

Alma Mater Studiorum – Università di Bologna

Dottorato di Ricerca in

CHIMICA INDUSTRIALE

Ciclo XXV

Settore Concorsuale di afferenza: *03/C2*

Settore Scientifico disciplinare: *Chim/04*

INNOVATIVE PROCESSES FOR SYNGAS PRODUCTION

Presentata da: *Dott. Barbera Davide*

Coordinatore Dottorato

Prof. Cavani Fabrizio

Relatore

Dott. Basile Francesco

Co-relatore

Prof. Trifirò Ferruccio

Prof. Vaccari Angelo

Esame finale anno 2013

Abstract

The research of new advanced processes for syngas production is a part of a European project for the production of a new Gas to Liquid Process (NextGTL). The crucial points in the production of GTL process are the energy required for the air separation used in autothermal reforming or the heat required for steam reforming and the efficiency in carbon utilization. Therefore a new multistep oxy-reforming process scheme was developed at lower temperature with intermediate H₂ membrane separation to improve the crucial parameter. The process is characterized by a S/C of 0.7 and O₂/C of 0.21 having a smoothed temperature profile in which kinetic regime is easily obtained. Active catalysts for low temperature oxy-reforming process have been studied working at low pressure to discriminate among the catalyst and at high pressure to prove it on industrial condition. It allows the selection of the Rh as active phase among single and bimetallic VIII group metal. The study of the matrix composition and thermal treatment has been carried out on Rh-Mg/Al hydrotalcite selected as reference catalyst. The research to optimize the catalyst lead to enhanced performances through the identification of a limitation of the Rh reduction from the oxides matrix as key point to increase the Rh performances. The Rh loading have been studied to allow the catalyst scale up for pilot process in Chieti in a shape of Rh-HT on honeycomb ceramic material. The developed catalyst has enhanced methane conversion in a inch diameter monolith reactor if compared with the semi-industrial catalyst chosen in the project as the best reference.

INDEX

1	Introduction.....	7
1.1	<i>NextGTL Project</i>	7
1.1.1	Motivations, Objectives and Concepts	9
1.1.2	Industrial Objectives and Project Structure	13
1.1.3	Natural Gas: Reserves and Options for Use	15
1.1.4	Line 1: Syngas Production	17
1.1.5	Membranes.....	19
1.2	<i>Processes for H₂ and/or syngas production</i>	20
1.2.1	Steam Reforming Process	21
1.2.1.1	Chemistry of Steam Reforming: Thermodynamics	22
1.2.1.2	Kinetics and Reaction Mechanism	27
1.2.2	Steam reforming catalysts	32
1.2.2.1	Carbon Formation on Reforming Catalyst	48
1.2.2.2	Sintering of Reforming Catalysts	58
1.2.2.3	Catalyst Shape and Dimensions	64
1.2.3	Practical Aspects of Steam Reformers	65
1.3	<i>Partial Oxidation of Fossil Fuels (POX).....</i>	69
1.4	<i>Autothermal Reforming (ATR).....</i>	71
1.5	<i>Catalytic Partial Oxidation of Methane (CPO).....</i>	72
1.6	<i>Aim of the Work.....</i>	78
2	Experimental Session	81
2.1	<i>Synthesis of Catalysts from Hydrotalcite Type Precursors.....</i>	81
2.1.1	Co-precipitation Method for Synthesis of Hydrotalcite-type Precursors	81
2.1.2	Calcination Procedure.....	82
2.2	<i>Synthesis of Impregnated Catalyst</i>	82
2.2.1	Incipient Wetness Impregnation (IWI).....	82
2.3	<i>Laboratory Plant Description.....</i>	83
2.4	<i>Description of Experiments.....</i>	85
2.5	<i>X-Ray Diffraction (XRD) Analysis.....</i>	86
2.6	<i>Surface Area and Porosimetry Analysis</i>	87
2.7	<i>Temperature Programmed Reduction (TPR) and Oxidation (TPO) analysis</i>	87

2.8	<i>H₂ Chemisorption Analysis</i>	87
2.9	<i>Scanning and Transmission Electron Microscopy Analysis</i>	88
2.10	<i>Infrared (IR) Spectroscopy Analysis</i>	88
3	Results and Discussion	90
3.1	<i>Studies and Selection of the Active Phase</i>	90
3.2	<i>Hydrotalcite-type Precursors</i>	90
3.2.1	Characterization of Rh 1% MgAl samples	95
3.2.1.1	Rh1% Mg ₆₈ Al ₃₂	95
3.2.2	Catalytic Tests	99
3.2.2.1	Comparison of Oxy-Reforming with Steam Reforming and CPO conditions	99
3.2.2.2	Catalytic Behavior: Rh1% Mg ₆₈ Al ₃₂	101
3.2.3	Study of the Rh or Ru Active Phase in the Mg/Al Matrix.	105
3.2.3.1	Characterization of Ru Catalyst	105
3.2.3.2	Comparison of the Catalytic Activity of Ru and Rh 1% Catalysts	106
3.2.3.3	Catalytic activity of Rh 0.1% and Ru 0.1%.....	107
3.3	<i>Effect of the Mg/Al ratio of the HT matrix</i>	107
3.3.1.1	Characterization of Rh1% Mg ₈₀ Al ₂₀ Catalyst	108
3.3.2	Comparison of the Catalyst Properties as Function of Mg/Al ratio	111
3.3.3	Effects of the Support: CeZrO ₂	116
3.3.4	Rh1% CeZrO ₂	116
3.3.4.1	Characterization.....	116
3.3.4.2	Catalytic activity.....	118
3.3.5	Comparison of the Selected Catalysts	119
3.4	<i>Bimetallic Active Phase</i>	120
3.4.1	Ni ₈ Rh _{0.15} Mg ₆₀ Al _{31.85} (NRexHT).....	121
3.4.1.1	Characterization.....	121
3.4.2	(Pt/Rh:2.5/1)1%/Ce _{0.75} Zr _{0.25} O ₂ (PRCZO)	122
3.4.2.1	Characterization.....	122
3.4.3	Comparison of the Bimetallic Catalyst Activity	124
3.5	<i>Industrial Catalyst (IC)</i>	126
3.6	<i>Scale-up of the Catalyst</i>	128
3.6.1	Rh2% Mg ₆₈ Al ₃₂	128
3.6.2	Comparison with the Rh1% Mg ₆₈ Al ₃₂	130
3.6.2.1	Catalytic Tests Comparison as Function of the Rh Content	132
3.6.3	Validation of the Results Obtained with Rh2% Mg ₆₈ Al ₃₂	136
3.6.3.1	New Study of Rh1% Mg ₆₈ Al ₃₂	139

3.6.4	Optimization of the Active by Different Thermal Treatment: Rh1% Mg ₆₈ Al ₃₂ tt	141
3.6.4.1	Characterization.....	141
3.6.4.2	Catalytic Activity	144
3.6.5	Rh3% Mg ₆₈ Al ₃₂	146
3.6.6	Structured Catalysts.....	148
3.6.6.1	Honeycomb catalyst	148
4	Conclusions.....	150
5	References	152

1 INTRODUCTION

1.1 NextGTL Project

Fast development of the world economy and increase of the international oil price have made the global energy and environmental problems increasingly serious. Gas-to-liquid (GTL) processes of Fischer-Tropsch (FT) synthesis, methanol synthesis, and dimethyl ether (DME) synthesis have become increasingly important and received much attention. Besides providing clean fuel, the products of GTL processes can be further processed to many other chemical products.

GTL fuels can be produced from natural gas, coal, and even biomass using the FT synthesis process. The entire process requires at least three stages. The first is the conversion of feedstock to synthesis gas (a mixture of CO and H₂). A second step is the FT synthesis which converts the syngas to waxy hydrocarbons. The third step is product upgrading which converts the waxy hydrocarbons into final products – naphtha and sulphur-free diesel. The resulting diesel can be used neat or blended with today's diesel fuel in existing diesel engines. The entire process is even more complex, because it includes also the preparation of the feed for syngas step, as summarized in Figure 1.

Although GTL fuels can be produced by different feedstocks, the use of coal or biomass requires more steps and has a higher impact on environment than starting from natural gas. In fact most of European companies have focused attention to natural gas to liquid, while starting from coal is mainly a primary interest of countries such as China.

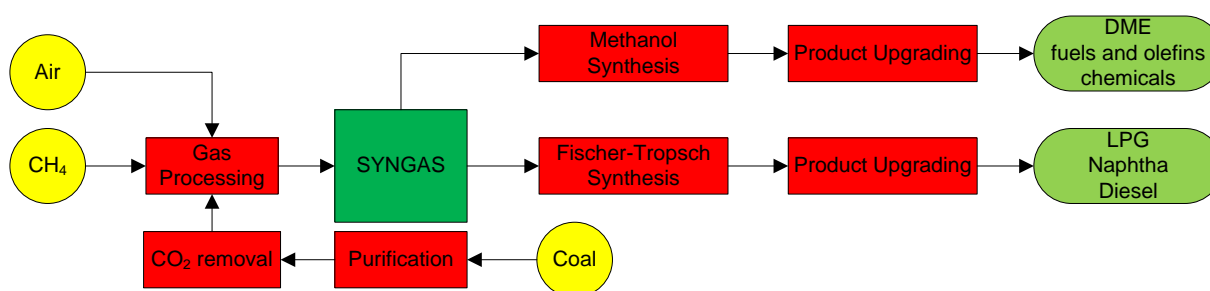


Figure 1. Main steps in the GTL process plant through indirect route.

The GTL technology is principally established, although there are still improvements necessary. Two large commercial scale GTL plant have been build and operate in Qatar. The Oryx process by Sasol uses ATR for syngas production and a FT carried out with Fe catalyst

and fluidized bed reactor (36'000 barrel per day) while the PEARL-GTL, developed by Shell uses an uncatalyzed POX process for syngas production and Co catalyst in a fixed bed reactor (140'000 barrel per day). Both process have still large space for improvement and optimisation. Some companies initially involved, such as Exxon, have stepped down, and others such as BP believe in opportunities to take conversion technologies even further to deliver a wider “gas to products” (GTP) portfolio. Critical issues are the large size of reactors and investments necessary for FT and the cost of syngas and the related air separation step. GTL is a capital-intensive process, with capital cost ranging from \$25'000 to \$45'000 per daily barrel.

Location:	Qatar, Ras Laffan Industrial City
Category:	Integrated gas and gas-to-liquids project
Ownership:	Development and Production Sharing Agreement with Government of the State Qatar, 100% Shell funding
Operator:	Shell
Development cost:	\$18 billion-\$19 billion
Peak: Production:	1,6 bcf/d of gas resulting in: <ul style="list-style-type: none"> • 140 kbo/d of gas-to-liquids products (2 trains) • 120 kbo/d of natural gas liquids and ethane
Total production:	3 billion boe of natural gas over the life of the project
Key contractors:	JGC/KBR joint venture

Table 1. Overview of Pearl GTL Project.

From syngas it is possible to produce methanol which can be used in part as gasoline blend (with opportune additives) or transformed to DME to be used also as fuel component. The main advantage of methanol over FT products is that it is much easier converted to chemicals, either by transformation to olefins using small-pore zeolites, or to other chemicals. The route through methanol offers thus better possibilities for an *integrated fuel and chemical*

production, an important concept for the future of refineries as shown, for example, in biorefineries.

The actual cost of production of fuel via FT or methanol routes is nearly equivalent, but the 1st is a target for diesel, while the 2nd is a target for gasoline. After several years of an increasing diesel car market, the trend was inverted in 2007. In addition, biodiesel is a more attracting route than bioethanol for the European market. Therefore, energy companies in Europe have reconsidered the need of FT to increase diesel production.

In conclusion, interest of producing methanol from NG particularly in remote areas (of the proven NG reserves, over 80% are too far to be transported by pipelines) is rising, for its potential to be a flexible intermediate for both fuel and chemicals, thereby minimizing risks in a fluctuating market. Direct methane to methanol is the grand-challenge. However, large progress has been made recently. The number of patents is raising, [1,2,3,4] showing that several companies are looking seriously into this route.

There are other interesting possible routes for direct conversion of methane, in particular the direct conversion of methane/natural gas to aromatics [5,6,7].

- Under non-oxidative conditions it is possible to form hydrogen as co-product and this is a first element of interest. Significant breakthroughs in the improvement of the catalyst stability and catalytic performance by modification of the catalyst and process parameters have been made recently. The selectivity to light aromatics can reach 80% at a methane conversion of 10-12%. The catalyst lifetime was extended to over 70h at an aromatics yields of 5%.
- High-value-added products such as aromatics are generated, answering the increasing aromatics demand in the chemical industry. Due to raising cyclohexane, cumene and phenol markets, the benzene price increased from about 2.40\$/gal (Jan. 2006) to about 3.50\$/gal (end 2007) with a peak of 4.40\$/gal in May 2007.
- The produced aromatics can be further converted to alkylaromatics for the chemical industry and the gasoline pool by reaction with other NG components (ethane, propane) using catalysts in the presence of a H₂-permselective membrane.

1.1.1 Motivations, Objectives and Concepts

The previous background section may be summarized as follows:

1. Conversion of natural gas to liquid is a primary driver over coal conversion, due to the environmental pressure and limited coal resources (in terms of competitive costs of extraction).
2. There is a renewed interest to produce methanol, for the possibility of a better integration between fuel and chemical production, an increasingly relevant factor in a market with fast raising costs of oil.
3. FT synthesis is highly interesting for diesel, but there are limited developments possible at the precompetitive stage necessary for an EU project;
4. The trend in the diesel car market has been inverted in direction and considering also the trends in biodiesel vs. biogasoline, should be revised the forecasts of increasing diesel vs. gasoline in refineries;
5. The syngas production is a critical element either to go to FT products or to methanol; in both cases it is the more costly stage of the production chain and the more energy-intensive. The syngas generation represents typically around 50-60% of the total cost, while FT conversion around 25% and product upgrading around 15-25% of the total cost. The present choice for large-scale FT plants based on natural gas is autothermal reforming. The main costs of an ATR unit are related to the manufacture of oxygen. Therefore, this is the stage which requires further development, even if a well-established process. Recent developments in membrane technology to remove H₂ and/or CO₂, and in O₂ separation from air open novel perspectives to reduce costs in syngas production. Approximately 60-70% of the capital cost of a methanol plant is associated with the syngas plant. A major breakthrough is required to substantially reduce the cost. The Argonne National Lab., in cooperation with Amoco, has pioneered in the use of membrane technology in the production of syngas, and have shown, that the membrane process could lower the cost of syngas production by about 30%. Recently an alliance of Amoco, BP, Praxair, Statoil and Sasol was announced to develop this technology. The US Dept. of Energy announced an \$84 million project to develop membrane technology for syngas production.
6. The direct conversion of CH₄ to CH₃OH or DME opens new routes to synthesize easily transportable liquid products suitable both for the fuel and the chemical market. Although for a long-time this has been an objective of research, the increasing knowledge on combining homo- and heterogeneous catalysts and on the fundamental understanding of the mechanisms of methane activation allows now to put the research

in this area on new bases/prospects. We do not consider the conversion to other chemicals such as formaldehyde, because they are not suitable for fuel transport applications.

7. Dimethylether (DME) is a very attractive synthetic transportation fuel, because of its properties close to LPG regarding storage (with advantages in terms of explosivity), very low toxicity, and high cetane number (around 55-60). In the presence of acidic sites methanol can be dehydrated to DME and it is thus possible to tailor the properties of a catalyst active in methane to methanol conversion to form DME or methanol/DME mixtures.

8. Many patents have been issued recently on non-oxidative gas to liquid conversion, i.e. methane to aromatics¹, for the interest in valorization of stranded natural gas resources. The advantage of non-oxidative conversion is the possibility to avoid separation of natural gas (NG) components and the co-production of H₂. However, due to the toxicity of benzene and the concomitant ever more stringent regulation of its content in gasoline, its further alkylation is necessary. As an important side effect, this step considerably increases the octane number and lowers vapour pressure. Alkylation of benzene-rich reformat with olefins is a common practice in refinery, where the olefins are readily available. However, for applications in remote areas close to NG wells, i.e. where the olefins are not available, it would be necessary to develop a completely innovative technology, which uses the alkanes (C₂-C₃), which could be recovered from the NG stream, as alkylating agents. The aromatization of methane and the alkylation of benzene to alkyl benzenes are fully complementary steps. Natural gas associated with crude oil always contains other light alkanes. The alkylation of benzene with ethane and propane ensures that the natural gas is used in total. It would neither be economic nor environmentally friendly to use just methane and to flare the rest.

9. Recent reconsiderations on the role of biofuels in Europe have further pushed the urgent need to develop alternative fuels for transport. Methane conversion is the most straightforward choice. In recent meeting of EU ministers (5-6 July 2008) it was concluded that the share of *biofuels* in transport (10% by 2020) had been misinterpreted and is not limited to them but to alternative fuels. Methane is among the options considered, but requires large investments in converting actual vehicles and distribution system. Therefore, conversion of methane to products, which can be used

¹ For example, in the period 2006-2008 ExxonMobil issued 11 patents extended worldwide

in the actual transport system, is the best solution. Products should be considered, which can be added to gasoline and diesel pools. Therefore, methanol, DME and alkylaromatics from natural gas are the natural choice.

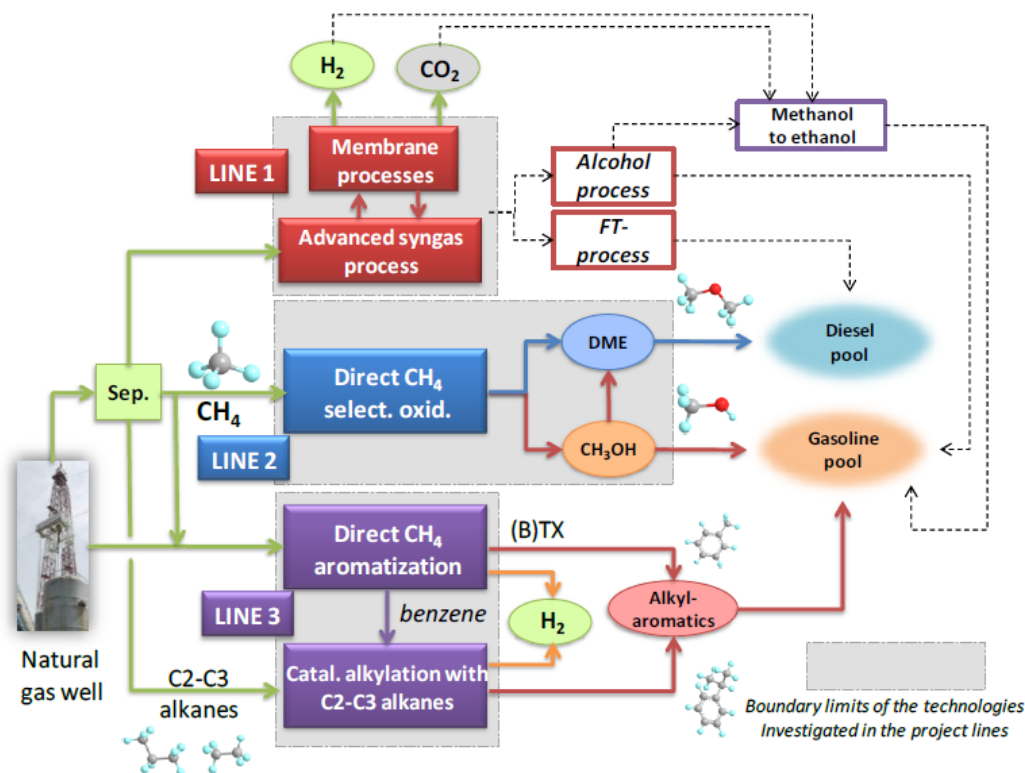


Figure 2. Overall conceptual scheme investigated in the project. In this scheme from natural gas to transport fuels we have outlined the general pathways considered and the specific aspects which are investigated in the project in the three main lines of activity.

Above considerations form the basis for the strategic planning of present projects. The general objective is to explore novel and innovative (precompetitive) routes for transformation of natural gas (NG) to liquid products, particularly suited for remote areas to facilitate the transport. The aim is an integrated multi-disciplinary approach to develop in a long term vision the next-stage catalysts and related precompetitive technologies for gas to liquid conversion. FT synthesis and hydrocracking, as well as the processes for coal to liquid conversion were not included.

The focal points of the project strategy are the following:

1. Improve the current gas to liquid (GTL) conversion chain by developing an improved technology for the most costly and energy-intensive step of syngas production; use the knowledge available on catalysis and membranes to develop this new technology.

2. Develop alternative direct routes (not via syngas) of methane to liquid conversion to transportable fuels, suitable for both gasoline and diesel pools, and eventually for chemical uses; explore both oxidative and non-oxidative routes for methane conversion to compare the two alternatives.
3. Develop technologies, which may be used close to NG production sites.

1.1.2 Industrial Objectives and Project Structure

The project addresses from one side the most critical and costly step to produce liquid fuel from natural gas using conventional routes, i.e. the stage of syngas production, and from the other side explores alternative routes (oxidative and non-oxidative) to convert natural gas to liquid transportable products for gasoline and diesel pools. The broader and ambitious organization of the project in three lines derives from the following industrial needs / objectives:

1. Reduce the cost and energy consumption (and related environmental impact) of the more costly step in the conventional GTL process, i.e. syngas production, and overcome the actual barriers in using catalysts in this process (mainly related to stability); this objective is implemented in Line 1 by developing a new low temperature catalytic syngas production based on the integration between catalysts and membrane.
2. Develop GTL technologies suitable for small-medium scale productions in remote NG areas; this objective is implemented in all the three lines of the project by using configurations, based on the integration with membranes, suited for this objective. Develop direct NG routes, in particular, is an important target to reach this objective. In addition, the possibility in Line 3 of using NG mixtures (instead of pure CH₄) in aromatization step and C2-C3 alkanes (instead of olefins) for converting benzene to alkylaromatics are further relevant components to reach the scope.
3. Develop processes for producing liquid fuels which can be blended in both gasoline and diesel pools, or which may be used for chemical purpose; after syngas production (Line 1) different products could be obtained (as schematically indicated in **Figure 1**), but in view of point 2, it is necessary also to develop direct conversion routes which could meet this objective. For this reason methanol, DME and alkylaromatics are targeted as products,.

Accordingly, three development lines are followed in this project:

Line 1: advanced, low temperature route for catalytic syngas formation from natural gas, in which reaction steps are integrated with different types of membranes for O₂, H₂ and CO₂ separation.

Line 2: direct low temperature catalytic conversion of methane to methanol/DME, utilizing several innovative concepts to overcome the drawbacks of previous approaches including the use of supported ionic liquids/molten salts

Line 3: direct catalytic conversion of methane to aromatics under non-oxidative conditions followed by upgrading of the products by alkylation with ethane/propane.

To enable these objectives within the timescale and partnership possible for the project specific aspects are investigated. The project will accordingly not fully develop the three process options, as this is not realizable within the project, but the aim is to develop the necessary knowledge to assess the feasibility of the three processes, which then should be further developed in a second phase. In particular the line 1 will be carried on till the development of a pilot scale process to be built in Chieti proving at least the multistage reactor for syngas production with intermediate hydrogen membrane separation.

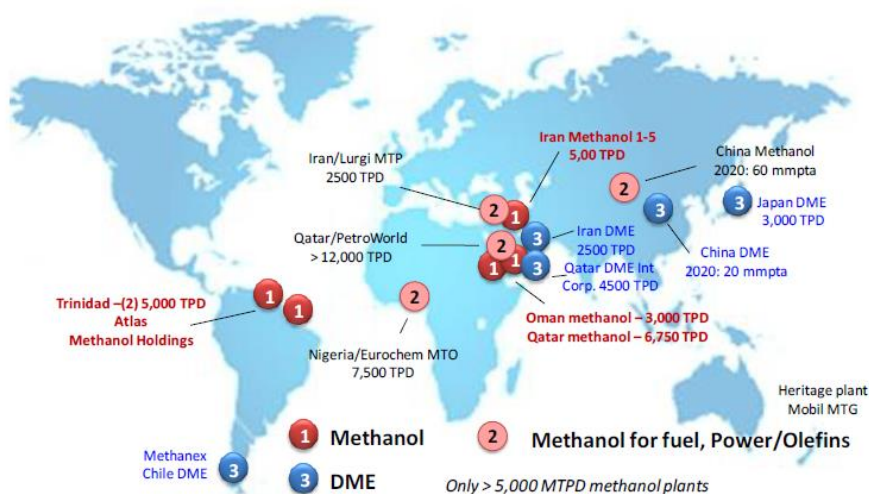
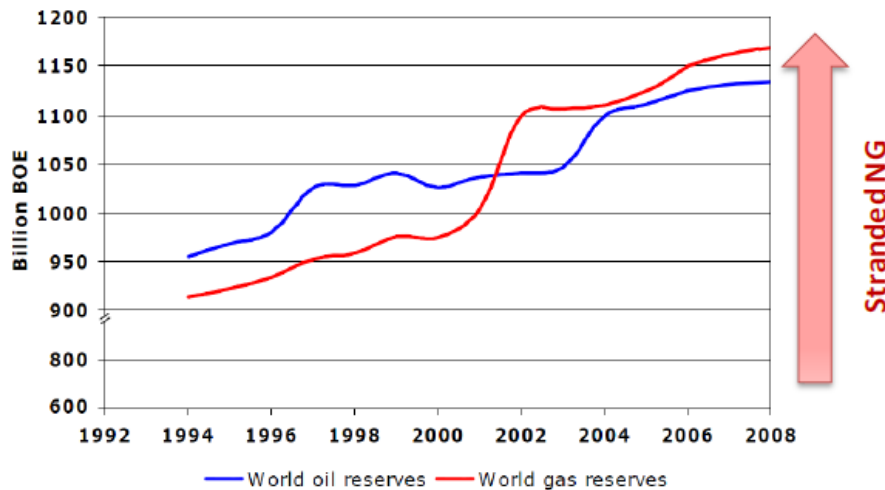


Figure 3. Methanol/DME projects: transition from chemicals to fuels.

1.1.3 Natural Gas: Reserves and Options for Use

From around 2001 the proven world gas reserves have overcome those of oil (Graph 1) to reach nearly 1'200 Billion BOE (Barrel of oil equivalent), e.g over 196 TSCM (thousand billion standard cubic meters) [8].



Graph 1. Proven world oil & gas reserves, with an indication of the amount of "stranded natural gas" [9].

The total amount of "Stranded Gas Reserves", i.e. the part which is not usable, has been estimated to be about 70 TSCM, about 40% of the gas proven reserves. Such an amount could, if converted to synthetic fuels, generate around 250 billion barrels of synthetic oil, a quantity equal to one third of Middle Est's proven oil reserves.

The possible options for remote gas monetization, when transport in pipelines is not possible, are the following:

- (i) LNG (Liquefied Natural Gas), i.e. cooling to about -160°C for transport followed by regasification and introduction in the local network;
- (ii) GTL (Gas to Liquid), i.e. conversion of NG to liquid transportation fuels. The economics of GTL versus LNG depends on the oil to gas price relationship which depends on various aspects.

The main *drivers for GTL* are the following:

- reduction in cost of transport of NG - monetization of stranded natural gas - economic utilization of associated gas;

- high current and projected demand for liquid transportation fuels - higher costs tied in with crude markets and refining capacity issues - need of clean fuels (sulphur free);
- flaring reduction and environmental concerns;

Currently the only industrial feasible option for GTL passes through the first step of conversion of NG to syngas (CO/H₂ mixtures) followed by conversion of syngas to either hydrocarbons via Fischer-Tropsch (FT) synthesis or oxygenated products (CH₃OH/DME, or higher alcohols) via well established technologies. While FT projects concentrate mainly in Qatar (Sasol “Oryx” and Shell “Pearl”, while other in the same region such as the ExxonMobil, ConocoPhillips, etc. were stopped or postponed for the risks and too large investment), there are many methanol/DME projects which clearly evidence a transition from chemicals to fuels (Figure 3). Note that in terms of *thermal/carbon efficiency*, GTL today is about 60-77%, while methanol/DME is about 70-83% [10]. In terms of economic competitiveness of methanol and DME in fuel markets, with respect to FT products, they are comparable [9].

A typical FT plant flow scheme is shown in Figure 4, while Figure 5 shows the cost breakdown for the main components [9]. The largest part of the cost (36-48%) is associated to air fractionation/syngas production. To reduce this cost, very large plants are necessary for FT production, but this is limited, because

- large investments and risks are necessary;
- there are only few gas fields for which these large investments could be justified.

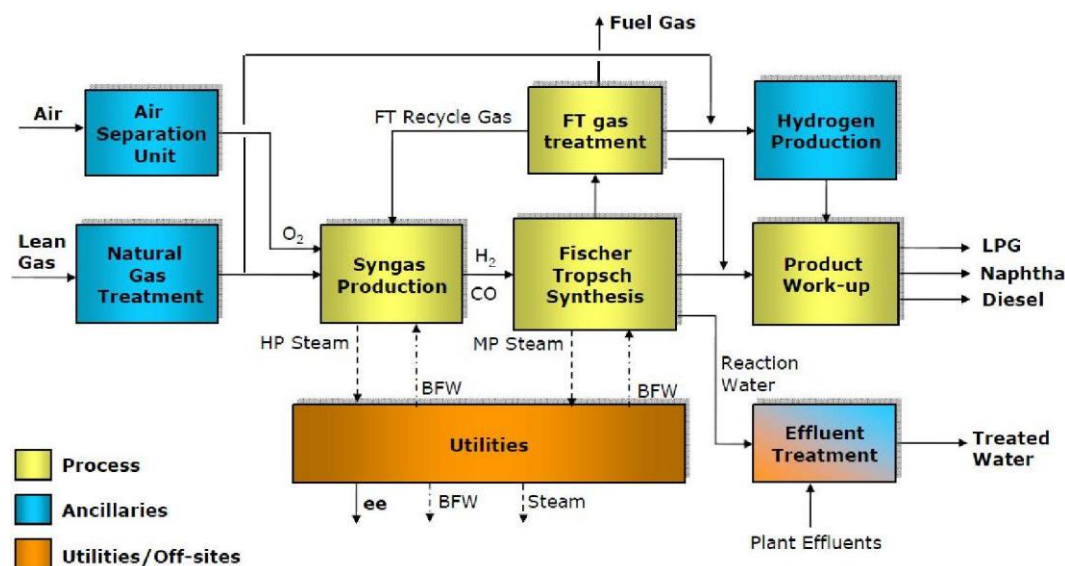


Figure 4. Fischer-Tropsch Plant Flow Scheme [11].

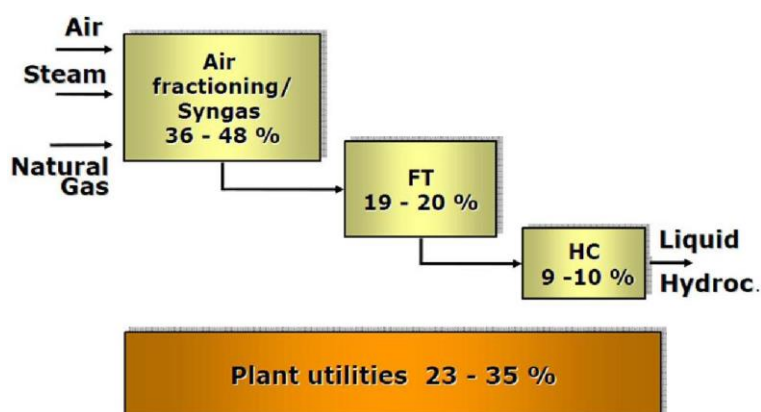


Figure 5. Costs breakdown for FT process [11].

As a consequence, the valorization of small/medium size gas fields for which pipelines and LNG are not convenient (Graph 1), require the development of alternative syngas technologies suited for this size, and direct routes for NG conversion. The project is thus motivated based on the following industrial objectives:

- to introduce a novel, less costly and more energetically efficient, scheme for syngas, based on membranes to develop GTL processes cost-effective on small-medium size;
- to develop new direct routes for GTL which avoid the costly syngas step;
- to synthesize liquid products which can go either to fuel or chemical production, and which realize a better balance between diesel vs. gasoline pools;
- to invest R&D to explore novel reactor/process concepts to maintain competitiveness of EU companies in the highly competitive field of sustainable energy;

1.1.4 Line 1: Syngas Production

The AutoThermal Reformer (ATR, Figure 6) is used for producing synthesis gas from NG for CH₃OH synthesis, FT and carbonylation processes, due to better CO/H₂ ratio. The ATR technology requires the use of pure oxygen or strongly enriched air for preventing the decrease in the partial oxygen pressure in the combustion chamber from causing the formation of carbonaceous residues. Membranes that selectively extract pure oxygen from air can provide oxygen at a low cost, reducing the whole syngas production charges in a remarkable way. This approach was developed by Air Product/Chevron for the US DoE using a La-Ca-Fe perovskite-based oxygen-membrane, but the membrane should operate at 900°C to have enough flux. MTR (Membrane Techn. Res., US) offers H₂ membrane separation for

the syngas process, but these are polymeric membranes, which thus require to cool down the feed to below 150°C and cannot be used for recycle. H₂ permselective membranes based on Pd-alloy are preferable for a separation integrated with syngas reactor. A recent review [12] discussed these aspects in details. In particular, it is evidenced that 450 trillion Btu/yr could be saved using H₂ membranes. The review emphasizes the flow sheet design modification with adsorption or membrane units being added downstream to the reactor for short-term impact, and an integrated membrane/reactor design for a longer-term sustainable impact. This corresponds to the approach proposed in this project.

In Europe, besides the TECHNIP/INSTM project [13] dedicated to the H₂ production process, there are few efforts exceeding the laboratory scale. The two main research activities to be cited are those at ECN (The Netherlands), who developed H₂ membranes based on a Pd-alloy film deposited by Electroless Plating on a ceramic tubular support, and at SINTEF (a Pd-Ag 1µm film deposited on Si wafer and after pull-off from this substrate rolled around a ceramic tubular membrane). They collaborate (together also with the Dalian Institute of Physical Chemistry, China) in the frame of the running EU project CACHET CO₂ dedicated to new options for CO₂ capture).

Steam reforming (SR) (Figure 6) is used for converting natural gas (NG) and naphtha into synthesis gas. Before being sent to SR, the hydrocarbon reagent is preheated and desulfurized; vapour is then added and the mixture is further preheated. The reforming takes place in an oven in which tubes are located filled with catalyst, through which the reaction mixture flows. The synthesis gas at the outlet of the tubes is rapidly cooled and can be sent to water-gas shift processes and separation/purification. SR requires considerable quantities of vapour to reduce the formation of carbonaceous residues. Vapour is also necessary for increasing the H₂ content in the synthesis gas produced which would otherwise prevalently contain CO, in case a higher H₂/CO ratio is required.

CPO (catalytic partial oxidation) with a short contact time [11] can use either oxygen, enriched air or air also in the absence of vapour, so the formation of carbonaceous compounds in produced synthesis gas is strongly reduced thus improving the efficiency of thermal recoveries and allowing the use of exchange systems (for syngas production) at a lower cost. By means of short contact time, CPO is capable of transforming hydrocarbon fractions which cannot be used by other known catalytic technologies (SR and ATR) and which can only be converted into synthesis gas by means of the PO technology but with high energy consumptions and investment costs. It is also possible to transform liquid hydrocarbons with a high content of aromatics and sulphur into synthesis gas avoiding the formation of carbonaceous residues and

NO_x , using air, enriched air or oxygen as oxidizing agents. The temperature is often close to 1000°C at the catalyst inlet and the catalyst active phase and structure is subject to sintering.

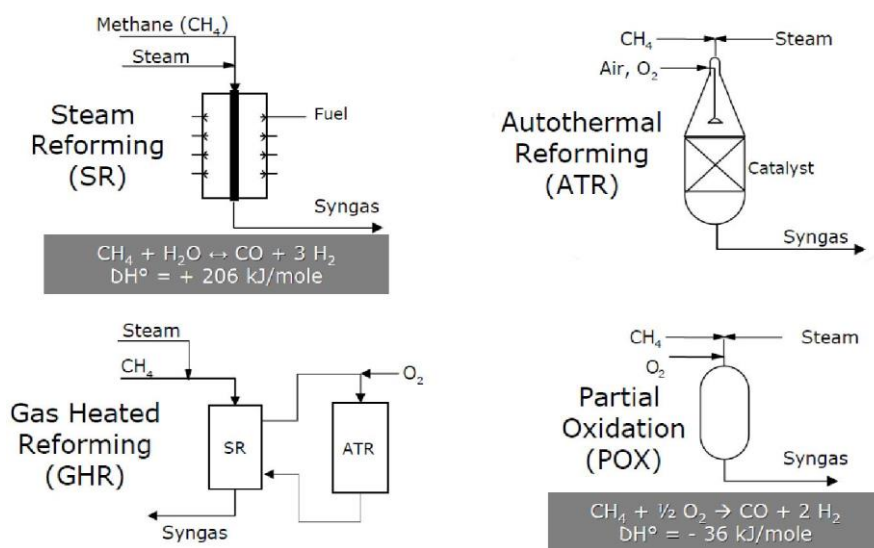


Figure 6. Syngas technologies to convert Natural Gas

A CPO/membrane reactor can then be a valuable alternative with respect to conventional SR or CPO reactors to transform methane into syngas. No attempt was previously made to integrate CPO upstream with an O_2 membrane separator and downstream with a H_2 membrane separator.

1.1.5 Membranes

Various articles and review have discussed the advances in this area. [14,15,16,17,18,19] The state-of-the-art can be summarized as follows:

- For H_2 -permselective membranes there are two approaches: (i) a thin Pd or Pd-alloy (Cu, Ag) layer in which the transport mechanism is based on H_2 dissociation and transport of H in atomic form by diffusion in the Pd (this mechanism provides a virtual 100% permeoselectivity), and (ii) the use of a zeolite-layer in which the selectivity is given by the faster kinetic diffusion of H_2 . They have both advantages and disadvantages. The main critical factors are the flux and the permeoselectivities which should be obtained, together with the stability in long term. No commercial membranes are available.
- Preparation of crack-free and robust membranes is an issue. Initial research was focused on planar-type membranes, but it is now focused on tubular types, which are more robust. In Pd-based membranes usually a ceramic membrane is utilized as the support, while metallic supports

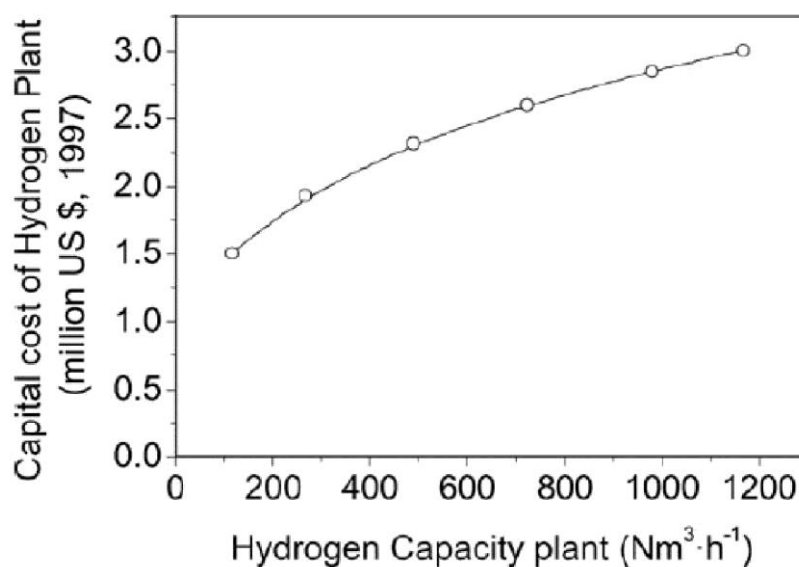
have been not successful up to now. Among the methods of preparation of Pd film, electroless plating deposition is one of the most common.

- Dense ceramic membranes for the separation of O₂ are mainly based on perovskites, or O²⁻ conducting materials as used in solid state fuel cells (Y-stabilized zirconia, Ce-gadolinia, etc.). O₂ flux at a given temperature and production of crack-free thin films are the main issues.
- For CO₂ separation, either nanoporous membranes (polymeric, or based on supported ionic liquids), or adsorbents based on zeolites (clinoptilolite or ion-exchanged zeolites) are utilized.

1.2 Processes for H₂ and/or syngas production

Although hydrogen can be produced from a large variety of sources by using different methods, up to now the most extensively used process is the steam reforming of hydrocarbons. Biomass can be also used to produce H₂ by thermochemical or biological processes. Metabolic processing appears as an interesting alternative for the treatment of wastes while generating H₂ as product. Some other approaches for hydrogen production from water or other hydrogen-containing materials such as photodecomposition or thermochemical processes are also in development. Solar photodecomposition of water still has many technical hurdles remaining that suggest it is decades away from large scale, cost-effective implementation [20]

The conversion of hydrocarbons to hydrogen and syngas will play an important role in the 21st century ranging from large gas to liquid plants and hydrogen plants for refineries to small units providing hydrogen for fuel cells. The choice of technology for manufacture of syngas depends on the scale of operation [21].



Graph 2. Capital cost of a hydrogen plant as a function of capacity [20].

Currently, steam reforming of hydrocarbons (SR) especially steam methane reforming (SMR) is the largest and generally the most economical way to make H₂. Alternative non-catalytic, industrial chemical approaches include partial oxidation (PDX) of heavy oil or coal. When electricity is available and relatively inexpensive, electrolysis of water offers an alternative commercial approach [22,23]. Industrially, two main reactions are important in the conversion of natural gas to syngas [24]:

- Steam reforming (SR),
- Non-catalytic partial oxidation (POX).

While most syngas is produced by steam reforming, two other processes may be more attractive, depending on factors such as H₂:CO ratio, downstream use, product purity, the presence of CO₂, N₂, H₂O and CH₄, plant capacity, feedstock availability, purity and cost, including O₂. These processes are:

- Autothermal catalytic reforming (ATR),
- Catalytic partial oxidation (CPO).

1.2.1 Steam Reforming Process

In areas where natural gas is available in large quantities, interest is centered on steam reforming of methane as hydrogen source [25]. The process is more economic than that based on coal. The hydrogen content of the hydrocarbon improved the yield of hydrogen per unit of carbon in the feedstock compared with coal, and there were also fewer unwanted byproducts. The methane steam technology was pioneered in the first quarter of 20th century by BASF who established the essential configuration of the primary steam reformer, and the technology was used in 1931 by Standard Oil of New Jersey to produce hydrogen from off-gases at its Baton Rouge and Bayway refineries.

The methane reforming process was adopted mainly in the US where natural gas was easily available as feedstock, whereas reformers in Europe were initially reduced to operate on propane and LPG [26].

The steam reforming reaction took place over catalyst in vertical tubes, which were supported in parallel rows in a radiant furnace. The endothermic heat of reaction was supplied by burning fuel in the furnace. The process was considerably improved by ICI, who developed the fundamental engineering data for the design of the furnace, improved the catalyst formulation and introduced the desulphurization step using zinc oxide. The process was used to produce hydrogen

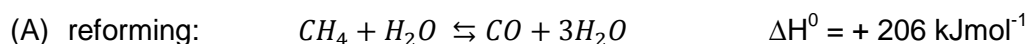
from off gases for coal hydrogenation plants, which ICI built in 1936 and 1940. The ICI technology was subsequently used in the development of the North American ammonia industry when plants were constructed at El Dorado, Baxter Springs, Ethers, Sterlington and Calgary. The plants used natural gas, which contained mainly methane with low concentrations of higher hydrocarbons, and nearly all used catalyst developed by ICI. Natural gas was not a readily available feedstock in the UK before the discovery in the North Sea, but as more refineries were built other hydrocarbons, such as naphthas, became increasingly available. It was apparent in the 1950s that if naphthas could be steam reformed economically they would provide a cheap source of hydrogen for the manufacture of ammonia. Work by ICI at this time led to the development of a catalyst, which would reform naphthas at economic steam ratios without carbon formation. The catalyst was stable, resistant to poisons and had an economical life.

In the 1959 ICI started up the first large scale pressure steam reformer using naphtha as a feedstock, and this became the precursor of over 400 plants subsequently licensed around the world in areas where natural gas was not available. From 1959 to date development of the catalyst continued in order to allow plants to be run at higher pressure and temperature, and with feedstocks containing quantities of unsaturated and aromatic compounds to be reformed. In more recent years the increasing availability of natural gas has resulted in its use as a major source of reformer feedstock, and this is likely to remain so for some time. Development of catalyst for natural gas reforming has concentrated on extending catalyst life, improving activity, inhibiting carbon-forming reactions, and by improving the physical properties.

1.2.1.1 Chemistry of Steam Reforming: Thermodynamics

The objective of the catalytic steam reforming process is to extract the maximum quantity of hydrogen/syngas held in water and in the hydrocarbon feedstock. Thereafter the subsequent manipulation of the gas stream depends on the purpose for which the gas is intended.

The reforming of natural gas utilizes two simple reversible reactions:



The reforming reaction (A) is strongly endothermic, so the reaction is favored by high temperature as well as by low pressure, while the shift reaction (B) is exothermic and is favored by low temperature but is largely unaffected by changes in pressure. To minimize the overall efficiency (and hence economics) of the conversion of carbon to carbon dioxide and the production of hydrogen, reformers are operated at relative high temperature and pressure. This is followed by the shift process that, by using two different catalysts, permits the shift reaction to be brought to equilibrium at as low temperature as possible. It can be seen that with methane the stoichiometric requirement for steam per carbon atom is 1.0. However, it has been demonstrated

that this is not reliable because all catalysts so far developed tend to promote carbon formation under steam reforming conditions. These reactions can be suppressed by using an excess of steam, with the results that the minimum ratio is in the region of 1.7. However, the reforming reaction itself is also promoted by an excess of steam and hence some advantage is derived from this. In practice ratio of 2.5 - 3.5 are commonly used, but in some cases, there can be economic attractions in using lower steams ratios and there is a trend in this direction.

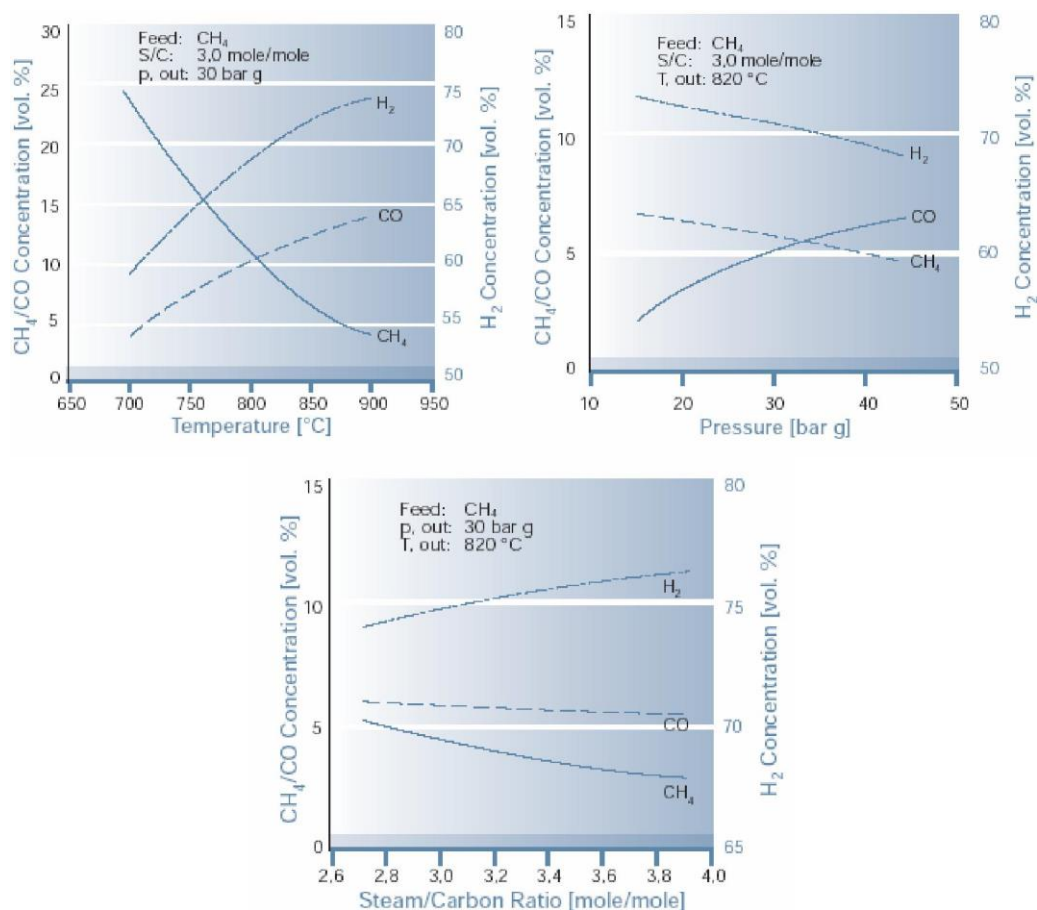
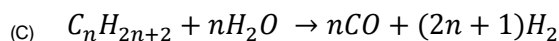


Figure 7. Variation of the reformed gas depending on: (a) outlet temperature; (b) outlet pressure; and (c) inlet S/C ratio.

The reforming of saturated naphthas of general formula C_nH_{2n+2} is based on the following reaction:



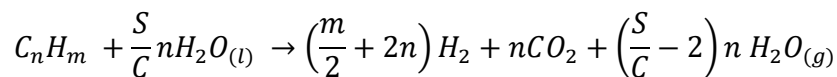
Reaction (C) is strongly endothermic, absorbing more heat than the following methanation reaction (D) and shift reaction (B) evolve, thus making the overall process normally an endothermic one.

Analogously to methane, the naphtha reforming reaction is favored by high temperature and low pressure, while the shift reaction is inhibited by high temperature but largely unaffected by

pressure. The tendency towards carbon formation on catalysts when stoichiometric ratios of carbon and steam are used is greater with naphtha than with methane, and the minimum practical ratio is about 2.2. As with methane, the excess steam favors the reforming reaction, and in practice S/C ratios of 3.5 - 4.5 are common. At low S/C ratio the methanation reaction begins to dominate, and under certain conditions of pressure and temperature can cause the overall reaction to be exothermic. As with methane reforming, it is possible to calculate the equilibrium methane, carbon monoxide, carbon dioxide, hydrogen and water concentrations from inlet steam/carbon ratios and the operating conditions of a reformer [25].

Lutz and co-workers [27] examined the thermodynamics of the steam reforming process. SR is achieved by reaction over a catalyst at high temperature. In addition to the energy required to provide the steam, the overall reaction is endothermic, so energy must be added to drive it. The process must burn either a second fuel, a fraction of the primary fuel, or the residual fuels that remain in the reformat stream. This last option is often done in practice to recover heating value that would otherwise be wasted. The analysis presented by Lutz considers two levels of sophistication in treating the chemistry. The first uses a global species balance that assumes that the reforming reaction goes to completion. An energy balance for the reaction allows to examine the definition of thermal efficiency. This analysis provides a theoretical upper limit on the thermal efficiency that is independent of temperature or other influences on the reaction kinetics. The second analysis replaces the global reaction step with a calculation of chemical equilibrium for the reforming reaction. The equilibrium computation brings in temperature dependence, without requiring detailed information regarding the specific reactions or catalyst performance.

To study the thermodynamics of steam reforming of hydrocarbon fuel at a basic level, a global reaction balance was examined:



where n and m define the composition of the fuel, and S/C is the steam-to-carbon ratio for the mixture. The term "global reaction" recognizes that the reaction is actually the net result of a series of elementary reactions, some of which include catalytic interaction with surfaces. This balance conserves elements with two assumptions: there is sufficient steam to react with the fuel ($S/C \geq 2$), and the reaction goes to completion. Using this reaction, the formation enthalpies of the species can be added to determine the net enthalpy change:

$$\Delta H_R = n h_{CO_2}^f + \left(\frac{S}{C} - 2\right) n h_{H_2O(g)}^f - (h_{C_n H_m}^f + h_{H_2O(l)}^f)$$

where h_k^f is the formation enthalpy per mol of species k at standard temperature and pressure. Note that $h_{H_2}^f = 0$, by definition (was dropped from the equation). Since water is liquid at room temperature it was considered that as the state for the reactant ($H_2O_{(l)}$). Since the reactants must be raised to higher temperatures to make the reaction proceed, Lutz et al [27] took the water in the products to be vapor, $H_2O_{(g)}$.

Using methane as example, with $S/C=2$, the net enthalpy change for the reaction is $\Delta H_R = +60 \text{ kcal} \cdot \text{mol}^{-1}$ of fuel, thus the process requires energy input. For heptane (C_7H_{16}) the net enthalpy is $\Delta H_R = +339 \text{ kcal} \cdot \text{mol}^{-1}$ of fuel. It appears that reforming heptane requires more energy than methane, but to put the comparison in perspective, note that these enthalpies changes are based on 1 mol of fuel. A more level comparison would be the energy cost per mole of H_2 produced. Methane takes $15 \text{ kcal} \cdot \text{mol}^{-1}$ of H_2 produced, compared to $15.4 \text{ kcal} \cdot \text{mol}^{-1}$ of H_2 for reforming heptane and cetane ($C_{16}H_{34}$) requires $15.9 \text{ kcal} \cdot \text{mol}^{-1}$ of H_2 . Therefore, the energy necessary to produce H_2 is roughly constant, at least for these saturated hydrocarbons. However, in the analyses Lutz et al [27] showed that the thermal efficiency of the process is not constant, but depends on the fuel.

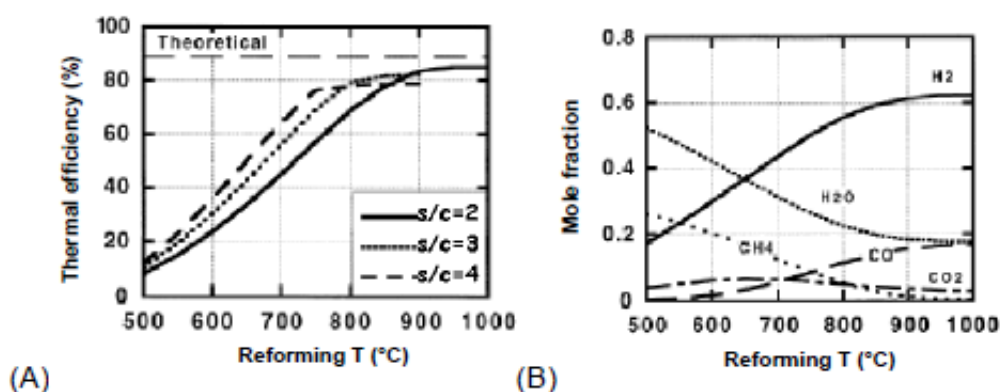


Figure 8. (A) Efficiency of methane steam reforming computed in equilibrium model versus reformer temperature at pressure of 10 atm at different S/C ratios. (B) Equilibrium composition leaving the methane steam reformer for $S/C = 2$ and pressure 10 atm [27].

The equilibrium model solutions show the effects of two parameters: the steam/carbon (S/C) ratio and the temperature (Figure 8 (A)). Focusing on the solid curve (Figure 8 (A)), for $S/C=2$, the effect of temperature is to increase the efficiency of the equilibrium reformer. This is simply due to the fact that at lower temperatures the equilibrium composition leaving the reformer (Figure 8 (B)) contains more unreacted methane and water. As the temperature increases, the equilibrium composition approaches the product stream expected from the global balance, except that there is still an excess of steam, and the CO concentration is 20% of the mixture.

The equilibrium solutions suggest that the reformer must operate at higher temperatures. There is, however, a limit to which higher temperature improves performance. The equilibrium does not shift much farther towards reaction completion as the temperature goes above 900°C. A secondary effect is that the reformat stream contains insufficient heating value, so supplemental fuel must be added prior to the burner. The effect of S/C ratio is complicated by the fact that its influence depends on the temperature. The three curves (Figure 8 (A)) at S/C ratios of 2, 3 and 4 show that at low temperature, where the reaction is far from completion, the efficiency increase with excess of steam. At high temperature, where maximum H₂ is obtained, the equilibrium model behaves like global analysis. In this limit, the excess of water does reduce the efficiency. The observation that the thermal efficiency intersect at some temperature means that there is a point where the chemical benefit of extra steam is offset by the energy required to generate it. Figure 9 shows that a higher exhaust temperature reduces the thermal efficiency.

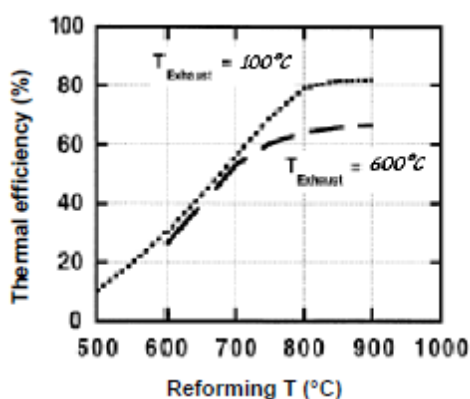


Figure 9. Thermal efficiency vs. equilibrium reformer temperature for steam reforming of methane at S/C=3 and two exhaust temperatures [27].

From thermal efficiency analysis, Lutz and co-workers concluded that definitions of thermal efficiency can be misleading. The definition should be accompanied by identification of the system boundary and the heat flows across it. The definition should include external heat addition. Comparisons of the equilibrium model for steam reforming to experimental data showed that the chemical equilibrium is appropriate for understanding the effect of temperature. Experimental thermal efficiencies for steam reforming were significantly lower than the thermodynamic limit predicted by the equilibrium model. Species measurements showed the deficiency was partly due to non-equilibrium composition, but other heat transfer losses are a dominant effect, especially for compact steam reformers. The effect of extra steam suggested by the equilibrium analysis is to increase the H₂ conversion and thermal efficiency, at least until a high temperature limit is reached where the H₂ conversion is maximized. Only in this limit is the global analysis valid. The global and equilibrium analyses both show a decrease in thermal efficiency for reforming larger hydrocarbons

compared to methane. Expect the efficiency of reforming diesel fuel to be at least 15 % lower than that of natural gas, from thermodynamic alone.

1.2.1.2 Kinetics and Reaction Mechanism

The results of a number of studies on the kinetics of the methane steam reforming have been published. There is general agreement that the reaction is first order in methane, but there is less agreement with other kinetic parameters. In part, this is due to the use of different catalysts and experimental conditions, but often it has resulted from a lack of consideration of diffusion and heat transfer limitations. Thus, reported activation energies are spread in a wide range of values due to different degrees of diffusion limitation, and these can also cause misleading total pressure effect. Indeed, with the relatively large catalyst particle sizes used in industrial steam reformers, these effects results in very low effectiveness of the catalyst. Effectiveness factors (η) may, depending on conditions, only be as high as 0.3 at the inlet region, and perhaps as low as 0.01 at the exit. Because of this, apparent activity increases as the particle size is made smaller, but the increased pressure drop, which arises across the reformer, restricts the size of the catalyst that can be used in practice [25].

There has been some debate about the first formed products of the steam reforming reactions, and it appears that the relative concentrations of carbon monoxide and carbon dioxide leaving the catalyst surface depend on the efficiency of the catalyst in the water gas shift reaction. With rhodium-based catalysts the CO/CO₂ ratio of the initially formed carbon oxides is relatively high (in keeping with poor shift activity), whereas with nickel catalysts the amount of carbon monoxide is lower [25].

A wide variety of rate expressions for the steam reforming of methane have been proposed. These models range in complexity from simple first order dependency on methane, involving two parameters, to complex Langmuir–Hinshelwood models with over ten parameters [28]. It is generally agreed that the rate of methane reforming has a first order dependency on methane. Furthermore, it is also agreed that the rate-determining step in the reforming process is the formation of adsorbed carbon species:



This mechanism leads to the formulation of rate equations of the following form:

$$r_{CH_4} = -kp_{CH_4}p_{H_2}^\alpha$$

In this equation, the value of α is found to depend on temperature, having a value close to -1 at low temperatures ($<700^\circ\text{C}$) and approaching 0 at high temperatures ($>700^\circ\text{C}$).

Kinetic rate expressions for the steam reforming of methane found in the literature use the steady state approximation and take the form:

$$r_{CH_4} = -k p_{CH_4} \frac{f(p_{H_2O}, p_{H_2})}{[1 + f(p_{CH_4}, p_{H_2O}, p_{H_2}, p_{CO}, p_{CO_2})]} * \left(1 - \frac{p_{CO} * p_{H_2}^3}{p_{CH_4} * p_{H_2O} K_1}\right)$$

Wei and Iglesia [29,30] measured CH₄ reaction rates on 7% Ni/MgO catalyst in the absence of detectable deactivation and of transport or thermodynamic corruption of rate measurement. CH₄ reaction rates remained constant for 100 h and transport artifacts were ruled out by dilution of the catalyst pellet with inert Al₂O₃ and dilution of the catalyst bed with ground quartz. Reforming rates can be rigorously obtained from measured net rates using an approach to equilibrium parameter (η) evaluated from CH₄-H₂O thermodynamic reaction data and measured reactant and product partial pressures:

$$\eta = \frac{[P_{CO}][P_{H_2}]^3}{[P_{CH_4}][P_{H_2O}]} * \frac{1}{K_{eq}}$$

In this expression, $[P_j]$ is the average partial pressure of species j (in atm); it is also used to correct for reactant depletion. K_{eq} is the equilibrium constant for CH₄ - H₂O reaction. Forward turnover rates (r_f) are given by:

$$r_f = \frac{r_n}{(1 - \eta)}$$

where r_n is the net CH₄ conversion turnover rate. CH₄ reaction rate increased linearly with increasing CH₄ pressure, but it is not influenced by H₂O pressure. H₂ and CO products added to CH₄ - H₂O reactant mixture influenced net CH₄ conversion rate at 600°C, but forward rates were unaffected, indicating that H₂ and CO affected only the extent to which reforming reactions approach equilibrium, but not the kinetics of CH₄ reforming reaction. Thus, previously reported inhibition of CH₄ reaction rates by products may reflect unrecognized contributions from reverse reaction rates. CO adsorption enthalpies are 135kJ* mol^{-1} at low coverage (<0.02) and much lower at higher coverage on Ni (100). These adsorption enthalpies indicate that CO coverage should be well below 0.01 monolayer at 600°C and even at equilibrium CH₄ conversions. The lower adsorption enthalpies typically reported for H₂ (92 kJ* mol^{-1}) would make hydrogen coverages even lower than for CO. Thus, competitive adsorption is unlike to influence the availability of metal sites for CH₄ activation and reported inhibition effects predominately reflect contributions from reverse reactions.

These kinetic responses to reactant and product concentrations are consistent with determining CH₄ activation steps on surfaces, essentially free of reactive intermediates or co-

adsorbed products. CH₄-derived chemisorbed intermediates appear to be readily removed via reactions with H₂O co-reactant; as a result, the identity and concentration of co-reactant become kinetically irrelevant and forward rate data for the steam reforming reaction is accurately described by:

$$r_f = kP_{CH_4}$$

Catalytic reaction of CH₄ with H₂O to form H₂-CO mixtures on Ni depends only on the rate of the initial activation of C—H bonds, catalyzed by surface Ni atoms. Co-reactant activation is easy and CH₄-derived intermediates, including reactive chemisorbed carbon, are kept well below monolayer coverages by their rapid reactions with intermediates derived from H₂O.

Isotopic tracing and exchange measurements confirmed the mechanism proposed based on measured kinetic effects of reactant and product concentrations of forward reaction rates.

Methane decomposes to chemisorbed carbon (C*) via sequential elementary H-abstraction steps, which become faster as H atoms are sequentially abstracted from CH₄ reactants. Density-functional theory led to an activation energy of 142kJ*mol⁻¹ for the first H-abstraction step in CH₄ on Ni clusters, which decreased to 25-40kJ*mol⁻¹ for CH₂ formation from CH₃. This cascade process leads to low CH* coverages and to C* as the most abundant carbon-containing reactive intermediate. Chemisorbed carbon is then removed using CO₂ or H₂O as co-reactants (Figure 10). These elementary steps are consistent also with kinetic and isotopic measurement on Ru, Pt, Ir and Rh catalysts. When exposed metal atoms (*) are the most abundant surface species, only the rate constant for the activation of the first C—H bond in CH₄ appears in the rate expression and reaction rates become first order in CH₄ and independent of the presence or concentration of H₂O or CO₂ co-reactants. Wei and Iglesia noted that these elementary steps provide pathways for reactions of CH₄ with either H₂O or CO₂ and also for water gas shift reaction which have been typically, but inappropriately and non-rigorously, treated as independent kinetic process during CH₄ reforming [29,30]

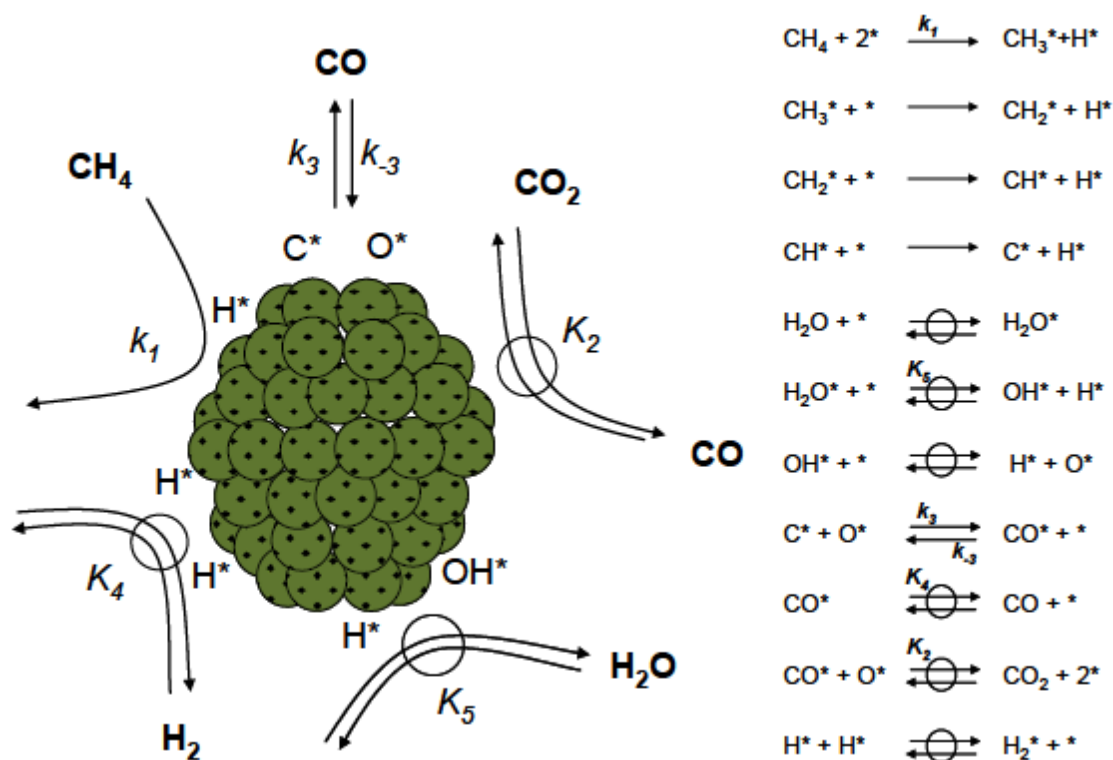


Figure 10. Sequence of elementary steps for CH₄ reforming and WGS reactions on Ni based catalysts. (→ irreversible step, \rightleftharpoons quasi-equilibrated step, \rightleftharpoons reversible step, k_i is the rate coefficient and K_i is the equilibrium constant for a given step i) [29].

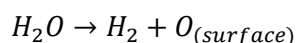
The mechanism of steam reforming of higher hydrocarbons is more complex than that of methane, since break of carbon-carbon bond is necessary to produce single carbon surface species. The order with respect to higher hydrocarbon in most published work is zero over nickel or rhodium catalysts, reflecting the ease of fragmentation of higher hydrocarbons and a consequent high surface coverage. The order with respect to water ranges from zero to one.

Microkinetic model assisted catalyst design seems to be a powerful tool for catalyst development and can be used to study methods for decreasing the carbon formation. Model simulations indicate that the use of Ni alloys and alkali promoters reduce the potential of carbon formation, but it also reduces the activity of methane reforming. Co, Pd, Pt, Ag and Au are candidates as dopants for Ni catalysts to form surface alloys [31].

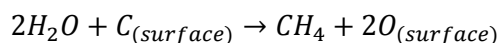
Decomposition of methane on nickel surface is believed the first step of the steam reforming of methane; then the carbon species formed on the surface react subsequently with steam or surface oxygen species. To follow the reaction steps, Matsumura and Nakamori [32] separately fed methane and steam to the catalysts at 500°C and analyzed the mechanism at the initial stage of the reaction in which surface-active species participate.

The rate of the reaction of methane in absence of steam is significantly lower than that of the steady steam reforming, suggesting that the presence of steam which can oxidize the surface of Ni accelerates the decomposition of methane to hydrogen [32]. The formation rate of hydrogen is high at the initial stage of the reaction with methane on Ni/SiO₂ and Ni/Al₂O₃ catalysts, and formation of carbon oxides, which evidences presence of surface oxygen species, is accompanied. Carbon monoxide is selectively formed in the reaction with methane over the catalyst containing NiO. Hence, the reduction of nickel oxide results in formation of carbon monoxide.

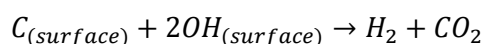
Formation of hydroxyl group on the surface of nickel (Ni-OH) is hypothesized in the reduction process of NiO particles. It is also supposed that the hydroxyl group is more reactive to methane and/or carbon monoxide than the lattice oxygen of nickel oxide. Accumulation of oxygen on the surface of these catalysts can be detected at the initial stage of the reaction with steam after methane decomposition. In this process, reaction of:



and



are also probable. However, the contribution will be small because formation of carbon monoxide, which is produced in presence of nickel oxide is small in the reaction with methane after the contact with steam. Since the formation rates of hydrogen and carbon dioxide increases gradually in the reaction with steam, carbon dioxide cannot be formed in the direct reaction between steam and surface carbon, but probably formed by the reaction with surface hydroxyl groups whose concentration should be saturated under the continuous feed of steam. That is:

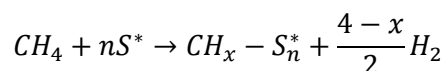


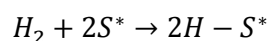
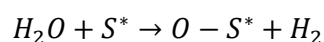
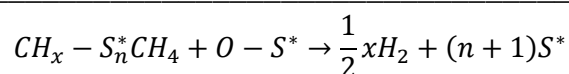
will take place on the surface. Little methane is formed after the formation rate of carbon dioxide is saturated, implying that the surface is mostly oxidized, because formation of methane does not proceed in absence of metallic nickel which accepts the oxygen in steam. After the feed of steam, following the reaction with methane, formation of carbon dioxide



can be observed with re-feed of methane, suggesting formation of surface hydroxyl groups during the previous reaction with steam.

Mechanism of methane steam reforming at low temperature can be schematized as:





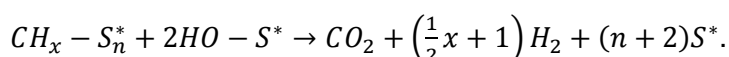
In the mechanism, where S^* represents an active site, the presence of oxide causes formation of carbon monoxide and the process is similar to:



in the reaction solely with the methane.

No reaction was observed at the initial stage of the methane decomposition over 20 % Ni/ZrO₂ without reduction, suggesting that methane does not reduce nickel oxide. Just after the induction period, CH_x is probably formed on the partially reduced surface and this leads to the formation of carbon monoxide and hydrogen which also reduces the surface. Thus, formation of CO in the steam reforming at 500°C will be caused from surface NiO species.

Since formation of carbon dioxide takes place in the presence of surface hydroxyl groups



may proceed on the surface in the steam reforming. Formation of hydroxyl groups on the surface should be an important step also in the steam reforming at 500°C. In the case of Ni/ZrO₂, accumulation of water on the support assists formation of the hydroxyl groups, and this is probably the reason why zirconia is an effective support of nickel in the steam reforming at 500°C. Formation of carbon dioxide from carbon monoxide by water–gas shift reaction is possible in the reaction mechanism, but no relationship between production of carbon monoxide and carbon dioxide can be found in the reactions solely with methane or steam [25].

1.2.2 Steam reforming catalysts

The catalyst must promote the desired reaction and be as inactive as possible towards unwanted side-reactions, particularly to the formation of carbon. The catalyst should also be as resistant as possible to poisons [25].

The catalyst must be able to maintain its activity under the demanding process conditions, necessary to promote the desired reaction (800-1000°C and 20-30bar). With impregnated catalysts, an important parameter in maintaining activity over prolonged periods is the nature of the support material and its pore structure [25].

The catalyst must be strong enough to withstand the handling it receives; from manufacture to charging into the reformer, as well as the stresses generated by the process conditions and the thermal cycles arising from plant start-up and shutdown. The catalyst also must be of a suitable physical shape to provide an appropriate geometric surface area to give an acceptable activity per unit volume of packed bed whilst possessing acceptably low-pressure drop characteristics. The support must not be affected by water condensing on it, nor must it produce an unacceptable quantity of dust and material carryover, which could foul heat exchangers and other catalysts downstream [25].

For many years nickel has been recognized as the most suitable metal for steam reforming of hydrocarbons, other metals can be used; for example cobalt platinum, palladium, iridium, ruthenium and rhodium. Although some precious metals are considerably more active per unit weight than nickel, nickel is much cheaper and sufficiently active to enable suitable catalysts to be produced economically.

The reforming reaction takes place on the nickel surface, so the catalyst must be manufactured in a form that produces the maximum stable nickel surface area available to reactants. This is generally done by dispersing the nickel as small crystallites on a refractory support, which must be sufficiently porous to allow access by the gas to the nickel surface.

This is usually achieved by precipitating nickel as insoluble compound, from a soluble salt, in the presence of a refractory support such as mixtures of aluminum oxide, magnesium oxide, calcium oxide and calcium aluminate cement. Alternatively, the nickel can be incorporated by impregnating a preformed catalyst support, such as alumina or an aluminate, with a solution of a nickel salt which is subsequently decomposed by heating to the oxide.

In either case, the nickel oxide is reduced to the metal by hydrogen supplied from another plant, or by cracking a suitable reactant gas (e.g. ammonia) over the catalyst as the reformer is being started up. In some instances process gas itself is used to reduce the nickel oxide to metal as the reformer is gradually brought on line.

Impregnated catalysts are generally stronger than precipitated catalysts, and this is one of the reasons for their widespread use.

The activity of a steam reforming catalyst in service is closely related to the available surface area of the nickel metal and the access the reactants have to it. Most commercial natural gas catalysts are now of the impregnated type and give a relatively high surface area when first reduced, but under normal reforming conditions the surface area falls as sintering of nickel crystallites occurs. The higher the temperature is, the more rapidly the sintering proceeds.

Activity is a function of the overall nickel content. However, it has been demonstrated that with both impregnated and precipitated catalyst there is an optimum beyond which an increase in nickel content does not produce any further significant increase in activity. Typically, these optima are approximately 20% for precipitated and up about 15% for impregnated catalyst, but this depends on the nature and physical properties of the actual support.

Steam reforming catalysts differ in the ease with which they reduce, and the extent of reduction is influenced by the chemical nature of the catalyst support, the reduction temperature and time, and the composition of the reducing gas. The highest initial nickel surface area is obtained when the reduction is done using pure hydrogen (rather than steam and hydrogen) and when the reduction temperature is ~600°C. Below this temperature, reduction can be slow and incomplete. Above 600°C, some sintering may take place, which lowers the nickel surface area.

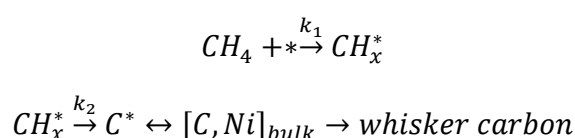
When steam is present, the surface areas can result lower, because sintering is enhanced, and this process proceeds further to give even lower surface areas if excessive reduction periods are employed. Nevertheless, for some catalyst, particularly precipitated catalysts for naphtha reforming, reduction periods up to twenty-four hours are recommended.

In order to optimize the development of superior catalysts, it is essential to understand the catalyst surface at the molecular level. Choudhary and Goodman [33] summarize the studies related to methane activation on Ni catalyst. The interaction of methane with Ni surfaces is of considerable importance because steam reforming of methane is carried out on nickel catalysts.

The dissociation of methane is considered to be the rate-limiting step in SMR. This has led to a great interest in investigating the fundamental sticking process of methane on nickel single crystals. Ni single crystal studies have shown methane dissociation to be structure sensitive [33].

At a given temperature and for a given hydrocarbon feed carbon will be formed below a critical S/C ratio [34]. This critical S/C ratio increases with temperature. By promotion of the catalyst, it is possible to push this limit towards the thermodynamic limit reflecting the principle of the equilibrated gas: "Carbon formation is to be expected on nickel catalysts if the gas shows affinity for carbon after the establishment of the methane reforming and the shift equilibria".

By use of noble metals or sulphur passivation, it is possible to push the limit at lower values. A safe design criterion is to require that the actual gas shows no affinity for carbon formation. Whether carbon free operation is possible depends on the kinetic balance as illustrated in the simplified two-step mechanism:





where * represents nickel site disregarding the ensemble size [25].

For a nickel catalyst, carbon is normally formed by the whisker mechanism. Adsorbed carbon atoms that do not react to gaseous molecules are dissolved in the nickel crystal and carbon whiskers nucleate from the nickel support interface of the crystal. Carbon formation is avoided when the concentration of carbon dissolved in the nickel crystal is smaller than that at equilibrium, in other words, when the steady state activity of carbon is smaller than one. The steady state activity is proportional with $[C^*]$ which can be expressed by:

$$a_c^5 \sim [C^*] \sim \frac{k_1 k_2}{k_3 k_4} * \frac{1}{[OH_y^*]^2}$$

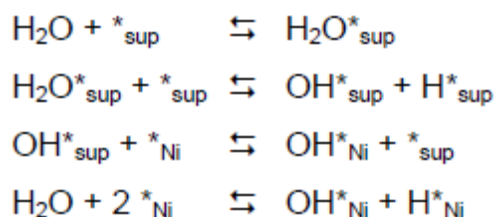
Hence, the steady state carbon activity can be decreased by:

- Enhancing the adsorption of steam or CO₂
- Enhancing the rate of the surface reaction
- Decreasing the rate and degree of methane activation and dissociation.

The whisker mechanism may also be blocked by use of noble metal catalysts because these metals do not dissolve carbon.

Kinetic studies indicated that the adsorption of steam was enhanced by active magnesia and alkali and that spill-over of adsorbed steam to the metal surface may play a role. This was reflected by negative reaction orders with respect to steam.

The improved adsorption of steam on magnesia supports, resulting in improved resistance to carbon formation, is not a static but a dynamic effect. Enhanced steam adsorption cannot reflect a true equilibrium constant. This would violate the principle of microscopic reversibility, because steam is also adsorbed directly on the nickel surface.



The above means that the spill-over of steam probably involves OH species instead of molecular water [25].

Apart from the enhanced steam adsorption on alkali promoted catalyst, it is well known that the addition of alkali to steam reforming catalysts results in a decrease of the reforming rate sometimes by more than one order of magnitude. The effect has been observed on a number of different group VIII metals and on a variety of supports. The decrease in reaction rate is due to lower pre-exponential factors whereas the activation energies are almost unchanged. In contrast, the enhancement of steam activation on magnesia-based catalyst has no impact on pre-exponential factor. It is remarkable that the decline in activity when promoting with alkali is also observed when testing the catalyst for hydrogenolysis of ethane, i.e. without the presence of steam.

The impact of alkali is stronger on less acidic supports, which suggest that the alkali partial pressure over the catalyst is important. A less acidic support has a weaker bounding of alkali resulting in easier transport (via the gas phase) from the support to the metal. This effect of alkali on the activity of nickel is not fully understood [25].

The influence of alkali on the chemisorption of a number of different molecules on transition metal surfaces has been explained as the result of electrostatic interaction. It was found that, above a critical alkali coverage, the adsorbed H_2O is dissociated into OH and H. The maximum OH coverage is equal to the alkali coverage. Both adsorbed H_2O and OH are strongly stabilized by the presence of alkali [25].

A direct blockage of surface nickel atoms, with resulting ensemble control, was observed over partly sulphur poisoned nickel catalysts. By controlling the sulphur content in the feed, it is possible to establish a situation on the nickel surface with ensembles available for the dissociation of methane, but not for the dissolution of carbon atoms into the nickel crystal and nucleation of the whisker carbon. This way of obtaining carbon free operation was brought into practice in the SPARG process. Carbon formation on noble metals is probably prevented because carbon is not dissolved in these metals, thus preventing the diffusion of carbon through the metal to form whisker carbon. Palladium is the only noble metal that still forms carbon, probably because of the formation of a carbide [25].

Takehira et al [35,36,37,38] proposed a solid phase crystallization (spc) method for the preparation of well-dispersed and stable metal supported catalyst, starting from perovskite compounds (PVK) and hydrotalcite-like compounds (HTlc) as the precursors. Starting from Mg–Al hydrotalcite precursors containing Ni at the Mg sites, spc-Ni/MgAl catalysts have been prepared and were successfully applied in the partial oxidation, the steam reforming, and the CO_2 reforming of CH_4 .

There has been for the past decade an increased interest in the preparation of mixed oxide catalysts using hydrotalcite-like compounds as precursors for various reactions. Recently it was reported that spc-Ni/MgAl catalyst showed high and stable activity for both steam reforming and autothermal reforming of CH₄. Such characteristics are equal to the ability of 1wt.% Rh/MgO, reported as the best catalyst. In spite of such good catalytic performance due to stable and highly dispersed Ni metal particles, spc-Ni/MgAl catalysts have a drawback. Active Ni species distribute uniformly from the surface skin to the core of catalyst particles, since the catalysts was prepared by heating Mg(Ni)-Al hydrotalcite to form Mg(Al)-Ni-O solid solutions, followed by the reduction of Ni(II) included in the structure. As a result, a considerable amount of Ni included in the catalyst bulk becomes irreducible and therefore ineffective for catalysis. The preparation of metal-loaded catalysts in egg shell-type will be anticipated, since active metal species are concentrated in the surface layer of the catalyst particles where gas-phase reactions preferentially proceed in the micro- or meso-porous space [37].

Hydrotalcite is an anionic clay, layered mixed hydroxide containing exchangeable anions and affords the mixed oxide by heating; it shows an interesting property, i.e., a “memory effect”. This “memory effect” allows the reconstitution of the original hydrotalcite structure under mild conditions when the product of the thermal treatment is brought into contact with aqueous solutions containing anions. By adopting this “memory effect” on the surface of Mg-Al mixed oxide particle after thermal treatment, Takehira and coworkers [37] have prepared egg shell-type Ni-loaded catalysts. When the Mg-Al mixed oxide particles were dipped in aqueous solution of Ni(II) nitrate, Mg-Al hydrotalcite was reconstituted on the surface of particles and Ni(II) substituted for the Mg(II) sites. After the calcination followed by the reduction of the particles, active spc-Ni/MgAl phase was formed in the surface layer of the particle, resulting in the formation of egg shell-type Ni-loaded catalyst as s-spc-Ni/MgAl (surface spc). The egg shell-type loading was substantially affected by the heating rate and the calcinations temperature of Mg-Al hydrotalcite to the mixed oxide and by the dipping conditions, i.e., pH of aqueous solution of Ni(II) nitrate and the dipping time.

Surface-solid phase crystallization (s-spc) Ni/MgAl catalyst was prepared by adopting the “memory effect”, i.e., reconstitution of Mg-Al hydrotalcite from Mg-Al mixed oxide and spc-method was just applied in the surface layer of the mixed oxide particle. Mg-Al (3/1) mixed oxide particles were prepared as the catalyst supports starting from Mg-Al (3/1) hydrotalcite, [Mg₆Al₂(OH)₁₆CO₃•4H₂O], and were dipped in an aqueous solution of Ni(II) nitrate. Upon dipping, reconstitution of Mg-Al hydrotalcite took place in the surface layer and a part of the Mg(II) sites were replaced by Ni(II). After the calcination, followed by the reduction, s-spc-Ni/MgAl catalysts were obtained and showed high activity due to surface enrichment of highly dispersed Ni metal particles. Egg shell-type Ni-loaded catalysts showed a high and stable activity in the steam

reforming of CH₄. It was concluded that the high activity is mainly due to the enrichment of stable and highly dispersed Ni metal particles in the surface layer of the catalyst particles [37].

Catalysts were prepared from hydrotalcite precursors, characterized and tested in the reaction of methane steam reforming to produce hydrogen also by Fonseca and Assaf [39]. The precursors were synthesized by the traditional technique, with co-precipitation of Ni, Mg and Al nitrates with carbonate; co-precipitation of Mg and Al nitrates with pre-synthesized nickel chelate and anion-exchange of (NO₃)⁻ of hydrotalcite with nickel chelate. The catalytic tests demonstrated high methane conversion, high activity for hydrogen production and high stability during the time of reaction for a molar ratio in the feed H₂O:CH₄ = 2:1. The low quantity of carbon formed on the catalysts surface confirmed the hypothesis that the structure of hydrotalcite layers leads to a homogeneous distribution of the active phase. Comparing the different methods of preparation, it was shown that the precursors obtained by means of Ni chelates were the most active in converting methane, with a high hydrogen yield, probably because they provided the best distribution of the active phase [39].

Strutzenegger and coworkers [40] have tested nickel iron oxide (NiFe₂O₄) as a combined catalyst precursor and oxygen transfer material for improved conversion of methane into syngas.

Alloying Fe₃O₄ with NiO to a spinel-type nickel iron oxide turned out to be a promising path for adding catalytic functionality to the native iron oxide. The reaction of the ternary metal oxide with humidified CH₄ comprises two characteristic phases. During the early phase, oxidation of methane by lattice oxygen is the prevailing reaction. This leads to a two-phase mixture consisting of a nickel-deprived spinel phase and a Ni-rich alloy. As the amount of the Ni-rich alloy increases, catalyzed steam reforming of CH₄ becomes increasingly important. Once all Ni is deprived from the spinel phase, the bulk reaction terminates and steam reforming of methane is the only reaction.

The reduction of the bed material is reversed by exposure to steam. Though this reaction is slower than that with pure or diluted O₂, it is advantageous because it produces H₂ rather than heat. The reaction with steam is also a key step in catalyst regeneration. First, oxidation and re-integration of Ni drives off many prominent catalyst poisons, specifically sulfur, as thermodynamics predicts conversion of nickel sulfides into nickel iron oxides at high water vapor pressure. Recycling of the parent spinel phase has thus a similar purification effect as re-crystallization and minimizes the accumulation of undesired elements in the fixed bed. Second, each recovery of the parent spinel phase re-disperses the nickel on an atomic scale, allowing for a repeated formation of fresh Ni-alloy particles under conditions similar to those during the first reduction. The benefit of re-dispersion was also emphasized by Provendier et al. [41] while

discussing regeneration of Ni/LaFeO₃/La₂O₃ to the parent perovskite-type LaNi_{1-x}Fe_xO₃ by calcination in air.

The design of a steam reforming catalyst support must reflect the need for it to be robust at high temperature and pressure. It must also be suitable for the dispersion of nickel crystallites and allow access of the reacting species, but it must not interfere with their activity. If possible, it should promote or at least sustain the activity of the nickel, but it must not catalyze side-reactions, particularly those which produce carbon deposits. Good physical properties can be obtained by using a simple γ -alumina that is calcined at 1500°C.

A particularly useful range of catalysts are produced from a support which is derived from a mixture of alumina and hydraulic cement that is processed to a porous calcium aluminate. This support is less acidic than α -alumina, and is therefore less susceptible to carbon formation initiated by hydrocarbon-cracking reactions.

Spinel is a ternary oxide with a chemical formula of AB₂O₄, where A is a divalent metallic cation in a tetrahedral site and B is a trivalent metallic cation in an octahedral site of the cubic structure [42]. Magnesium aluminate spinel (MgAl₂O₄) has a specific combination of desirable properties such as: high melting point (2135°C), high resistance to chemical attack, good mechanical strength from room temperature to high temperatures, low dielectric constant, excellent optical properties, low thermal expansion and good catalytic properties. Conventionally, the spinel (MgAl₂O₄) is prepared through a reaction in the solid state using MgO and Al₂O₃. In this process, the mixture is calcined at high temperatures such as 1400–1600°C. An effort to synthesize MgAl₂O₄ at lower temperatures has been reached by using chemical synthesis processes, especially chemical co-precipitation and sol–gel processes, where the spinel phase is formed at temperatures around 700°C. The MgAl₂O₄ can be formed at temperatures lower than 675°C by the co-precipitation method involving the dehydration of a solution of metallic ion complexes with tri-ethanolamine. However, these chemical processes have disadvantages over the conventional solid-state reaction. The co-precipitation method has difficulties in pH control because there is solid precipitation and the removal of anions that are in the solids as impurities, changing the final composition. The sol–gel method, which uses a mixture of aluminum and magnesium salts that are submitted to pyrolysis, also has impurities in the solids. Catalysts obtained through nickel impregnation in inorganic supports have been employed in industry to catalyze the steam reforming of hydrocarbons. Due to its resistance to sintering, the magnesium aluminate spinel has been used as a catalyst support for methane reforming. It was observed a high activity and stability of a Ni/MgAl₂O₄ catalyst for dry reforming of methane, which was attributed to the interaction between the active phase Ni and the support, resulting in highly dispersed active Ni

species. This catalyst exhibited higher activity and better stability when compared to Ni/ γ -Al₂O₃ and Ni/MgO- γ -Al₂O₃ catalysts.

The addition of small amounts of Pt (0.09%) to Ni/Al₂O₃ catalyst resulted in a significant increase of its activity in methane reforming with CO₂ and O₂. It was found that the addition of Pt, Pd and Ir (< 0.3%, w/w) in Ni/ γ -Al₂O₃ catalysts (15% Ni, w/w) strongly promoted conversion of methane in an autothermal reforming reaction.

MgAl₂O₄ was synthesized by Foletto and coworkers [42] through hydrolysis of metallic alkoxides of Mg²⁺ and Al³⁺. The formed spinel precursor phase was calcined at temperatures between 600 and 1100°C, for 4h. The spinel was utilized as a Ni/Pt catalyst support. The Ni/MgAl₂O₄ catalysts (15% Ni, w/w) containing small amounts of Pt were tested for methane steam reforming. The spinel phase was formed at temperatures above 700°C. The addition of small amounts of Pt to Ni/MgAl₂O₄ promoted an increase in surface area. This noble metal promoted an increase in the surface area. This probably caused the considerable increase in methane conversion [42].

Nickel is increasingly studied for the methane-reforming catalysis with various oxides, either classical (Al₂O₃, SiO₂, MgO, TiO₂) or less conventional ones (ThO₂, CeO₂, ZrO₂, Cr₂O₃, Nb₂O₅) [43]. It appears that, besides the elaboration process, the nature of the interaction between the nickel and the support, in the form of specific phases, plays a determinant role for the catalytic properties. For example, the formation of phases, such as nickel aluminate spinel, NiAl₂O₄, on alumina leads after reduction to highly dispersed catalysts with a high selectivity and a great resistance against sintering and poisoning. However, these phases are only partially reduced by conventional methods (hydrogen reduction at high temperature) and their activity is drastically low. Nevertheless, even though the role of the tight interaction support metal is widely studied, it is still subject to discussion and yet far from being well understood. The catalyst properties may be due to a combination of intrinsic size effects and support effects [43].

As an alternative way, irradiation has been proven to be a powerful tool to reduce metal ions into highly dispersed and size-controlled metal clusters. Actually, the specific properties, distinct from the bulk, of 'quasi-atomic' metal were demonstrated for the first time for nascent metal produced by irradiation. The aggregates of a few atoms only were much easily oxidized than the bulk metal. These new specific properties could explain why nanosized metal clusters are difficult to stabilize but they could induce higher activity. The radiation-induced reduction of metal ions into atoms is achieved by solvated electrons generated from the solvent and by electrons generated from the support, both having the strongest reducing power. Therefore, all ions, including non-noble metals, are reducible by electrons. Due to the radiation penetration, the reducing species are produced - without any chemical additive. In addition, the reduction is carried out at room

temperature, which is favorable to prevent sintering. The radiolytic process has been extensively used to synthesize noble metals as nanocolloids or supported clusters. Using the radiolytic technique in both regimes (steady-state and pulsed radiolysis), it was improved the understanding of the primary steps of the formation of mono- and multi-metal aggregates and the nucleation–coalescence processes. This has permitted to obtain clusters of controlled size and structure (alloyed or core shell) [43].

Non-noble metal clusters are still more difficult to synthesize at very small sizes, since their fragility to oxidation still exists up to high nuclearities. The atoms and the primary oligomers are highly oxidable and can be corroded as soon as they are produced. However, using appropriate conditions, nickel and other metal nanocolloids were produced by radiation-induced reduction. Irradiation has also been used in some cases as a complementary treatment of Ni-alumina samples, before or after the classical reduction by hydrogen gas, in view of creating defects in the support and improving the catalytic properties of the solids [43]. A series of Ni aggregates supported on α -Al₂O₃ at different nickel contents are prepared by ionic exchange of Ni²⁺ followed by γ -irradiation under inert atmosphere. The radiation-induced reduction of Ni ions and the synthesis of Ni clusters, under wet conditions already known for nanocolloids, was successfully adapted to the elaboration of Ni particles supported on α -alumina. When used as catalysts for the steam-reforming methane reaction to produce synthesis gas, they act with a remarkable high selectivity in CO (80%), even at low temperature (550°C). The reasons are probably due to combination of the influence of the radiation on both the metal and the support, particularly on the interface [43].

The presence of silica would further increase the already adequate strength of the support, but as silica is volatile in the presence of steam at high temperatures only very small quantities can be used, except in naphtha steam reforming catalysts when it is combined with potassium which significantly reduces its partial pressure under reforming conditions.

Magnesia can also be included in some formulations, but has to be used with caution and understanding, however, as under certain conditions, it can hydrate and markedly weaken the catalyst. During start-up or shutdown in the presence of reaction steam only, hydration of the magnesia can take place below 425°C and, since the molar volume of Mg(OH)₂ is almost twice that of MgO, a dramatic weakening of the support may result unless the MgO is formulated in such a way that is chemically associated with other refractory oxides. If this is not done reformer start-ups and shutdowns must ensure that, the catalyst is in a dry atmosphere whilst temperatures are below the critical hydration temperatures [25]. Effects of supports such as silica, γ -alumina, and zirconia for nickel catalysts have been studied in steam reforming of

methane at 500°C [32]. The activity of the nickel supported on silica reduced with hydrogen at 500°C decreases with oxidation of nickel particles by steam during the reaction. Nickel supported on ψ -alumina is not much reduced with hydrogen at 500°C and is inactive in the reforming at 500°C. However, the catalyst reduced at 700°C is fairly active while nickel is partially oxidized during the reaction. Nickel supported on zirconia is the most effective in the steam reforming at 500°C [25].

Fujimoto and coworkers [44] studied a Ni-Mg-O solid solution with low Ni content ($\text{Ni}_{0.03}\text{Mg}_{0.97}\text{O}$, atomic ratio) which was reduced at high temperature ($> 800^\circ\text{C}$) and was found to be an active and stable catalyst for the steam reforming of methane in a S/C ratio of 1.0. The reduced $\text{Ni}_{0.03}\text{Mg}_{0.97}\text{O}$ catalyst showed higher activity and much higher stability than a commercial reforming catalyst ($\text{Ni}/\text{Al}_2\text{O}_3\text{-MgO}$). The catalyst kept its activity for 60h or more at 900°C and a steam to carbon ratio of 1.0, giving little coke on the catalyst ($<1\text{wt } \%$), whereas the commercial steam reforming catalyst lost its activity at 20h because of severe coking under the same reaction conditions. For both $\text{Ni}_{0.03}\text{Mg}_{0.97}\text{O}$ and $\text{Ni}/\text{Al}_2\text{O}_3\text{-MgO}$, the rate equations were similar. Thus, it was suggested that the suppressed coke formation of the $\text{Ni}_{0.03}\text{Mg}_{0.97}\text{O}$ catalyst is caused by the very small nickel particles and the difference in the composition of surface carbonaceous species on the Ni metal particles as the reaction intermediate.

$\text{Ni}_{0.03}\text{Mg}_{0.97}\text{O}$ solid solution catalyst has high resistance to carbon deposition in steam and dry reforming of methane, but the deactivation due to oxidation of active nickel species was observed under some reaction conditions. This deactivation was avoidable by the addition of hydrogen to reactant gas. On $\text{Ni}_{0.03}\text{Mg}_{0.97}\text{O}$ catalyst, nickel particles were much more dispersed than that on 3mol% Ni/MgO and CO_2 was adsorbed on $\text{Ni}_{0.03}\text{Mg}_{0.97}\text{O}$ similarly to MgO. In addition, CO_2 was activated on $\text{Ni}_{0.03}\text{Mg}_{0.97}\text{O}$ at 60°C lower temperature than on 3mol% Ni/MgO. This is suggested to be promoted by large interface between metal and support, and strong interaction of CO_2 with support surface. Combined with the results of reaction order, it is suggested that high resistance to carbon deposition in methane dry reforming is closely related to high ability of CO_2 activation and this causes rapid oxidation of carbon species on nickel before converting to deposited carbon [45].

Reactions used to model the steam reforming of natural gas show that the influence of the support on the performances of the metal is minimal. On the other hand, hydrogen produced during the reactions adsorbs on the metal and can spill over to the support. The spilt over hydrogen could be responsible in part for the gasification of carbonaceous residues [46].

In the industrial viewpoint, Al_2O_3 -based supports are preferred because of their easier availability in the reforming processes. Therefore, $\text{Ni}/\text{Al}_2\text{O}_3$ and $\text{Ni}/\text{MgAl}_2\text{O}_4$ have been used as

catalysts for SMR. As an alternative, Ni/ γ -Al₂O₃ could be considered. However, it is unstable at high temperature (>700°C) because of the thermal deterioration of the γ -Al₂O₃ support that causes sintering and leads to pore closing and reduction in surface area as well as phase transformation into α -Al₂O₃ which changes an active surface layer and promotes a low surface area structure. Thus, Jun and coworkers [47,48,49] carefully changed γ -Al₂O₃ into θ -Al₂O₃ and modified θ -Al₂O₃ with CeZrO₂ because Ni/CeZrO₂ exhibited good performance in methane reforming reactions. The catalyst was remarkably deactivated by steam treatment but reversibly regenerated by H₂-reduction. The steam treatment resulted in the formation of NiAl₂O₄, which is inactive for SMR, but it was reversibly converted to Ni by the reduction. The reversible oxidation-reduction of Ni state was evidenced and it was observed that the formation of NiAl₂O₄ is more favorable at higher temperature. It is most likely that the alumina support is only partially covered with CeZrO₂ and most Ni directly interacts with θ -Al₂O₃, which would probably make easy formation of NiAl₂O₄ in the presence of steam alone. The results imply that, during the start-up procedure in SMR, too high concentration of steam could deactivate seriously Al₂O₃ supported Ni catalysts [47].

Xu et al [50] had explored the use of oxide nanoparticles for catalysts founding that the Ni catalyst 'supported' by small nanoparticles of ZrO₂ (7–25nm) or MgO (10–12nm) can be highly active and extremely stable for the steam and the dry methane reforming reactions at 700–800°C. In contrast to conventional oxide-supported metal catalyst having discrete metal nanocrystals (1–20nm) supported on oxide particles that are often one to several orders of magnitude larger than the metal nanocrystals, the stable Ni/ZrO₂ catalysts appear as nanocomposites of comparably sized Ni-metal (10–15nm) and zirconia nanocrystals (7–25nm). Ni catalysts supported on conventional oxide supports are not able to avoid coking and deactivate rapidly under the same conditions. They tested nanocomposite Ni/ZrO₂ catalyst for the SMR reaction with a stoichiometric mixture of steam and methane in a wide range of feed space velocities. The nanocomposite catalyst is claimed to be superior to Ni catalysts supported on bigger particles of conventional oxides (Ni/ZrO₂ and Ni/Al₂O₃) for the SMR reaction [50].

Addition of promoters into the catalysts is the simplest and cheapest way to improve their quality. For example, molybdenum added to nickel catalysts in small amounts (≤ 0.5 wt.%) is a promoter, which significantly increases catalysts resistance to coking in the steam reforming (decreasing coking rate and lengthening induction time). With the addition of such amounts of Mo, loss of catalytic activity was not observed [51]. Effectiveness of promoter depends on the type of hydrocarbon reaction (reforming, hydrogenolysis, cracking), and in the case of steam reforming on the ratios of reactants (H_2O/C_nH_m) and p_{H_2O}/p_{H_2} in the reaction mixture. The

prepared catalyst [51] was Ni–Mo/ γ -Al₂O₃. Heating of the catalysts in the H₂O:H₂ mixtures at the temperature 500–600°C caused important changes in the mean oxidation number of surface Mo atoms. The same treatment at the higher temperature resulted in the bulk changes and the formation of MoO₂ phase. H₂O into gaseous atmosphere affects the oxidation states of Mo and Ni. Concentration of oxygen atoms on the surface of Ni–Mo/Al₂O₃ catalysts after heating in the H₂O:H₂ mixture (so at conditions similar to the steam reforming of hydrocarbons) was higher than that on the nickel catalyst surface. The experiments confirmed surface reactions between water vapor and molybdenum under the conditions of steam reforming of hydrocarbons, which change the oxidation state of promoter atoms due to their oxidation. Hence, it was supposed that in the steam reforming reaction of hydrocarbons the presence of larger number of oxygen atoms on the surface of Ni–Mo catalysts may facilitate gasification of the “CH_x species” and limit their transformation into inactive deposit. It decreases the rate of carbon deposit formation [51].

Nickel catalysts supported on silica–zirconia mixed oxides were prepared [52] by homogeneous precipitation in sol–gel-derived wet silica gel. Their structural properties and catalytic performance in steam-reforming of methane were investigated from the viewpoint of steam resistance. Ni/SiO₂ without zirconia readily loses its catalytic activity during the reaction because the coarsening of silica that occurs in the presence of high-temperature steam hinders the active surface of Ni. The addition of zirconia drastically increases the steam resistance of silica. Ni/SiO₂-ZrO₂ catalyst shows steady activity in steam-reforming of methane without any changes in pore structure [52].

From an industrial point of view, the development of nickel catalysts with greater resistance to coking is thus an attractive research goal [53].

An effective approach to developing such nickel catalysts is to focus on the selection and modification of catalyst supports. It is widely accepted that the addition of alkali, alkali earth oxides and rare earth metal oxides to the α -Al₂O₃ support or the use of basic metal oxides as the support improves resistance to coking. This positive effect is understood to result from the enhancement in steam adsorption, in the oxidation rate of CH_x fragments adsorbed on metallic nickel and/or the reduction of methane activation and dissociation.

Although improvements of the support greatly influence catalytic activity and/or resistance to coking, limited attempts have been made to apply oxygen-ion conducting oxides, for instance CeO₂ and perovskite-type oxides, to the steam reforming catalysts.

It is mechanistically expected that oxidation of CH_x fragments adsorbed on metallic nickel would be promoted by the lattice oxygen in oxygen-ion conducting oxides and that the consumed lattice oxygen would be regenerated by steam. Such a mechanism has specifically been proposed for CO oxidation and dry reforming of methane. Huang and coworkers [54] [55] [56] have evaluated the activity of nickel supported on ceria-based ion-conducting oxides for dry reforming of methane and have pointed out that the lattice oxygen in modified ceria may play some positive roles in the activation of methane and carbon dioxide. Takehira et al. [35] have reported that the perovskite-type oxides such as SrTiO_3 , CaTiO_3 , BaTiO_3 that contain a small amount of nickel in the titanium sites show high catalytic activities with high resistance to coking, due to the high dispersion of nickel. These researchers also examined oxygen mobility in perovskites, and found that the high resistance to coking might be partly due to the migration of mobile oxygen from the perovskite support to the metallic nickel particles.

The catalytic activity and resistance to coking of nickel catalysts supported on a variety of the perovskite-type oxides (LaAlO_3 , LaFeO_3 , SrTiO_3 , BaTiO_3 , $\text{La}_{0.4}\text{Ba}_{0.6}\text{Co}_{0.2}\text{Fe}_{0.8}\text{O}_{3-\delta}$) were compared to those of the conventional $\text{Ni}/\alpha\text{-Al}_2\text{O}_3$ catalyst for steam reforming of methane under the conditions of 800°C , atmospheric pressure and a molar $\text{H}_2\text{O}/\text{CH}_4$ ratio of 2 [53]. To investigate differences in catalytic activity among the Ni/perovskite catalysts examined, the dispersion and reduction properties of nickel and the roles of the lattice oxygen on the catalytic activity and carbon deposition were examined. Ni/LaAlO_3 and Ni/SrTiO_3 showed high catalytic activities among the Ni/perovskites and longer-term stabilities than the conventional catalyst. Temperature programmed oxidation of carbon deposited on used catalysts revealed that inactive carbon species detected on $\text{Ni}/\alpha\text{-Al}_2\text{O}_3$ were not formed in the case of Ni/LaAlO_3 . The results of temperature programmed reduction confirmed that consumption and recovery of the lattice oxygen in perovskites occurred during the reaction, and that the reducibility of perovskites had a great impact on the steam reforming activity. The lattice oxygen in perovskites is considered to play important roles in promoting the oxidation of CH_x fragments adsorbed on metallic nickel.

Both the reducibility and the particle size of nickel were found to be related to catalytic activities. These results suggest that the lattice oxygen in LaAlO_3 and SrTiO_3 accesses CH_x fragments adsorbed on nickel readily due to the large amount of lattice oxygen near the surface of the perovskite, and interfaces between the nickel particles and the support. Thus, Ni/LaAlO_3 and Ni/SrTiO_3 have high catalytic activities. The lattice oxygen in LaAlO_3 and SrTiO_3 , thus plays a positive role in both promoting the oxidation of CH_x fragments adsorbed on metallic nickel and in hindering the production of inactive carbon species [53].

A novel anode $\text{La}_{1-x}\text{Sr}_x\text{Cr}_{1-y}\text{Ni}_y\text{O}_{3-\delta}$ ($x=0.1, 0.2, 0.3, 0.4$ and $y=0.05, 0.1$) for solid oxide fuel cells (SOFCs) operated under methane has been tested regarding its catalytic activity for methane steam reforming and its structure characterized [57]. Powders were synthesized by solid-state reaction. The steam/methane ratio was between 0.5 and 1.

The strontium and nickel-doped lanthanum chromite has been shown to have some catalytic activity for methane steam reforming. The main point was the absence of carbon deposition for a steam/methane ratio equal to 1 or less at 850°C. The highest catalytic activity was obtained with 30mol% of strontium and 5mol% of nickel, synthesized at 1400°C during 4h. This synthesis temperature seems to be necessary in order to obtain a complete solid-state reaction. The maximum in conductivity seemed to be either between 30 and 40mol% of strontium, or slightly above 40mol%. With nickel content higher than 5mol% of nickel, the catalytic activity decreased and some nickel/chromium agglomerations were observed after catalytic tests [57].

Wang et al prepared a series of Rh/MgO- Al_2O_3 catalysts with varying Rh loadings (1, 5 and 10%) and 6wt% MgO by an incipient wetness method. Rh loading was optimized on a stable MgO- Al_2O_3 support to improve the volumetric productivity for methane conversion. Catalyst activities were stable over a wide range of steam/carbon ratios. In particular, experimental results demonstrated that Rh/ MgO- Al_2O_3 catalysts are extremely active for methane steam reforming and are resistant to coke formation at stoichiometric steam/carbon ratio of 1 for over 14h time-on-stream with no sign of deactivation. Methane steam reforming activities on this catalyst were compared in both a micro-channel reactor and a conventional micro-tubular reactor. Significant performance enhancement was observed in micro-channel reactors owing to improved heat and mass transfer [58].

Highly active and coke-resistant Rh catalysts were developed for methane steam reforming in micro-channel chemical reactors [58]. Conventional methane steam reforming processes suffer severe mass and heat transfer limitation, and the effectiveness factors of catalysts are typically less than 5%. Micro-channel reaction technology, which has been developed over the past decade, provides a potential breakthrough solution to the challenge of methane steam reforming processes. Micro-channel reactors have a sandwich-like multi-layer structure consisting of a large number of closely spaced channels with a gap of less than 1mm, which reduces heat and mass transport distance and thus enhancing the overall efficiency. Consequently, micro-channel reactors allow process intensification and unprecedented temperature control. Heat transfer coefficients in micro-channel reactors are as high as 10'000–35'000 $\text{Wm}^{-2}\text{K}^{-1}$ compared to 100–700 $\text{Wm}^{-2}\text{K}^{-1}$ in conventional reactors. Such

high heat transfer coefficients coupled with the high surface-to-volume ratio achievable in micro-channel reactors permit the operation of highly endothermic methane steam reforming at near isothermal conditions and provide the potential to improve significantly the efficiency of methane steam reforming process [58].

The effect of Ru loading added to the Ni-catalyst was investigated [59], it was found that the presence of Ru strongly enhances the catalytic performance of the Ni-based catalyst when increasing Ru loading up to 2wt%. Effect of Ni loading to the Ru-based catalyst system was also investigated. It was found that the addition of nickel to the Ru-based catalyst up to 15wt% enhanced significantly the catalytic activity of the catalyst. The lifetime of the Ru–Ni catalysts in the reforming of m-cresol was tested at 750°C (m-cresol was used as a representative model compound for the coal tar or lignin-derived oils). In agreement with general observations of the use of Ni monometallic catalyst, deactivation of the catalyst due to the carbon deposition reaction already occurred in the reforming of the oxygenated compound. On the other hand, a reasonable high resistant on the carbon deposition in the reforming of m-cresol was given by the 2wt%Ru–15wt% Ni catalyst system. An effort in improving the strength of the catalyst support with this catalyst system was also conducted, and the catalyst showed significant increase in the stability of the reforming of oxygenated aromatic compound [59].

Palladium (Pd) supported on CeO₂-promoted γ -Al₂O₃ with various CeO₂ crystallinities, were used as catalysts in the methane steam reforming reaction [60]. Pd was found present on the oxidized CeO₂-promoted catalysts as Pd⁰, Pd⁺ and Pd²⁺, at ratios strongly dependent on CeO₂ structure. Pd was well dispersed (particles <2nm) on crystalline CeO₂ and was agglomerated as large clusters (particles in 10–20nm range) on amorphous CeO₂. After pre-treatment under H₂ or in the presence of amorphous CeO₂, partial encapsulation of Pd particles occurred. CeO₂ structure influenced the CH₄ steam reforming reaction rates. Crystalline CeO₂ and dispersed Pd favor high reaction rates (low activation energy). The presence of CeO₂ as a promoter conferred high catalytic activity to the alumina-supported Pd catalysts. The catalytic activity was significantly lower on Pd/ γ -Al₂O₃ or on amorphous (reduced) CeO₂/Al₂O₃ catalysts. The reaction rates were found two orders of magnitude higher on Pd/CeO₂/ γ -Al₂O₃ than on Pd/ γ -Al₂O₃, due to a catalytic synergism between Pd and CeO₂. The low rates on the reduced Pd/CeO₂/Al₂O₃ catalysts were correlated with the loss of Pd sites through encapsulation or particle agglomeration, a process found mostly irreversible after catalyst regeneration [60].

CeO₂ has been extensively employed as a textural and structural promoter for supported noble metal catalysts. Its promotion effect was attributed to excellent thermal and mechanical

resistance, propensity to non-stoichiometry and oxygen-storage capacity. Due to its properties, structure and capabilities of storing and releasing oxygen, CeO₂ is an important component in automotive, emission-control (oxidation) catalysts, selective oxidation in fine chemicals synthesis and solid oxide fuel cell applications.

CeO₂ addition to a Ni-supported catalyst was found to decrease carbon deposition and increase the catalyst life and activity. Noble metal based catalysts (Pt, Pd and Rh) deposited on various supports such as Al₂O₃, CeO₂, ZrO₂, or NiO, tested in regular tubular reactors or more recently in membrane design reactors, provided good catalytic activity in methane, propane or n-butane steam reforming reactions. The promoting effect of CeO₂ on Pt, Pd and Rh catalysts was proven for CO oxidation, water gas shift and CH₄ steam reforming. The state of CeO₂ reduction affects the activity of Pt/Ce–Zr oxides in CO oxidation. For various CeO_x stoichiometries corresponding to various degrees of reduction, the activation energy increases as the degree of ceria reduction increases.

1.2.2.1 Carbon Formation on Reforming Catalyst

Coking or the formation of carbonaceous deposits is an important side reaction in many industrial processes. Very often, measures to eliminate or depress coke formation are more decisive for the process layout than, for instance, the activity of the catalyst [61].

Deactivation of supported metal catalysts by carbon or coke formation is a problem of serious magnitude in steam reforming. Its causes are generally threefold:

1. fouling of the metal surface,
2. blockage of catalysts pores and voids,
3. actual physical disintegration of the catalyst support.

Carbon may chemisorb strongly, as a monolayer, or physically adsorb in multi-layers and, in either case, block access of reactants to metal surface sites. Furthermore, carbon may totally encapsulate a metal particle, and thereby completely deactivate that particle, and plug micro- and macropores such that access of reactants is denied to many crystallites inside this pores. Finally, in extreme cases, strong carbon filaments may build-up in pores to the extent that they stress and fracture the support material, ultimately causing disintegration of catalyst pellets and plugging of reactor voids [62].

Since loss of catalytic activity and physical destruction of the catalyst by carbon deposits can occur rapidly (within hours or days) under unfavorable conditions, understanding and control of these effects are of major technological and economical importance [63].

Carbon accumulation can also cause spalling and pulverization of catalysts, which can also lead to poor heat distribution [64].

Carbon is a product of CO disproportionation while coke is produced by decomposition or condensation of hydrocarbon on metals. Nevertheless, coke forms may vary from high molecular weight hydrocarbons such as condensed polyaromatics to carbon such as graphite, depending upon the conditions under which the coke was formed and aged (Figure 11).

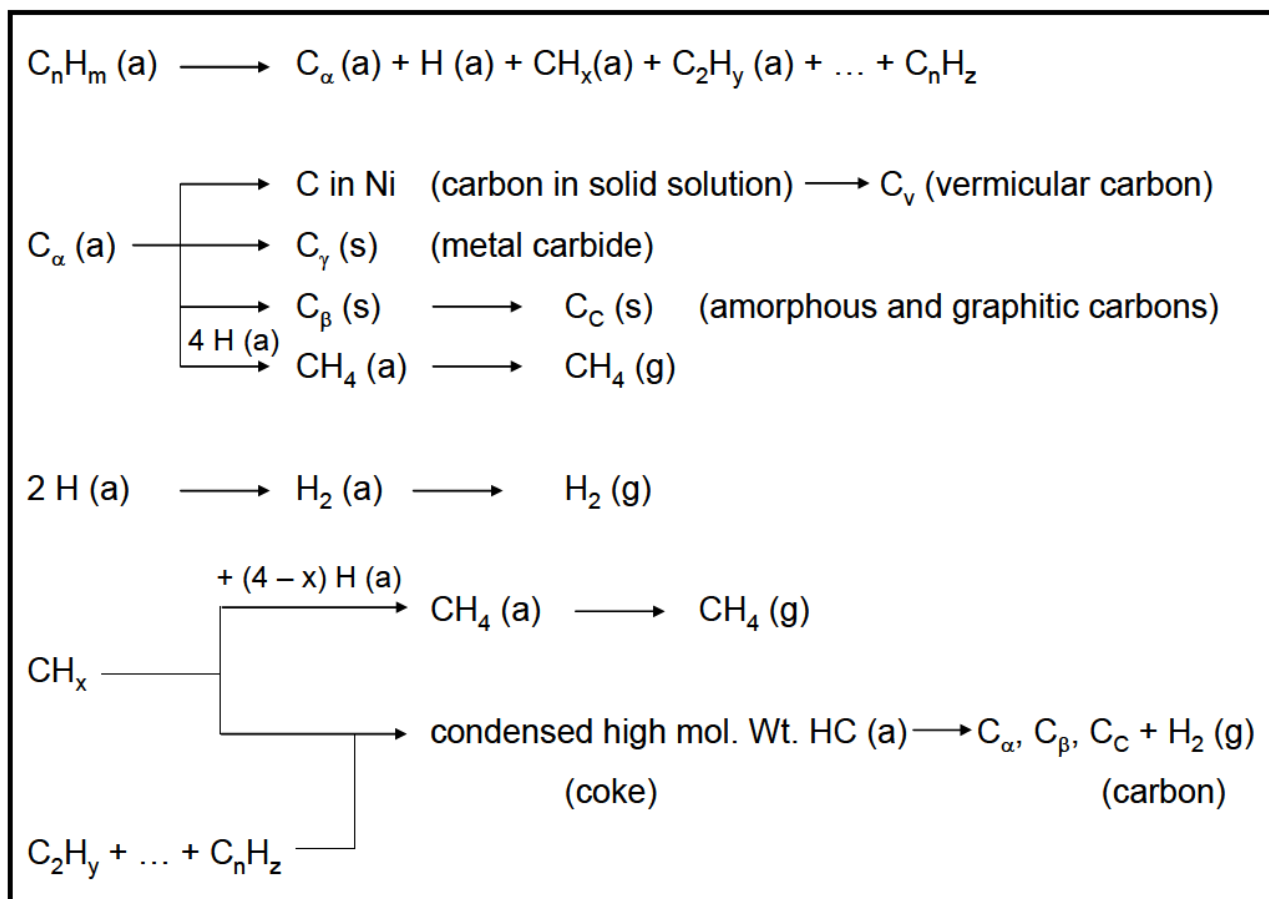


Figure 11. Formation, gasification and transformation of coke and carbons on metal surfaces from hydrocarbons (a= adsorbed, g= gaseous, s= solid).

Three different kinds of carbon or coke species are observed in steam reforming (Table 2):

1. whiskers like carbon formed at temperature greater than 450°C,
2. encapsulating hydrocarbon films formed by polymerization at less than 500°C,
3. pyrolytic carbon from cracking of hydrocarbon above 600°C.

Formation of carbon deposits via CO decomposition (Figure 12) may involve the production and transformation of various carbon forms, adsorbed atomic carbon (C_α), amorphous carbon (C_β), vermicular carbon (C_v), bulk nickel carbide (C_γ) and crystalline, graphitic carbon (C_c), the

structural reactivities of which are summarized in the Table 3. The presence of dispersed or atomic carbon, stable below 325°C, which can be also surface nickel carbide, and polymerized carbon stable above 325°C was confirmed. Nickel carbide can be easily removed by H₂ at the same temperature.

	Whisker like	Encapsulating film	Pyrolytic carbon
Formation	Diffusion of C through Ni crystal, nucleation and whisker growth with Ni crystal at top	Slow polymeraization of C _n H _m radicals on Ni surface into encapsulating film	Thermal cracking of hydrocarbon. Deposition of C precursors on catalyst
Temperature range	> 450°C	< 500°C	> 600°C
Critical parameters	High temperature. Low H ₂ O/C _n H _m No enhanced H ₂ O adsorption Low activity Aromatic feed	Low temperature Low H ₂ O/C _n H _m Low H ₂ /C _n H _m Aromatic feed	High temperature High void fraction Low H ₂ O/C _n H _m High pressure Acidity of catalyst

Table 2. Carbon species formed in steam reforming of hydrocarbons [63].

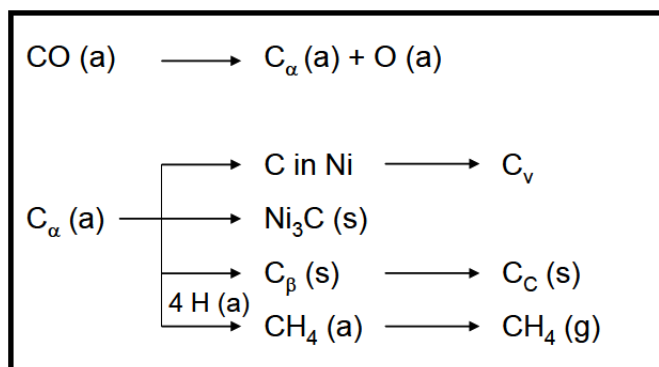


Figure 12. Formation, gasification and transformation of carbon on nickel from carbon monoxide (a= adsorbed, g= gaseous, s= solid).

Structural type	Designation	Temperature formed	Peak temperature for reaction with H ₂
Adsorbed, atomic (dispersed, surface carbide)	C _α	200-400°C	200°C
Polymeric, amorphous films or filaments	C _β	250-500°C	400°C

<i>Vermicular (polymeric, amorphous)</i>			
a. <i>filaments</i>	C _V	300-1000°C	400-600°C
b. <i>fibers</i>			
c. <i>whiskers</i>			
<i>Nickel carbide (bulk)</i>	C _V	150-250°C	275°C
<i>Graphitic (crystalline)</i>			
a. <i>platelets</i>	C _C	500°C	550-850°C
b. <i>films</i>		550°C	

Table 3. Forms and reactivities of carbon species formed by decomposition of CO on nickel [63].

Several studies of carbon deposition on nickel powders, foils and single crystals show direct evidence of low density filamentous (amorphous) and high density, crystalline graphitic forms, such as platelets observed after treatment in carbonizing atmospheres at temperature above 550°C. It should be emphasized that at high temperature amorphous carbon may convert to more graphitic forms in terms of their reactivity and even crystallinity while retaining their overall film or vermicular structure.

Furthermore, some forms of carbon results in loss of catalytic activity and some do not. For example, at low temperature (<300-375°C), condensed polymer or β-carbon films and at high temperature (>650°C) graphitic carbon films encapsulate the metal surfaces of steam reforming catalysts.

Deactivation of steam reforming catalysts at high temperature (500-900°C) may be caused by precipitation of atomic (carbide) carbon dissolved in the Ni surface layers to a depth of more than 50-70nm. If it accumulates on the metal surface, at high or low temperatures, adsorbed atomic carbon can deactivate metal sites for adsorption and/or reaction. For example, carbon atoms residing in the four fold hollow sites of Rh (100) block the adsorption of hydrogen and hence could block sites for hydrogenation [62]. In the intermediate temperature range of 375-650°C, carbon filaments are formed by precipitation of dissolved carbon at the rear side of metal crystallites causing the metal particles to grow away from the support. Filament growth stops when sufficient carbon accumulates on the free surface to cause encapsulation by a carbon layer; however, encapsulation of the metal particles does not occur if H₂/CO or H₂O/hydrocarbon ratios are sufficiently high. Thus, carbon filaments sometimes formed in CO hydrogenation or steam reforming of hydrocarbons would not necessarily cause a loss of intrinsic catalyst activity unless they are formed in sufficient amount to cause plugging of the pores or loss of metal which occurs as the carbon fibers are removed during regeneration. However in practice, region of carbon forming potential in steam reforming must be carefully avoided, since once initiated, the rate of filamentous carbon formation are

sufficiently high to cause catastrophic pore plugging and catalyst failure within a few hours to days.

The rate at which deactivation occurs for a given catalyst and reaction depends greatly on reaction conditions, especially temperature and reactant composition. A fundamental principle for coke insensitive reactions on metals (in which relatively reactive coke precursors formed on active sites are readily removed by hydrogen or other gasifying agents) is that deactivation rate depends greatly on the difference in rate of formation and gasification of carbon/coke precursors:

$$r_d = r_f - r_g$$

If the rate of gasification, r_g , is equal to or greater than that of formation, r_f , carbon/coke is not deposited. Rates of carbon/coke precursor formation and gasification both increase exponentially with temperature, although the difference between them varies a great deal with temperature because of differences in pre-exponential factors and activation energies. Thus, carbon/coke formation is avoided in region of temperature in which precursor gasification rate exceeds deposition rate. Since at temperature below 320°C ($1/T > 1.66 \times 10^{-3} \text{K}^{-1}$) the rate of C_α gasification exceeds that of C_α formation, no carbon is deposited. However, above 320°C, C_α accumulates on the surface since the rate of C_α formation exceeds that of C_α gasification. As C_α accumulates (at 320-520°C), it is converted to a C_β polymeric chain or film which deactivates the nickel catalyst; however, above 520°C ($1/T < 1.43 \times 10^{-3} \text{K}^{-1}$) the rate of C_β hydrogenation exceeds that of formation and no deactivation occurs.

In steam reforming, filamentous carbon formation rate is strong function of hydrocarbon structure; for example, it decreases in the order acetylenes, olefins, paraffins, i.e. in order of decreasing reactivity, although activation energies for nickel are in the same range independent of hydrocarbon structure and about the same as those observed for formation of filamentous carbon from decomposition of CO. This latter observation suggests that the reaction of CO and different hydrocarbons to filamentous carbon proceed by a common mechanism and rate-determining step, probably the diffusion of carbon through the metal crystallites [62].

The rate at which carbon or coke is accumulated in a given reaction under given conditions can vary significantly with catalyst structure, including metal type, metal crystallite size, promoter, and catalyst support. For example, Co, Fe and Ni are active above 350-400°C for filamentous carbon formation from CO and hydrocarbons. Pt, Ru and Rh catalysts, on the other hand, while equally or more active than Ni, Co, or Fe in steam reforming produce little or

no coke or carbon. This is attributed to reduced mobility and/or solubility of carbon in the noble metals, thus retarding the nucleation process. Thus, it is not surprising that addition of noble metals to base metals retards carbon formation; for example, addition of Pt in Ni lowers carbon deposition rate during methanation, while addition of Cu to Ni substantially lowers carbon formation in steam reforming.

Since carbon formation and gasification rates are influenced differently by modifications in metal crystallite surface chemistry, which are in turn a function of catalyst structure, oxide additive or oxide supports may be used to moderate the rate of undesirable carbon or coke accumulation [62].

The high temperatures associated with steam reforming favor the formation of carbon [65]. Four reactions may be involved:

Thermal cracking or decomposition of methane:



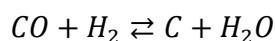
Thermal cracking or decomposition of hydrocarbons:



CO disproportionation (Boudouard):



CO reduction:



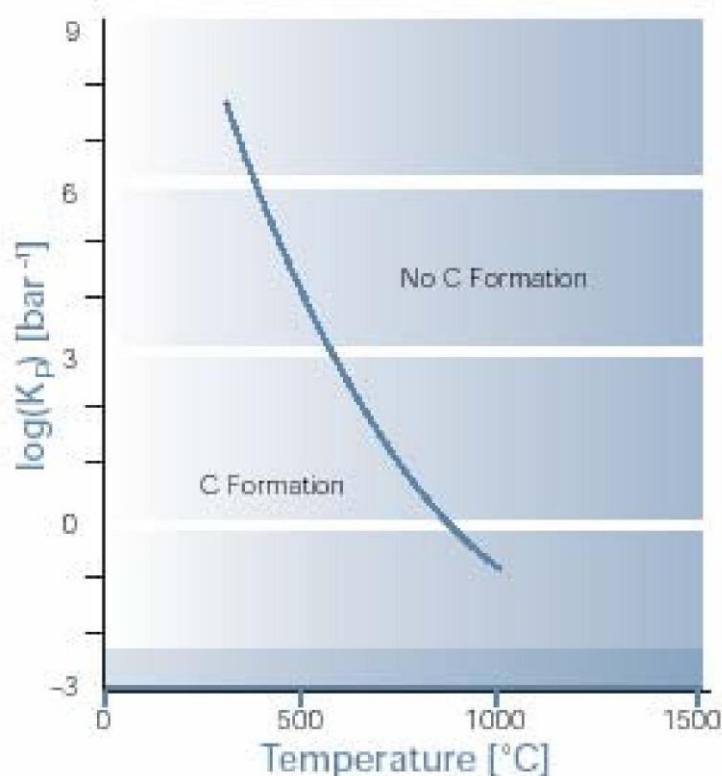


Figure 13. Boudouard reaction: equilibrium constant.

For naphtha the decomposition is more complex because carbon can be formed by direct thermal cracking and also from various intermediates, particularly unsaturated species.

When methane or naphthas are reformed, the formation of carbon within the nickel catalyst can be prevented by ensuring the steam/hydrocarbon ratio (S/C) exceeds a certain minimum ratio. This minimum varies with pressure and temperature, and thermodynamic data can be used to calculate the minimum S/C ratio under different conditions. The exact values calculated depend on thermodynamic parameters assumed for “carbon”, and a considerable amount of research has shown that different forms of carbon can be produced, depending on the prevailing conditions. There is a greater tendency for higher hydrocarbon than for methane to form carbon, because on pyrolysis the readily formed initial intermediates is an important factor, and is critical in influencing the delicate balance between carbon-forming and carbon-removing reactions.

Both the nickel and the support play dual roles, contributing to the reforming process and to the formation of carbon. This problem was solved (by ICI) by introducing an alkali metal component into the catalyst. This accelerates the carbon-steam reaction and, at the same time, the alkali neutralizes the acidity in the catalyst support, so retarding cracking and

polymerization. The most effective alkali was found to be K_2O (potash). The potassium is effective by being mobile on the catalyst surface.

Accurate formulation combines the potassium as a complex potassium alumina-silicate (Kalsilite: $K_2O-Al_2O_3-SiO_2$) and monticellite ($CaO-MgO-SiO_2$). The potassium is liberated at a very slow rate as non-volatile K_2CO_3 which is hydrolyzed as fast it is formed, producing KOH, which is very mobile on the catalyst surface and is the effective carbon-removing agent. Potassium is therefore slowly lost from the catalyst into the product gases, but the rate of evolution is very slow, being kinetically controlled by its release from the Kalsilite compounds. The higher the temperature and the higher the feedstock throughput, the more rapid is the potassium depletion. Careful formulation of the catalyst ensures that lives of several years are obtained in most reformers.

Most of the complex reactions associated with naphtha reforming are completed in the top half of the catalyst bed, with methane reforming taking place in the lower part of the tubes. It is therefore possible to use a non-alkalized steam reforming catalyst in the bottom half of the reformer tube. This has several beneficial effects. It reduces the total quantity of potash in the reformer, and takes potash out of the hottest part of the reformer. Since the potash depresses the activity of the nickel catalyst to some degree with respect to the methane reforming, a non-alkalized catalyst at the bottom of the reformer improves the approach to equilibrium at the exit of the reformer for a given throughput and exit temperature.

Non-acidic magnesium spinel ($MgAl_2O_4$) based catalysts containing no mobile alkali are effective under certain operating conditions, but formulation is critical. However, given good control of temperature throughout a reformer, it is possible to achieve the delicate balance between carbon formation and removal. Systems of this sort have lower tolerance to variation in operating conditions, changes in reformer firing patterns or temperature profiles which can disturb the balance and give carbon lay-down [25].

The reduction or elimination of coke formation often results in constraints on the operating conditions to be applied. Steam and hydrogen are the most important retarding reactants. In steam reformers, carbon will be formed below a certain steam to carbon ratio which means that in many cases the steam reformer has to operate with a surplus of steam and, hence that a larger reformer is required. When using a catalyst with enhanced steam adsorption, the critical steam to carbon ratio can be reduced. This can be obtained by adding alkali to the catalyst or using active magnesia as support. In tubular reforming, no carbon is accepted because of the break-down of the catalyst will result in buildup of pressure drop with uneven

flow distribution and hot spots. The progressive deactivation can be followed from the movement of temperature profile of the catalytic bed.

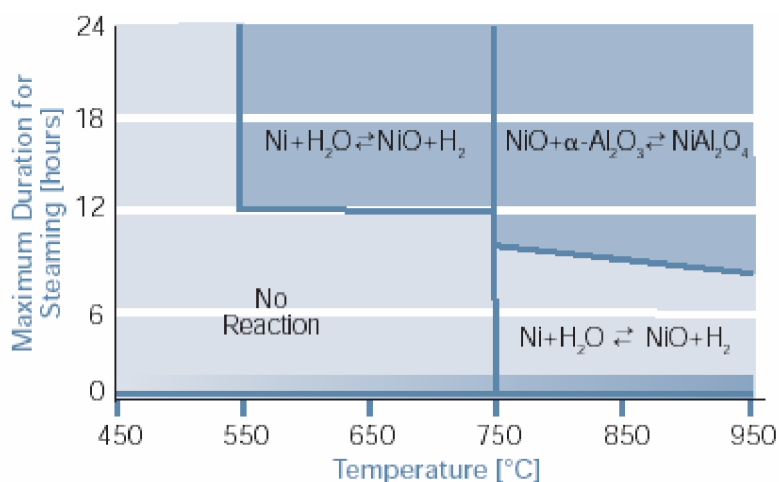


Figure 14. Steaming: recommended durations.

Regeneration of coke deposits can be carried out in various ways depending on the reactivity of the coke. The encapsulating deposits which cause deactivation of the nickel based catalysts can be removed by treatment in hydrogen at 500°C depending on the age of the carbon. Newly formed carbon in tubular steam reformers can be removed by increasing the S/C ratio or by steaming of the catalyst (Figure 14. Steaming: recommended durations. Figure 14). However, aged coke deposits require regeneration by means of air. At sufficiently high temperatures (typically above 500°C), the regeneration process becomes limited by the diffusion of the oxygen through the carbon free pores as the burn-off progresses after a core/shell mechanism. If the carbon is highly reactive, the regeneration may easily become heat transfer limited meaning that the temperature of the catalyst pellet may be heated up to a temperature corresponding to the adiabatic temperature increase of the combustion process. In the case of a metal catalyst, the metallic phase will also be oxidized. Therefore, in many cases it is necessary to carry out the regeneration with controlled addition of air to nitrogen or steam [61].

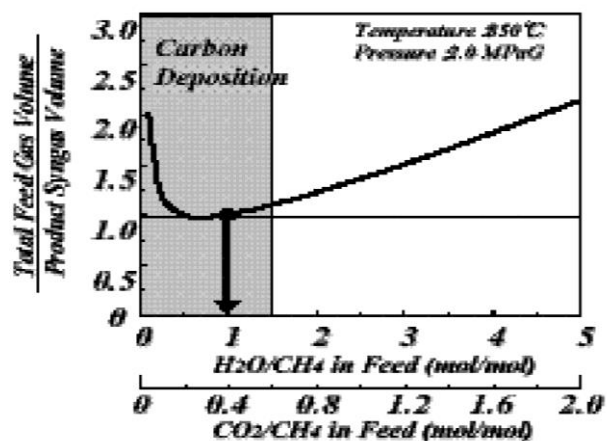


Figure 15. Optimal values of H₂O/CH₄ and CO₂/CH₄ ratios.

Because of the reactions that lead to carbon formation are reversible, and it is possible to calculate limits based on the ratio of carbon in the feedstock to steam beyond which carbon will not be formed, there is a continuing pressure to work at high steam/carbon ratio [65]. The situation can be worse when dealing with heavier feedstocks. The first problem arises with traces of sulphur that may be present in the feed. When the level of sulphur is very low, this may be advantageous. Under most circumstances, however this leads to the formation of nickel sulphide and to catalyst deactivation.

So, the carbon formation may be avoided by controlling the surface reactions, by sulphur addition. It has been demonstrated that minimal coking can be observed, during steam reforming, if traces of sulphur are added to the feed [66], [67]. Sulphur obtained from traces of hydrogen sulphide in the feed chemisorbs on the surface. At low coverages on a (100) surface, sulphur occupies a fourfold hollow site independent of coverage. At higher coverages the surface involves a (2x2) structure on the (100) surface, which is probably best described as a nickel sulphide surface containing islands of free nickel sites [65].

Adsorbed sulphur will deactivate nickel but will also delineate ensembles of sites where sulphur is not adsorbed. Rostrup-Nielsen [67] suggested that the size of these ensembles was critical in allowing steam reforming with minimal formation of coke. Steam reforming was found to involve ensembles of 3-4 nickel atoms, while carbon formation required six or seven atoms.

Dissociation of methane to form C_α requires a given number of sites. If the formation of dissolved carbon occurs mainly through C_β, then polymerization/isomerization of C_α to C_β is required. This, in turn, requires at least twice the number of sites associated with the formation of C_α. The critical ensemble size was found to be generated at sulphur coverages in excess of 0.7-0.8 (corresponding to H₂S/H₂ ratios of greater than about 7.5x10⁻⁷). The rate of steam

reforming was decreased, but carbon formation was essentially eliminated. Some amorphous carbon was laid down and it was possible, under extreme conditions, to produce carbon whiskers [65].

The formation of carbon is very dependent on the system pressure, and the industry seeks high pressure H₂/CO, not low-pressure product. It is known that if one operates these reforming reactions at elevated pressures (~12atm), dramatic increases in the rates of coke formation are observed over most types of Ni based catalysts. Formation of carbon on a catalyst can be difficult to follow at elevated pressure running in continuous mode [64].

Carbon formation may also have an effect on construction materials. Pyrolytic coke deposited on the tube walls may lead to harmful carburization of the high alloy steel tubes. A critical phenomenon is metal dusting corrosion, which may take place if a CO-containing process gas is cooled below the equilibrium temperature of the CO-decomposition reaction. The resulting carbon will typically react with the steel forming iron carbide which will decompose and fall off leaving the construction material with heavy pitting [61].

1.2.2.2 Sintering of Reforming Catalysts

Nickel steam-reforming catalysts are subject to several deactivation mechanisms including coking, poisoning, and sintering. Sintering is the reason for loss of activity for many industrial catalyst systems.

Thermally induced deactivation of catalysts results from [62]:

- loss of catalytic surface area due to crystallite growth of the catalytic phase;
- loss of support area due to support collapse and of catalytic surface area due to pore collapse on crystallites of the active phase,
- chemical transformations of catalytic phases to non-catalytic phases.

Sintering processes generally take place at high reaction temperatures (> 500°C) and are generally accelerated by water vapor. Sintering of heterogeneous catalysts is often referred to as the loss of catalytic surface area due to growth of large particles at the expense of smaller particles. Sintering is complex and may be influenced by many parameters such as sintering time, temperature, chemical environment, catalyst composition and structure, and support morphology. A good understanding of the sintering mechanism is necessary, both to predict the extent of deactivation by sintering and to design catalysts that maintain a high activity [68].

Particle growth via sintering influences the resistance of the catalyst toward coking and poisoning with sulfur. The coking limits are affected by the nickel particle size and the nickel

surface area determines the sulfur capacity of the catalyst. Furthermore, the activity of a steam-reforming catalyst is related to the nickel surface area. To model an industrial reformer with regard to activity and the effect of sulfur poisoning, it is necessary to know the nickel surface area as a function of time, temperature, feed gas composition, chemical composition including promoters, and extent of poisoning.

Several studies of sintering of Ni particles supported on a ceramic carrier are reported in the literature. The most important parameters are the sintering temperature and the composition of the gas over the catalyst. Increasing temperature and the presence of steam accelerates the sintering process. High surface areas of the carrier, on the other hand, increase the stability toward sintering.

Three mechanisms for the metal particle growth have been proposed:

1. particle migration, where entire crystallites migrate over the support followed by coalescence;
2. Ostwald ripening (atom migration), where metal atoms emitted from one crystallite migrate over the support and are captured by another crystallite;
3. vapor transport between particles (at high temperatures).

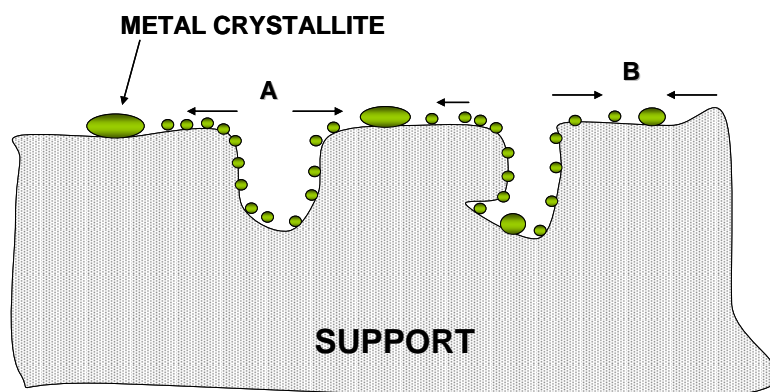


Figure 16. Two conceptual models for crystallite growth due to sintering by (A) atomic migration or (B) crystallite migration [62].

Crystallite migration involves the migration of entire crystallites over the support surface followed by collision and coalescence. Atomic migration involves detachment of metal atoms from crystallites, migration of these atoms over the support surface and ultimately, capture by large crystallites^[62].

Each of the three sintering mechanisms is a simplification, which ignores the possibility that all mechanisms may occur simultaneously and may be coupled with each other through complex physicochemical processes including:

1. dissociation and emission of metal atoms or metal-containing molecules from metal crystallites,
2. adsorption and trapping of metal atoms or metal-containing molecules on the support surface,
3. diffusion of metal crystallites across support surfaces,
4. metal or metal oxide particle spreading,
5. support surface wetting by metal or metal oxide particles,
6. metal particle nucleation,
7. coalescence of, or bridging between, two metal particles,
8. capture of atoms or molecules by metal particles,
9. liquid formation,
10. metal volatilization through volatile compound formation,
11. splitting of crystallites in O₂ atmosphere due to formation of oxides of a different specific volume,
12. metal atom vaporization.

Depending upon reaction or redispersion conditions, a few or all of these processes may be important; thus, the complexity of sintering/redispersion process is emphasized.

In general, sintering processes are kinetically slow at moderate reaction temperature and irreversible or difficult to reverse. Thus, sintering is more easily prevented than cured⁷⁷.

Temperature, atmosphere, metal type, metal dispersion, promoters/impurities and support surface area texture and porosity, are the principal parameters affecting rates of sintering. Sintering rates increase exponentially with temperature. Metals sinter relatively rapidly in oxygen and relatively slowly in hydrogen, although depending upon the support. Water also increases the sintering rate of supported metals. In reducing atmosphere, metal crystallite stability generally decreases with decreasing metal melting temperature, in the order: Ru>Ir>Rh>Pt>Pd>Ni>Cu>Ag, although this order may be affected by relatively stronger metal–support interactions.

Promoters or impurities affect the sintering by either increasing (chlorine and sulphur) or decreasing (oxygen, calcium and cesium) metal atom mobility on the support. Similarly,

support surface defects or pores impede surface migration of metal particles, especially micropores and mesopores with pore diameters about the same size as the metal crystallite.

Sehested et al. [69] studied the mechanism for sintering of nickel steam-reforming catalysts at 500°C, 30bar, H₂O:H₂=10:1 and concluded on the basis of the particle size distributions that sintering occurred via the crystallite migration mechanism. For this sintering mechanism, mass transport by diffusion of nickel atoms on the nickel crystallite surfaces is necessarily an important step, so the diffusivity and concentration of single metal atoms and small clusters are central parameters in the understanding of the sintering phenomenon.

Campbell et al. [70] reported that the heat of adsorption of metal atoms to metal particles depends more strongly on the particle size than assumed previously leading to faster rates of sintering via both Ostwald ripening and particle migration and coalescence. This phenomenon is most important for small particles (diameter <50Å for Pb particles). A nickel particle with a diameter of approximately 36Å contains the same number of atoms as a Pb particle with a diameter of 50Å due to the size difference of the atoms. In the study of Sehested [68], the nickel particles are generally larger than this particle size. The smallest average nickel particle diameters estimated from the nickel surface areas in the catalysts used are of the order of 75–90Å, indicating that the effect of fast sintering of small particles can be ignored. On the contrary, ASAXS (anomalous small angle X-ray scattering) gives lower estimates of the nickel particle diameters, indicating that sintering of small particles is significant. However, they believe that the measurements of the nickel areas in that case give the most reliable estimates of the nickel particle diameters as these measurements are carried out using reduced catalysts as opposed to ASAXS, where passivated catalysts are used. Nickel may move significantly during passivation.

Recently, a simple expression for the development of the nickel surface area as a function of time, temperature, nickel loading, and carrier surface area was derived [71].

$$A_{Ni} = \pi c_{cat} d_{Ni}^2 = const. X_{Ni} d_{Ni}^{-1} \approx const. \frac{X_{Ni}^{0.86} (1 - X_{Ni})^{0.14} A_{car}^{0.14}}{K_1^{0.14} D_{Ni}^{0.14} t^{0.14}}$$

A_{Ni} = nickel surface area

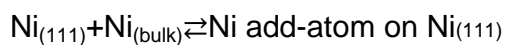
c_{cat} = number of particles per gram of catalyst

d_{Ni} = number averaged particle diameter

X_{Ni} = fractional mass of nickel (g metal/g catalyst)

A_{car} = surface area of the carrier (m^2/g of the carrier)

K_1 = equilibrium constant for the reaction:



D_{Ni} = diffusion coefficient of an add-atom on a Ni surface

t = time

To obtain the expression it was assumed that the sintering mechanism was particle migration and coalescence, that the particle sizes were log normally distributed with constant relative standard deviation, and that the carrier acted only as an area dispersing the metal particles. The expression included a parameter, which depends on the atmosphere over the catalyst and the chemical environment on the catalyst. It was investigated experimentally and theoretically the effects of steam and hydrogen over nickel catalysts as a function of temperature. The relative nickel areas of Al_2O_3 and MgAl_2O_4 -supported nickel catalysts are determined after sintering at 1, 31, and 40 bar total pressure at various steam and hydrogen ratios. The increased rate of sintering in the presence of steam is attributed to formation of $\text{Ni}_2\text{-OH}$ species at the surface of nickel particles. The energy of formation of this species at the nickel surface is low, compared to that of nickel atoms while the energy of diffusion is highest for the $\text{Ni}_2\text{-OH}$ complex. It was concluded that, in the presence of steam and hydrogen, the surface transport at nickel particles will be dominated by $\text{Ni}_2\text{-OH}$ dimers. The calculated energies of formation and diffusion are used in a simple model that is able to predict the rate of sintering of nickel catalysts. The predicted dependencies of temperature, $P_{\text{H}_2\text{O}}$, and P_{H_2} are in good agreement with those obtained experimentally.

The experimental data showed a change in the activation energy of sintering at high temperatures. The temperature for this change is at approximately 600°C at 40bar total pressure and $\text{H}_2\text{O}:\text{H}_2=2.5:1$ when the catalyst is sintering for 700h. At ambient pressure, the change is observed to happen at approximately 700°C after sintering at 1bar total pressure and $\text{H}_2\text{O}:\text{H}_2=1:1$ for 50h. It is speculated that the rate of sintering, at high temperatures, may be determined by Ostwald ripening [68].

Sintering of the support may also occur. Single-phase oxide carriers sinter by one or more of the following processes:

1. surface diffusion,
2. solid-state diffusion,
3. evaporation/condensation of volatile atoms or molecules,

4. grain boundary diffusion,
5. phase transformation.

Additives and impurities affect the thermal properties of carriers by occupying defect sites or forming new phases. Alkali metals, for example, accelerate sintering, while calcium, barium, nickel and lanthanum oxides form thermally stable spinel phases with alumina. Steam accelerates support sintering by forming mobile surface hydroxyl groups that are subsequently volatilized at higher temperatures. Chlorine also promotes sintering and grain growth in magnesia and titania during high temperature calcination.

Dispersed metals, in supported metal catalysts, can also accelerate support sintering, for example, dispersed nickel accelerates the loss of Al_2O_3 surface area in $\text{Ni}/\text{Al}_2\text{O}_3$ catalysts [62].

1.2.2.3 Catalyst Shape and Dimensions

Reforming catalysts can be produced in different shapes and sizes by pelleting or extrusion technique. Since it is used in tubular reactors, it must be of a shape and size which packs easily and homogeneously into the tubes to give an active bed which does not have an unacceptably high pressure drop. As much as possible of the active nickel surface must be accessible to the reactant gas, while the catalyst must be strong enough to resist abrasion and breaking during handling or during any thermal cycling that might occur. It must also generate enough turbulence in the gas to give good heat transfer between the tube wall and the body of the catalyst [25].

Obvious, possible simple shapes are pellets, spheres, rings and various extrusions in the shape of tubes, cylinders, rods and bars of different sizes and cross sections

For reforming it has been found that a thick-walled ring meets all of the above criteria, and the dimensions most commonly used are a diameter of 17mm with lengths of 17mm, 10mm and even 6mm. If the outside dimensions of the ring are reduced, then an equivalent packed volume will have an increase of pressure drop and slightly higher activity resulting from the larger geometric surface area. By using different ratio of the various sized catalyst, it is possible to balance gas flows through individual reformer tubes and to compensate for asymmetric heat fluxes in the furnace [25]. To enhance steam reformer performances a possible route can be to modify catalyst shape rather than changing the fundamental chemistry of the support or the catalytically active phase.

The two main objectives are to reduce pressure-drop across the reformer, and/or lower tube wall temperatures (particularly in the region of maximum heat flux) via increased activity through higher geometric surface area and heat transfer properties. The major benefits that can be obtained are either longer life or the possibility of increased throughput, or a combination of both effects [25].

In designing shaped steam reforming catalysts a number of factors have to be taken in account. These include the packing characteristics of the catalyst particles in relatively narrow tubes, pressure drop, geometric surface area, heat transfer properties and physical strength. Whilst some of these properties may be enhanced with a particular shape, others may be diversely affected. For example, some high geometrical surface area shaped particles tend to bridge across the tube walls when they are being charged, and this makes uniform packing difficult. Subsequently, when the reformer is running, this problem can lead to severe hot spots at regions where there is little catalyst in the tube. Other high geometric surface area shapes may have low strength. A further consideration is the pattern of breakage of the catalyst

particles. If a ring breaks, it is preferable that forms two large pieces, which do not cause a detrimental increase in pressure drop. However, with shapes having open structures there is the danger of them shattering into a number of small pieces when they break and these can give rise to a high-pressure drop [25].

1.2.3 Practical Aspects of Steam Reformers

Although steam reforming is the most mature and the best established technology for hydrogen production, the continuous research on reforming catalysis, reactor engineering, and process modeling brought several improvements in the new installed plants.

A typical design for a SMR reactor and a scheme for the whole process of hydrogen production are presented in Figure 17. For this kind of endothermic process, the catalyst is usually loaded into a number of tubes and placed inside of a furnace. There are several factors that are of fundamental importance in the reformer design: i.e., the geometry and number of single reformers; the heat transfer from the burners to the reforming units; and the catalyst design, including its intrinsic activity and physical properties (size, form, etc.) [20].

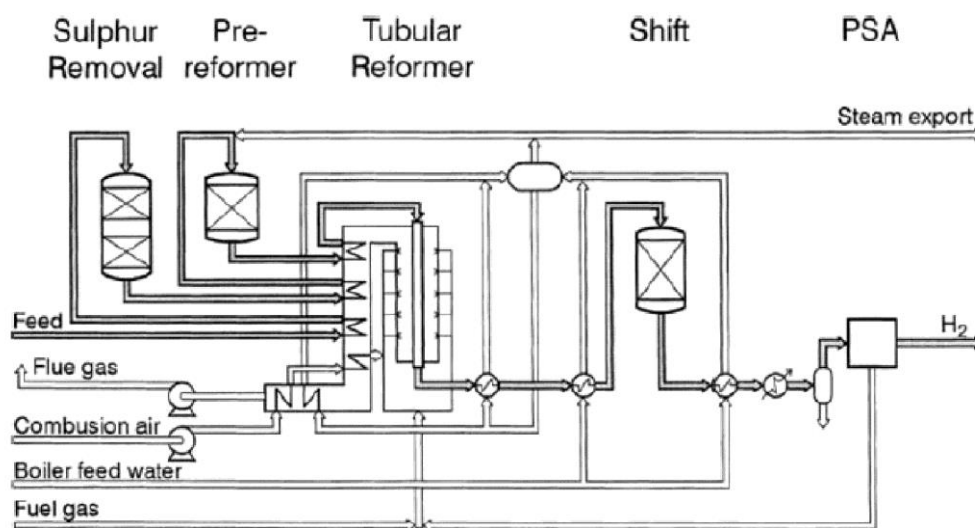


Figure 17. Typical process layout for a hydrogen plant based on advanced tubular steam reforming technology. The hydrogen is purified by shift conversion followed by pressure swing adsorption (PSA) to delivery pressure [20].

The primary reformer consists essentially of two main sections: the furnace, containing the tubes charged with the catalyst, and the convection section, where heat is recovered from the

flue gas by such duties as preheating feedstock, process air and/or combustion air, boiler feedwater heating and steam raising, and super heating.

The steam reforming reactions are usually carried out at a pressure up to 35bar and temperatures of 800°C or higher, while the flue gas may reach a temperature in excess of 1000°C. Consequently, the design of the primary reformer is complex and depends on the duty and on the philosophy of the chemical contractor engineering the plant. The furnace can be top-fire, terrace wall-fire or side-fire, and in the case of small hydrogen plants it can be of a bottom-fired design [20]

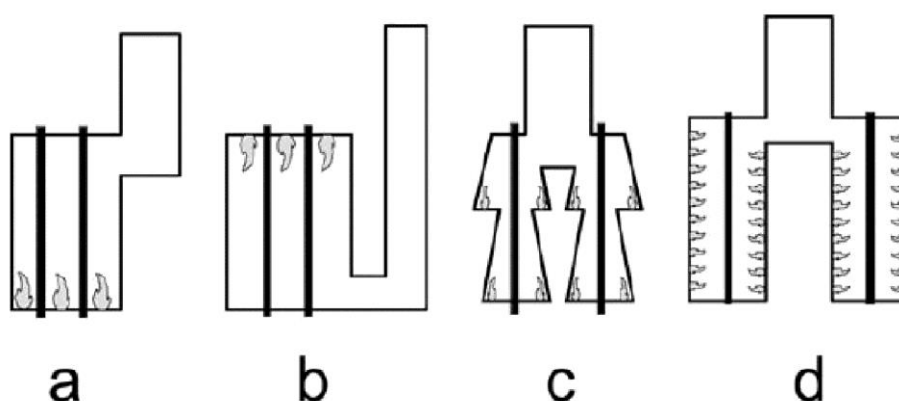


Figure 18. Typical configurations of reformer furnaces: a) bottom fired, b) top fired, c) terrace wall, d) side fired [20].

Typical throughput, which is usually expressed as the amount of steam plus feedstock per hour per liter of catalyst, is in the range 2-7 Kg h⁻¹L⁻¹. The overall length of reformer tubes is usually in the range 7.5–12.0m although the heated charged length may be up to 9.0m; tube diameter usually lies between 7cm and 13cm. The number of tubes depends on output, and for a large reformer there may be as many as 650 tubes [25].

Conventional steel tubes do not possess the material characteristics to withstand the pressure and temperature at which a modern reformer operates. A suitable cost-effective material is a chromium/nickel alloy with the following composition: Cr 24-28 %, Ni 18-22%; C 0.35-0.45%; Mn 2 %; Si 2 %; P and S 0.05 %. The melting point of the alloy is close to 1370°C, and it is suitable for use at temperatures up to 1150°C. Other materials such as Pyrotherm G24/24 Nb and Manaurite 36X can also be used, since they allow operation of the reformer at higher temperatures and pressures. However, they are more expensive [25].

If the diameter of the tube is too large, heat transfer to the catalyst in the center of the tube will be restricted and the reaction rate limited. On the other hand, if the tube diameter is too small the pressure drop will be high.

In operation, there is a gradation of temperature longitudinally from the inlet to the outlet of the tube, as well as radially across the wall of the tube. Creep occurs with time at normal operating conditions. The temperature which the tube wall experiences depends on the distribution of heat input and the heat adsorbed by the reaction taking place on the catalyst in the tubes. Uneven heat input uneven catalyst activity caused by uneven packing or catalyst poisoning will cause local overheating, resulting in excessive creep in that location, which will hasten tube rupture. Normally reformers are designed with a tube life of about 10 years using creep strength data based on creep-rupture tests of varying duration available from a number of sources [25]. The higher the temperature and pressure are, the greater the creep and the shorter the tube life. This applies to all parts of each tube, and if part of any tube is subjected consistently to higher-than-average temperatures, it will fail prematurely. It is therefore important that hot spots, due to catalyst poisoning or carbon deposition, are removed as soon as possible.

Other practical aspects of steam reformers are:

- Reactant gas distribution (both steam/feedstock and fuel for the burners)
- Firing the reformer
- Expansion and contraction of reformer tubes
- Facilities to charge and discharge catalyst
- Designing a reformer for efficient operation
- Catalyst reduction (with hydrogen, with ammonia, with methanol, with natural gas or other hydrocarbons)

The life of a catalyst can be affected by the following factors: catalyst breakdown, tube blockage, overheating of the catalyst, poisoning of the catalyst, and thermal ageing. Catalyst breakage and blockage of the tubes causes an increased pressure drop across the reformer, and if the effect is random, it shows as an uneven appearance of the tubes in the furnace. More fundamentally, it can lead to overheating of the catalyst, loss of activity and a reduction of throughput. All of these effects may be caused by the deposition of carbon. Overheating of the catalyst can also be caused by maloperation of the reformer. Loss of activity through poisoning by contaminants in the process gas is important, since this can cause carbon deposition and result in overheating, catalyst breakage and, in extreme cases, even partial blocking of the tubes. Gradual loss of activity or thermal ageing caused by progressive loss of

nickel surface area through sintering places a limit on the life of a catalyst charge, and for a particular catalyst, this depends on the actual operating conditions. In practice, the most important effects are catalyst sintering, catalyst poisons and carbon formation. Carbon can be deposited in primary reforming catalyst by different mechanisms and to varying degrees. Complete loss of reaction steam results in a massive deposit of carbon, and the reformer will develop a very large pressure drop within a few seconds. It will not then be possible to run the reformer again without replacing the catalyst. Running a reformer with a slightly deficient steam/carbon ratio will result in slight carbon deposition, which will slowly increase the reformer pressure drop, and the tubes will appear hotter than normal. If detected soon enough this carbon can often be removed satisfactorily, but this depends on the type of catalyst being employed. Removing the feed flow and sustaining normal reformer temperatures with only steam and hydrogen will convert the carbon to carbon dioxide, which can be detected by an analyzer at the reforming exit. The hydrogen will keep the catalyst in a reduced form. When the carbon has been deposited within the catalyst pores by carbon monoxide disproportionation, steaming will increase the reformer pressure drop. In this case, the carbon expands within the catalyst pores and cracks the pellet and, although the carbon in situ retains the pellet strength, when the carbon is removed, the pellet collapses. If this happens, it is necessary to change the catalyst [25].

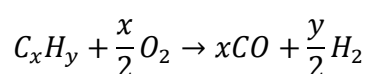
Slow deposition of carbon can occur for a number of reasons. Careful catalyst formulation is essential to maximize selectivity, and to eliminate acid sites, which can promote carbon formation. When a predominantly methane feedstock is reformed, low catalyst activity in the inlet portion of the tube can lead to carbon deposition, which restricts heat transfer and give rise to the phenomenon known as "hot bands". Both the CO disproportionation and reduction reactions are always in the carbon-free side of the equilibrium throughout the reformer tube, regardless of catalyst activity. However, the methane cracking reaction is on the carbon forming side equilibrium for a significant portion of the tube. Carbon is not, however, produced at the lower temperatures near the inlet, because both reactions which remove carbon (reverse CO disproportionation and reverse CO reduction) are faster at these temperatures than the rate of carbon formation by methane cracking. However, as the temperature increases, so does the rate of carbon formation and at a temperature of about 650°C, the carbon forming reaction becomes faster than the carbon removing ones. If the rates of these reactions are fixed, then it is essential that the catalyst has enough activity to produce sufficient hydrogen via steam reforming below this temperature, so that the gas composition lies on the carbon removal side of the methane cracking equilibrium.

"Hot bands" always format about the same position on all tubes in the furnace and approximately the same position in all reforming furnaces.

As expected, heavily loaded top-fired furnaces are the most susceptible to forming “hot bands”. The low catalyst activity can arise from a number of causes – catalyst may be old and at the end of its useful life, it may be poisoned or inadequately reduced. If no hydrogen is recycled with the feedstock, then the catalyst in the inlet portion remains in the oxidized state until reforming or cracking of the feedstock occurs, and produces some hydrogen. This increases the load on the catalyst further down the tube, since the inlet portion is then functioning simply as a heat exchanger. Further, if reformer conditions change, then unreduced catalyst may be called upon to do some reforming. It will be unable to do so, carbon will be deposited and hot areas will appear at the top of the tubes.

1.3 Partial Oxidation of Fossil Fuels (POX)

The other major route to hydrogen is non-catalytic partial oxidation of fossil fuels, often referred to as POX (or gasification). One key advantage of this approach is that it accepts all kinds of hydrocarbon feeds. The thermal oxidation is run at 30-100 atm with pure O₂ using a special burner inside a refractory lined vessel at ~1300°C. The general reaction is described by:



There are several plants that produce hydrogen by the partial oxidation of hydrocarbons. In the non-catalytic process, a mixture of oxygen and natural gas is pre-heated, mixed and ignited in a burner. In the absence of catalyst, the reactor temperature must be high enough to reach complete CH₄ conversion. Combustion products like CO₂ and H₂O are also formed to a certain extent. Subsequently, endothermic reaction as steam reforming is also involved, which determine the outlet temperature in the order of 1000-1200°C. At this stage, the gas composition is near thermodynamic equilibrium. According to the stoichiometry of reaction the consumption of O₂ should be, in the absence of combustion products, approximately 0.5 O₂/CH₄. However, actual use requires O₂/CH₄ ratio of about 0.7. It appears that if the reactor in principle is simple, the cost of an oxygen plant is considerable. One advantage of this process is that it can work at high pressures, thereby saving costly compressors. Some carbon is formed by the thermal cracking of methane and has to be removed by washing. The outer reactor walls are cold being insulated on the inside. Using this technology, Texaco and Shell commercialize this conversion process [24].

In non-catalytic partial oxidation process, steam is not used as a feed, but with higher hydrocarbon feeds there can be a lot of coke as by-product. Since conditions are maintained

net reducing, no NO_x or SO_x are produced; however, if the feed contains any sulfur compounds, H_2S and COS are by-product which must be scrubbed. A clear disadvantage is the need to have huge quantities of O_2 available continuously, thus requiring the substantial investment in an adjoining O_2 plant [24].

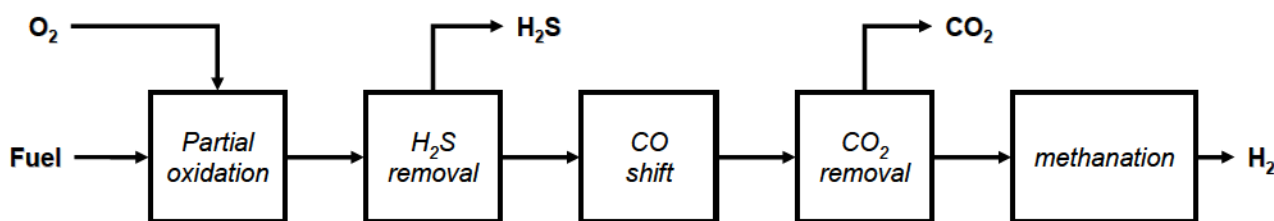


Figure 19. Block diagram of the whole non catalytic partial-oxidation of methane.

Methane is reacted with O_2 in a flame, then after desulphurization, the WGS reaction is used to shift essentially all CO to H_2 , and CO_2 is removed. If complete removal of residual CO and CO_2 is required, methanation on a Ni catalyst can reduce carbon oxides to less than 10 ppm (Figure 19) [24].

Since CO is also a co-product, one has to use high temperature water gas shift to convert CO with steam to H_2 . Additional unit operations are required for gas purification (largely to remove H_2S) and to remove soot from the waste water. In addition, the CO_2 can be removed by adsorption, and final traces of CO destroyed by follow-up methanation. Thus POX operations can get quite complex, and in comparison to SMR they are less energy efficient, while eliminating more CO_2 co-product [22].

In the Figure 20 it is only shown part of the POX process, steam must also be generated and the product CO/H_2 must also be purified. A strong feature of POX technology versus SMR is that the former is a very attractive process when dealing with the increasing amounts of bottom-of-the-barrel feedstocks. It was estimated that the thermal efficiency of a POX plant feed with heavy hydrocarbons to be ~70 % versus 81% with SMR. Secondary reforming with added O_2 is used in some operations employing SR technologies, especially in connection for the high H_2 demands of ammonia synthesis. In the exothermic, secondary reforming, air is added to the effluent of the primary reformer. The residual methane reacts with the air providing heat for this CO producing reaction, and the unreacted N_2 is used for NH_3 synthesis [22].

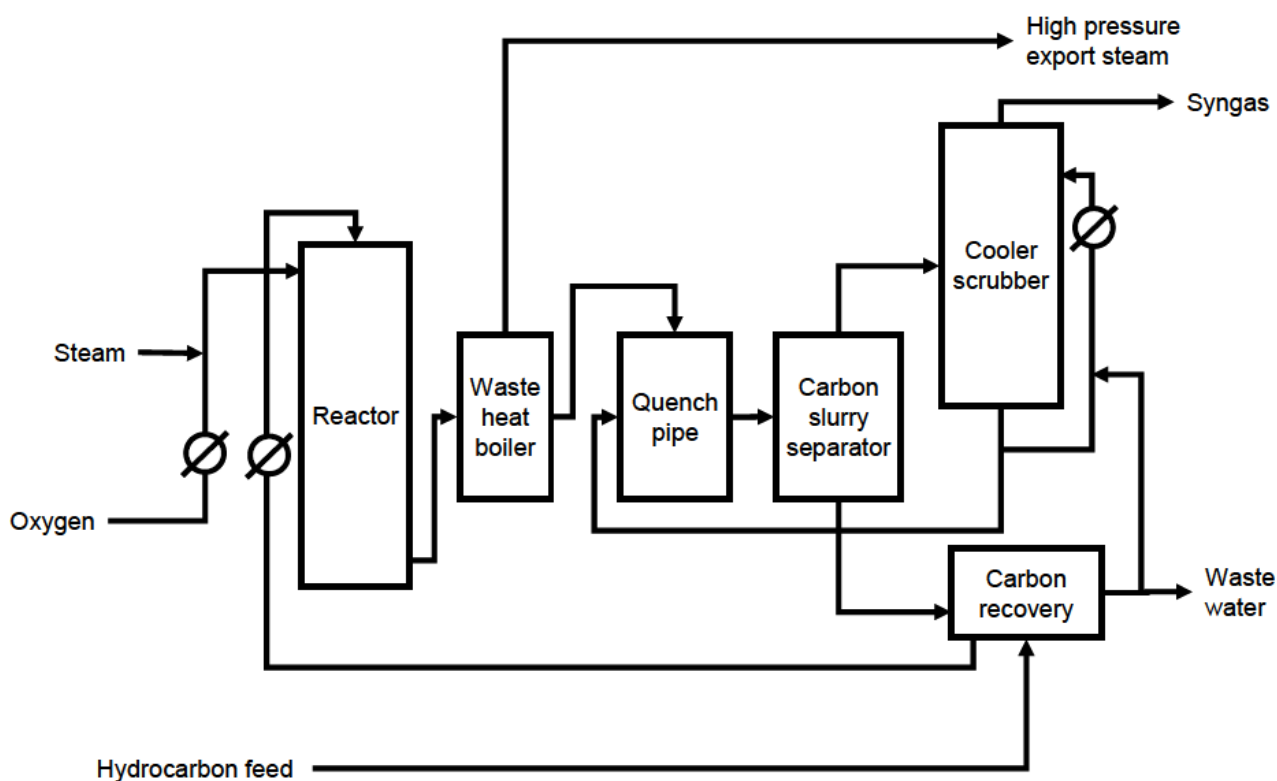


Figure 20. Process flow diagram for POX

1.4 Autothermal Reforming (ATR)

An alternative approach to POX and SMR is autothermal reforming (ATR), which is a combination of both technologies.

This process was developed by Haldor Topsoe in the late 1950s with the aim of performing reforming in a single reactor. In autothermal reforming, the energy for the production of CO and H₂ is produced by partial oxidation of the hydrocarbon feedstock. Like POX, the feeds first react in a large refractory lined vessel with O₂ for non-catalytic combustion at 1200-1250°C. If the product H₂ is intended for NH₃ production, an air feed could be used.

The reformer basically consists of a ceramic lined tube and a fixed catalyst bed for equilibration of the gas. The preheated streams (CH₄ + H₂O and H₂O + O₂) are mixed in a burner placed at the top where the POX reactions take place. The final steam reforming and equilibration take place in the catalyst bed below the burner. Typically, the ATR operates at high temperatures ca. 1200-1300°C in the combustion zone and 950-1200°C in the catalytic zone. This results in a lower oxygen consumption (O₂/CH₄=0.55-0.60), however, with a certain amount of steam added to the feedstock to eliminate carbon formation. Carbon and soot formation in the combustion zone is an undesired reaction, which leads to carbon deposition

on downstream tubes causing equipment damage, pressures losses and heat transfer problems.

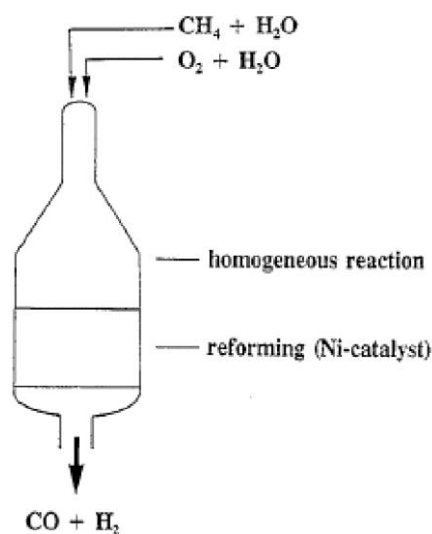


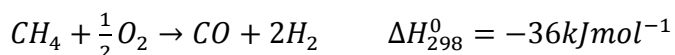
Figure 21. Autothermal reformer.

Although the ATR was originally used to maximize H_2 production in ammonia plants, it can be applied in the production of CO rich gases. In all cases, the H_2/CO ratio at the outlet of the reactor can be precisely adjusted by varying the H_2O/CH_4 and/or O_2/CH_4 molar ratios in the feed.

Since autothermal reforming uses less O_2 than POX, the economics are less sensitive to the price of O_2 when O_2 is cheap. It requires no external fuel while offering some flexibility in feedstock.

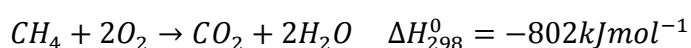
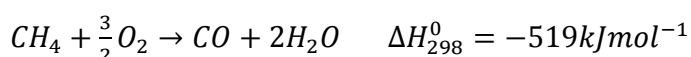
1.5 Catalytic Partial Oxidation of Methane (CPO)

A new interesting process for conversion of methane into synthesis gas is catalytic partial oxidation. In the 1940s, Prettre et al first reported the formation of synthesis gas by the catalytic partial oxidation of CH_4 :



They used a Ni-containing catalyst. In contrast to steam reforming of methane, methane partial oxidation is exothermic. However, the partial oxidation requires pure oxygen, which is produced in expensive air separation units that are responsible for up to 40% of the cost of a synthesis gas plant (in contrast, the steam reforming process does not require pure oxygen) [72].

In the early 1990s, several papers [73,74,75,76,77] reported that one can reach CO and H₂ concentrations in excess of those expected at thermodynamic equilibrium by operating the CH₄ oxidation reaction at exceptionally high space velocities (GHSV=52,000ml(g_{catalyst})⁻¹h⁻¹) in a fixed-bed reactor. The following catalysts were employed: Ni/Yb₂O₃, Co/rare earth oxide, Co/MgO, and Ni/Al₂O₃. According to the partial oxidation reaction, such a process yields the desired H₂/CO molar ratio of 2 required for methanol or Fischer-Tropsch synthesis. From thermodynamic simulations, it is clear that the reaction is favored at T>850°C in excess of CH₄, although both CO and H₂ selectivities are modified by the formation of CO₂ and H₂O in combustion reactions which are much more exothermic:



Since CPO reaction is slightly exothermic, a process based on this reaction would be much more energy efficient than the energy intensive SMR process. In addition the partial oxidation reaction is also much faster than the reforming reactions, suggesting that a single stage process for syngas production would be an attractive alternative to SMR and also results in smaller reactors and higher productivity.

The direct oxidation has not been developed at industrial scale, and it is difficult to study because it involves co-feeding CH₄/O₂ mixtures and reaction close flammable or even explosive conditions. Local hot spot are usually formed which can irreversible damage the active catalyst. Moreover the gas phase reactions in a high reducing atmosphere can led to carbon and soot deposition over the catalyst surface.

The actual reaction temperatures could be much higher than those reported. By using an optical pyrometer, it was found that, during the catalytic oxidation of methane to CO and H₂, the combination of a high space velocity, an exothermic reaction, and an active catalyst (Ni/Yb₂O₃) gave rise to steep temperature gradients (hot spots). Furthermore, the temperature of the hot spot was greater by as much as 370°C than the temperature measured with a thermocouple located at a distance of only 1 mm from the hot spot in the catalyst bed. If a temperature lower than that of the hot spot is used to calculate the equilibrium concentrations of CH₄, CO, CO₂, and H₂, one can draw the conclusion that the concentrations of CO and H₂ exceeded their thermodynamic equilibrium values. However, if the true maximum (hot spot) temperature is used in the calculation, the observed concentrations are found to be somewhat less than those predicted at equilibrium. Indeed, using a careful temperature measurement method, in which a thermocouple end contacted just the top surface of the catalyst bed, it was

found that the CH₄ conversion in the presence of Ni/Al₂O₃ catalyst was less than that predicted by thermodynamic equilibrium.

Furthermore, Hu and Ruckenstein [78] observed hot layers (thinner than 1mm) in NiO/MgO solid solution catalysts and in NiO/Al₂O₃ and NiO/SiO₂ catalysts during the partial oxidation of methane in a fixed-bed reactor. The hottest layers were located at the top of the bed of the NiO/MgO and NiO/Al₂O₃ catalysts, but they were observed to move down and then up for the NiO/SiO₂ catalyst bed. The down-and-up movement resulted in an oscillatory temperature of the NiO/SiO₂ catalyst at a given position in the bed, which was absent when the catalyst was NiO/MgO or NiO/Al₂O₃.

The different temperature behaviors of the three catalysts were attributed to the different strengths of the interactions between the metal oxide and the support. Temperature-programmed reduction (TPR) experiments with 4% H₂ in argon indicated that the initial reduction temperature was about 330°C for 13.6wt% NiO/SiO₂, which is near that of pure NiO (about 300°C). In contrast, for 13.6wt% NiO/Al₂O₃ the initial reduction temperature was high (670°C) and no marked reduction peak could be detected even at 800°C for 13.6wt% NiO/MgO. These results clearly indicate that there are weak interactions between NiO and SiO₂ and much stronger interactions between NiO and Al₂O₃ and between NiO and MgO. The weak interactions in Ni/SiO₂ might have been responsible for the temperature oscillation by allowing a facile redox behavior of the active nickel sites, namely, the oxidation of Ni⁰ to NiO by O₂ and the reduction of NiO to Ni⁰ by CH₄. The strong interactions characteristic of NiO/Al₂O₃ and NiO/MgO were inferred to inhibit in part the redox behavior of the nickel sites. In the case of NiO/SiO₂, according to this interpretation, the freshly reduced NiO located at the inlet of the bed became highly active, causing a hot layer to be generated. The high temperature of this hot layer resulted in sintering of the nickel particles, which led to the loss of activity. Therefore, the reaction is inferred to have taken place in the neighboring section of the catalyst. As a result, a hot layer propagated downward in the reactor. However, the sintered nickel particles were re-dispersed on the SiO₂ support when they were re-oxidized by O₂, because the oxygen concentration is high when the reaction of CH₄ with O₂ does not take place. After a certain time, the re-oxidized layer near the entrance was again reduced by CH₄ and became active again, resulting in a hot layer. The following part of re-oxidized nickel on SiO₂ can be reduced rapidly by H₂ and CO generated near the entrance of the reactor. The redox of the Ni/SiO₂ catalyst constitutes a cycle of deactivation and reactivation in each part of the catalyst. The hot layer moved downward in the bed during the time required for the reduction of the entrance layer. Consequently, the time scale of the oscillations was determined by the time scale of the reduction–oxidation process.

Furthermore, Basile et al. [79] used IR thermography to monitor the surface temperature of the nickel foil during the methane partial oxidation reaction by following its changes with the residence time and reactant concentration. Their results demonstrate that the surface temperature profile was strongly dependent on the catalyst composition and the tendency of nickel to be oxidized.

In the 1940s, Prettre et al. reported the formation of synthesis gas via the catalytic partial oxidation of CH₄ catalyzed by a 10 wt % refractory supported nickel, at temperatures between 700 and 900°C. Thermodynamic equilibrium corresponding to the catalyst bed exit temperature was achieved under all conditions investigated. In 1970, it was examined the effect of diffusion on methane partial oxidation catalyzed by a single grain of Ni/mullite catalyst in the temperature range of 760 and 900°C and examined the ignition and extinction characteristics of this catalyst. It was observed that the nickel catalyst deactivated in an oxidative environment but could recover on reduction. In 1984, Gavalas et al [80] investigated the effects of the calcination temperature, pre-reduction, and feed ratio on the reaction of CH₄/O₂ mixtures catalyzed by NiO/α-Al₂O₃ at 570–800°C. However, under their experimental conditions, the main products were CO₂ and H₂O. Since 1990, researchers have continued to examine nickel-containing catalysts for the partial oxidation of methane, and they also started to use noble metals as catalysts. In 1990, it was reported a methane conversion of about 90 % and more than 90 % selectivity to CO and H₂ at 770°C, atmospheric pressure, and at the high GHSV of $4 \times 10^4 \text{ ml}(\text{ml}_{\text{catalyst}})^{-1} \text{ h}^{-1}$ for a reaction catalyzed by lanthanide ruthenium oxides, such as Pr₂Ru₂O₇, Eu₂Ru₂O₇, Gd₂Ru₂O₇, Dy₂Ru₂O₇, or Lu₂Ru₂O₇. In 1992, Hickman and Schmidt [81] used platinum monoliths to achieve high selectivity to CO and H₂ in the partial oxidation of methane. In the following 10years, various noble metal catalysts have been examined. Compared with the non-noble metal catalysts, the noble metals exhibit high stability with excellent activity and selectivity. The major drawback of the noble metal catalysts is their high cost, which restricts their potential use in industrial processes. Non-noble metal catalysts, particularly those containing nickel, have also been investigated extensively since 1990.

The authors observed that, under their operating conditions, the calcined catalyst bed consisted of three regions, NiAl₂O₄ (upstream, section), NiO + Al₂O₃ (middle section), and reduced Ni/Al₂O₃ (downstream section). In the upstream section of the reactor, the CH₄/O₂/He feed contacted NiAl₂O₄, which exhibited only a moderate activity for the complete oxidation of methane to CO₂ and H₂O. The next section of the reactor contained NiO + Al₂O₃, which catalyzed the complete exothermic oxidation of methane to CO₂. Because of the complete consumption of O₂ in the second section, the third (downstream) section of the catalyst bed consisted of a reduced Ni/Al₂O₃. The formation of the CO and H₂ products, corresponding to

thermodynamic equilibrium at the temperature of the bed exit, occurred in this section, as a result, of the reforming reactions of CH₄ with CO₂ and H₂O produced during the complete oxidation reaction catalyzed by the NiO/Al₂O₃.

The activity of NiO in the total oxidation reaction was excluded by Basile et al [79] using IR thermography and evidencing the low temperature of oxidized Ni particles placed at the entrance of the bed.

Choudhary et al. reported a high conversion of CH₄ and high selectivities to CO and H₂ with Ni/CaO, Ni/Al₂O₃, NiO-rare earth oxide, and Co/rare earth oxide catalysts [73,74,75,76,77].

The major problem encountered with these non-noble metal catalysts is their relatively low stability. The main causes of the deactivation of the catalysts are carbon deposition and metal sintering in the catalyst. Nevertheless, numerous effective nickel-containing catalysts have been developed by incorporation in suitable supports, such as La₂O₃, MgO, SrTiO₃, and CeO₂; effective promoters, including La₂O₃, Li₂O, and iron oxide; and novel preparation methods, such as a solid phase crystallization method, a sol–gel method, and a citrate method [72]. However, because the high stabilities reported for these effective nickel-containing catalysts were based on short-term tests (<100h), it is unclear how stable these catalysts will be in long term tests (>1000h), which is the first step that any candidate catalyst for commercialization must pass.

In the last decade, numerous attempts have been made to understand the mechanism of the partial oxidation of methane. Mechanistic investigations of the partial oxidation are still challenging, because this exothermic reaction is very fast and causes extremely high catalyst temperature rises, so that the usual methods of investigation are unsuitable.

Two kinds of pathways have been suggested:

1. a combustion-reforming pathway, in which CO₂ and H₂O are the primary products, and CO and H₂ are formed by their reactions with CH₄,
2. a pyrolysis or dissociative adsorption pathway, in which CO is the primary product formed by the dissociation of methane, CH₄→CH_x + (2 – 1/2x)H₂; followed by the oxidation of carbon containing species to give CO without the pre-formation of CO₂.

For methane partial oxidation to syngas, the thermodynamic calculation results suggest a high temperature is advantageous for high methane conversion and selectivity to CO and H₂. However, increasing the pressure in the reactor is unfavorable for CH₄ conversion and CO and

H₂ selectivity. The prediction of the CH₄ conversion and product selectivity under specific conditions is shown in two-dimensional forms (Figure 22). Apparently, under 1bar at 800°C, theoretical CH₄ conversion should be up to 90%, and selectivities to CO and H₂ are 97%. At 8bar and 800°C, CH₄ conversion is only 70%, and CO and H₂ selectivities are around 85%.

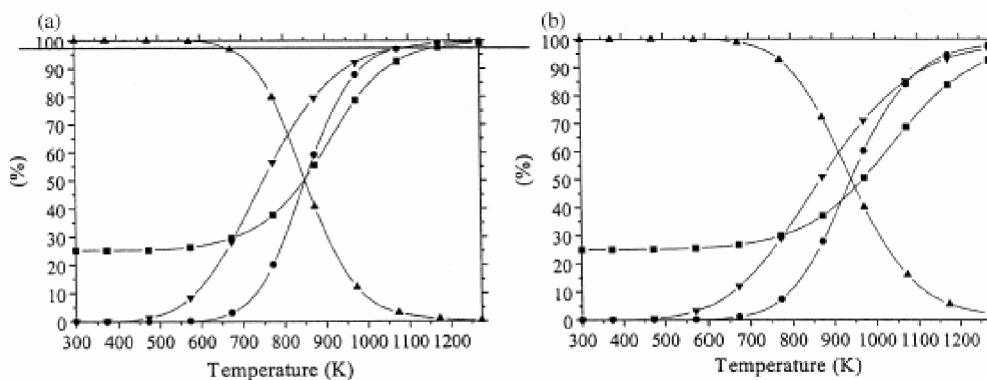


Figure 22. Thermodynamic equilibrium calculations at: (a) atmospheric pressure and (b) at 8 bar; (■) XCH₄; (●) S[CO], (▲) S[CO₂], (▼) S[H₂] [82].

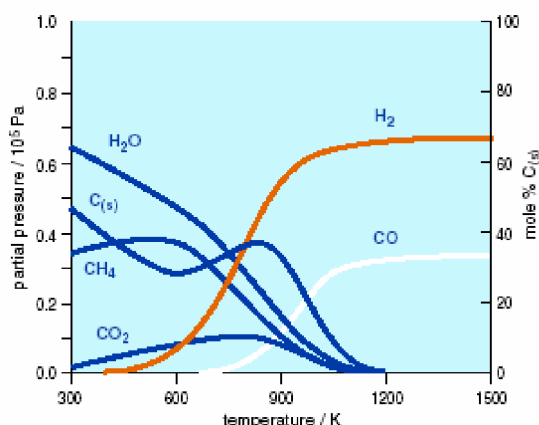


Figure 23. Composition of equilibrium mixture as a function of temperature when oxygen and methane are mixed in a 2/1 ratio [83].

This process is likely to become more important in the future of methane conversion due to the thermodynamic advantages this process has over steam reforming:

1. Partial oxidation is mildly exothermic, while steam reforming is highly endothermic. Thus, a partial oxidation reactor would be more economical to heat. In addition, it can be combined with endothermic reactions, such as steam reforming or dry reforming with carbon dioxide to make these processes more energy efficient.

- The H₂/CO ratio produced in stoichiometric partial oxidation is around 2, and this ratio is ideal for downstream processes, in particular methanol and FT synthesis. This avoids the need to reverse shift hydrogen, which is produced in excess in steam reforming.
- The product gases from methane partial oxidation can be extremely low in carbon dioxide content, which must often be removed before synthesis gas can be used downstream.
- Partial oxidation technology avoids the need for large amounts of expensive superheated steam. However, an oxygen separation plant, which is also costly, may be required in cases where nitrogen (from air) is undesirable in high-pressure downstream processes.

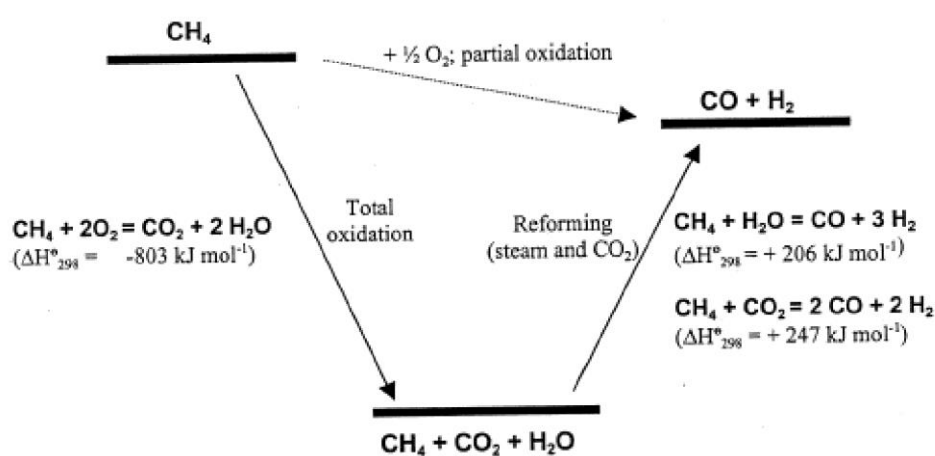


Figure 24. Thermodynamic representation of the partial oxidation of methane.

1.6 Aim of the Work

A *new process architecture* is proposed to produce syngas from methane partial oxidation where reaction steps are integrated with different types of membranes for O₂, H₂ and CO₂ separation (Figure 25).

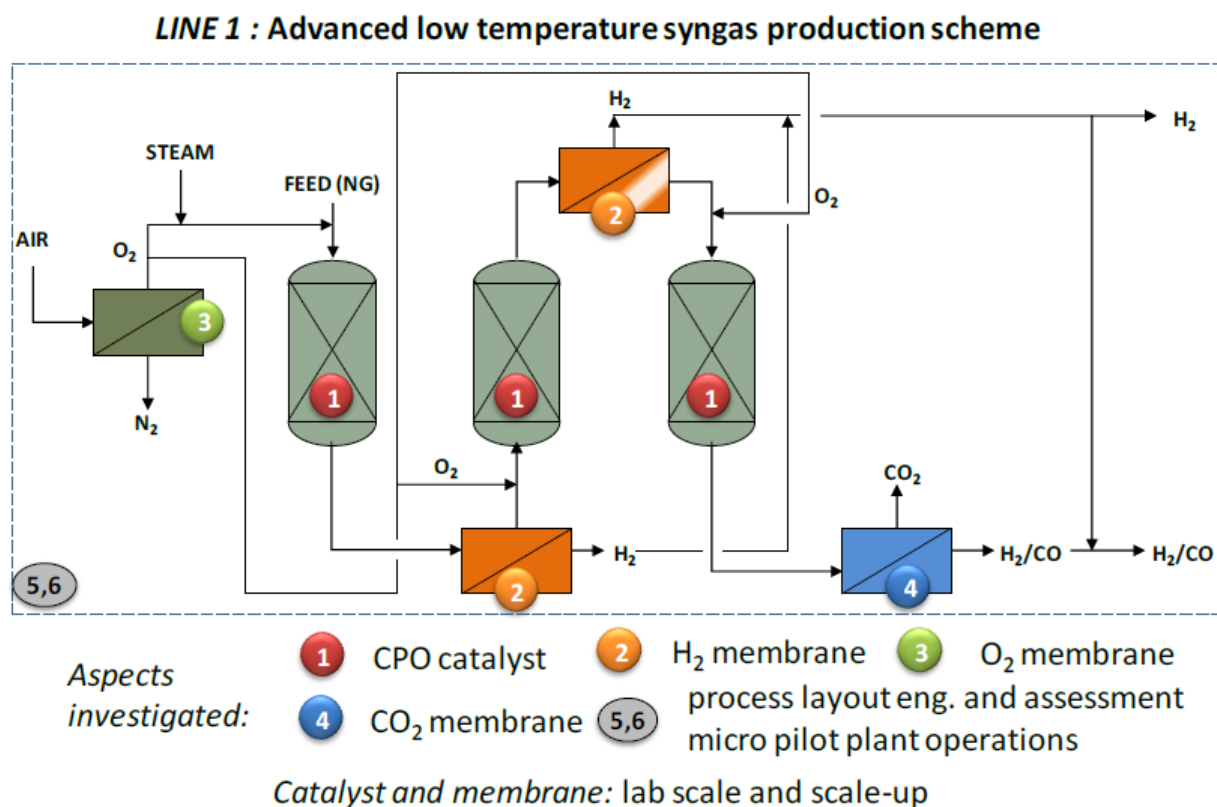


Figure 25. Conceptual scheme of the proposed advanced syngas production.

According to the US DOE financing a large project on OTM (oxygen transport membranes), a reduction of 30% of costs is to be expected, based on such a design. The use of membrane reactors allows enhancing feed conversion at lower temperature in the range of 600-700°C, because the selective removal of hydrogen from the reaction environment enables the multistep integrated process to overcome the thermodynamic equilibrium conversion of a single step process carried out at higher temperature. The development of the multistage reactor with only the intermediate hydrogen membrane separation can allow a reduction of operational cost of 13% with respect to the CPO process that is the best case for syngas production

Lowering the reaction temperature will in turn reduce the oxygen demand and together with air membrane separation not only improves the overall energy efficiency of the process but also reduces the plant capital investment. The splitting of oxygen feed rate over two or more reactors minimizes also the thermal shock on the monolith and catalyst sintering which are major pending issues.

Moreover, the installation of the membranes outside the reactor simplifies either the reactor mechanical design or the membrane geometry.

The new scheme allows operating at mild conditions, with improved life-time of the catalysts, minimized overall energy consumption for syngas production and eventually production of H₂ and CO₂ side streams which can be used for other reactions.

Such a conceptual membrane reactor scheme derives from recent experience developed by TECHNIP/INSTM in combination with other partners in the frame of a large national project to develop a membrane reactor architecture unit for producing H₂ from steam methane reforming. Other firms and academic expertise on membrane are integrated here to address this more complex scheme for syngas production, under the TECHNIP company leadership. Together with the development of a proper process scheme with heat or material balance for large capacity applications, an experimentation from lab scale to pilot plant unit is also programmed to test such a concept. The innovative aspects of the process can be summarized as follows:

- Use of permselective H₂ membranes to allow operations at low temperatures (600-700°C); at these temperature, the overall energy efficiency is higher (at the usual reaction temperature, i.e. higher than 900°C, the performance are governed by heat transfer limitations), the problems of stability for CPO (catalytic partial oxidation) catalysts are largely eliminated and new catalysts formulations could be adopted; the scheme allows thus the development of a catalytic process of syngas production, for which commercialization has previously been hindered due to lacking catalyst stability.
- Introduction of permselective O₂ membrane to enrich oxygen feed and reduce the costs of air separation, one of the more costly components of the overall GTL process.
- Use of permselective CO₂ membranes to separate carbon dioxide to reduce greenhouse gas emissions and allow its reuse.
- A process layout feasible for applications in remote areas (stranded methane).
- Experimentation both at the lab scale and micro pilot plant unit.

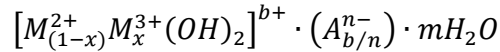
2 EXPERIMENTAL SESSION

In this chapter will be described the synthesis routes for the catalysts production, the laboratory plant with the operating guidelines and the techniques for the characterization of catalysts.

2.1 Synthesis of Catalysts from Hydrotalcite Type Precursors

The route for the production of the catalysts follows these general steps:

Synthesis by coprecipitation method of hydrotalcite type precursor with general formula:



with: $M^{2+} = Mg^{2+}$ and/or Ni^{2+}

$M^{3+} = Al^{3+}$ and/or Rh^{3+}

$A^{n-} = CO_3^{2-}$

1. Calcination step for generation of mixed oxides phases
2. Shaping of the powder
3. Formation of the active phase by reduction with diluted hydrogen.

2.1.1 Co-precipitation Method for Synthesis of Hydrotalcite-type Precursors

The method consists in a simultaneous precipitation of metals hydroxides at controlled pH and temperature.

1. Preparation of aqueous solution (1.5M) of the nitrate of the desired metals cations:
 - $Mg(NO_3)_2 \cdot 6H_2O$ (99%, *Sigma Aldrich*)
 - $Al(NO_3)_3 \cdot 9H_2O$ (98%, *Sigma Aldrich*)
 - $Ni(NO_3)_2 \cdot 6H_2O$ (99%, *Sigma Aldrich*)
 - $Rh(NO_3)_3$ (10%w/w, *Sigma Aldrich*)

The solution with cation is stored in a separatory funnel.

2. Preparation of aqueous carbonate solution (4 times in excess with respect to the amount required by the stoichiometry)

- $Na_2CO_3 \cdot 10H_2O$ (99% Sigma Aldrich)

The solution is stored in a becker glass.

3. The pH of the solution with anion is adjusted to a pH value of 10.5 with nitric acid while the temperature is maintained in between of 50-60°C under vigorous magnetic stirring.
4. The cations solution is slowly dropped in the anion solution keeping the pH value at 10.5 ± 0.1 with simultaneous dropping of a solution of NaOH 3M. The temperature is maintained constant in between of 50-60°C, the system is constantly under vigorous magnetic stirring. Once the dropping of the cation solution is finished, the dispersion is maintained under stirring at constant pH (10.5) and temperature (50-60°C) for 45 minutes.
5. The solid is separated from the mother liquor by vacuum filtration then washed with abundant hot water (60°C) until nitrate free. The solid is dried at 100°C overnight then grinded in order to obtain a fine powder.

2.1.2 Calcination Procedure

The fine powder obtained in 2.1.1 is thermally treated for obtain a mixture of oxide powder. The sample is placed in a temperature programmed oven in which the sample is maintained at 900°C for 12h. The set point is reached increasing the temperature 10°C/min. After 12h the sample is cold down to room temperature, both the weight and the volume are reduced.

2.2 Synthesis of Impregnated Catalyst

In this method of preparation of catalysts the active phase is introduced on the support after the synthesis of the support itself by impregnation of a solution containing a salt of the active phase then the solution is dried and the salt of the active phase remains inside the pores of the support; a thermal treatment is necessary for stabilize the active phase on the support generating the oxide of the active metal. In this work only the Incipient Wetness Impregnation method have been used.

2.2.1 Incipient Wetness Impregnation (IWI)

The IWI is a method in which the amount of solution used for the supporting active phase is only the volume of solution corresponding to the volume of the pores of the support. The

volume of solution needed to fill all the pores is called Water Uptake (WU), is different for each material and is necessary to know before the impregnation in order to prepare the correct starting impregnation solution [84] [85]. The WU is measured by slowly dropping water (or another solvent but the same of the impregnation) on a known amount of support keeping it mixed with a spatula. When the drop will form a kind of mud and will not be absorbed this means that the pores are filled and the volume of water used is the water uptake. The procedure for the production of the supported catalyst is as follows [86]:

1. Take the weight of the support
2. Prepare the volume of solution with the correct amount of salt containing the precursor of the active phase
3. Drop slowly the solution mixing the powder with a spatula in order to impregnate all the pores
4. Once the dropping is complete dry the solid at 120°C overnight
5. Calcine the solid for 12h at 500°C.

2.3 Laboratory Plant Description

The reactions were carried out in two different reactors. Both materials and dimensions are different in order to focus the study on a particular aspect of the reaction itself or on the effects of the scale up and on the supporting of the catalyst. The A-reactor is a 500mm long INCOLOY 800HT tube with an internal diameter of 10mm and an external diameter of 28mm; it can work up to 1000°C and 20bar. The B-reactor is a 500mm long quartz tube with an internal diameter 26mm; it can work up to 1000°C at 1bar. All the reactors are filled as fixed bed reactor.

The desired amount of catalyst is placed inside the reactor as the scheme showed in a zone in which the temperature of the oven is constant and defined. Inside the reactor is also inserted a thermocouple shell type K thermocouple inside used for measure the temperature along the catalytic bed. Inert phase before the catalyst is used for different purposes:

- Static mixer for fuel and oxidant
- Prevent explosion
- Homogenize the temperature of the gas

The reactor is placed inside an electric oven which can reach temperature up to 1150°C.

The laboratory plant showed in could be subdivided in three zone for simplicity of explanation:

1. Feeding zone
2. Reaction zone
3. Post-treatment and analysis zone

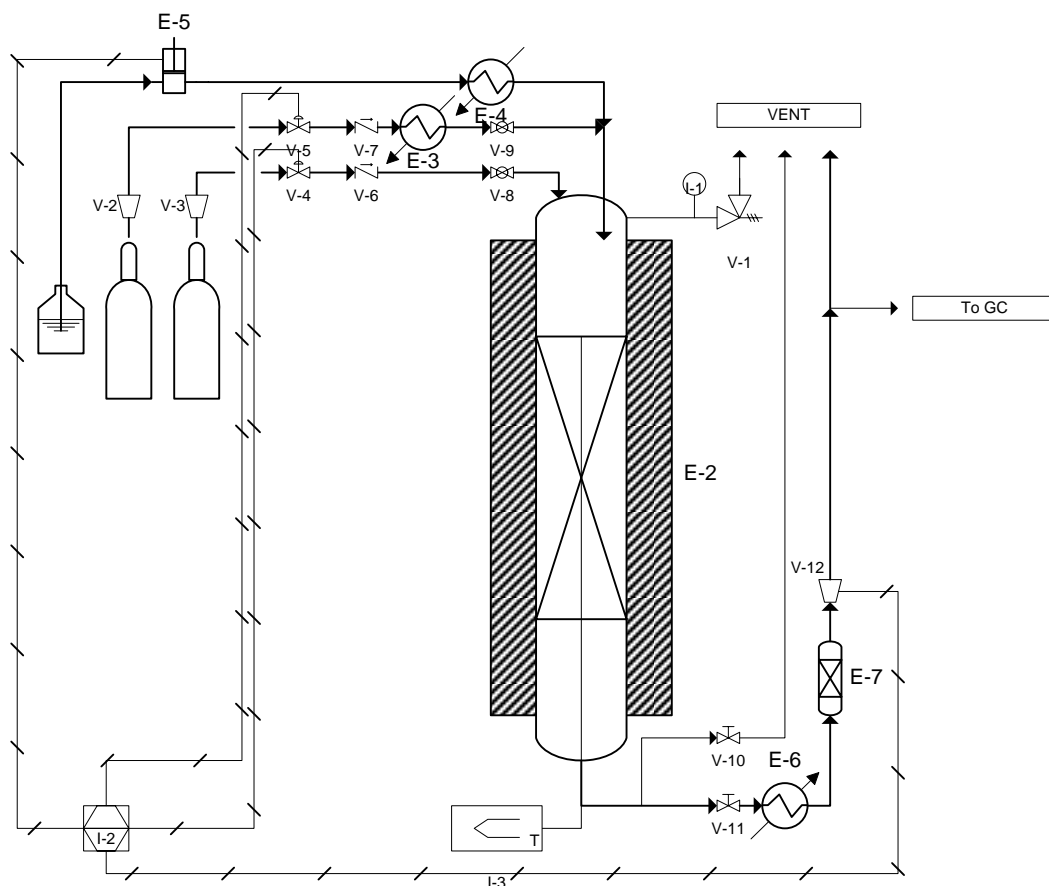


Figure 26. Flow-sheet of the laboratory scale plant.

In the first zone each bottle of gas (CH_4 , O_2 , H_2) is connected to a mass flow controller by a two stage pressure regulator followed by a check valve; mass flow controllers are regulated by a central electronic unit. Deionized water is stored in a plastic vessel and pumped in a vaporizer by an HPLC pump then mixed with the hot O_2 stream. Methane is direct injected in the upper part of the reactor while the overheated vapor mixed with oxygen is injected on the reactor in the part already filled with inert in order to avoid explosion inside.

In the third zone the outlet stream is cold down to ambient temperature then dried and split into three streams, one directed to the vent while the other two to directed to the gas analysis system. The gas analysis system consisted into two gas chromatographs, one dedicated to

the hydrogen quantification (Thermo Scientific Focus GC, Restek packed column Shincarbon ST 100/120 2m x 1mm, TCD detector, N₂ as carrier and reference gas) while the second one dedicated to the quantification of CH₄, CO and CO₂ (Perkin Elmer Clarus 500, Perkin Elmer packed column Carbosphere 80/100 6ft x 1/8inch, TCD detector, He as carrier and reference gas).

2.4 Description of Experiments

The volumetric ratio of the of the feed mixture was decided in collaboration with Tecnimont KT simulating the real feed which will be used in the pilot plant and in the industrial plant.

	Wet %	Dry %
CH ₄	52	82
O ₂	11.2	18
H ₂ O	36.8	//

Table 4. Composition of inlet stream

From the composition is possible to calculate the steam to carbon ratio and oxygen to carbon ratio:

- S/C: 0.7
- O₂/C: 0.22

The O₂/C ratio is calculated considering only the free oxygen of the stream while if we take in consideration the total amount of oxygen in the stream the O₂/C ratio become 0.57, a value typical for classical CPO reaction. The temperature for the reaction is fixed to 750°C, the pressure can be changed from 1 to 20bar and the GHSV can be changed from 24'000h⁻¹ to 100'000h⁻¹.

For each day of work no more than three tests were possible due to the time of stabilization and due to the analysis time. During a set of tests, the first test is periodically repeated. These tests, also called reference tests, are used for evaluate the activation or the deactivation of the catalyst comparing the performance with the first test after several hours of work.

The start-up of the plant follows some few rules in order to do not create variation of activity due to an incorrect procedure. Starting from a new load of catalyst not calcined:

1. Open all the vent valves and isolate the post treatment and analysis zone

2. Feeding N₂ then startup heating up to temperature of reduction
3. Open the valves of H₂ and leave the reduction process go on overnight
4. Close the H₂ valve
5. Set up the reaction temperature
6. Set the values for the CH₄, H₂O and O₂ the close the N₂ valve while open the CH₄ valve then the valve of H₂O and the valve of the O₂
7. After 10 minutes close the Vent_1 valve and then open the post-treatment and analysis zone
8. Close the other vent valves and start with the analysis

2.5 X-Ray Diffraction (XRD) Analysis

The XRD powder analyses were carried out using a Philips PW1050/81 diffractometer equipped with a graphite monochromator in the diffracted beam and controlled by a PW1710 unit (Cu K α , $\lambda = 0.15418$ nm). A 2θ range from 5° to 80° was investigated at a scanning speed of $70^\circ/\text{h}$.

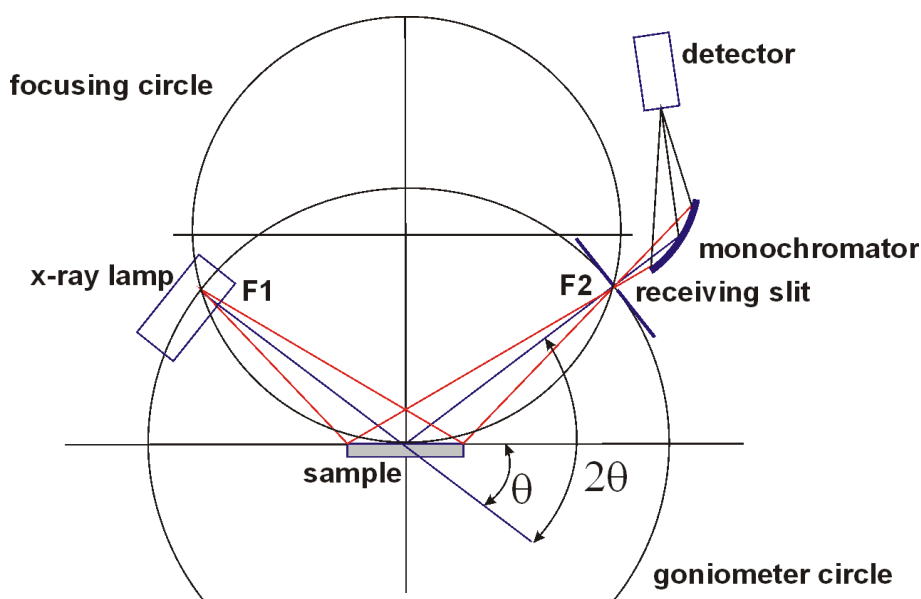


Figure 27. Scheme of the instrument for the X-ray diffraction analysis

The analysis of the phases present in the patterns were analyzed using the Bragg's Law:

$$n\lambda = 2d\sin\theta$$

in order to calculate the d values to compare with those reported in the literature [Powder Diffraction Files - Inorganic Phase, ICDD (International Centre for *Diffraction Data*)]. In addition, the particle sizes are calculated using the Sherrer's Law:

$$D = \frac{k\lambda}{\cos\theta\sqrt{B^2 - b^2}}$$

2.6 Surface Area and Porosimetry Analysis

Specific surface area and porosimetry analysis were carried out in a Micromeritics ASAP 2020 instrument (Accelerated Surface Area and Porosimetry System). This instrument measures the adsorption and desorption isothermal curve (at 77 K) by the volume of adsorbed/desorbed N₂, as a function of relative pressure (via-multi-point method).

BET analyses were performed for the precursors of catalysts and for calcined catalysts. The precursors were previously degassed under a vacuum at 120 °C until a pressure of 30 mmHg was reached and maintained for 30 min. Calcined solids were heated up to 150 °C until a pressure of 30 mmHg was reached, then kept 30 min at this temperature and finally heated up to 250 °C and maintained for 30 min.

Each analysis required about 0.3-0.5 g of catalyst sample.

2.7 Temperature Programmed Reduction (TPR) and Oxidation (TPO) analysis

The reduction and oxidation profiles have been measured using a ThermoQuest Instrument TPD/R/O 1100 Catalytic Surface Analyzer. The analyses were carried out loading 0.1 g of sample, using the following procedure:

- **Pre-treatment** : the sample was pre-treated under N₂ (20mL*min⁻¹) from room temperature to 150°C (temperature rate of 20°C*min⁻¹) and hold for 30 minutes at 150°C.
- **Reduction** : after cooling until 100°C, the reduction analysis was carried out with 5% of H₂ in Ar (20mL*min⁻¹) from 60 to 950°C (temperature rate of 10°C*min⁻¹) and hold for 30 minutes at 950°C.

2.8 H₂ Chemisorption Analysis

The instrument used for the H₂ chemisorption analysis is a ASAP 2020C (Micromeritics) in which the analysis were carried after a pre-treatment under vacuum at 100°C, reduction with a H₂ flow at 750°C for 2hours and again vacuum treatment at 740°C for 2h for the cleaning of the surface of the catalyst. The analyses are carried out at different H₂ pressure and 35°C. The H₂ chemisorbed is calculated from the difference of two consecutive analyses: in the first the

measured adsorbed H_2 correspond to chemisorbed and physisorbed H_2 , while in the second to H_2 only physisorbed.

2.9 Scanning and Transmission Electron Microscopy Analysis

A high-resolution scanning electron microscope equipped with a Field-Emission Gun FEG-SEM (JEOL-6700F), equipped with an EDS detector (PGT Spirit, Si(Li) diode detector), was used to observe the microstructure of the surface and of the bulk of alumina foam after coating. Samples were prepared by attaching the foam struts to brass sample carriers with a silver paste.

Transmission Electron Microscopy (TEM, JEOL 2010), combined with Energy Dispersive X-ray Spectrometry (EDS) was used to study rhodium particle size before and after reaction. Before measurement every sample was reduced under H_2 .

2.10 Infrared (IR) Spectroscopy Analysis

For the IR spectroscopy characterization the powder was pressed in a thin self-supported pellet, placed inside a gold hand-made envelope and located in the IR cell (Figure 28).

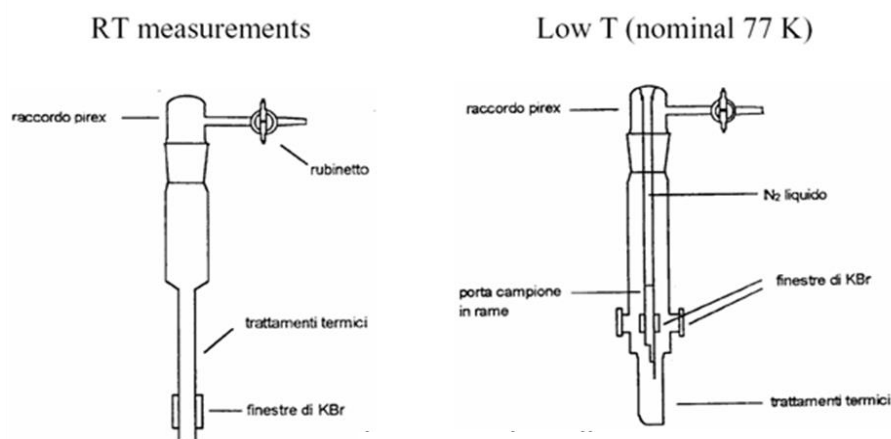


Figure 28. Self-made cells for IR measurements.

The IR cell allows thermal treatments in vacuum as well as in presence of gas at controlled pressure (static conditions) in the temperature range 20-800 °C.

After thermal or reduction treatment the sample was cooled down and IR spectra were collected on a Bruker IFS 55 Equinox instrument equipped with an MCT cryodetector working with 2cm^{-1} resolution. The dosing of gas/vapours was carried out by connecting the IR cell to a vacuum ramp, equipped with one Pirani vacuum gauge and one manometer. In a typical

adsorption measurement, a set of spectra is recorded, where each spectrum refers to a specific gas equilibrium pressure. In order to carry on a comparative semi-quantitative characterization, the spectra are normalized with respect to the sample amount, so that intensities of bands observed for different samples may be used to evaluate the concentration of adsorbed species (and the concentration of adsorbing sites).

Powders were pressed into thin self-supporting pellets and then placed into a quartz IR cell. The activation treatment was carried out by connecting the cell to a vacuum-adsorption frame with a residual pressure below 10^{-3} mbar. In particular, prior to the adsorption measurements, all samples were activated by a treatment in H_2 (200 mbar) at 750°C (heating rate $2.5^\circ\text{Cmin}^{-1}$) for 1h, outgassed under dynamic vacuum at 650°C for 2h and then cooled to room temperature under Ar atmosphere. FT-IR spectra were collected by using a Bruker Equinox 55 spectrometer, equipped with MCT cryodetector, at a spectral resolution of 2cm^{-1} and accumulation of 32 scans. CO were dosed in the pressure range from 0.1 to 35 mbar by connecting the IR cell to a vacuum frame. The interaction with CO was studied both at r.t. and at the nominal temperature of -196°C by using liquid nitrogen as coolant. The actual temperature of the sample is about -173°C , due to the heating effect of the IR beam.

3 RESULTS AND DISCUSSION

In this chapter will be shown and discussed all the tests obtained from experiments performed in the laboratory plant described in 2.3. The aim of this work was to find a new stable and active catalyst for the production of syngas from methane through a new, low temperature, oxyreforming process.

The study can be subdivided into 5 parts

- Identification of the active phase
- Effect of the support
- Effect of the active phase (bimetallic phases)
- Activity of an industrial catalyst
- Scale up of the catalyst

The first three parts will be focused on the pure activity of the self-made catalyst while the other two parts will be focused on the comparison with an industrial catalyst and on the supporting of the self-made catalyst on a possible industrial support as monolith or foam.

3.1 Studies and Selection of the Active Phase

3.2 Hydrotalcite-type Precursors

The hydrotalcite is an anionic clay, called also layered double hydroxide (LDH), of lamellar mixed hydroxides separated from layer of exchangeable anions with general formula: $[M_{(1-x)}^{2+}M_x^{3+}(OH)_2]^{b+} \cdot (A_{b/n}^{n-}) \cdot mH_2O$. The hydrotalcite can be used as precursor of bulk catalyst or support: In that case the prepared material is calcined allowing the lost of water and the anion present in the interlayer (usually carbonate) and producing an homogeneous mixed metal oxide. This metal oxides have several important properties:

- High surface area
- Basic properties
- High stability to thermal treatment material
- Small crystal size of the oxides

To understand the structure of these compounds, it is necessary to start from the structure of brucite, $(Mg(OH)_2)$, where octahedral of Mg^{2+} (6-fold coordinated to OH^-) share edges to

form infinite sheets. These sheets are stacked on top of each other and are held together by hydrogen bonding as shown in Figure 29.

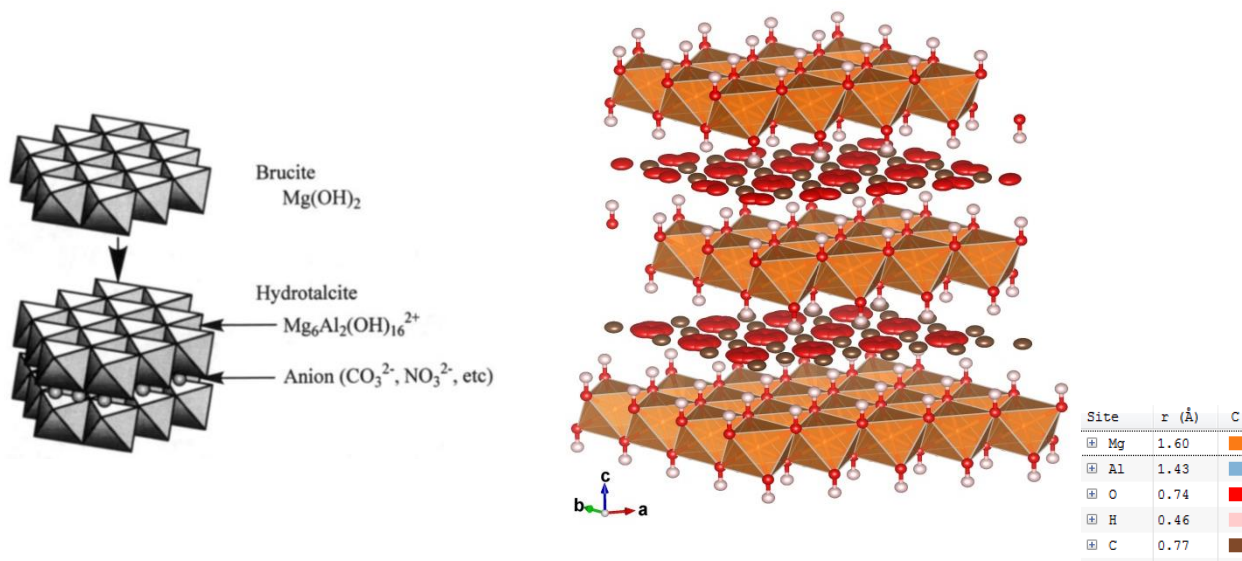
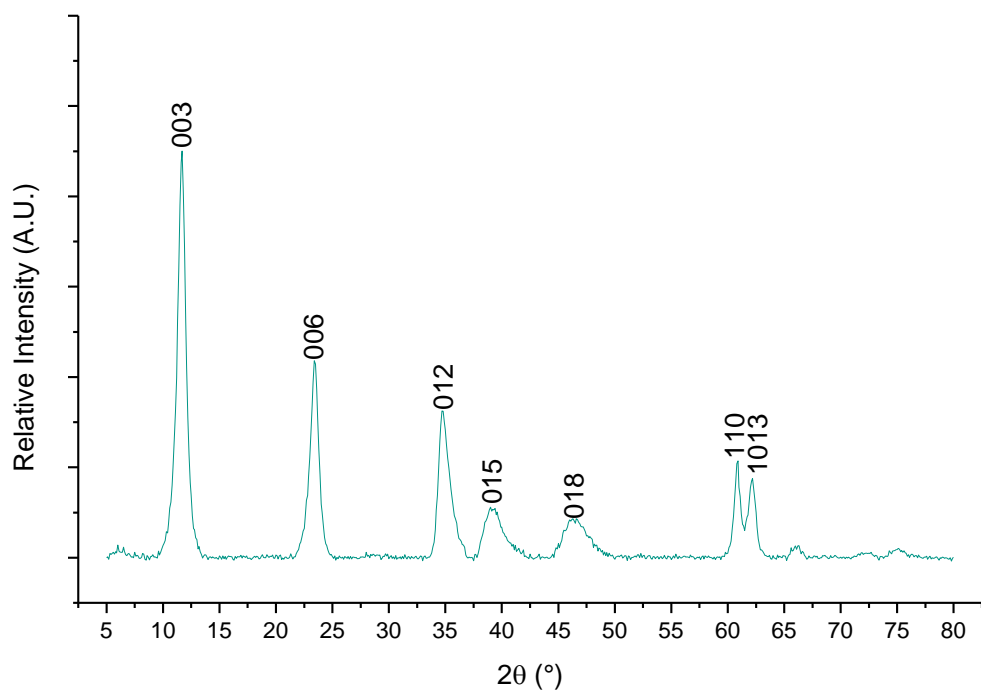


Figure 29. Crystal structure of the hydrotalcite-like compounds [87]left image; [88] right image.

When Mg^{2+} ions are substituted by a trivalent ion having a similar ionic radius (such as Fe^{3+} for pyroaurite and Al^{3+} for hydrotalcite, respectively), a positive charge is generated in the hydroxyl sheet. This net positive charge is compensated by $(\text{CO}_3)^{2-}$ anions, which lie in the interlayer region between the two brucite-like sheets, in the free space of this interlayer the water also finds a place interacting with H-bond with interlayer and brucite layer [87]. In the right picture of Figure 29 the $(\text{CO}_3)^{2-}$ is showed with its indetermination of the position.



Graph 3. XRD pattern of Mg/Al=68/32 HT in which all the planes are indicated on the reflections.

Most of the LDH's are well described by hexagonal unit cell with $a=b\approx 3\text{\AA}$, $c=m*c_0$, $\alpha=\beta=90^\circ$ and $\gamma=120^\circ$ in which m is the number of brucite-like layers in the unit cell and c_0 depends from the type of anion present in the interlayer. For $(\text{CO}_3)^{2-}$ bearing LDHs c_0 is from 7.5 to 7.8Å. [89].

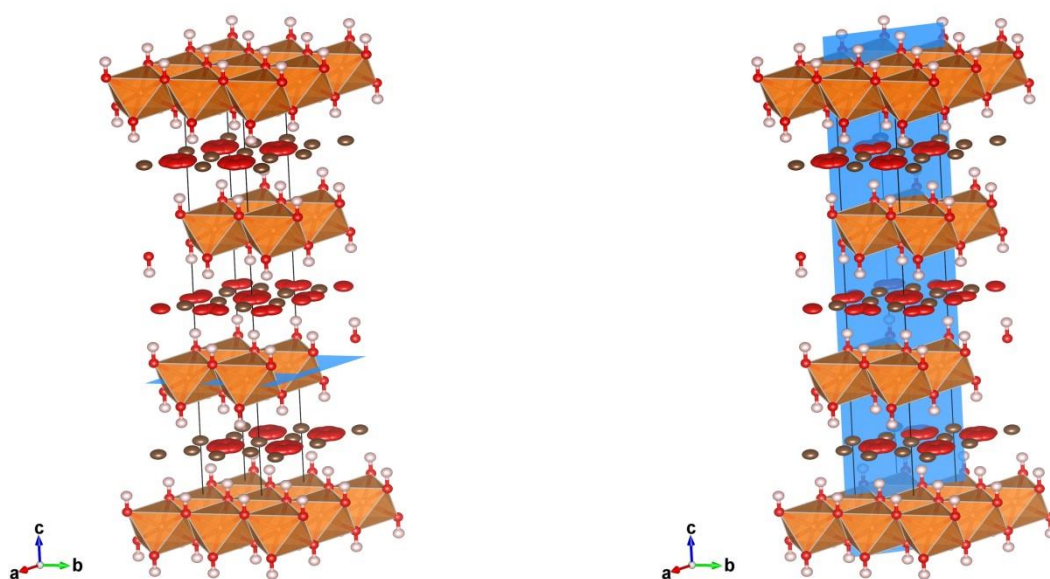


Figure 30. Graphical representation of plane 003 (on the left, $c_0=7.60333\text{\AA}$) and 110 (on the right, $a=b=3.054\text{\AA}$)

Calcination cause deep changes in the structure together with changes in its specific surface area and pore development. The structure collapses at temperature ranging from 200 to 500°C losing water and $(\text{CO}_3)^{2-}$ and forming defective mixed oxide material [90], above this temperature crystallization of new phases takes place. Up to medium calcination temperature (500-600°C) the specific surface area increase due to the water escaping during collapsing of layered structure. Increasing the calcination temperature above 750°C segregation and crystallization of MgO and spinel MgAl_2O_4 take place causing a collapsing of the specific surface area (Figure 31).

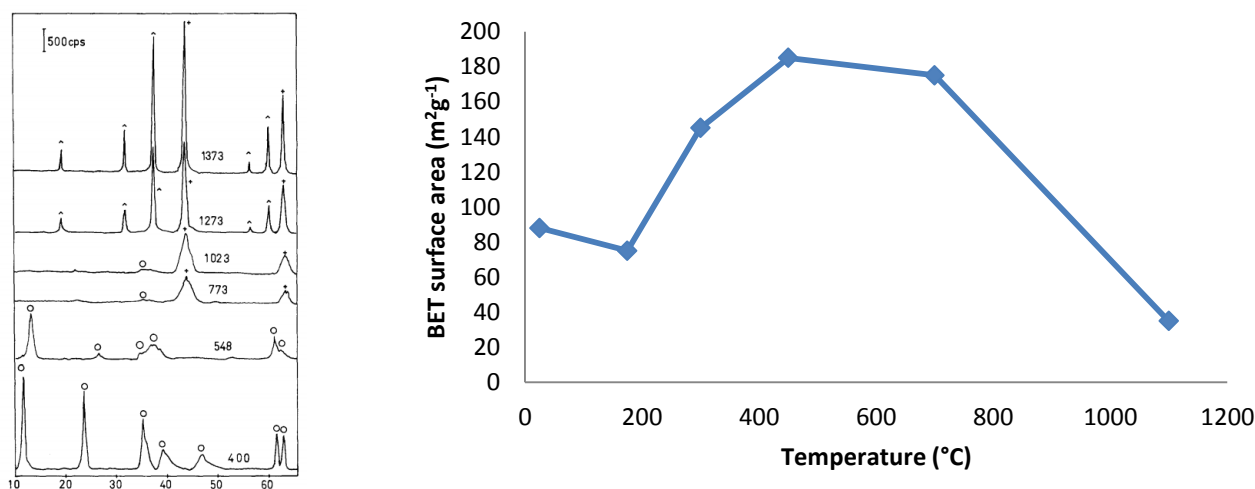


Figure 31. XRD patterns of thermal evolution of Mg/Al/ CO_3 -bearing LDH [91] (on the left relative intensity on the y axis and $^\circ 2\theta$ on the x axis). Specific surface area evolution with temperature for exHT with Mg:Al=80/20 [92] (on the right).

The variation of Mg/Al ratio in the starting HT material causes a changing to the ratio between the MgO phase and the spinel MgAl_2O_4 phase (Figure 32). The MgO phase still contains some Al^{3+} ion and the excess of positive charge is compensated by vacancies in the OH site. The sample prepared in the present thesis have two different Mg/Al ratio and give rise to the following phase distribution.

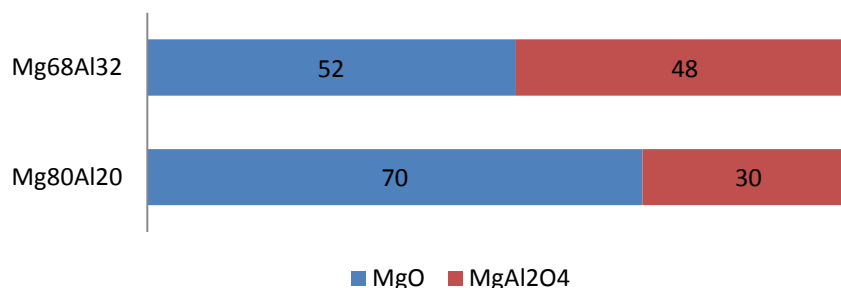
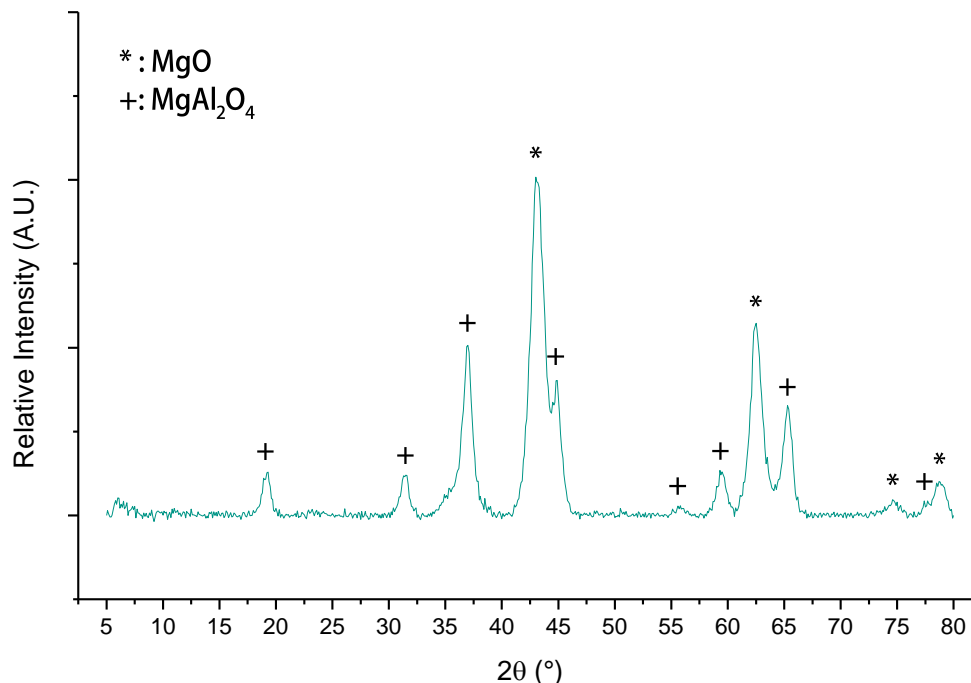


Figure 32. Phase obtained after calcination at 900°C for 12h in static air of Rh1% $\text{Mg}_{80}\text{Al}_{20}$ and Rh1% $\text{Mg}_{68}\text{Al}_{32}$.

Catalyst derived from HT containing Rh, Ni and Rh & Ni are widely studied in literature [93,94,95,96,97] and the study of the material after calcination revealed that the structure is made of MgO phase and of spinel MgAl_2O_4 phase containing the active phase (Graph 4).



Graph 4. XRD pattern of calcined sample (900°C, 12h in air) with Mg/Al=68/32. Phases identified: brucite MgO phase (*) and spinel MgAl_2O_4 (+).

The high activity of the catalyst may be due to the highly dispersed metal particles. Considering the Ni as third metal, on MgAl hydrotalcite precursor, a part of the Mg sites were substituted by Ni, decomposed to Mg(Al)O mixed oxide still containing Ni^{2+} at the Mg^{2+} site. When the mixed oxide was reduced, Ni^{2+} was reduced to Ni^0 migrated to the surface, and crystallized to form fine Ni metal particles on Mg(Al)O mixed oxide as the support. The Ni can be present, in some extent, in the spinel phase substituting the Mg^{2+} with a similar reducing mechanism which nevertheless occur at higher temperature. The amount present in the spinel increase with the Ni loading which increase the Ni reducibility

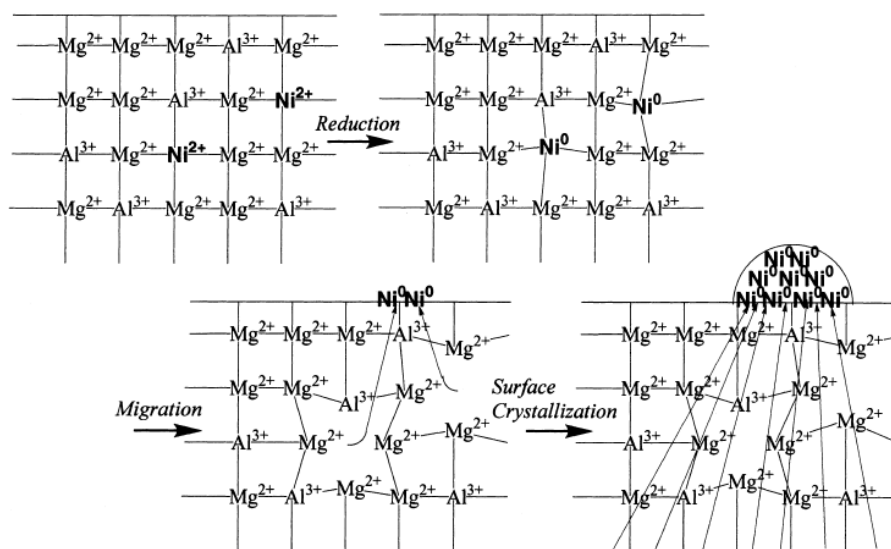


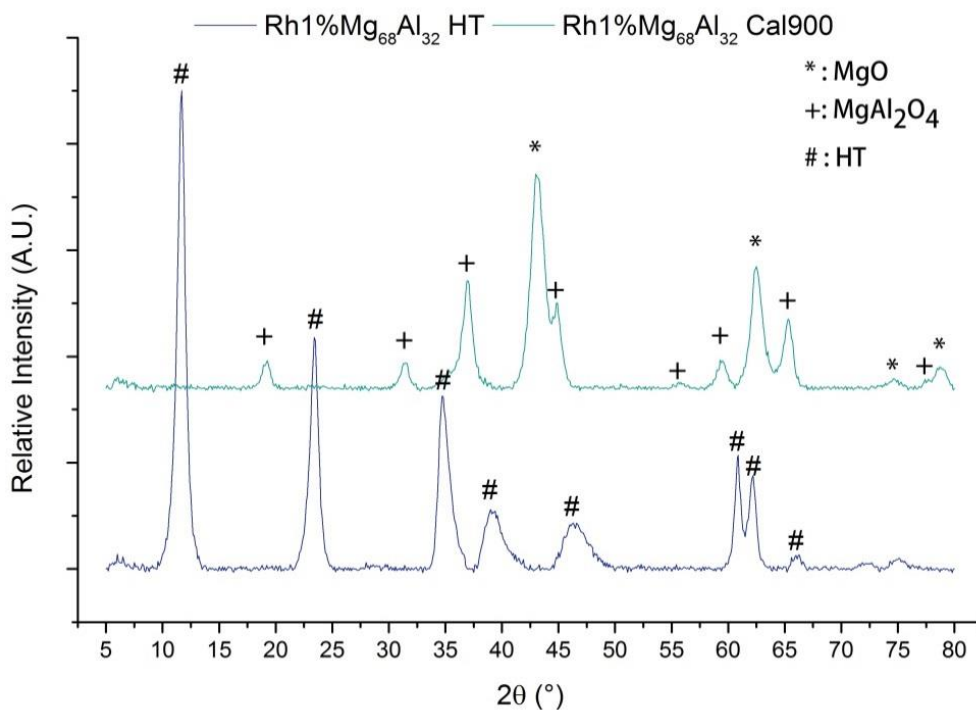
Figure 33. Plausible mechanism of Ni metal crystallization from Mg(Al)O mixed oxide [87]

For the Rh the process could be similar. It is present as Al³⁺ substitute in the HT phase and after calcination the Rh is present either in the MgO phase, in higher extent than Al, than in MgAl₂O₄ phase [98]. The combined (XRD and neutron diffraction) Rietveld analysis, carried out on a Rh³⁺:Mg²⁺:Al³⁺=5:71:24 sample allowed to identify the position of Rh, Mg and Al in the calcined samples. It shows that after calcination at 650°C the (Mg/Al)O cubic phase is a defective rock salt phase in which part of the Mg occupies tetrahedral sites [99,100]. By calcination at 900°C this phase is less defective and closes to an ideal MgO phase nevertheless, some Al and Rh are still present. The analysis of the Rh distribution shows that, Rh was more concentrated in a spinel-type phase, even if the MgO phase was more abundant (69%), as a consequence, the Rh amount in the two phases was similar (59% in the MgO and 41% in the spinel phase).

3.2.1 Characterization of Rh 1% MgAl samples

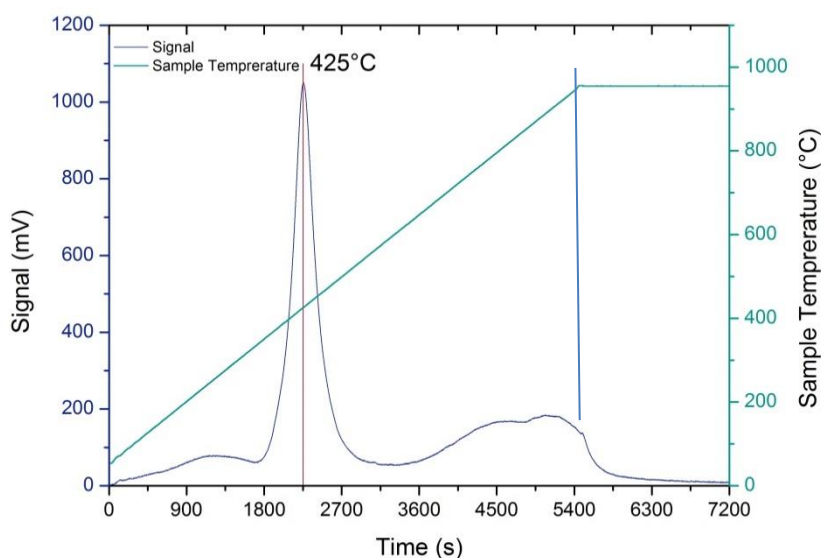
3.2.1.1 Rh1% Mg₆₈Al₃₂

The catalyst has been prepared by co-precipitation route then calcined at 900°C for 12h. The XRD analysis of the sample before calcination shows a typical pattern for an HT precursors in which the active metal is not directly detectable due to its homogeneous dispersion in the HT phase more than its low concentration. This is confirmed by the XRD of sample with high Rh concentration (Rh 5% a.r.) in which Rh phase are still not present. The calcined sample shows only two phases: MgO and MgAl₂O₄ in which the third metal is solved.

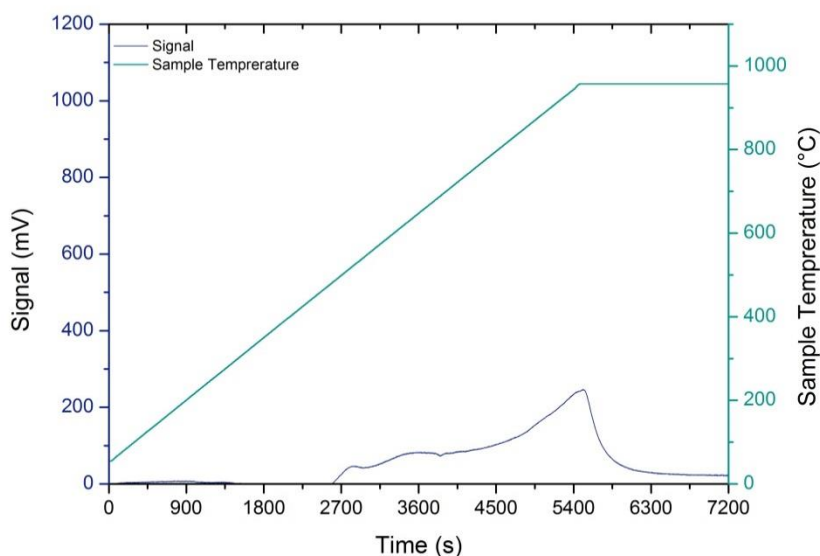


Graph 5. XRD patterns of HT precursor and calcined sample.

The TPR analysis in Graph 6 shows an intense H₂ consumption at 425°C (2'250s) and a shoulder from 3'600 to 5'600s that can be attributed to Rh in the structure even if it is overlapped with the instrumental base line shown in the analysis carried out on a sample not containing Rh in the starting material (Mg₆₈Al₃₂) (Graph 7).

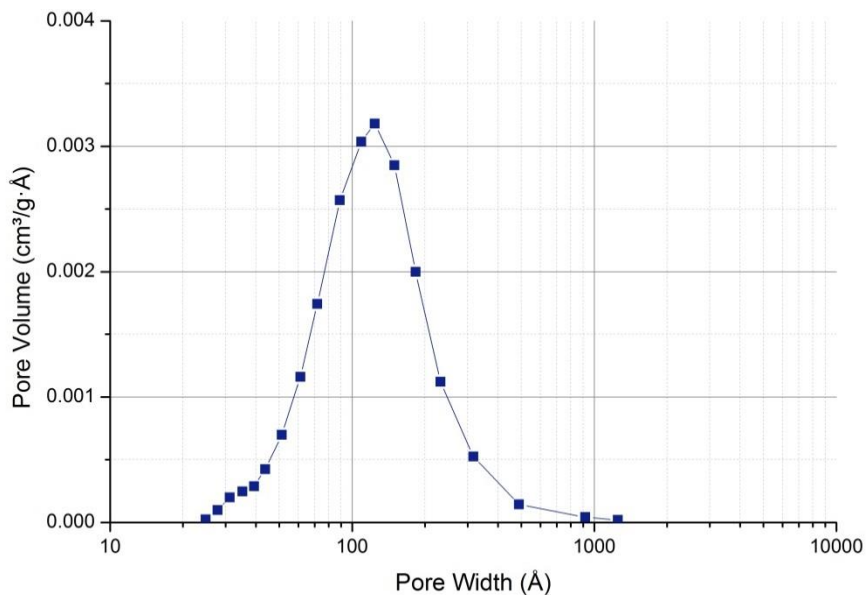


Graph 6. Temperature programmed reduction of Rh1%Mg₆₈Al₃₂exHT.



Graph 7. Temperature programmed reduction of $Mg_{68}Al_{32}exHT$.

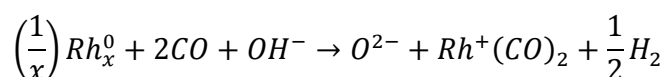
The pore size distribution of Rh1% $Mg_{68}Al_{32}exHT$ sample shows mainly monomodal and quite broad pore distribution curve around 10nm; BET surface area is $124m^2g^{-1}$.



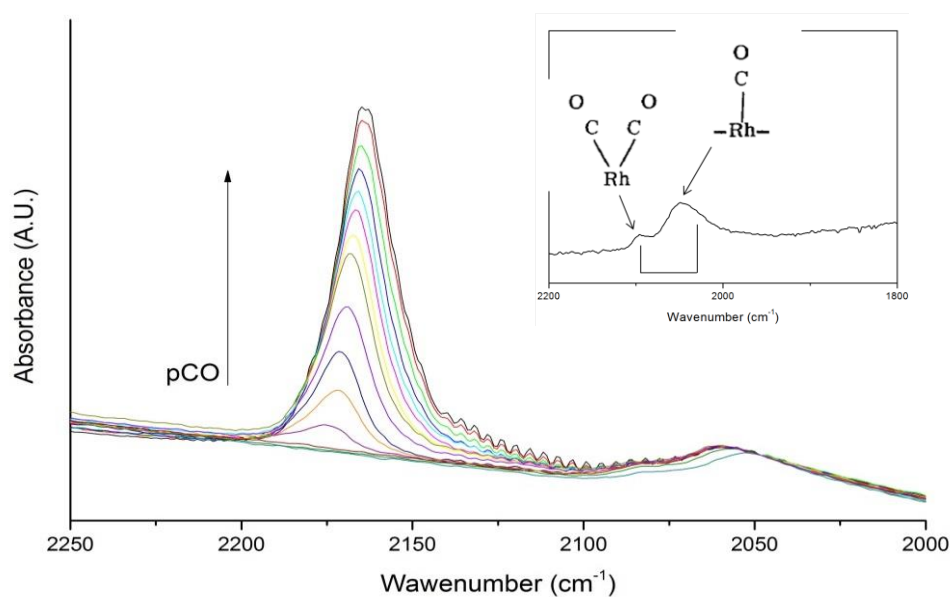
Graph 8. BJH pore size distribution of fresh Rh1% $Mg_{68}Al_{32}exHT$.

IR spectroscopy of the adsorbed CO is widely used to characterize Rh supported catalyst [101,102,103,104,105,106] and has been studied in order to evaluate the properties of the Rh present on the surface of the different catalysts and then understand the effect of the matrix on the activity of the catalyst. After reduction three kind of chemisorbed CO are detectable

identifying three different Rh sites: linear monocarbonyl species, $Rh^0(CO)$, bridging CO species, $Rh^0_2(CO)$, and gem-dicarbonyl complexes on oxidized Rh sites, $Rh^1(CO)_2$. The detection of the latter is considered significant for the existence of highly dispersed Rh, whereas linear and bridged carbonyl species are usually considered to form on extended Rh surface [101,103,105]. The existence and the formation of $Rh^1(CO)_2$ is still under debate in literature but it has been suggested that Rh-Rh bonds can be disrupted at room temperature and under CO pressure due to the higher energy of the Rh-CO bond as compared to the Rh-Rh one [107] in small Rh_x particles. The process of formation is described to be:



In which O^{2-} chemisorbed should be produced and also involvement of OH^- species [105] [108] [109].



Graph 9. IR spectra of Rh1% $Mg_{68}Al_{32}$ at different pressure of CO.

At very low pressure of CO only two bands are identified at $2'050cm^{-1}$ and at $2'080cm^{-1}$ the first attributed to linear chemisorbed carbonyl, $Rh^0(CO)$, while the latter is attributed to $Rh^1(CO)_2$.

Increasing the pressure of CO on the cell sample another band appears at $2'175cm^{-1}$ that is shifted at $2'160cm^{-1}$ when pressure is higher. This band is attributed to the CO interacting with the atoms of the support in particular unsaturated octahedral Al sites and unsaturated Mg sites that are medium acidic Lewis site. The band at $2'050cm^{-1}$ is shifted at $2'060cm^{-1}$ due to

the dipole coupling between adjacent chemisorbed CO molecules. No variation in the OH stretching region has been observed so the mechanism of formation of $\text{Rh}^1(\text{CO})_2$ cannot be proved. Bridging CO species, $\text{Rh}^0_2(\text{CO})$, has not been observed. Disproportion of CO took place (Boudouard reaction: $\text{CO} + \text{CO} \leftrightarrow \text{CO}_2 + \text{C}$) observed indirectly with the formation of carbonate species ranged from 1750cm^{-1} to 1200cm^{-1} (not shown). Basile et al [110] studied also the same catalyst at higher temperature of reduction (950°C) obtaining similar conclusion but they observed the formation of bridging CO species, $\text{Rh}^0_2(\text{CO})$, a less intense $\text{Rh}^1(\text{CO})_2$ band with a small disproportion effect. This effect is due to the growth of the Rh crystals by the increased temperature causing a different ratio between $\text{Rh}^1(\text{CO})_2$ and $\text{Rh}^0_2(\text{CO})$.

3.2.2 Catalytic Tests

3.2.2.1 Comparison of Oxy-Reforming with Steam Reforming and CPO conditions

The process is characterized by the contemporary presence of steam reforming and catalytic partial oxidation. Both the reactant, H_2O and O_2 , are present in sub-stoichiometric ratio with respect methane therefore the two reaction are pushed to occur already in the first part of the bed if not simultaneously. In particular the O_2/C ratio is 0.21 while the S/C ratio is 0.7. In terms of atomic ratio the overall O/C ratio is 1.1, just above the stoichiometry for the CO formation while the H/C ratio is 5.4 which means intermediate between the CPO and reforming stoichiometry. The present conditions have two type of consequences:

- 1) The thermodynamic limit of carbon formation is close to the real conditions and in specific have been calculated by the CEA-NASA program. The graph shown the equilibrium composition re-adjusted on a dry bases for an easy comparison with the exit gas analysis. It shown that at 1bar the formation of carbon occur at a temperature below 720°C . The carbon formation limit became narrow at high pressure and are present only among 600 and 700°C with a low amount due to the favorable conditions for the presence of methane.

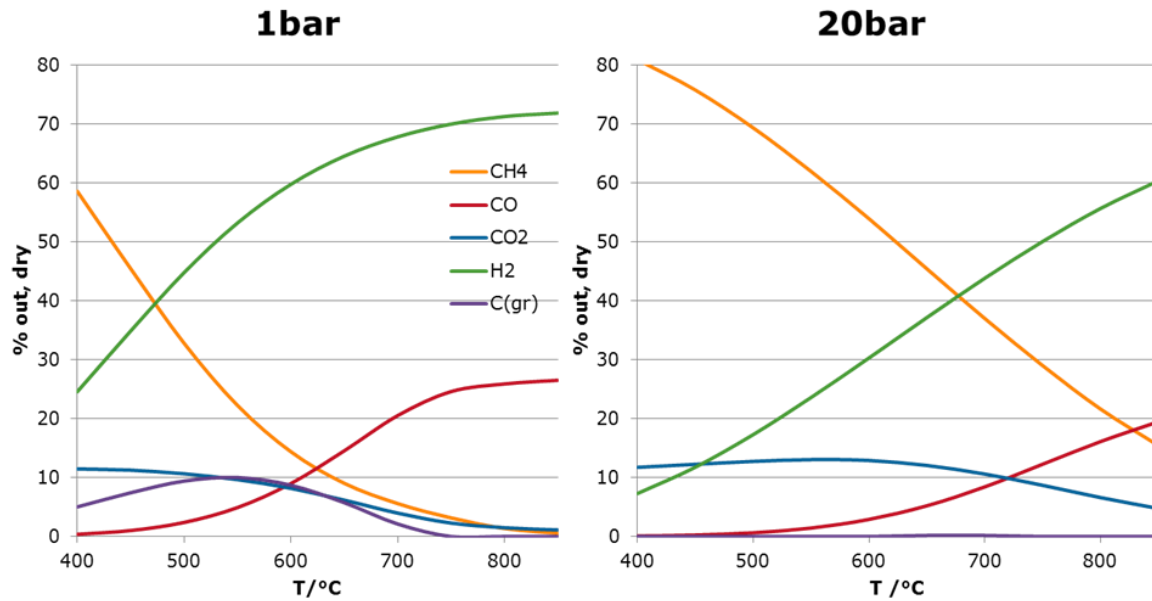


Figure 34. Thermodynamic equilibrium curves calculated with CEA-NASA at 1bar (on the left) and at 20bar (on the right) with real input concentration gases.

2) The presence of oxygen which react very rapidly through oxidation reactions in the very first zone could increase the temperature of the bed is compensated by the water presence which give rise to highly endothermic reforming reaction thanks to the low amount of oxygen present in the so called oxy-reforming process. Therefore at 1bar a small increase of temperature is present followed by a decrease of temperature of less than 30°C at 150ms. The changes in temperature are even smaller at high pressure where the overlapping between endothermic and exothermic reaction increases due to the increasing of the reaction rate (either by increase of reactant concentration and mass transfer rate). This conditions are very different from that generated in the CPO reaction where a temperature increase can easily reach 200-400° and differently from reforming where a ΔT is generated radially in the bed and axially the latter again reaching 200°C due to the limitation of the heat coming from external heating equipment [111]. The significant ΔT , the importance of the heat transfer and temperature profile in the system and along the bed is, in most of the case, the dominant parameter for the catalyst behavior. Therefore a catalyst comparison and ranking is very difficult in real conditions and usually low temperature and high dilution are used to limit these phenomena. Furthermore, it is very difficult to have kinetically controlled performances, since by reducing the residence time the thermal profile changes dramatically. In particular in CPO if the residence time is decreased by changing the flow rate, the increase of heat produced give rise to an increase of temperature and an increase of the conversion is usually observed [112,113]. In the present conditions the axial temperature profile is much less sharp and the

ΔT is limited, furthermore the presence of heat produced inside the reactor by oxidation reaction decreases a radial temperature profile usually present in the reforming reaction. In conclusion the thermodynamic reaction conditions are very favorable for the catalysts comparison differently from reforming and CPO and the comparison have been usually performed having the same oven temperature with a very limited shift of exit gas temperature.

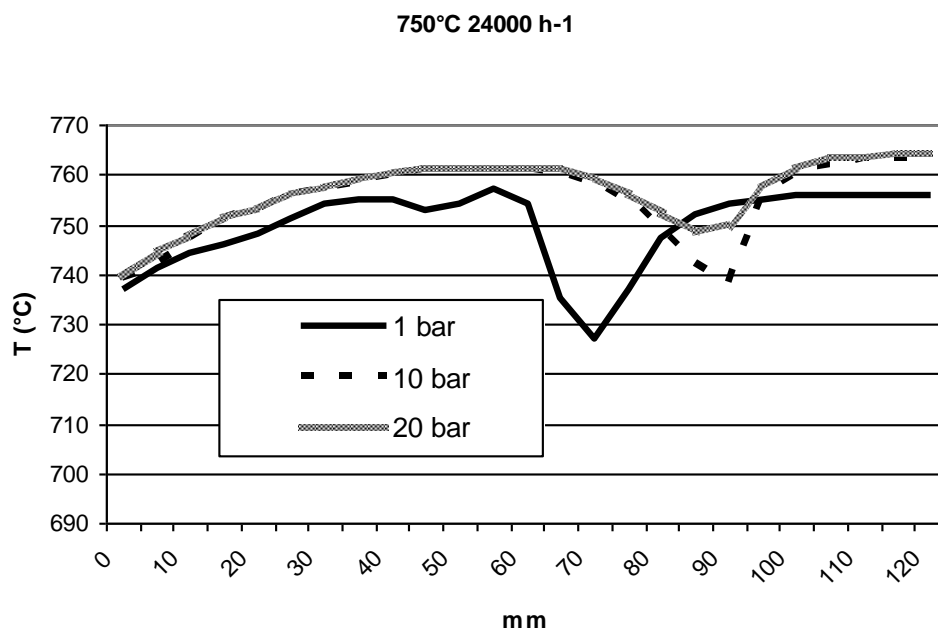


Figure 35. Temperature profiles of the catalytic bed at 24'000h⁻¹ and oven temperature of 750°C at 1, 10 and 20bar.

3.2.2.2 Catalytic Behavior: Rh1% Mg₆₈Al₃₂

The conditions and characteristics of the reaction will be shown and discussed on the sample Rh1% Mg₆₈Al₃₂ that is the most extensively studied in the present research activity. In particular two type of conditions will be used. A low pressure (1bar) condition useful to discriminate among the catalyst and an high pressure condition utilized to confirm the results in real industrial conditions used in NEXT GTL project. The performances of the catalysts are also studied as a function of the residence time and some tests of reforming at low temperature have been carried out to show the possibility of a low temperature multistage process carried out with interstage membrane H₂ separation to simulate the NEXT GTL concept process in different conditions. The graph (Figure 36, left) of the dry composition as function of the gas space velocity (GHSV) shows the increase of the methane exit concentration and the decrease of the H₂ exit concentration while the space velocity increase i.e. the residence time decreases from (150ms to 72ms and 36ms). The comparison of the methane exit percentage calculated from equilibrium show that even at high residence time

the equilibrium is not reached (Figure 36, right). Furthermore considering that the exit temperature from the catalyst bed show only slight changes, the comparison with the equilibrium curve show clearly the effect of a kinetically controlled reaction.

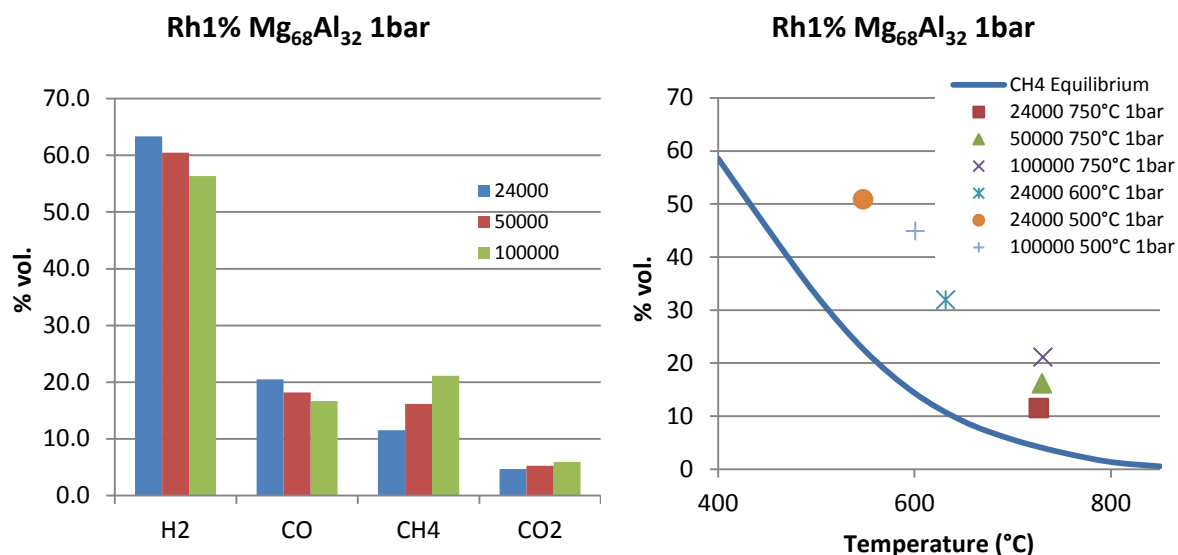


Figure 36. (left) Dry outlet composition at 1 bar at 24'000h⁻¹, 50'000h⁻¹ and 100'000h⁻¹. (right) Comparison of methane outlet with the equilibrium curve. Catalyst for each test: Rh1% Mg₆₈Al₃₂.

By increasing the pressure the exit methane increases and the presence of hydrogen decreases, a further decrease it is observed by increasing the flow rate (i.e. decreasing the residence time) At 20 bar the H₂ content of the dry gas is close to 50% while the methane content is higher than 40% (Figure 37).

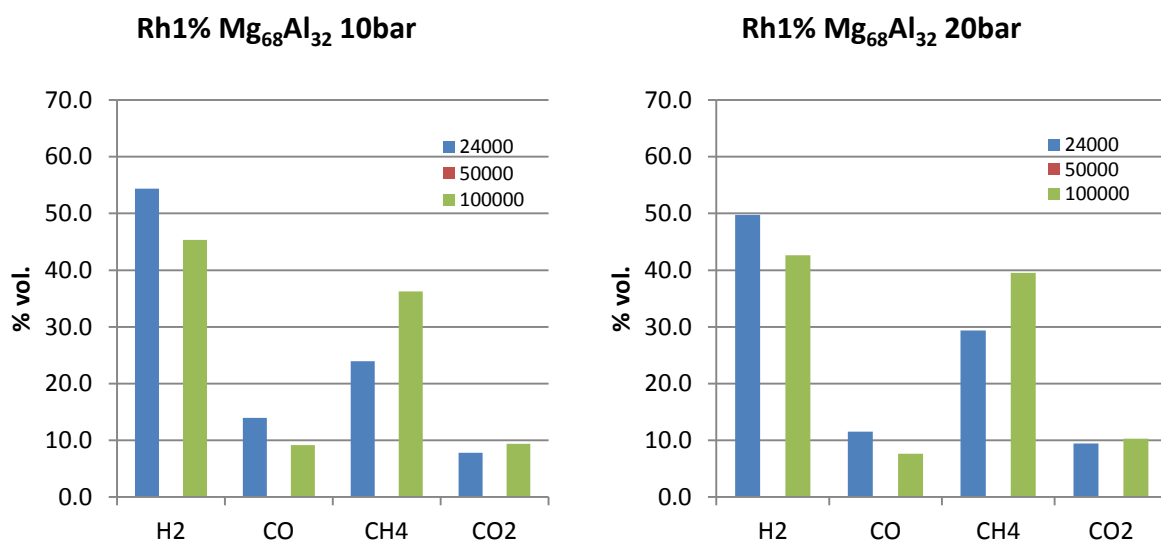


Figure 37. Outlet dry composition at 10bar (left) and 20bar (right) at 750°C with different GHSV: 24'000h⁻¹, 50'000h⁻¹ and 100'000h⁻¹.

The comparison with the equilibrium show that increase methane content as function of the pressure is due to the change of the thermodynamic equilibrium composition. In fact at 20bar and 150ms the equilibrium composition is reached. This is due to the increasing reaction rate by increasing the reactant partial pressure. The differences with flow rate (36ms as residence time) can be mainly correlated with a decrease of the exit gas temperature which change the exit value at the equilibrium. The results show also differences at high residence time with respect to the thermodynamic value this is due by both low residence time and lower bed temperature with respect the high residence time tests. Interestingly at high pressure the results are more close to the equilibrium even at 32ms and therefore this catalyst can be considering as a reference catalyst for the industrial reaction.

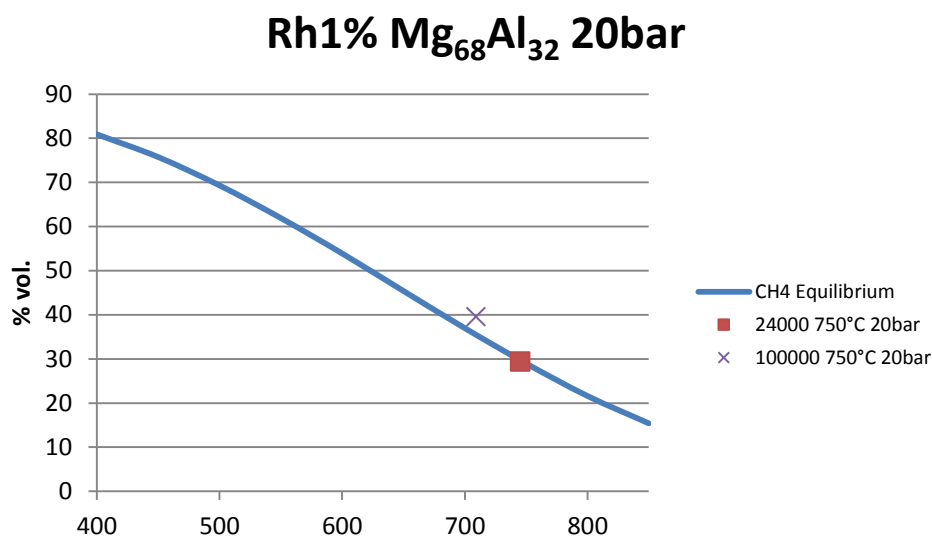


Figure 38. Methane outlet composition compared with the equilibrium curve.

In this conditions (20bar) is also crucial to evaluate the gas temperature profile as function of the gas flow rate due to the fact that the exit temperature change of about 50°C affecting the activity of the catalyst then the conversion of the catalyst.

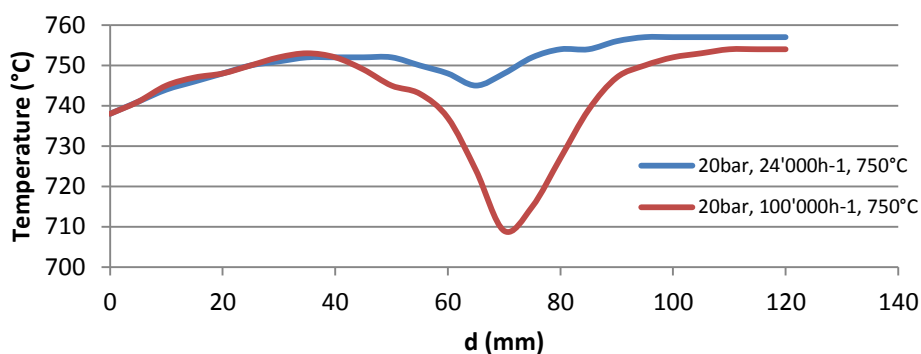


Figure 39. Temperature profiles of the catalytic beds at 24'000h⁻¹ and 100'000h⁻¹.

RESULTS AND DISCUSSION

Some test have been carried out at very high space velocity at $240'000\text{h}^{-1}$ 10atm and $480'000\text{h}^{-1}$ 20atm, i.e. with analogous linear velocity of the tests at 1bar and $24'000\text{h}^{-1}$, the results are far from the equilibrium and the methane conversion decrease nevertheless the thermal effect of the heat released and consumed are important and can affect the results.

The detailed results of the Rh1% Mg₆₈Al₃₂ are also reported in Table 5 with the related methane conversion, product selectivity and H₂/CO ratio for reference and completeness. In table are also reported the tests at 600°C and 500°C at 1bar. The decrease of the temperature give rise to a decrease of the methane conversion as expected by the kinetic and thermodynamic consideration. Interestingly at 500°C increasing the flow rate give rise to a significant increase of temperature and increase methane conversion, similar to the CPO reaction. This is due to the fact that in this conditions the reforming reaction occur less and the reforming rate is lower, i.e. the thermal effect of the oxidation reaction prevail. Furthermore this effect is enhanced by the fact that the external heat delivered by the oven at 500°C is lower therefore the effect of the internal heat produced or consumed are enhanced.

Finally these conditions are not thermodynamically save from carbon formation nevertheless the return tests at 750°C, which repeat the starting tests with the fresh catalyst show quite constant results evidencing high stability with time on stream and with carbon formation of this catalysts.

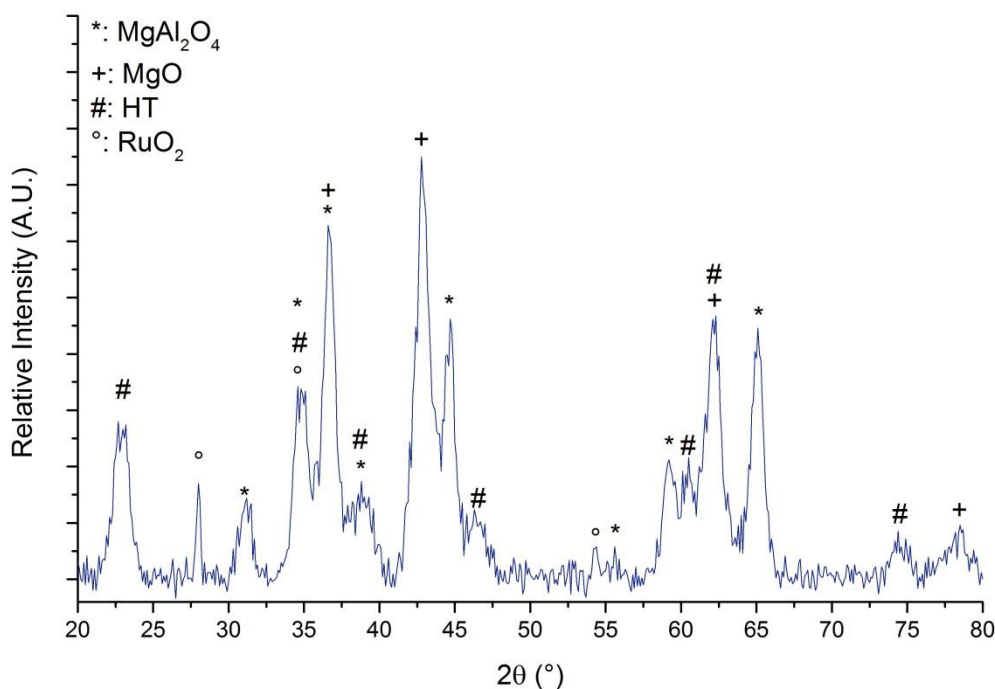
T (°C):	750	750	750	750	750	750	750	750	750	600	500	500	750
GHSV (h-1):	24000	24000	24000	24000	50000	100000	100000	100000	100000	24000	24000	100000	24000
P(bar):	1	10	20	1	1	1	10	20	1	1	1	1	1
H ₂ (%)	63.4	54.4	49.7	63.4	60.5	56.3	45.3	42.6	48.9	34.0	38.8	62.7	62.7
CO (%)	20.5	13.9	11.5	20.4	18.1	16.7	9.1	7.6	8.3	2.8	6.8	21.1	21.1
CH ₄ (%)	11.5	23.9	29.4	12.2	16.1	21.1	36.2	39.5	31.9	50.8	44.8	12.5	12.5
CO ₂ (%)	4.6	7.8	9.4	4.1	5.3	5.9	9.4	10.2	10.9	12.3	9.5	3.6	3.6
Tot (%)	100.0	100.0	100.0	100.0	100.0	100.0	100.0	100.0	100.0	100.0	100.0	100.0	100.0
X _{CH₄} (%)	68.6	47.6	41.6	66.8	59.2	51.7	33.8	31.1	37.6	22.9	26.7	66.4	66.4
S _{CO} (%)	81.7	64.1	55.0	83.3	77.4	73.9	49.2	42.7	43.2	18.5	41.7	85.4	85.4
H ₂ /CO (%)	3.1	3.9	4.3	3.1	3.3	3.4	5.0	5.6	5.9	12.1	5.7	3.0	3.0
Catalytic bed outlet temperature (°C)	727	734	745	737	730	731	701	709	632	548	601	737	737

Table 5. Test carried out with Rh1% Mg₆₈Al₃₂ exHT, in blue are evidenced the control tests. All the value are expressed in %v/v dry base

3.2.3 Study of the Rh or Ru Active Phase in the Mg/Al Matrix.

3.2.3.1 Characterization of Ru Catalyst

A catalysts containing 0.1wt% of Rh and two catalyst containing respectively 0.1wt% and 1wt% of Ru have been prepared in order to evaluate the difference in activity of the two noble metals. In terms of XRD characterization the precursor and the catalyst containing 0.1% of Rh and Ru are not different for a Mg/Al samples and the surface area of the calcined samples are $92\text{m}^2\text{g}^{-1}$ and $86\text{m}^2\text{g}^{-1}$ respectively for Rh and Ru catalysts. On the other hand the Ru1% sample show a different behavior when is calcined at 900°C according to Basile et al [99] that studied the noble metal distribution at different temperature and different concentration. Rh and Ru behave in a different way at a calcination temperature of 900°C where the MgO-type and the spinel (MgAl_2O_4) phases are usually formed; in fact if Rh is widely soluble in the MgO and spinel phase the Ru segregate as RuO_2 even using a low concentration of Ru (1% as atomic ratio). In that case the amount of segregated Ru is only partial while the remaining Ru is present solved in the MgO phase and is not present in the spinel phase and the extent of its segregation decrease with the amount of Ru [99]. The Graph 10 about Ru1% $\text{Mg}_{68}\text{Al}_{32}$ (corresponding to 0.43 as a.r.) shows the presence of the spinel phase MgAl_2O_4 , the MgO, a bit of HT reconstruction and a segregated RuO_2 as confirmation of its low solubility in MgO and spinel MgAl_2O_4 .

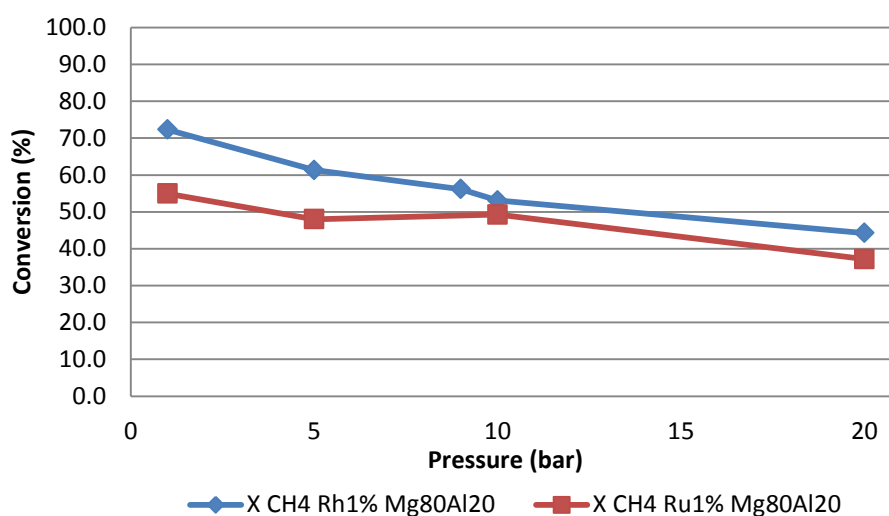


Graph 10. XRD pattern of Ru1% $\text{Mg}_{68}\text{Al}_{32}$ evidence the segregation of RuO_2 also at this low concentration.

The segregation of the RuO₂ phase already present at 1% of metal loading can affect the metal dispersion justify the choice to carried out the catalytic comparison using also 0.1% of atomic ratio where presumably the segregation of Ru is not occurring. Even if the low amount of Ru cannot exclude the segregation of a RuO₂ phase undetectable with powder XRD.

3.2.3.2 Comparison of the Catalytic Activity of Ru and Rh 1% Catalysts

The comparison have been carried out reducing overnight at 750°C with H₂ diluted in N₂ (10% v/v) in situ and then tested at 24'000h⁻¹ at 750°C and 1, 5, 10, 20bar.



Graph 11. Conversion of CH₄ at 24'000h⁻¹, 750°C vs pressure for Rh1% Mg₈₀Al₂₀ and Ru1% Mg₈₀Al₂₀

As visible in Graph 11 the conversion of CH₄ is always higher for the catalyst containing Rh at every pressure. The trend shows a constant decrease of conversion increasing the pressure; this is expected from equilibrium of reaction with increased number of moles in the products. Also the temperature profiles on the catalysts evidence a different activity of the noble metal present on the catalysts. The gap on the temperature in the profile is different; in particular the ΔT of the Rh catalyst is much larger than that of the Ru catalyst along the catalytic bed, as visible in Table 6 due to an high reaction rate and degree of methane conversion.

	Rh1%	Ru1%
1bar	$\Delta T: 40^\circ\text{C}$	$\Delta T: 14^\circ\text{C}$
20bar	$\Delta T: 45^\circ\text{C}$	$\Delta T: 16^\circ\text{C}$

Table 6. Maximum and minimum temperatures of the catalysts along the catalytic bed. GHSV: 24'000h⁻¹; T_{oven}: 750°C.

This can be attributed to an higher activity of the Rh probably due to the segregation of Ru which decrease its dispersion

3.2.3.3 Catalytic activity of Rh 0.1% and Ru 0.1%

The use of 0.1% of low amount of Ru can prevent the RuO₂ segregation and therefore a new comparison is needed with the Rh catalyst containing an analogous metal loading. Also in this case the catalyst have been reduced for 6h at 750°C. Considering the Rh0.1% a relative low methane conversion is observed that is below 50% at 750°C, 24000 h⁻¹ and 1bar. with an exit methane of 22.4% which is very far from the thermodynamic equilibrium. The results are much lower than that observed using Rh1% (exit methane 12%) confirming the importance of the metal loading and the kinetic controlled regime in which the reaction is carried out. Using the Ru0.1% catalyst the exit methane concentration is much higher and the conversion is 32% at low pressure. The results are much lower than that obtained using the Ru1% confirming the need for 1% metal catalyst. In conclusion the tests carried out with the Ru and Rh catalysts indicate that the Rh insertion the HT precursor is much more active than analogous samples prepared with Ru and that the reaction carried out at 150ms requires a significant amount of catalyst to approach the thermodynamic equilibrium conversion and gas composition.

Pressure (bar):	1	
GHSV (h ⁻¹):	24000	24000
H ₂	56.2	46.1
CO	15.2	9.9
CH ₄	22.4	37.0
CO ₂	6.2	7.1
TOT.	100	100
X _{CH4}	48.9	31.5
S _{CO}	71.0	58.2
H ₂ /CO	3.7	4.7
Catalytic bed outlet temperature (°C)	740	746

Table 7. Catalytic data of Rh0.1% Mg₆₈Al₃₂ and Ru1% Mg₆₈Al₃₂.

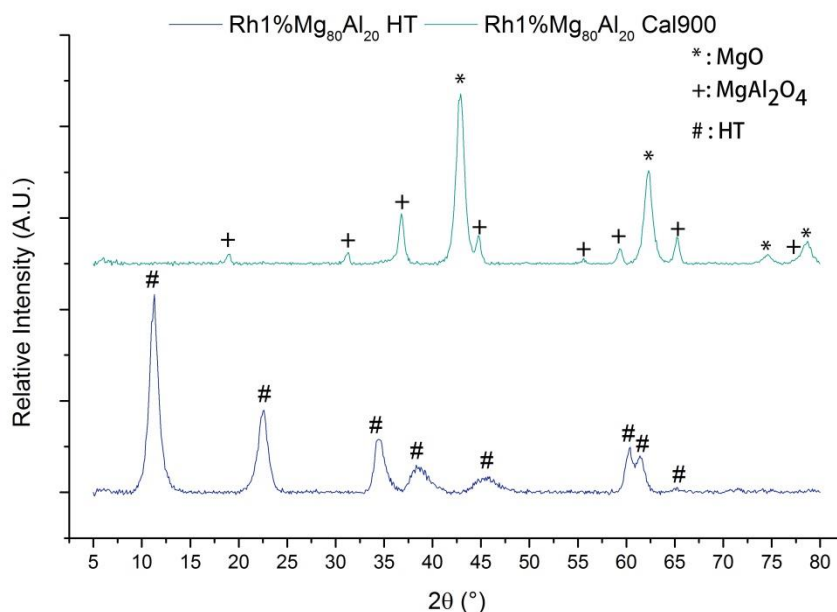
3.3 Effect of the Mg/Al ratio of the HT matrix

In every catalytic process the active phase is not the only important part of a catalyst. The support has generally an important role in the process stabilizing the active phase and the

dispersion of the active phase or the surface area. It gives also mechanical properties to the final material but can also promote the reaction and the activity of the active phase giving acidity, basicity or improve the redox property to the system. This is especially through when a catalyst is obtained by reduction of a solid solution containing the active phase. For this reasons the effects of the matrix will be evaluated in order to optimize the material for the oxy-reforming reaction.

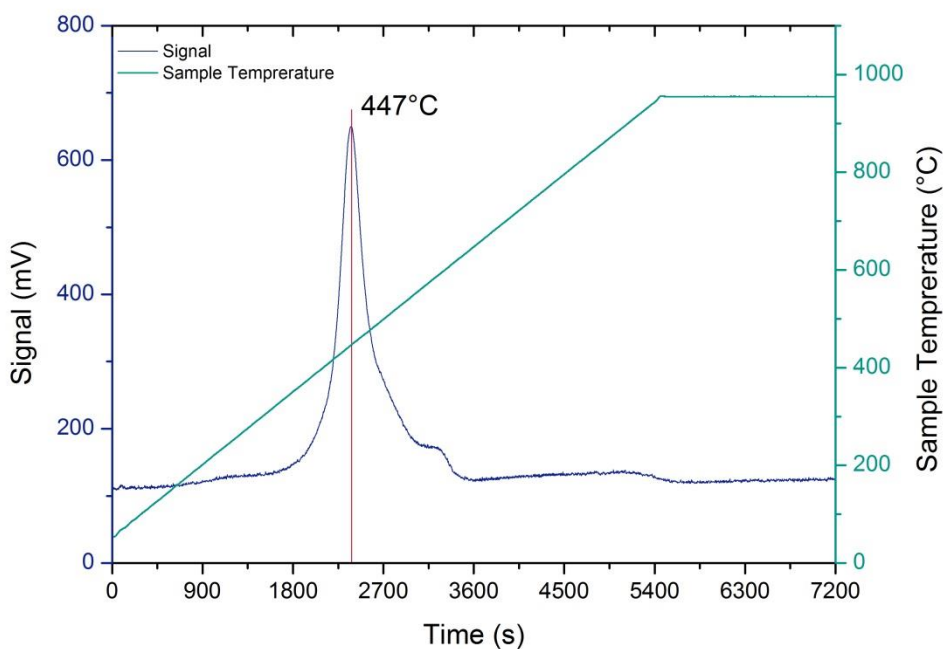
3.3.1.1 Characterization of Rh1% Mg₈₀Al₂₀ Catalyst

The catalyst has been prepared by co-precipitation route then calcined at 900°C for 12h. The XRD analysis of the sample before calcination shows a typical pattern for an HT precursors in which the active metal is dispersed. The calcined sample shows only two phases: MgO and MgAl₂O₄ in which the third metal is solved.



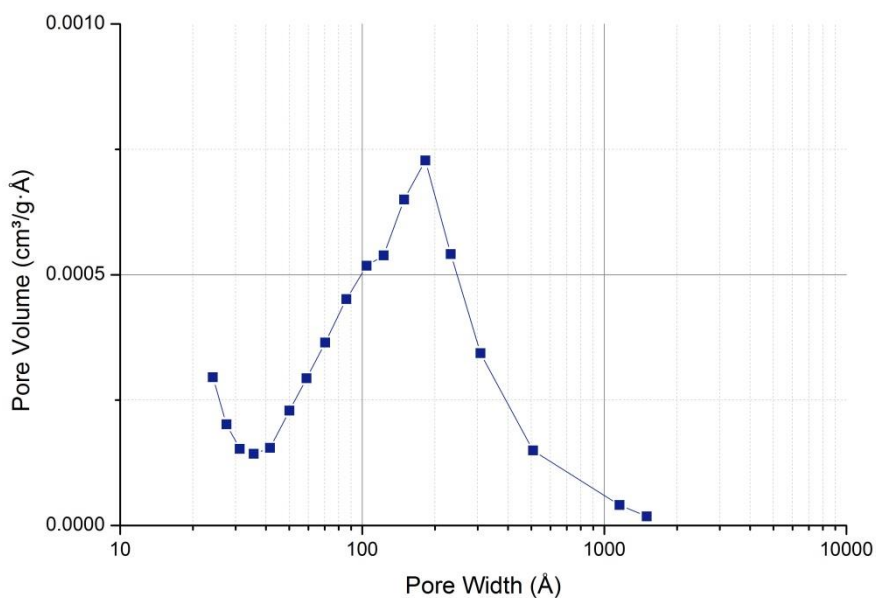
Graph 12. XRD patterns of HT precursor and calcined sample.

The temperature programmed reduction shows an important H₂ consumption at 447°C associated to the presence of Rh oxide inside the structure.



Graph 13. Temperature programmed reduction of Rh1% Mg₈₀Al₂₀.

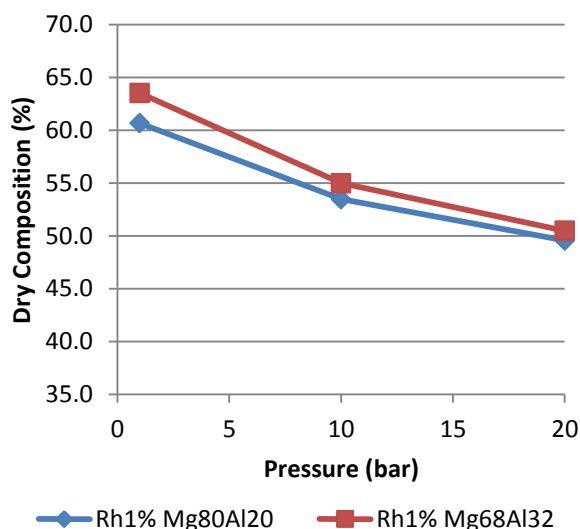
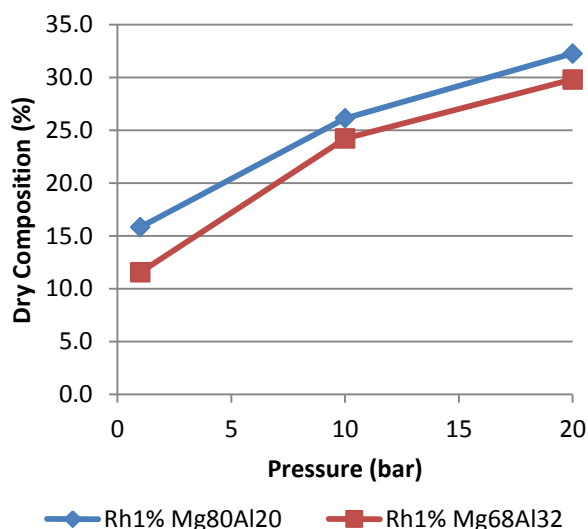
The pore size distribution of Rh1% Mg₈₀Al₂₀exHT sample is ranged from 50Å to 150Å; BET surface area is 105m²g⁻¹.



Graph 14. BJH pore distribution of Rh1% Mg₈₀Al₂₀

The two catalysts (Rh1% Mg₆₈Al₃₂ and Rh1% Mg₈₀Al₂₀) have been tested in the oxy-reforming reaction after activation carried out in H₂/N₂ 10%v/v at 750°C overnight.

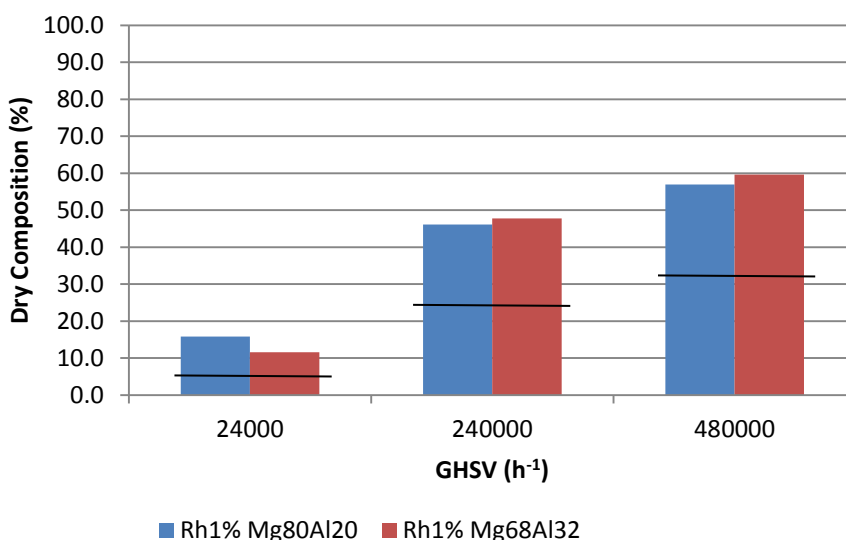
RESULTS AND DISCUSSION



Graph 15. Methane outlet composition for reaction carried out at 750°C and 24'000h⁻¹ for catalysts containing 1% of Rh and Mg/Al ratio equal to 80/20 (blue line) and 68/32 (red line).

Graph 16. Hydrogen outlet composition for reaction carried out at 750°C and 24'000h⁻¹ for catalysts containing 1% of Rh and Mg/Al ratio equal to 80/20 (blue line) and 68/32 (red line).

The graphs show the outlet composition of CH₄ and H₂ for three tests carried out at 750°C and 24'000h⁻¹ at different pressure indicated on the x axis. As easily visible the composition of the methane is always lower for the reaction carried out with the catalyst with Mg/Al:68/32 than 80/20. Also the H₂ composition is always higher for catalyst with Mg/Al ratio equal to 68/32. Increasing the pressure is possible to see a more similar behavior of the catalyst due to the almost reached equilibrium values.



Graph 17. Outlet methane composition at equal feed linear velocity varying pressure and GHSV for catalyst containing 1% of Rh and Mg/Al:80/20 (blue bar) and Mg/Al:68/32 (red bar). The black line identify the equilibrium % of the methane at the outlet calculated at 750°C for test at 24'000h⁻¹ and 1bar,

at 690°C for test at 240'000h⁻¹ and 10bar and at 695°C for test at 480'000h⁻¹ and 20bar.

Increasing the pressure but maintaining constant the linear velocity a similar behavior is observed, At 480'000h⁻¹ the conversion of the methane is low due to the very short contact time ($7.5 \cdot 10^{-3}$ sec) and due to the lower temperature on the catalyst. In this condition diffusion problem should be taken in consideration.

3.3.2 Comparison of the Catalyst Properties as Function of Mg/Al ratio

As already discussed, in the Mg and Al HT, after calcination, different ratio of MgO and spinel MgAl₂O₄ are present in the final support as function of the Mg/Al ratio and the active metal can be differently distributed from the two phases. In particular the Rh is differently solved in the spinel phase and also in the MgO phase and this can vary the availability of the Rh and its characteristics in the oxy-reforming reaction. In this work only two different ratios will be evaluated: Mg/Al:80/20 and Mg/Al:68/32. This two ratios has been already studied for CPO reaction and reforming of ethanol reaction [114,115]. The samples Rh1% Mg₈₀Al₂₀ and Rh1% Mg₆₈Al₃₂ have been prepared with the co-precipitation method as described in 2.1.1. The comparison of surface areas shows different surface area for the each sample a higher for the sample with Mg/Al:68/32 as visible in Table 8.

Composition	M ²⁺ /M ³⁺	HT (m ² g ⁻¹)	Cal(m ² g ⁻¹)
Rh1% Mg ₈₀ Al ₂₀	80/20	20	105
Rh1% Mg ₆₈ Al ₃₂	68/32	133	124

Table 8. Surface areas of samples containing Rh1%. Values are expressed in m²/g before calcination (HT column) and after calcination at 900°C for 12h (Cal column).

Each catalysts have been analyzed with TEM microscopy. The image of the Rh1% Mg₆₈Al₃₂ shows the typical mixed oxide structure in which the MgO phase and the spinel phase are highly interconnected [100]. The TEM shows also average Rh particle size of 1.4nm. the sample Rh1% Mg₈₀Al₂₀ which show similar morphology and even slightly smaller Rh particle size (1.1 nm).

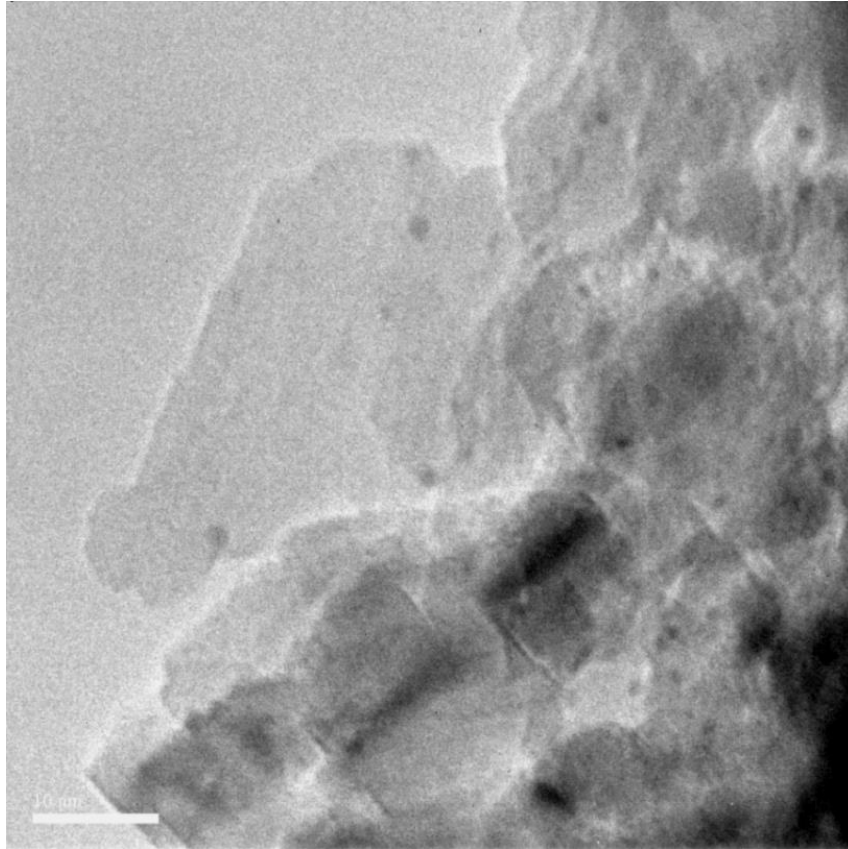


Figure 40. TEM image (200'000x) of the Rh1% Mg₆₈Al₃₂ after calcination at 900°C and reduction at 750°C.

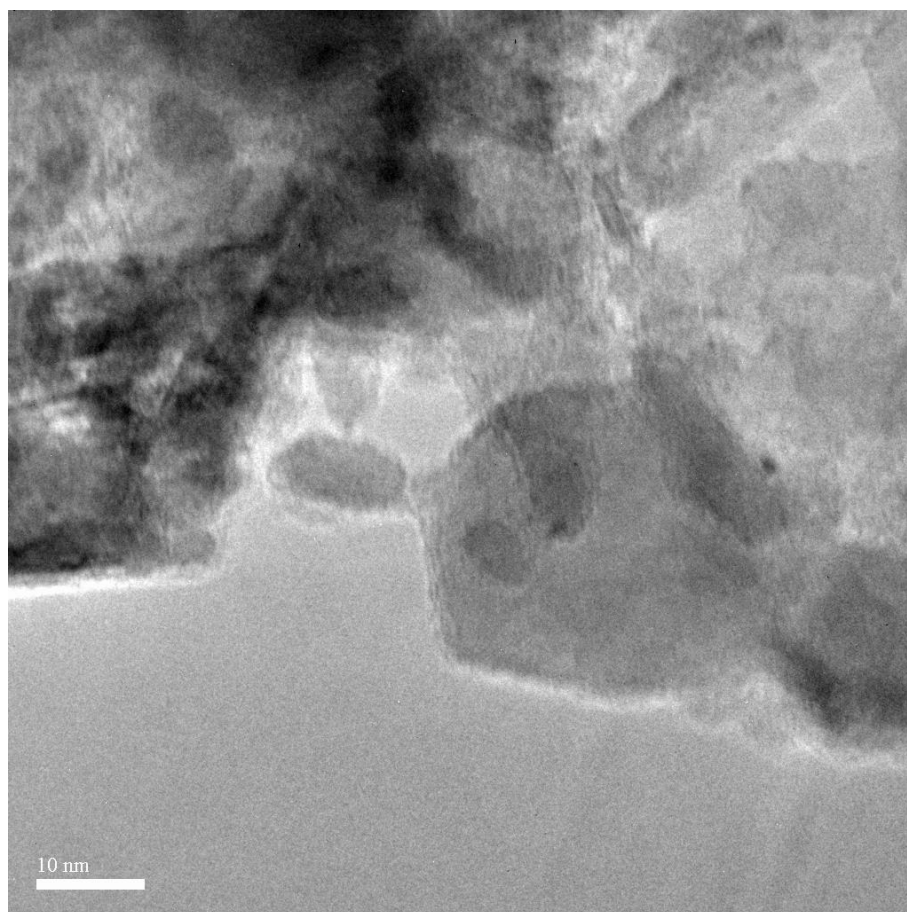
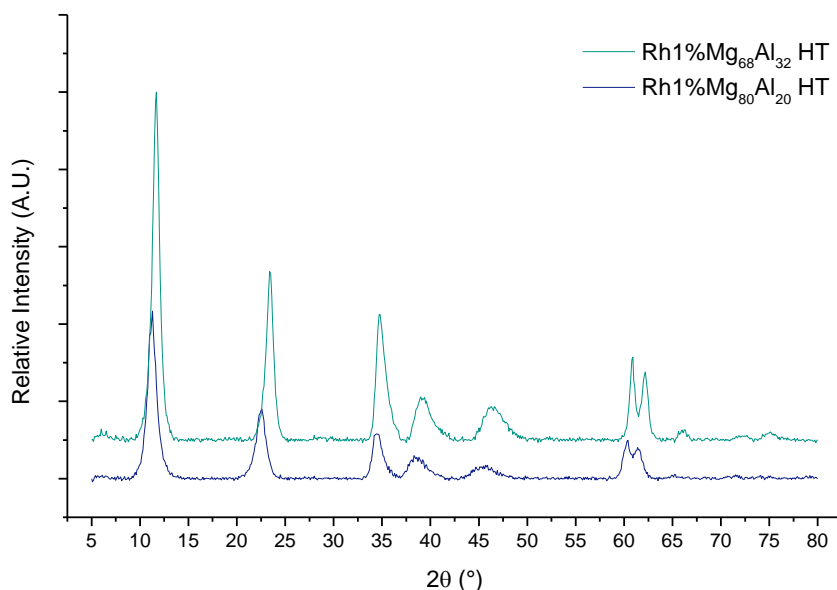


Figure 41. TEM image (200'000x) of the Rh1% Mg₈₀Al₂₀ after calcination at 900°C and reduction at 750°C.

In Graph 18 and Graph 19 XRD patterns of the precursors and of the calcined samples are reported. The precursors show the typical reflections of the hydrotalcite-like compounds but Rh is not observed due to its statistical distribution in the solid phase. A shift of all the reflections is showed for the sample with less Mg²⁺ evidencing smaller unit cells according to the smaller dimension of the Al³⁺ ion (0.82 and 0.59 respectively for Mg²⁺ and Al³⁺) with respect to the A parameter and an increasing electrostatic interaction due to the increasing amount of trivalent cation which significantly affect the c parameter.

	<i>a=b</i> (Å)	<i>c</i> (Å)	<i>D</i> (Å) (particle size from Sherrer's Law, plane 003)
Rh1%Mg ₈₀ Al ₂₀ HT	3.0703	7.8652	88
Rh1%Mg ₆₈ Al ₃₂ HT	3.0447	7.5934	112

Table 9. Crystal parameters for Rh1%Mg₈₀Al₂₀ and Rh1% Mg₆₈Al₃₂ calculated from XRD patterns.

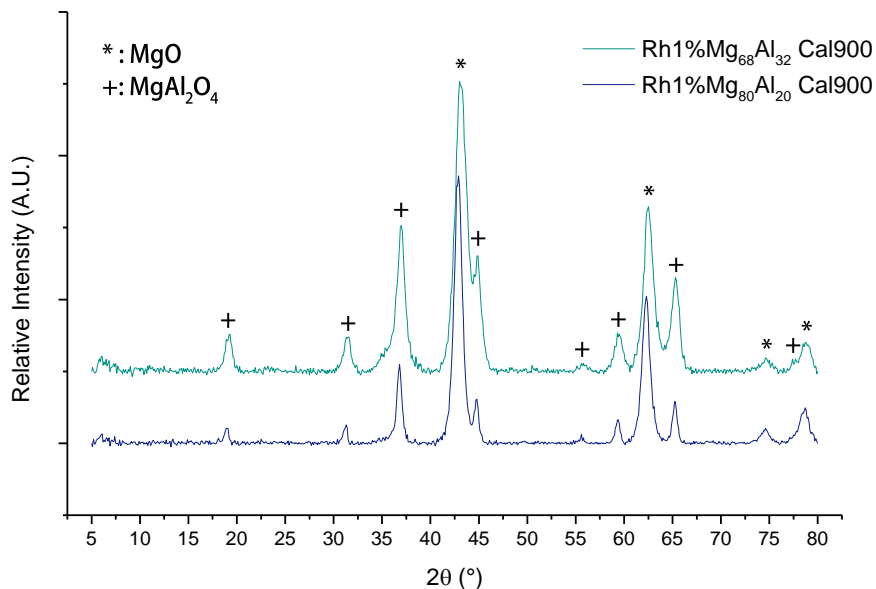


Graph 18. XRD patterns of the HT's with 1% of Rh prepared with co-precipitation method. Green line represents Rh1% Mg₆₈Al₃₂ HT, the blue line represents the Rh1% Mg₈₀Al₂₀ HT.

After calcination only 2 phases have been observed in each sample: MgO and MgAl₂O₄ according with literature and no reflections of Rh can be observed thanks to the formation of mixed oxide solid solution of Rh with the present oxide phases. In the sample with Mg/Al ratio equal to 80/20 the reflection of the MgO phase have an higher intensity than the sample with Mg/Al ratio equal to 68/32 evidencing a different ratio between the two phases present in the calcined material as shown in Figure 42 with an increasing amount of the MgO phase with respect to the theoretical due to the presence of Al³⁺ in the MgO phase [99].

	Rh1%Mg ₈₀ Al ₂₀		Rh1%Mg ₆₈ Al ₃₂		Reference [116]	
	MgO	MgAl ₂ O ₄	MgO	MgAl ₂ O ₄	MgO	MgAl ₂ O ₄
a (Å)	4.219	8.085	4.193	8.081	4.212	8.080
V (Å³)	75.107	528.486	73.718	527.639	74.709	527.514

Table 10. Cell parameters of phases obtained after calcination of Rh1%Mg₈₀Al₂₀ and Rh1%Mg₆₈Al₃₂ and reference values from [116]



Graph 19. XRD patterns of the calcined samples containing 1% of Rh. Green line represents Rh1% Mg₆₈Al₃₂ after calcination at 900°C for 12h, the blue line represents the Rh1% Mg₈₀Al₂₀ after calcination at 900°C for 12h.

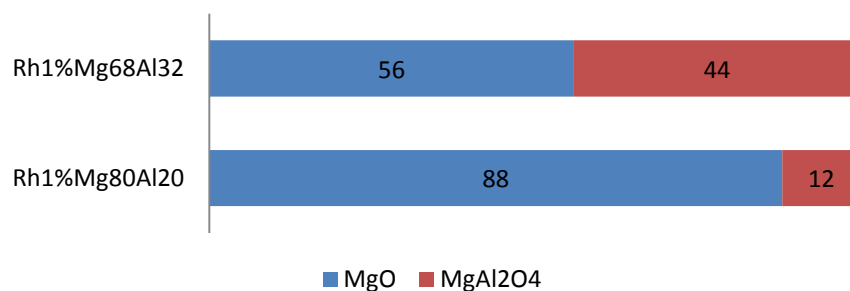
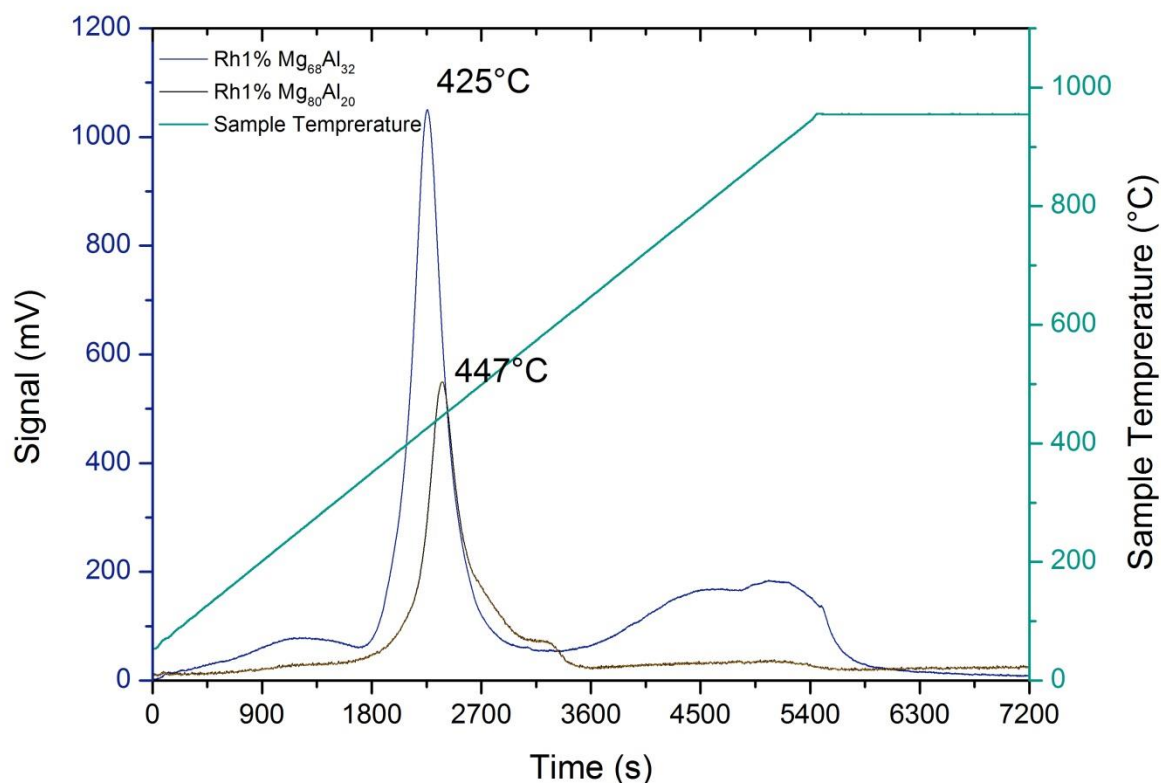


Figure 42. Phase obtained (calculated) after calcination at 900°C for 12h in static air of Rh1%Mg₈₀Al₂₀ and Rh1%Mg₆₈Al₃₂.

The presence of a different phase distribution affect the TPR. In fact if a reduction is visible in the high temperature region for the Rh1% Mg₆₈Al₃₂ this second reduction is not present in the Rh1% Mg₈₀Al₂₀ (Graph 20).



Graph 20. Comparison of the H₂ consumption of samples with different Mg/Al ratio.

The lower degree of reduction could also explain the lower particle dimension observed in TEM and the lower catalytic activity of the sample.

3.3.3 Effects of the Support: CeZrO₂

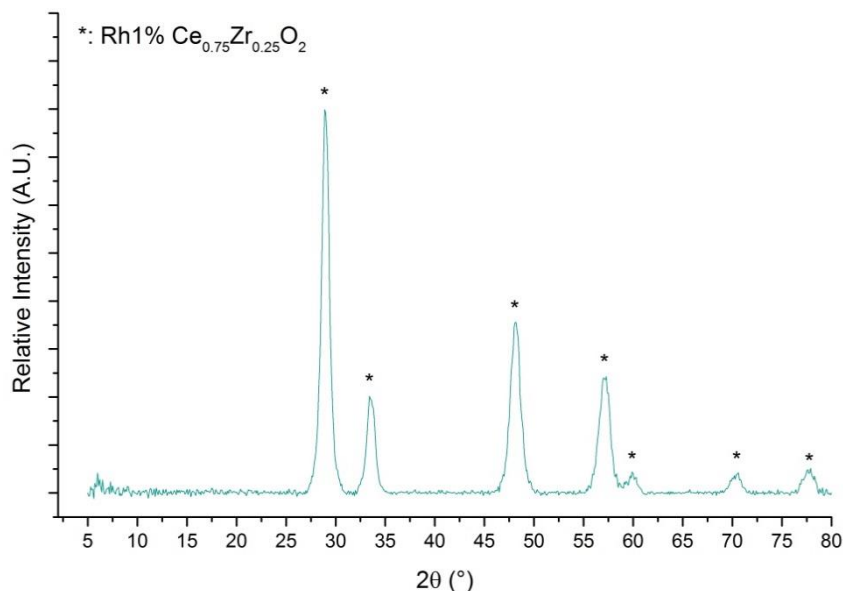
In order to observe if the support can modify the activity of the Rh, a catalyst based on a redox material has been tested. Ce_{0.75}Zr_{0.25}O₂ is well known as sink of O²⁻ [117,118,119,120,121] usually exhibiting properties of oxygen mobility that can help the CO formation.

3.3.4 Rh1% CeZrO₂

3.3.4.1 Characterization

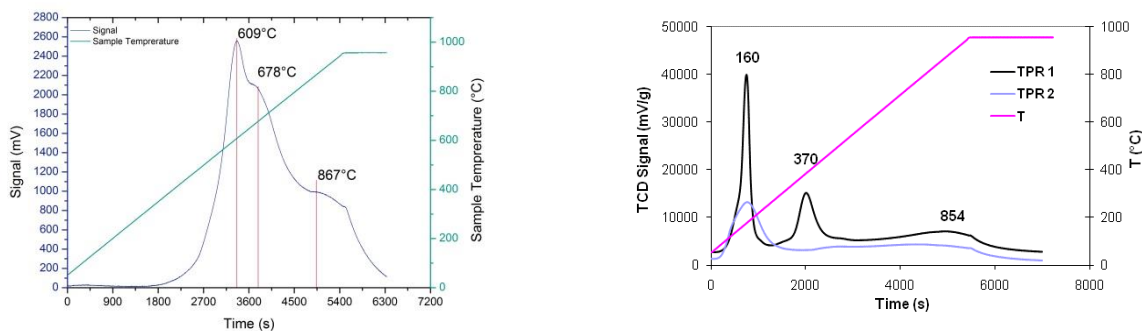
The Ce_{0.75}Zr_{0.25}O₂ catalyst was prepared by co-precipitation of nitrates of Rh, Ce and Zr. To obtain the precipitation of all hydroxide species the pH was kept over 6.5 at 20°C by adding drop by drop ammonia under vigorous stirring. Then the precipitate was centrifuged and dried

at 70°C. After that the powder was calcined at 700°C for three hours. The XRD pattern shows typical $\text{Ce}_{0.75}\text{Zr}_{0.25}\text{O}_2$ reflections while Rh is partially solved in the CeZrO_2 structure. Its presence as separated phase is not detectable due to the low amount.



Graph 21. XRD patterns of HT precursor and calcined sample.

The TPR profile of RCZO shows 3 peaks of H_2 consumption at ca. 160, 370 and 850 °C. The low temperature of first peak is associated to rhodium free on the surface of catalyst and it can attributed mainly to Rh_2O_3 while the second peak is attributed to the Rh^{3+} inside the CeZrO_2 others a higher temperature are due to the reduction of Ce^{VI} in the CeZrO_2 . TPR profile of CeZrO_2 without Rh shows two peaks at 600 and 850 °C which are associated with the reduction of the surface and the bulk. The presence of Rh determines a significant promotion in the reduction due to the spillover of H_2 onto the support, i.e. the reduction peaks at 600 °C shift to lower temperatures.

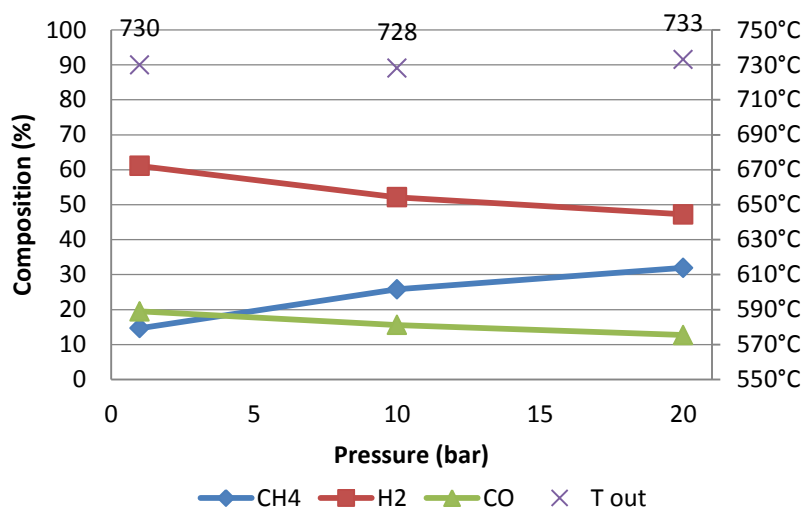


Graph 22. TPR comparison of CeZrO on the left and Rh1\% CeZrO on the right

The surface area of the sample is close to $10 \text{ m}^2\text{g}^{-1}$ but is a typical value for a CeZrO_2 material.

3.3.4.2 Catalytic activity

The catalyst, after reduction at 750°C overnight have been tested in the oxyreforming conditions showing the results in the Graph 23.



Graph 23. Dry composition of outlet stream for catalyst with 1%Rh on $\text{Ce}_{0.75}\text{Zr}_{0.25}\text{O}_2$. 750°C GHSV: $24'000\text{h}^{-1}$

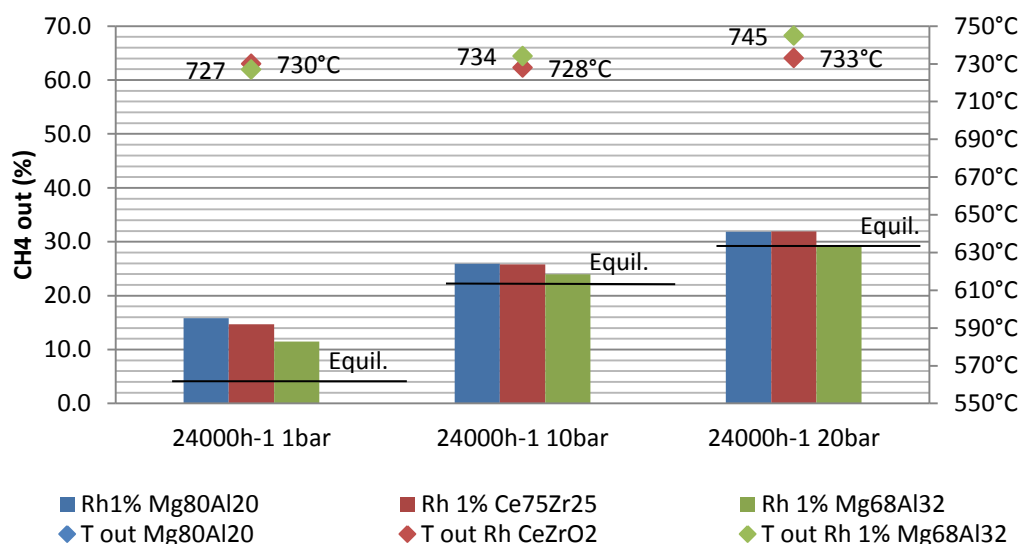
The tests with $\text{Rh}1\%/\text{Ce}_{0.75}\text{Zr}_{0.25}\text{O}_2$ show the same trend of the other tested catalysts decreasing the conversion of methane increasing the pressure. A complete table with test results is showed.

P (bar):	1	10	20	
GHSV (h-1):	24000	240000	480000	Control test
H ₂	61.1 %	40.5 %	32.9 %	61.2 %
CO	19.5 %	7.7 %	7.2 %	19.0 %
CH ₄	14.7 %	41.9 %	50.8 %	14.2 %
CO ₂	4.7 %	9.8 %	9.0 %	5.7 %
TOT.	100 %	100 %	100 %	100 %
X _{CH4}	62.2 %	29.5 %	24.2 %	63.5 %
S _{CO}	80.6 %	44.0 %	44.4 %	76.9 %
H ₂ /CO	3.1 %	5.3 %	4.6 %	3.2 %
Catalytic bed outlet temperature (°C)	730	728	733	728

Table 11. Table with complete catalytic activity of $\text{Rh}1\%/\text{Ce}_{0.75}\text{Zr}_{0.25}\text{O}_2$.

3.3.5 Comparison of the Selected Catalysts

Rh1% Mg₈₀Al₂₀, Rh1% Mg₆₈Al₃₂ and Rh1%/Ce_{0.75}Zr_{0.25}O₂ have been compared directly in order to better understand which one is the best candidate for further studies. The catalysts have been tested in the same condition at 750°C, 24'000h⁻¹ and the same time on stream.

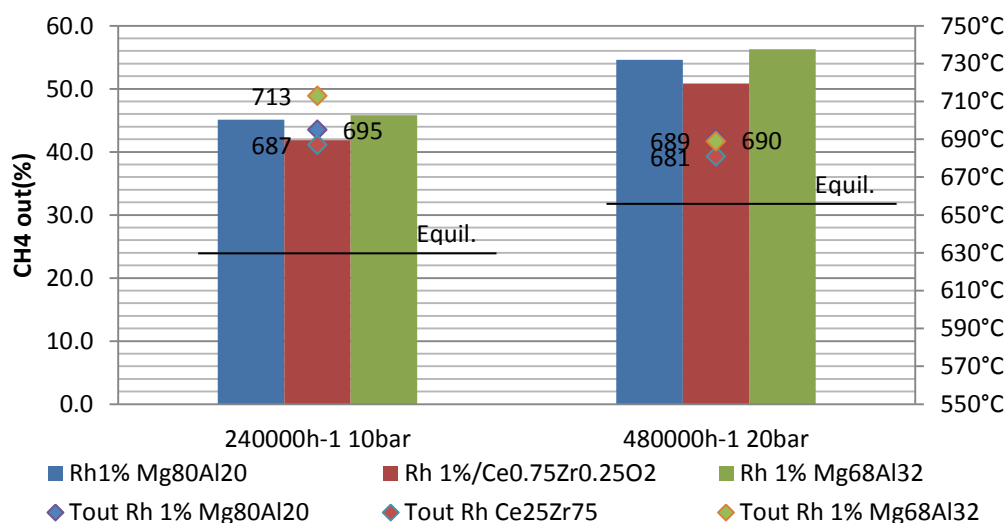


Graph 24. Methane outlet composition for Rh1% Mg₈₀Al₂₀, Rh1% Mg₆₈Al₃₂ and Rh1%/Ce_{0.75}Zr_{0.25}O₂ compared at 750°C and 24'000h⁻¹. The bars are referred to the left while temperature on the right. The equilibrium lines are calculated at 730°C for tests at 1 and 10 bar while at 740°C for the tests at 20bar.

The results show a significant higher methane conversion and synthesis gas selectivity at low pressure for the Rh1% Mg₆₈Al₃₂. At high pressure conditions, 10 and 20bar, the Rh1% Mg₆₈Al₃₂ is still the best catalyst. Particularly at 20bar the thermodynamic equilibrium is reached and as a consequence the difference among the catalysts decreases. This is good from the point of view of the activity but means that comparison at this pressure is very difficult due to the thermodynamic limitations. To compare the catalyst at high pressure a very high space velocity have been testes at 10 and 20 bar and the activity ranking changes and the Rh1%/Ce_{0.75}Zr_{0.25}O₂ has the best performances nevertheless the presence of hot spot have been observed in the catalytic bed which may affect the comparison.

Furthermore the in the evaluation of the results of the Rh1%/Ce_{0.75}Zr_{0.25}O₂ catalyst has to be taken into consideration the presence of a higher weight amount of catalyst due to the differences in density. Ex-HT catalysts have very close bulk density (2g*mL⁻¹) so the amount of Rh in the final material is almost the same while the density of the Ce_{0.75}Zr_{0.25}O₂ is 6.5g*mL⁻¹ i.e. the real amount of Rh in in the Ce_{0.75}Zr_{0.25}O₂ catalyst, keeping constant the volume, is more than three times the Rh present in the exHT catalyst. Notwithstanding the higher Rh

loaded in the reactor the activity in controlled condition at low pressure show the higher performance of Rh1% Mg₆₈Al₃₂.



Graph 25. Methane outlet composition for Rh1% Mg₈₀Al₂₀, Rh1% Mg₆₈Al₃₂ and Rh1%/Ce_{0.75}Zr_{0.25}O₂ compared at 750°C and at constant linear velocity. Equilibrium values are calculated at 690°C for the tests at 10bar and 240'000h⁻¹ and at 695°C for the tests at 20bar and 480'000h⁻¹

3.4 Bimetallic Active Phase

Basile et al [122] studied the effects of introducing a second metal as active phase in the CPO reaction, autothermal CPO and dry reforming of the methane pointing out the effect of the Rh on the temperature distribution of the catalytic bed during reaction. Ni is partially oxidized and less active in the oxygen rich part of the catalytic bed [123] while the Rh is more active in the oxidation part therefore the Rh/Ni composition can determine the tailoring of the thermal profile while both are active in the reforming resulting in a synergic effect that allow an increase of activity and stability towards the coke formation. Starting from this consideration, two different bimetallic catalysts have been prepared. A Rh/Ni catalyst on HT in which the Ni sites play the role of modulating the redox properties, more specifically, by increasing the oxygen lattice availability for the reaction in the oxidation zone and by increasing the number of active sites for the methane activation in the reforming zone. A Rh/Pt on an a support having a good oxygen mobility such as CeZrO₂ in which the Pt increase the metallic character of the active phase in the oxygen reach zone and is active in methane activation during reforming.

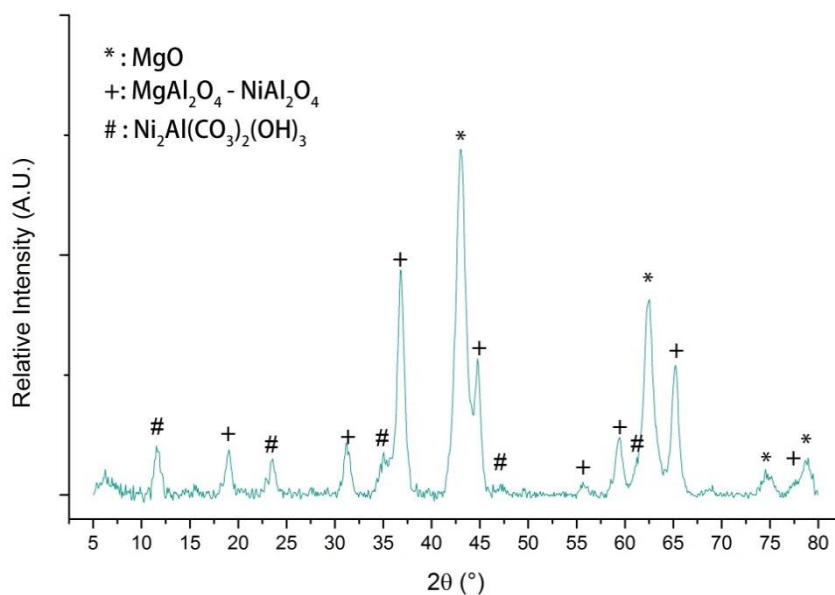
- Ni₈Rh_{0.15}Mg₆₀Al_{31.85} (NRexHT)
- (Pt/Rh:2.5/1)1%/Ce_{0.75}Zr_{0.25}O₂ (PRCZO)

$\text{Ni}_8\text{Rh}_{0.15}\text{Mg}_{60}\text{Al}_{31.85}$ have been prepared via co-precipitation method, dried overnight at 120°C , calcined at 900°C for 12h then reduced at 750°C overnight under H_2/N_2 10%v/v. $(\text{Pt}/\text{Rh}:2.5/1)1\%/\text{Ce}_{0.75}\text{Zr}_{0.25}\text{O}_2$ have been prepared via IWI method, calcined at 600°C for 12h then reduced as the previous one. The two catalysts have been tested at the same condition of the monometallic ones for better understanding the effect of the second metal on the activity of the catalyst.

3.4.1 $\text{Ni}_8\text{Rh}_{0.15}\text{Mg}_{60}\text{Al}_{31.85}$ (NRexHT)

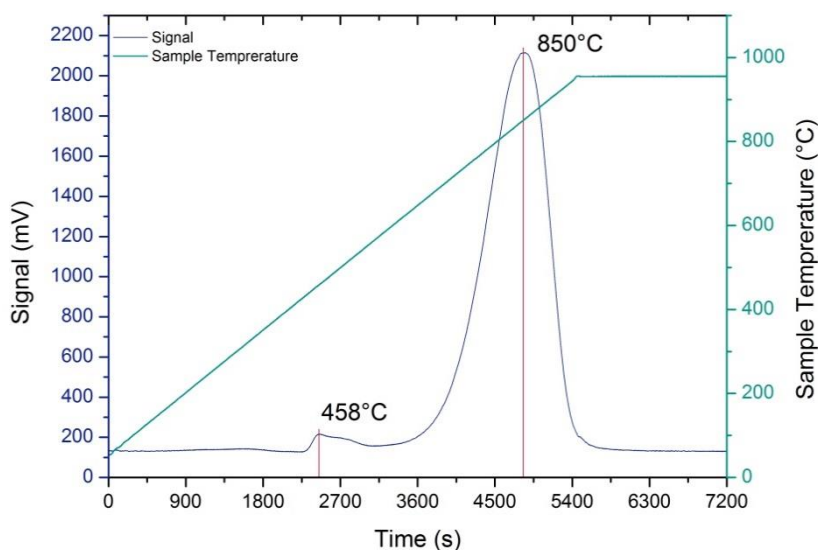
3.4.1.1 Characterization

The catalyst has been prepared by co-precipitation route then calcined at 900°C for 12h. The XRD analysis of the sample before calcination shows a typical pattern for an HT precursors (not shown). The calcined sample shows only two phases: MgO and MgAl_2O_4 in which the Rh and Ni are present forming a solid solution.



Graph 26. XRD patterns of HT precursor and calcined sample.

The temperature programmed reduction analysis shows hydrogen consumption at two different temperature: one small consumption at 458°C attributed to Rh and one large hydrogen consumption at 850°C attributed to Ni present in the MgO phase

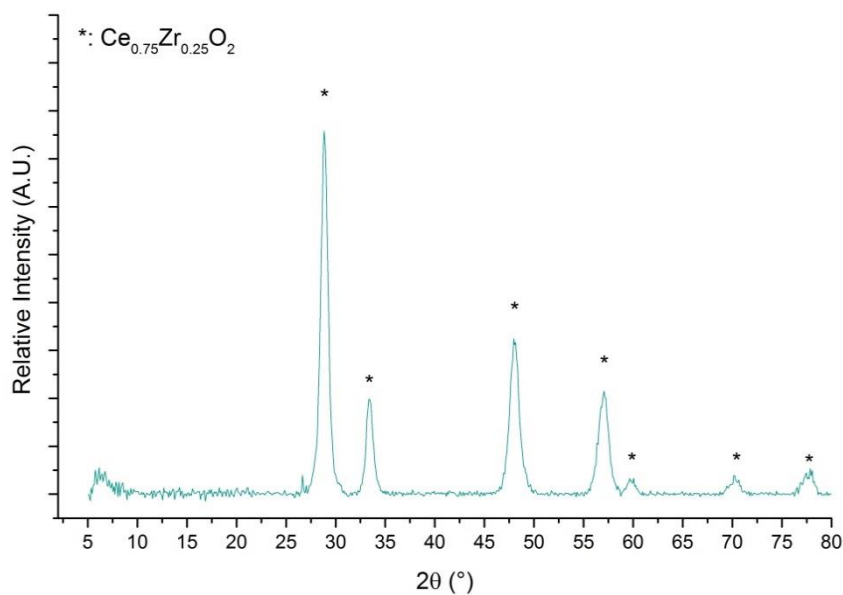


Graph 27. Temperature programmed reduction of $\text{Ni}_8\text{Rh}_{0.15}\text{Mg}_{60}\text{Al}_{31.85}$ exHT.

3.4.2 (Pt/Rh:2.5/1)1%/Ce_{0.75}Zr_{0.25}O₂ (PRCZO)

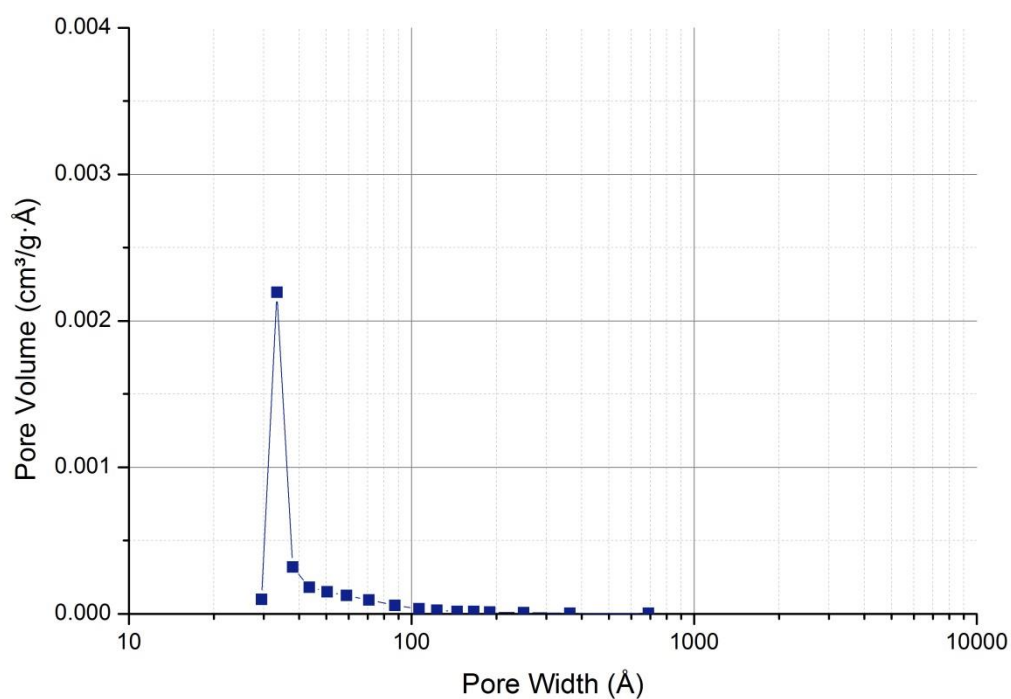
3.4.2.1 Characterization

The sample has been prepared by IWI route after synthesis of the $\text{Ce}_{0.75}\text{Zr}_{0.25}\text{O}_2$ by co-precipitation route, then calcined at 600°C for 12h. The XRD pattern shows only the reflections of $\text{Ce}_{0.75}\text{Zr}_{0.25}\text{O}_2$ but with cell parameter larger than the pure oxide. $\text{Ce}_{0.75}\text{Zr}_{0.25}\text{O}_2$ has a cubic cell system with $a=5.349\text{\AA}$ while this material with Pt and Rh supported has $a=6.18\text{\AA}$ due probably to an insertion of the active phase inside cavities of the structure after calcination.



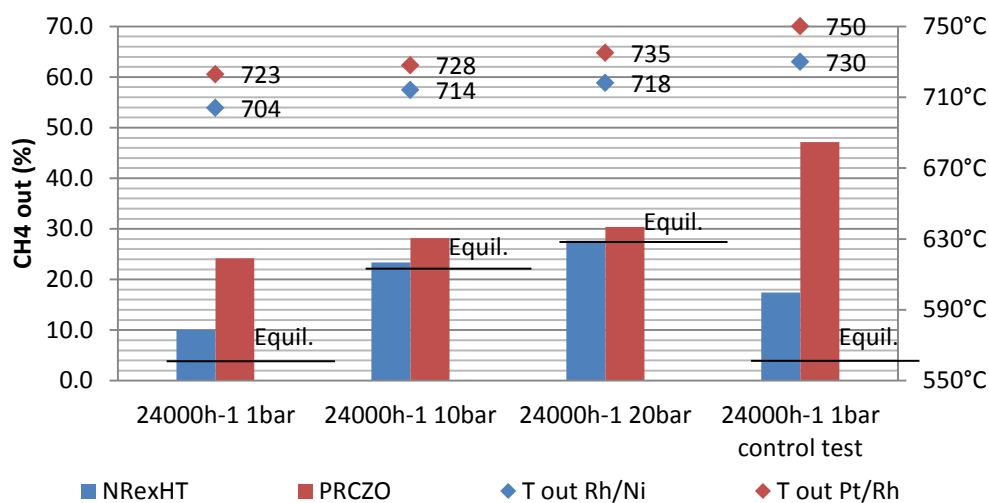
Graph 28. XRD patterns of HT precursor and calcined sample.

The surface area of the sample is very low $9\text{m}^2\text{g}^{-1}$ but is a typical value for a CeZrO_2 material and the measure of the porosimetry confirm the absence of pore volume in the material.



Graph 29. BJH pore size distribution of fresh PRCZO.

3.4.3 Comparison of the Bimetallic Catalyst Activity



Graph 30. Methane outlet composition for NRexHT and PRCZO compared at 750°C and 24'000h⁻¹. The bars are referred to the left while temperature on the right. The equilibrium lines are calculated at 740°C for tests at 1 and 10 bar while at 720°C for the tests at 20bar.

As already seen for the single metal catalysts the general trend is an increase of outlet methane by increasing the pressure, in agreement with the thermodynamic equilibrium. The comparison with the equilibrium curves shows, in addition, that the tests carried out with increasing pressure become more close to the equilibrium values and therefore that at high pressure is much more difficult to discriminate the catalysts behavior.

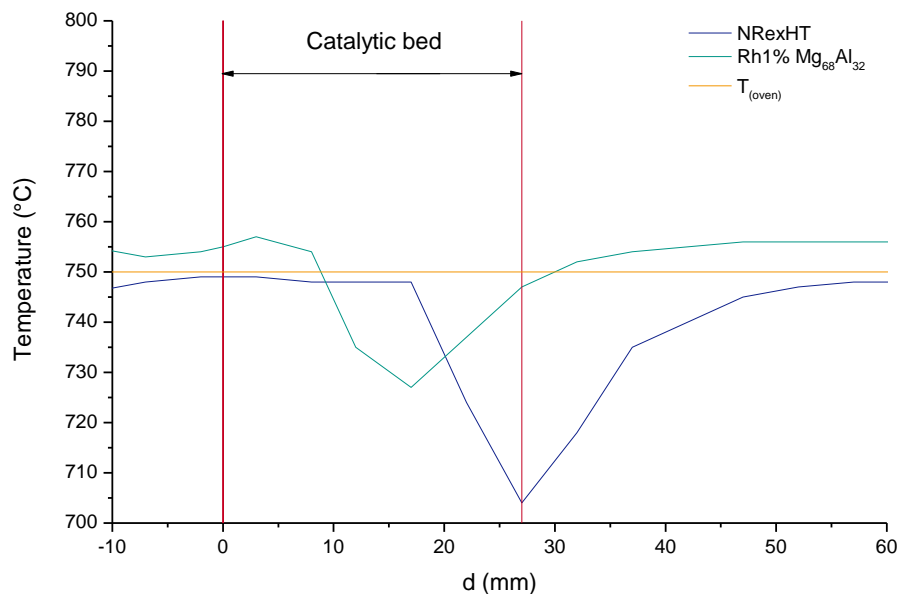
P (bar):	Ni/Rh	Pt/Rh	Ni/Rh	Pt/Rh
GHSV (h ⁻¹):	240000 10 bar	240000 10 bar	480000; 20 bar	480000 20 bar
H ₂	39.9 %	26.5 %	32.7 %	20.7 %
CO	7.8 %	9.7 %	6.5 %	9.6 %
CH ₄	42.5 %	57.8 %	51.2 %	64.7 %
CO ₂	9.8 %	6.0 %	9.5 %	5.0 %
TOT.	100 %	100 %	100 %	100 %
X _{CH₄}	29.3 %	21.4 %	23.8 %	18.4 %
S _{CO}	44.3 %	61.8 %	40.6 %	65.8 %
H ₂ /CO	5.1 %	2.7 %	5.0 %	2.2 %
Catalytic bed outlet temperature (°C)	678	723	666	724

Table 12. Comparison of outlet composition for bimetallic catalyst.

The NRexHT is more active than the PRCZO in every condition, also at 20bar where the PRCZO does not reach the equilibrium (Graph 30). Even in the tests carried out at high space velocity and lower contact time the Rh/Ni show higher conversion as visible in the following table.

After 50h of tests a control test have been carried out in which the conditions of the first test have been repeated. This test is used for evaluate the performance of the catalyst during time. Is possible to observe that the two bimetallic catalyts does not confirm the results obtained during the first test at 750°C and 24'000h⁻¹ in particular the PRCZO that show very low conversion after the series of tests. The presence of carbon have been identify in the NRexHT sample while the deactivation of the PRCZO is probably due to the sintering of the metal on the surface which have been demonstrated using Pt in oxidizing atmosphere.

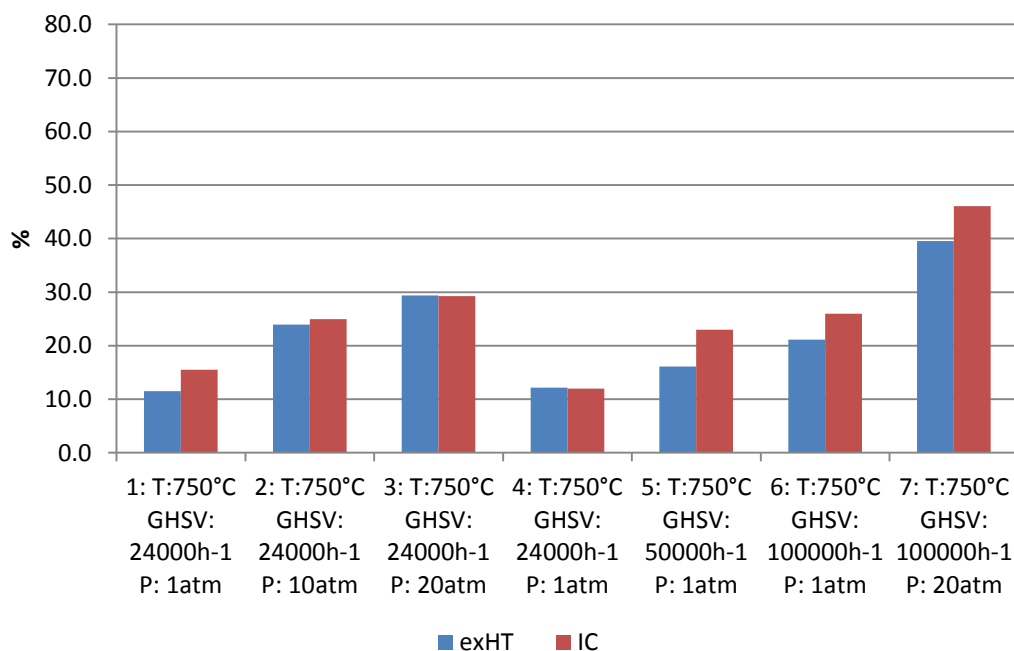
If compared, the NRexHT is more active of the Rh1% Mg₆₈Al₃₂ identified as best catalyst in 3.3.5 but while it lose activity during time on stream the monometallic one keep constant its methane conversion and also after all the tests no presence of coke on the surface is observed. The temperature profiles of the two catalyts are similar but an important thing is showed that confirm the different behavior in the oxidation zone [122]. In the catalyst with only Rh a marked hot spot in the first part of the catalytic bed is showed, Rh is active in oxidation indeed resulting in an increased temperature in the first part of the catalytic bed. In the second part of the catalytic bed dry and steam reforming reaction occur so a decrease of temperature is observed. For catalyst containing Ni the first part of the catalytic bed does not present the temperature increase while the reforming zone is more marked and shifted along the catalytic bed.



Graph 31. Example of temperature profiles NReXHT and Rh1% Mg₆₈Al₃₂ for reaction at 750°C and 24'000h⁻¹.

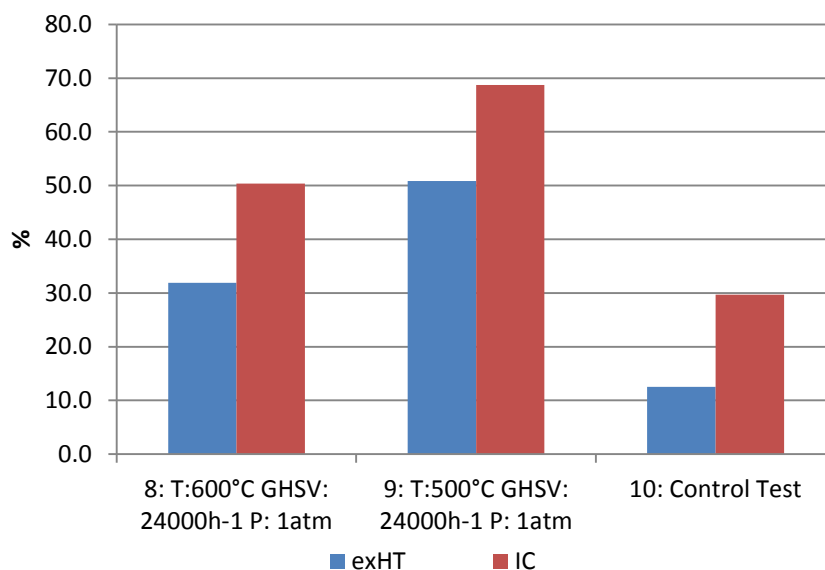
3.5 Industrial Catalyst (IC)

Investigation of a semi-industrial catalyst with analogous amount of noble metal have been used to compare the obtained results with an available catalyst. CPO reaction and reforming reaction have been well studied and many industrial process have been developed but operative conditions are often different from the operative conditions chosen for the oxy reforming process so the classical catalysts are not well optimized. A possible candidate as best catalyst have been chosen in the next GTL project as reference for comparison tests with the Rh1% Mg₆₈Al₃₂. The possible industrial catalyst shipped is a honeycomb shaped catalyst of 25.4mm of diameter and 250mm long with 1% w/w on the total weight of active phase (mixture of noble metals). No more indication can be inserted for this scope. For a direct comparison with the tests already carried out, considering the same total amount of active metal on the IC, the IC has been crushed and sieved as the bulk catalyst and the same weight, resulting also approximately the same volume, of self-made catalyst has been loaded inside the reactor, reduced at 750°C overnight then the classical tests have been carried out.



Graph 32. Comparison of methane outlet composition for Rh1% Mg₆₈Al₃₂ (exHT) and semi industrial catalyst at different pressure and GHSV.

In Graph 32 has been reported the direct comparison between the IC and the Rh1% Mg₆₈Al₃₂ catalyst (exHT) in the oxy reforming of methane. First test shows a better performance for exHT catalyst while increasing pressure this difference is no more observed because equilibrium is reached. CT#4 shows a further activation of IC catalyst, performance now are the same. Changing the GHSV (CT#5 and CT#6) a better performance of exHT catalyst is observed. Also increasing GHSV and pressure exHT catalyst is better than the other.



Graph 33. Comparison of methane outlet composition for Rh1% Mg₆₈Al₃₂ (exHT) and semi industrial catalyst at different temperatures. Final control test is showed.

Graph 33 shows tests carried out at lower temperature (600°C and 500°C) in which the results are from the thermodynamic equilibrium, exHT catalyst is always more active than IC catalyst. In CT#10, a control test repeating the first test conditions an important deactivation of IC catalyst is observed. For validate these data some of these tests have been repeated keeping the original shape of the IC catalyst for better use the intrinsic heat transfer capacity of the honeycomb. For this new shape a quartz reactor with an appropriate internal diameter has been used.

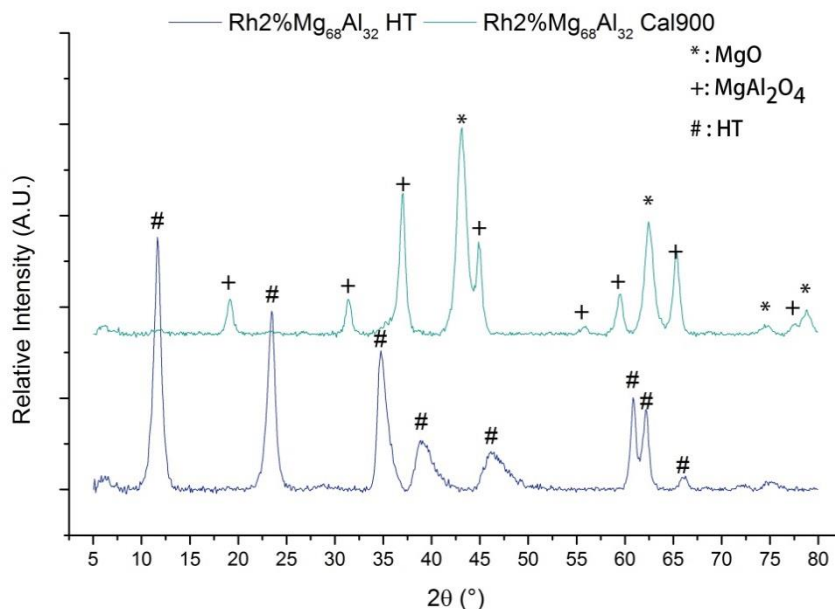
3.6 Scale-up of the Catalyst

Due to the encouraging results obtained with the Rh1% Mg₆₈Al₃₂ catalyst prepared in UNIBO the active phase will be supported on a honeycomb to have the same shape and noble metal content than the IC catalyst. The coating of the ceramic honeycomb has been developed from a project partner. To obtain a catalyst with similar noble metal content using Rh/Mg/Al on the honeycomb an increase of Rh concentration in the HT is required. The catalyst with increasing concentration have been tested to verify the performance.

3.6.1 Rh2% Mg₆₈Al₃₂

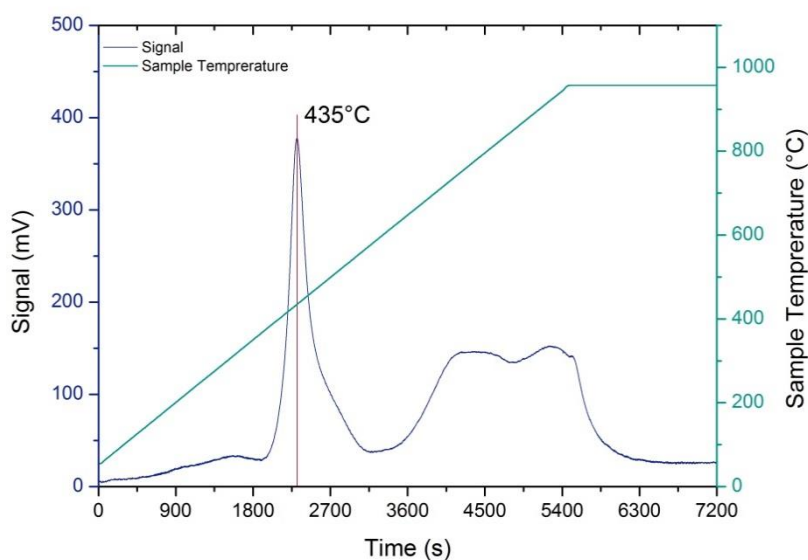
The catalyst has been prepared by co-precipitation route then calcined at 900°C for 12h. The XRD analysis of the sample before calcination shows a typical pattern for an HT

precursors in which the active metal is not directly detectable due to its dispersion in the cationic layer of the HT phase. The calcined sample shows only two phases: MgO and MgAl₂O₄ in which the third metal is solved.



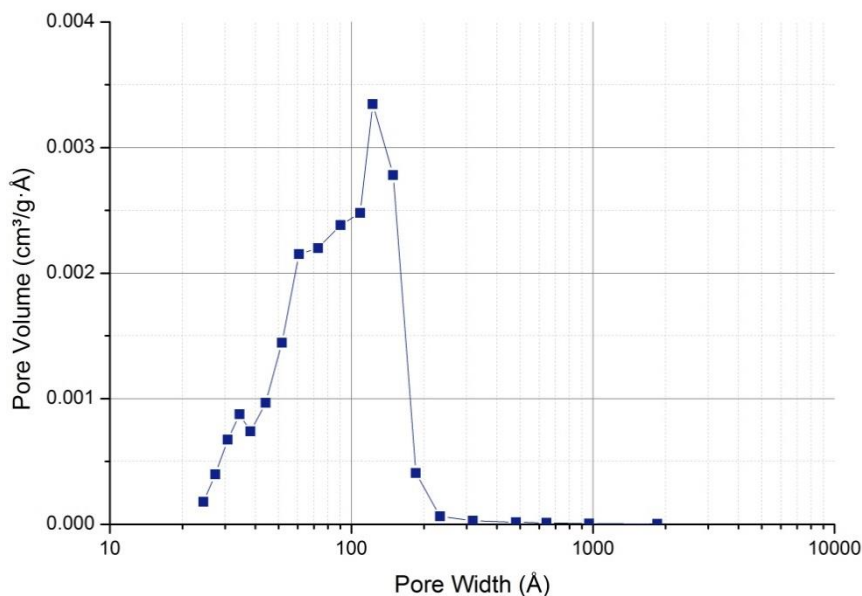
Graph 34. XRD patterns of HT precursor and calcined sample.

The TPR analysis in Graph 35 shows an intense H₂ consumption at 435°C (2'310s) and a shoulder from 3'600 to 5'600s (Mg₆₈Al₃₂) can be attributed to the Rh present in solid solution with Mg and Al (Graph 7) analogously to the Rh1%.



Graph 35. Temperature programmed reduction of Rh₂%Mg₆₈Al₃₂exHT.

The pore size distribution of Rh2% Mg₆₈Al₃₂exHT sample shows three different pore regions in the range of pore distribution curve at 35Å, 60Å and 105Å; BET surface area is 101m²g⁻¹.



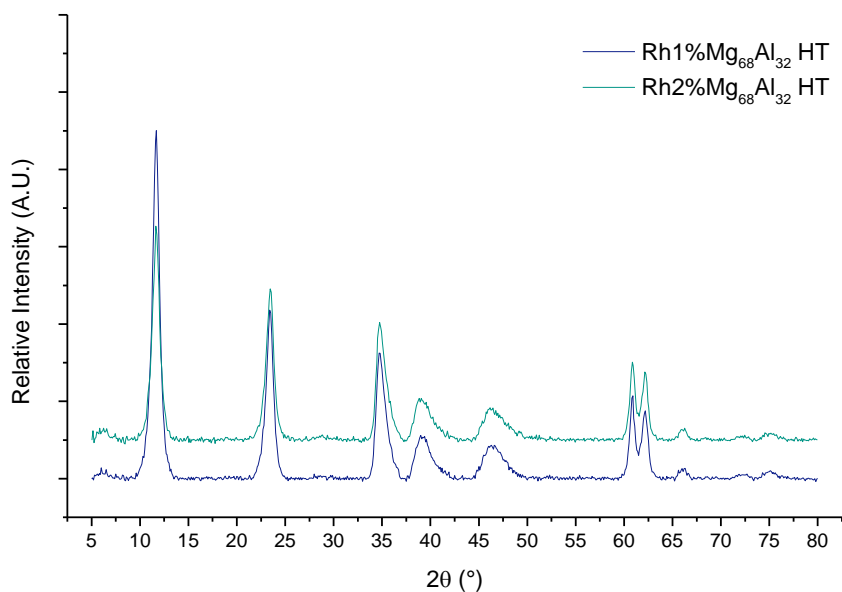
Graph 36. BJH pore size distribution of fresh Rh1%Mg₆₈Al₃₂exHT.

3.6.2 Comparison with the Rh1% Mg₆₈Al₃₂

Composition	M ²⁺ /M ³⁺	HT	Cal
Rh1% Mg ₆₈ Al ₃₂	68/32	133	124
Rh2% Mg ₆₈ Al ₃₂	68/32	101	86

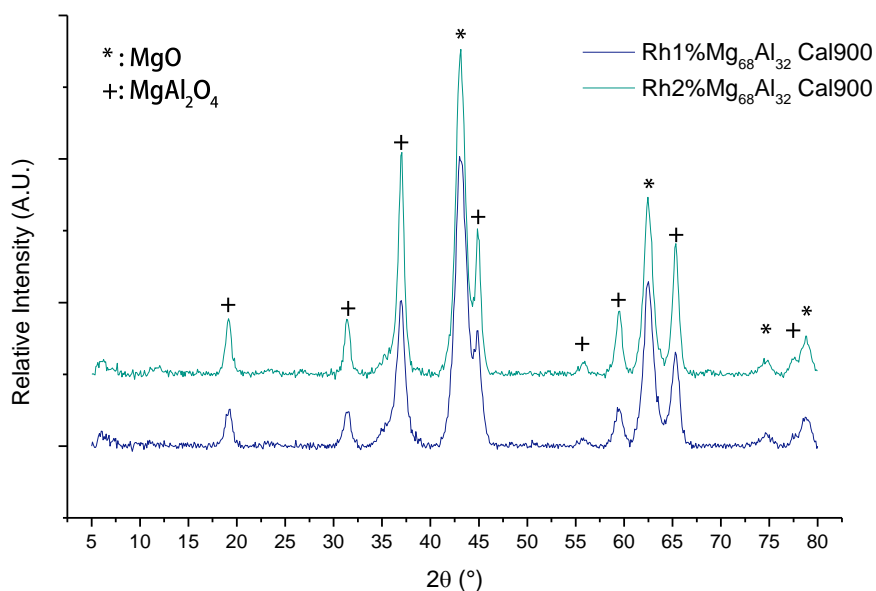
Table 13. Surface areas of samples containing Rh1%. Values are expressed in m²/g before calcination (HT column) and after calcination at 900°C for 12h (Cal column).

In Graph 37 XRD pattern of the precursor of the Rh2% Mg₆₈Al₃₂ is reported compared to the Rh1% Mg₆₈Al₃₂ XRD pattern. The precursor show the typical reflections of the hydrotalcite like compounds but no presence of Rh is showed due to the low amount and no crystallinity.



Graph 37. XRD patterns of the HT's with 1 and 2% of Rh prepared with co-precipitation method. Blue line represents Rh1% $Mg_{68}Al_{32}$ HT, the green line represents the Rh2% $Mg_{68}Al_{32}$ HT.

In Graph 38 XRD pattern of the calcined Rh2% $Mg_{68}Al_{32}$ HT is reported compared to the Rh1% $Mg_{68}Al_{32}$. The precursor show the typical reflections of the hydrotalcite like compounds but no presence of Rh is showed due to the low amount and no crystallinity.

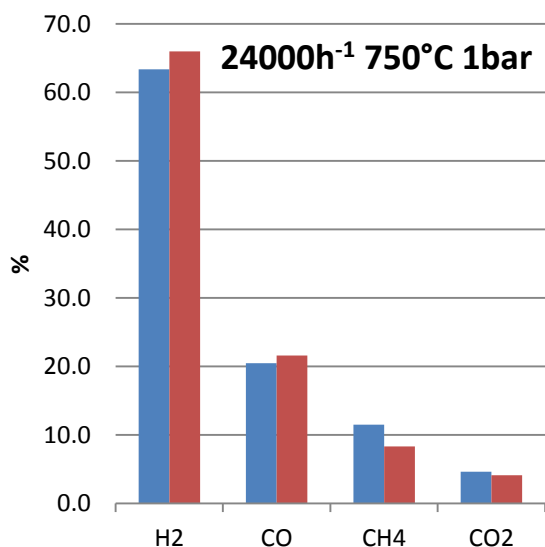


Graph 38. XRD patterns of the calcined samples containing 1% of Rh. Green line represents Rh1% $Mg_{68}Al_{32}$ after calcination at 900°C for 12h, the blue line represents the Rh1% $Mg_{80}Al_{20}$ after calcination at 900°C for 12h.

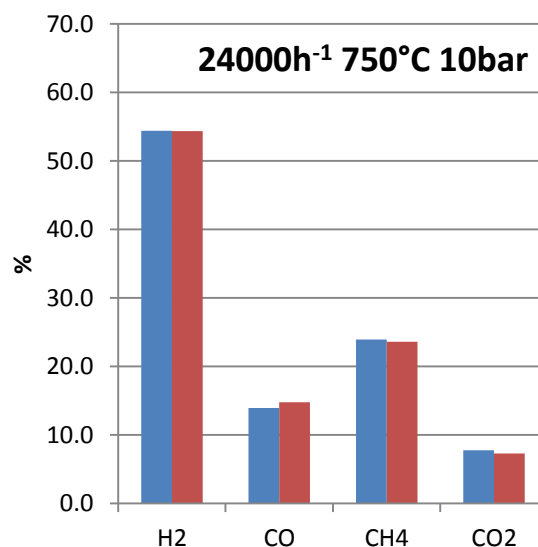
As already seen in 3.3.2 after calcination 2 phases have been identified the MgAl_2O_4 and the MgO . Rh have been not identified due its low concentration and its statistical distribution in the material.

3.6.2.1 Catalytic Tests Comparison as Function of the Rh Content

The data obtained with Rh2% $\text{Mg}_{68}\text{Al}_{32}$ will be reported compared with the data obtained with the Rh1% $\text{Mg}_{68}\text{Al}_{32}$ in order to evaluate the effects to increase the active phase.

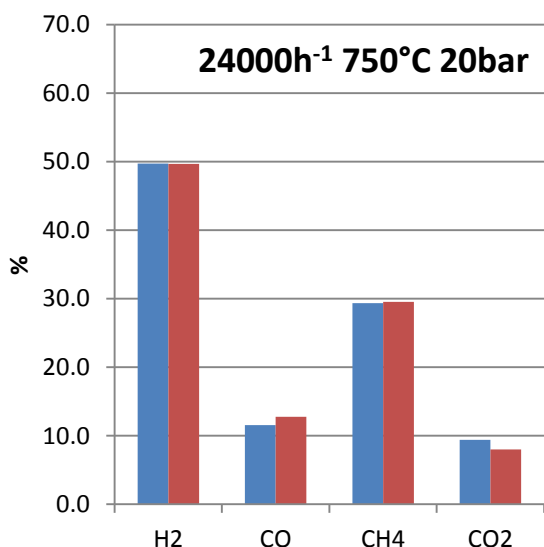


Graph 39. Outlet composition for Rh1% $\text{Mg}_{68}\text{Al}_{32}$ (blue bars) compared with Rh2% $\text{Mg}_{68}\text{Al}_{32}$ (red bars) at 1bar, 24'000h-1 and 750°C.

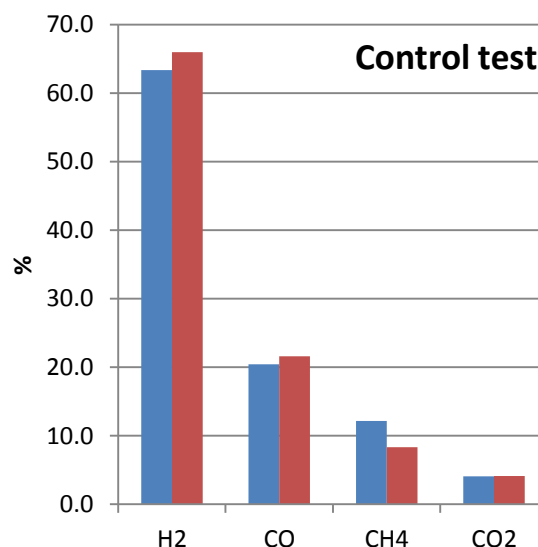


Graph 40. Outlet composition for Rh1% $\text{Mg}_{68}\text{Al}_{32}$ (blue bars) compared with Rh2% $\text{Mg}_{68}\text{Al}_{32}$ (red bars) at 10bar, 24'000h-1 and 750°C.

In the first test showed in Graph 39 high conversion is observed for the Rh2%. advantages are observed, the conversion of the methane is a bit lower than the same test with the half amount of Rh, as already discussed elsewhere the equilibrium is not reached. In Graph 40 and Graph 41 GHSV is maintained constant and only pressure has been changed. In this case the equilibrium is reached and no significant difference between the two catalysts have been observed.

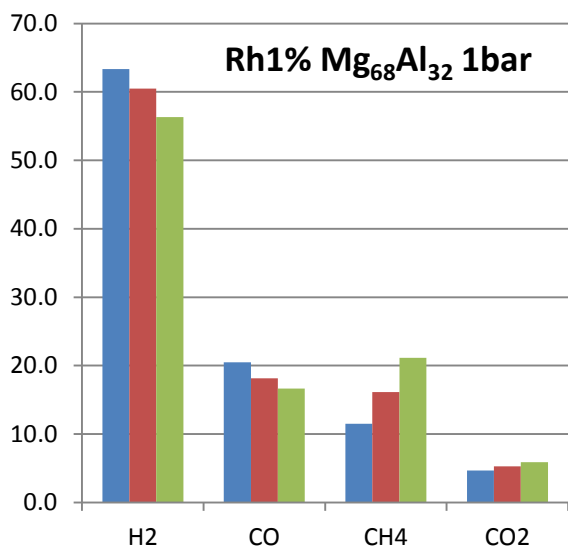


Graph 41. Outlet composition for Rh1% Mg₆₈Al₃₂ (blue bars) compared with Rh2% Mg₆₈Al₃₂ (red bars) at 20bar, 24'000h⁻¹ and 750°C.

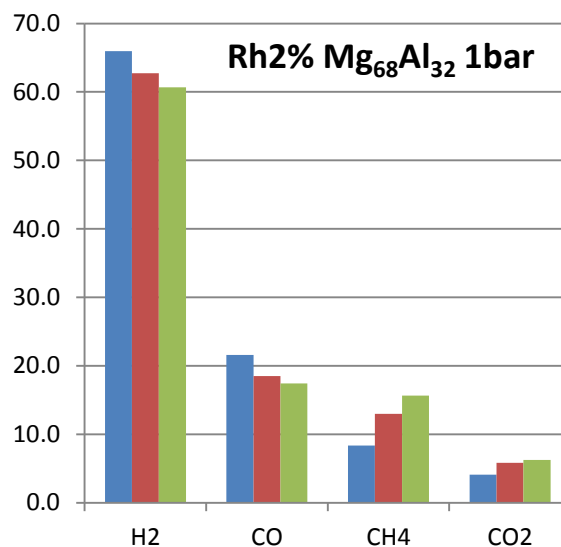


Graph 42. Outlet composition for Rh1% Mg₆₈Al₃₂ (blue bars) compared with Rh2% Mg₆₈Al₃₂ (red bars) at 1bar, 24'000h⁻¹ and 750°C. Control test.

The control test in Graph 42 shows better performance of the Rh2% reversing the situation showed in Graph 39. This highlights a probable lack of reduction of the Rh in the bulk material.



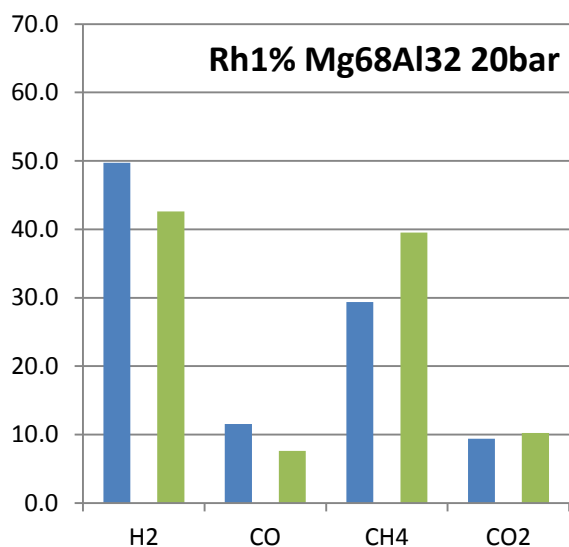
Graph 43. Outlet composition for Rh1% Mg₆₈Al₃₂ at 1bar, 750°C and different GHSV: 24'000h⁻¹ (blue bars), 50'000h⁻¹ (red bars) and 100'000h⁻¹ (green bars)



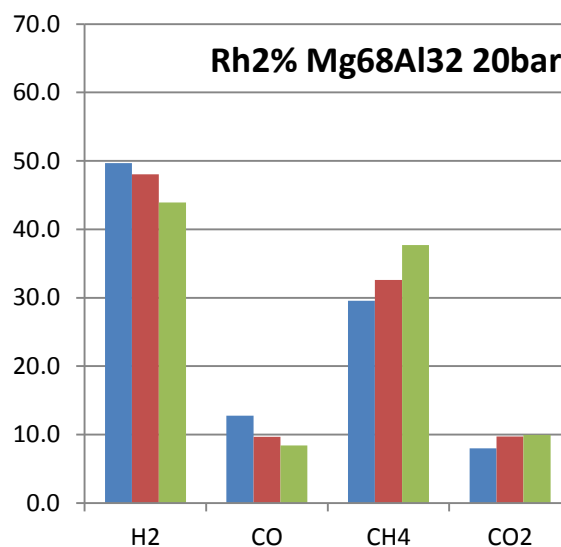
Graph 44. Outlet composition for Rh2% Mg₆₈Al₃₂ at 1bar, 750°C and different GHSV: 24'000h⁻¹ (blue bars), 50'000h⁻¹ (red bars) and 100'000h⁻¹ (green bars)

Continuing the test from this point demonstrate that increasing the amount of active phase the performances where the equilibrium is not reached are always improved. Increasing the GHSV from 24'000h⁻¹ to 100'000h⁻¹ at 1bar and 20bar best performances of the Rh2% is

showed as expected due to a more available Rh is present on the catalyst (Graph 43 and Graph 46).



Graph 45. Outlet composition for Rh1% Mg₆₈Al₃₂ at 1bar, 750°C and different GHSV: 24'000h⁻¹ (blue bars), 50'000h⁻¹ (red bars) and 100'000h⁻¹ (green bars)



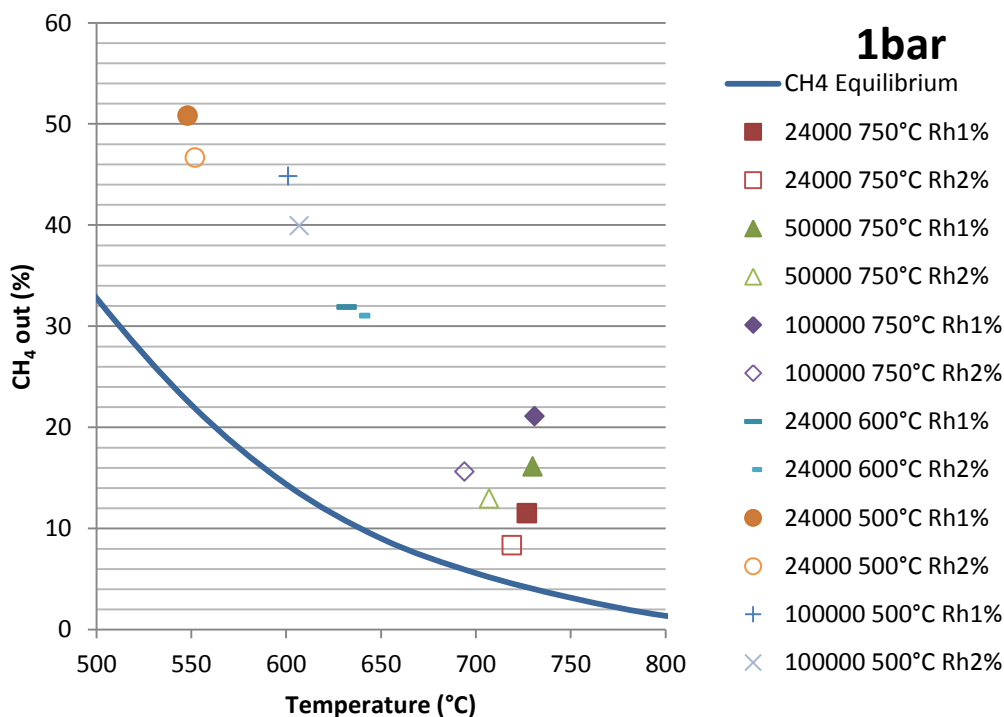
Graph 46. Outlet composition for Rh1% Mg₆₈Al₃₂ at 1bar, 750°C and different GHSV: 24'000h⁻¹ (blue bars), 50'000h⁻¹ (red bars) and 100'000h⁻¹ (green bars)

For better understanding room of improvements a direct comparison of the two catalysts studied with the equilibrium curves is necessary (Graph 47). With this comparison is more clear as the methane at the exit of the catalytic bed at one bar is closer to the equilibrium value when Rh2% is used as catalyst in the oxy-reforming reaction. If pressure is increased up to 20bar these differences are no more visible.

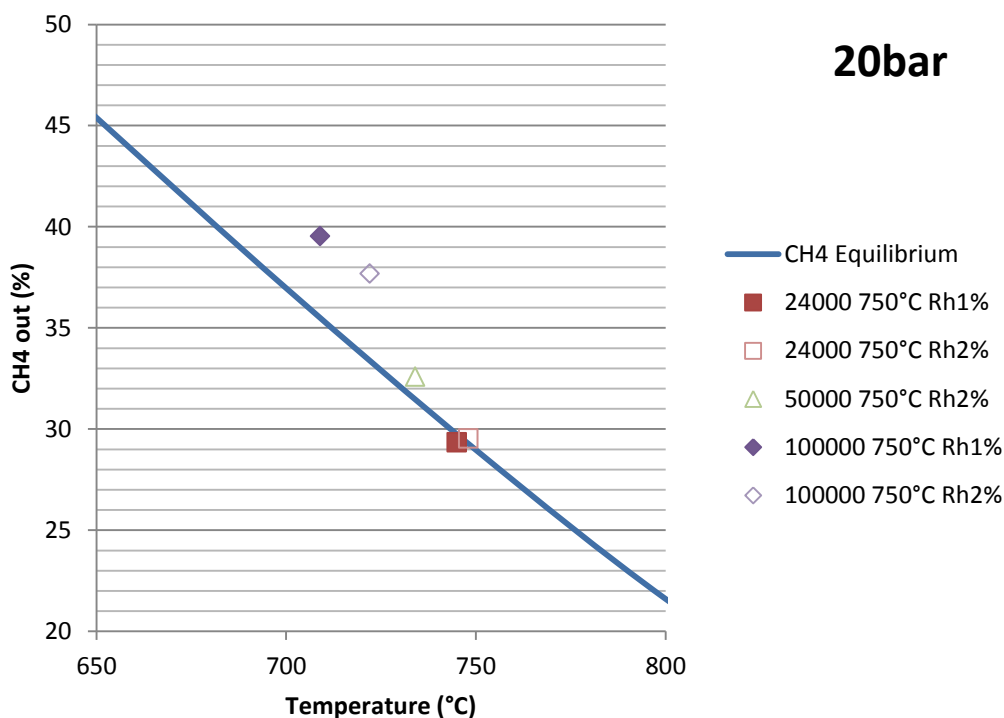
T (°C):	750	750	750	750	750	750	750	750	750	600	500	500	750
GHSV (h-1):	24000	24000	24000	24000	50000	100000	50000	100000	100000	24000	24000	100000	24000
P(bar):	1	10	20	1	1	1	10	10	20	1	1	1	1
H ₂	62.1	54.3	49.7	66.0	62.7	60.7	53.3	46.2	43.9	49.4	37.2	42.0	62.8
CO	19.1	14.7	12.8	21.6	18.5	17.4	13.4	9.4	8.4	8.8	3.4	7.5	20.4
CH ₄	13.5	23.6	29.5	8.3	13.0	15.6	25.6	34.7	37.7	31.0	46.7	39.9	12.9
CO ₂	5.3	7.3	8.0	4.1	5.8	6.3	7.7	9.8	10.0	10.8	12.7	10.5	3.9
Tot	100.0	100.0	100.0	100.0	100.0	100.0	100.0	100.0	100.0	100.0	100.0	100.0	100.0
X _{CH₄}	64.4	48.2	41.4	75.6	65.1	60.3	45.2	35.6	32.8	38.7	25.6	31.1	65.3
S _{CO}	78.3	66.8	61.5	84.0	76.1	73.4	63.5	49.0	45.7	44.9	21.1	41.7	84.0
H ₂ /CO	3.3	3.7	3.9	3.1	3.4	3.5	4.0	4.9	5.2	5.6	10.9	5.6	3.1
Catalytic bed outlet temperature (°C)	719	738	748	719	707	794	715	709	722	639	549	607	733

Table 14. Complete results from test with Rh2% Mg₆₈Al₃₂

Increasing the GHSV also at 20bar equilibrium is not reached, the values are closer to the equilibrium line but they still do not reach it. The role of increasing the active phase was not focused on an improving of the catalytic activity but on the confirmation of the catalytic activity thinking on a preparation of slurry for coating a classical industrial ceramic honeycomb generally used for this applications.



Graph 47. Equilibrium curve for the CH₄ outlet composition compared with the real composition obtained with exHT's catalysts containing 1% and 2% of Rh. Equilibrium curve is calculated with CEA-NASA.



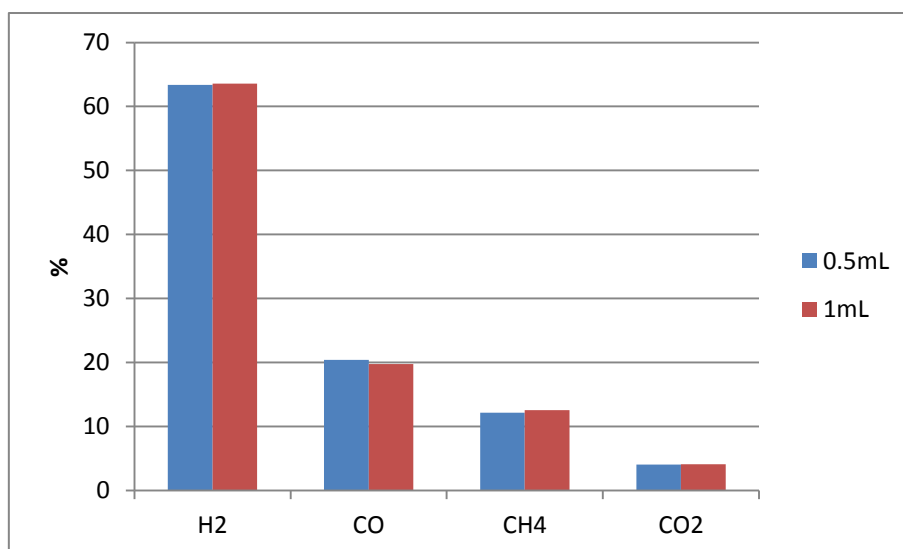
Graph 48. Equilibrium curve for the CH₄ outlet composition compared with the real composition obtained with exHT's catalysts containing 1% and 2% of Rh. Equilibrium curve is calculated with CEA-NASA.

3.6.3 Validation of the Results Obtained with Rh2% Mg₆₈Al₃₂

To validate the results obtained with Rh1% Mg₆₈Al₃₂ analogous reaction conditions with differences in fluid dynamics parameters have been carried out.

- Different amount of catalyst at the same space velocity in the same reactor have been tested to compare results doubling the linear velocity.
- Different pellet dimension keeping constant the total weight of the catalyst

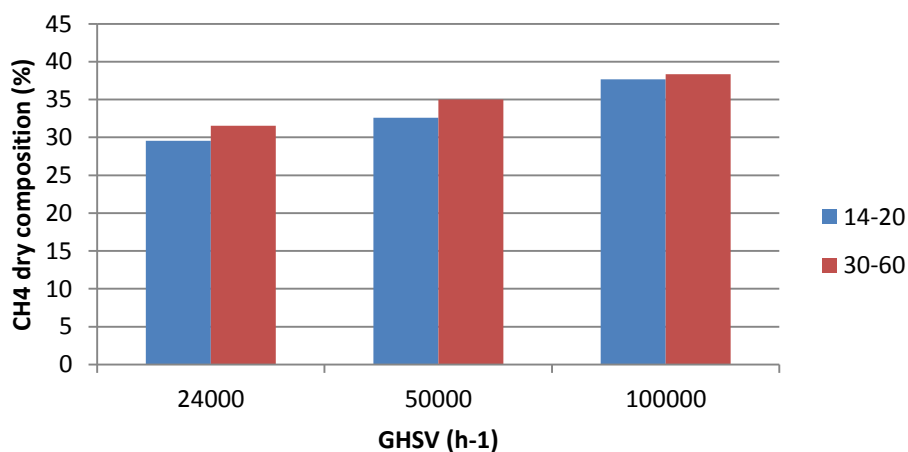
The different amount of catalyst at the same space velocity in the same reactor with i.d. of 10mm have been tested to compare results doubling the linear velocity. The tests show similar results both at low and high pressure. In Graph 49 are reported conditions in which the results are far from the thermodynamic equilibrium and thermal input from the reaction is minimum and therefore minimum is the change in thermal profile; i.e. P=1bar, GHSV=24'000 h⁻¹.



Graph 49. Comparison of dry outlet composition doubling quantity of catalyst. GHSV: 24'000h-1; T(oven): 750°C; P: 1bar.

By changing the pellets dimension from 1.4-0.8mm to 0.6-0.3mm results do not change and only a slight decrease of conversion (<2%) are present using smaller pellets. The decrease excludes significant effect of mass transfer limitation while it can be an indication of differences in the heat transfer between the reactor wall and the center of the catalytic bed.

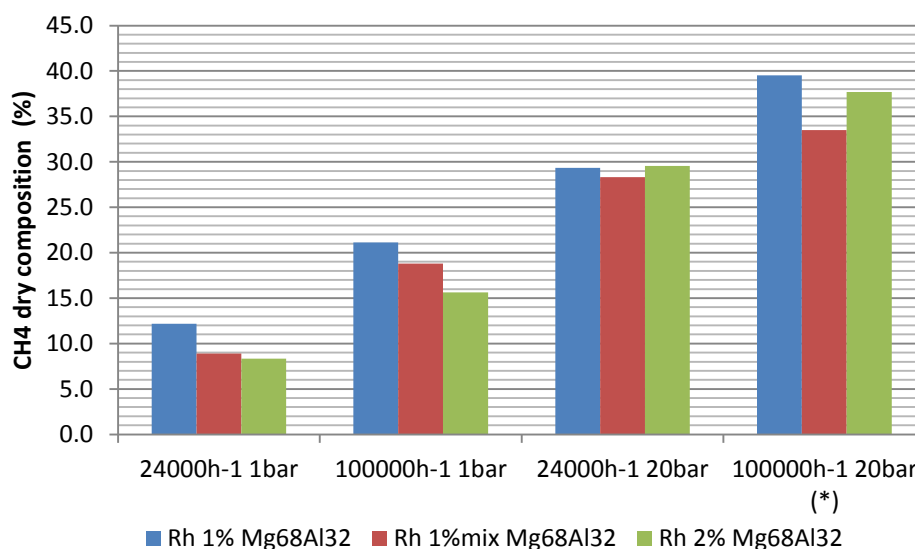
20bar 750°C



Graph 50. Comparison of methane outlet composition for Rh1% Mg₆₈Al₃₂ at 20bar and 750°C among two different particle size: 14-20MESH (1.4-0.8mm) and 30-60MESH (0.6-0.3)mm

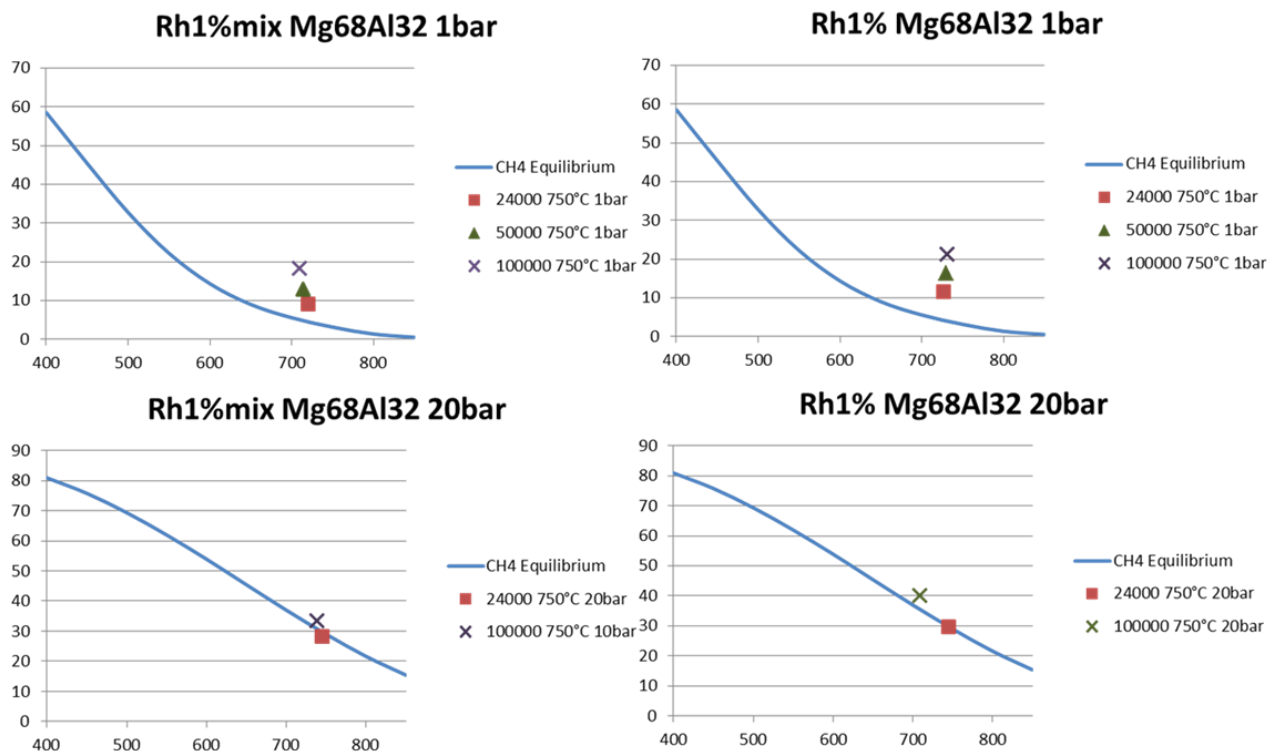
As conclusion the constant results changing the fluid dynamics parameter and the better results obtained in all the tests using Rh1% Mg₆₈Al₃₂ with respect to other catalysts validate the selection of this catalytic system as candidate for scale up.

The calcined Rh1% Mg/Al 68/32 (atomic ratio) and with a catalyst produced by mixing 1:1 a calcined Rh 2% Mg/Al 68/32(a.r.) with a calcined Mg/Al 68/32(a.r.) hydrotalcite i.e. producing by mixing a Rh1% catalyst called Rh1% mix. For a complete comparison the Rh2% Mg/Al 68/32(a.r.) is also shown. The results of Graph 51 show at low pressure a scale of activity Rh2% > Rh1% mix > Rh1%. The higher conversion of Rh2 % can be attributed to the higher methane loading while it seems that the higher conversion of Rh1% mix can be due to either to an increase Rh reducibility (due to the higher concentration in the Rh2% matrix) which allow an increase of availability of Rh on the surface or a slight increase of the particle dimension which increase the specific activity. Increasing the pressure at high residence time (GHSV=24'000h⁻¹) allows to reach the equilibrium while the comparison at low residence time (GHSV=100'000h⁻¹) is difficult due to the significant differences in temperature among the three catalysts ((* bars in Graph 51); being the outlet temperature of the Rh1% mix 30°C and 18°C higher than the Rh1% and Rh2% respectively.



Graph 51. Methane outlet composition for different catalyst at different condition, (*) the three catalyst have an outlet temperature of 709, 735 and 722°C respectively.

The comparison using the equilibrium curves between Rh1% and Rh1%mix show that the Rh1%mix is closer to the equilibrium at lower pressure while at high pressure both catalyst shows performances very close to the equilibrium value.



3.6.3.1 New Study of Rh1% Mg₆₈Al₃₂

The tests on the Rh1% mix have shown that the increasing Rh concentration can affect the catalytic performances. To verify the Rh reducibility a CO chemisorption have been carried out on the Rh1% Mg/Al:68/32 (atomic ratio).

The Dispersion calculated with the chemisorption was very low if compared with that expected on the bases of the Dp calculator using TEM image being less than 2 nm

Metal Dispersion:	10.7%
Metallic Surface Area:	0.47m²/g sample
Metallic Surface Area:	47m²/g metal

Table 15. Chemisorption analysis of Rh1%Mg₆₈Al₃₂.

An attempt to increase the reduction temperature have been carried out to increase the reducibility. A reduction at 1000°C for 30 minutes and 180 minutes have been carried out and the TEM image show an increase of the particle size together with an increase of the concentration of particles probably due to the decrease of the surface area of the sample to approximately 30 m²g⁻¹.

R1% Mg ₆₈ Al ₃₂	Rid 1000°C 30'	Rid 1000°C 180'
Dp* (nm)	1.8	2.6

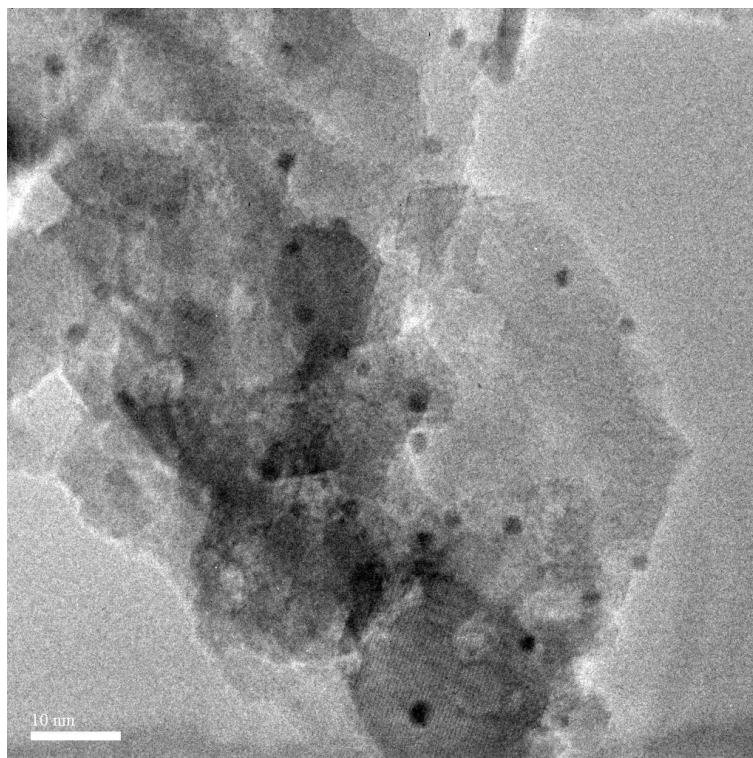


Figure 43. TEM image of Rh1% Mg₆₈Al₃₂. Black dots are Rh particles.

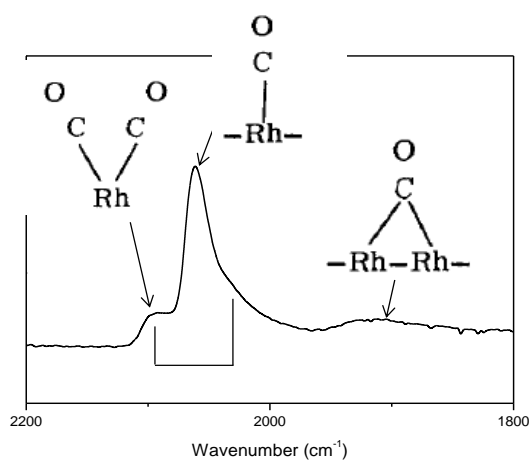


Figure 44. IR bands identification

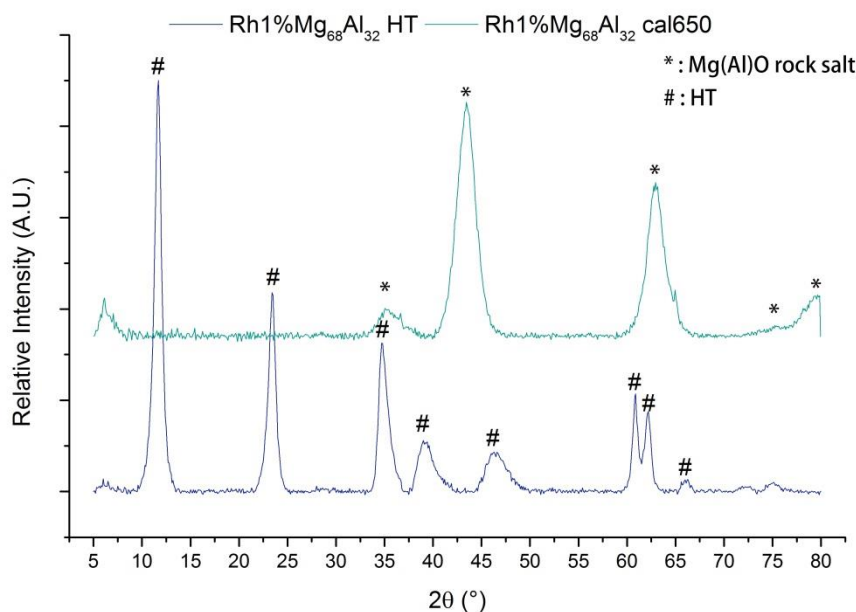
IR spectroscopy of the adsorbed CO at low pressure of CO shows three bands; beside the two band at 2'050cm⁻¹ and at 2'080cm⁻¹ attributed respectively to linear chemisorbed carbonyl, Rh⁰(CO), and Rh¹(CO)₂ identified for the sample reduced at 750°C, bridged carbonyl have been detected at low wavenumber indicating and confirming the increase of the particle size [110].

The sharp increase of the particle dimension with time show that is not a reproducible way to increase the reducibility especially on industrial catalyst therefore a new studies on therma treatment have been carried out reducing the Rh from the MgAl matrix before the formation of the two MgO MgAl₂O₄ oxide phases, using the defectivity of the MgAlO_x phase present below 750°C to increase the Rh mobility and its reducibility.

3.6.4 Optimization of the Active by Different Thermal Treatment: Rh1% Mg₆₈Al₃₂ tt

3.6.4.1 Characterization

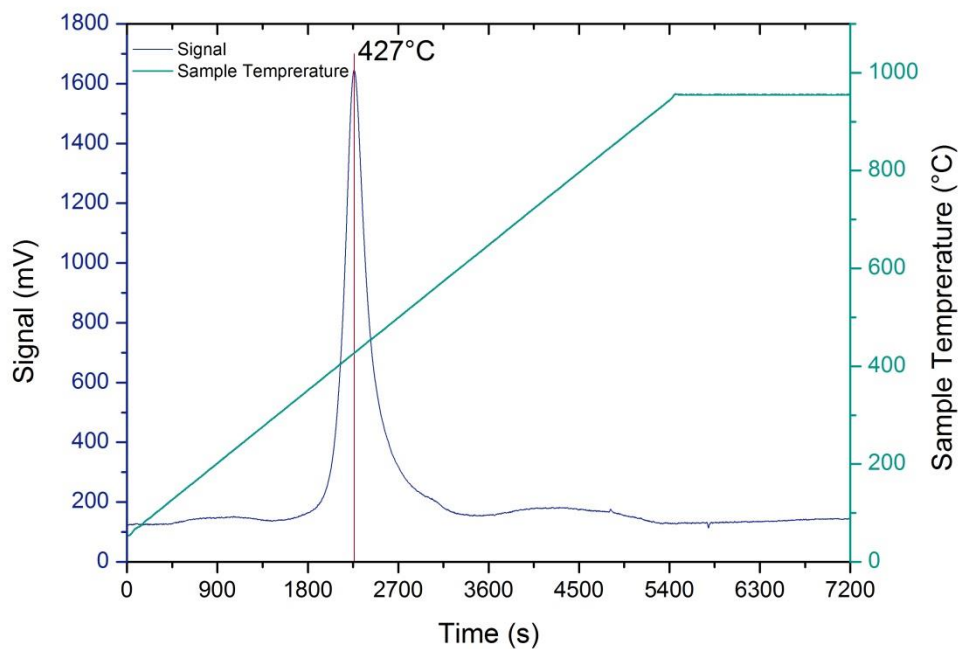
The XRD pattern of Rh1% Mg₆₈Al₃₂ HT after calcination at 650°C show a defective structure, already observed from Basile [99] [100] that is a defective Mg(Al)O rock salt with solved atoms of active phase. The idea is to promote the active phase reducing it before the formation of the stables MgO and MgAl₂O₄ and then calcine not in static air but in nitrogen directly inside the reactor.



Graph 52. XRD pattern of Rh1% Mg₆₈Al₃₂ HT before and after calcination at 650°C

The XRD pattern after first calcination at 650°C shows the formation of the mixed oxide Mg(Al)O in which the Rh is solved. Spinel phase and MgO phase are not still formed. The TPR analysis shows an intense peak at 427°C and a shoulder at high temperature. The comparison

with the Rh1% Mg₆₈Al₃₂ calcined at 900°C is not significant and therefore deeper characterization is required..



Graph 53. Temperature programmed reduction of Rh1% Mg68Al32 HT after calcination at 650°C.

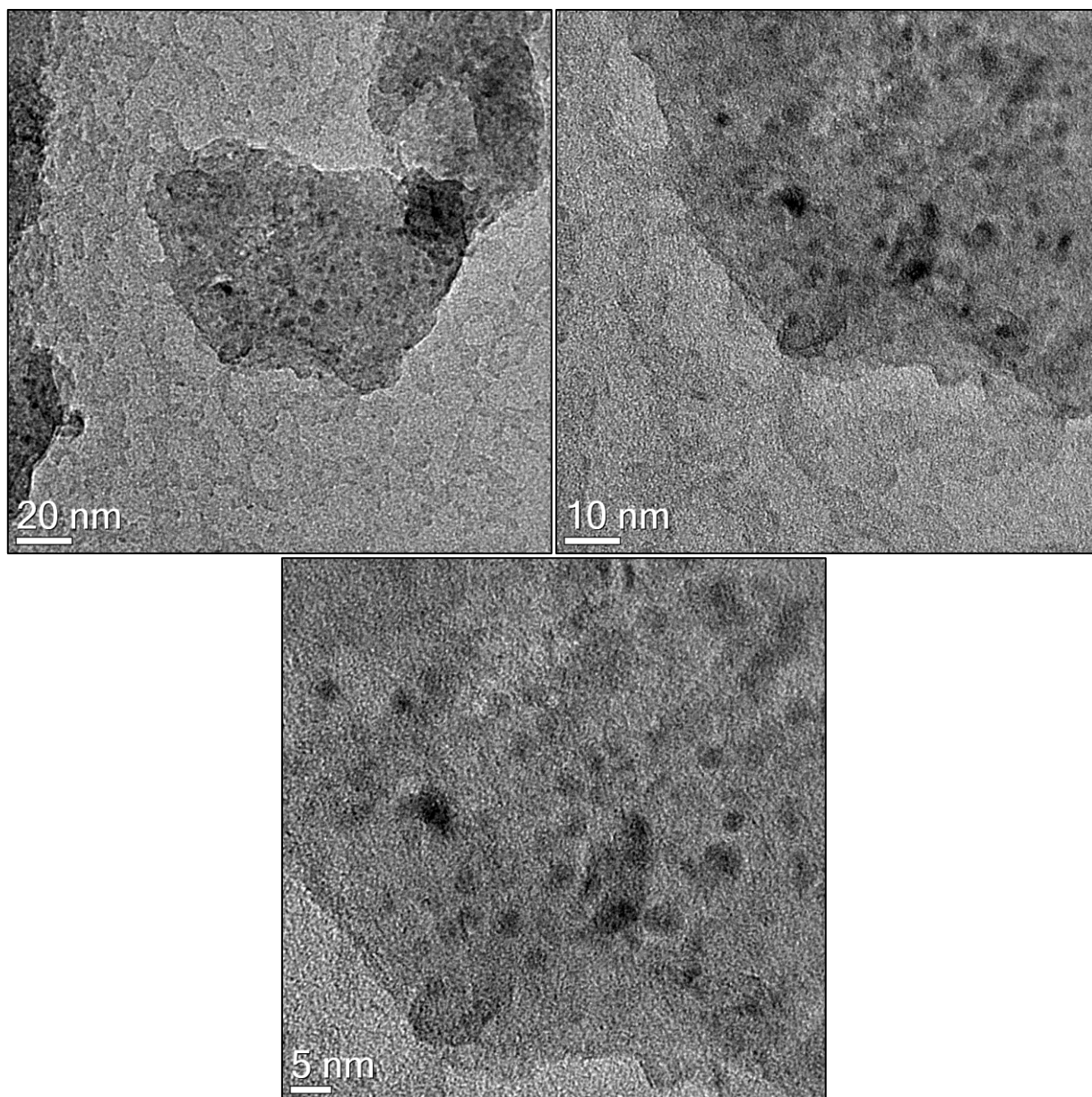


Figure 45. TEM images for Rh1% Mg₆₈Al₃₂tt, particle dimension (black dots) of 2.5nm.

750°C reduced samples	Rh1% Cal900	Rh1% Cal650
Metal Dispersion:	10.7%	46%
Metallic Surface Area:	0.47m ² /g sample	2.00 m ² /g sample
Metallic Surface Area:	47m ² /g metal	200 m ² /g metal

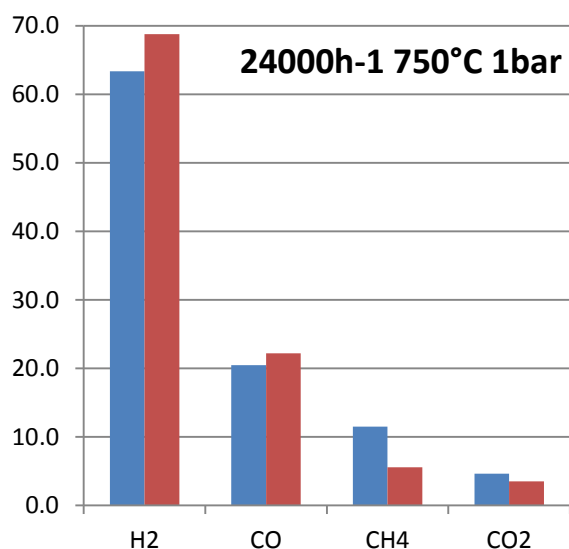
Table 16. Chemisorption analysis of Rh1% Mg₆₈Al₃₂tt compared with Rh1% Mg₆₈Al₃₂.

The TEM images shows particles of Rh a bit larger (2.5nm) from the ones of the sample calcined at 900°C (1.4nm). The high number of particles presents on the surface and their dimension are probably due to an increase reduction of R. The comparison of the chemisorption metallic surface area and dispersion give clear indication of an higher

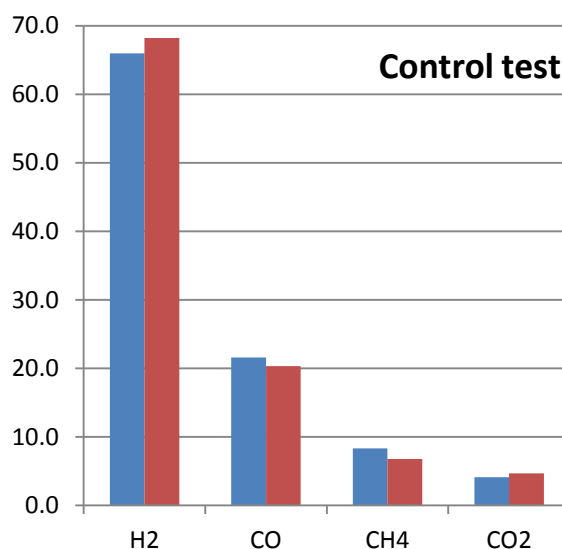
availability of Rh on the surface and therefore of a large increase of the reducibility allowing high catalytic performances.

3.6.4.2 Catalytic Activity

If the Rh1% Mg₆₈Al₃₂ is thermally treated in a different way after synthesis the activity of the catalyst change. Instead of a direct calcination in air at 900°C after drying and the reduction of the active phase at 750°C overnight the HT after drying is calcined at 650°C in air for 12h, reduced in diluted H₂ stream as the classical way then calcined at 900°C for 12h under N₂ stream.

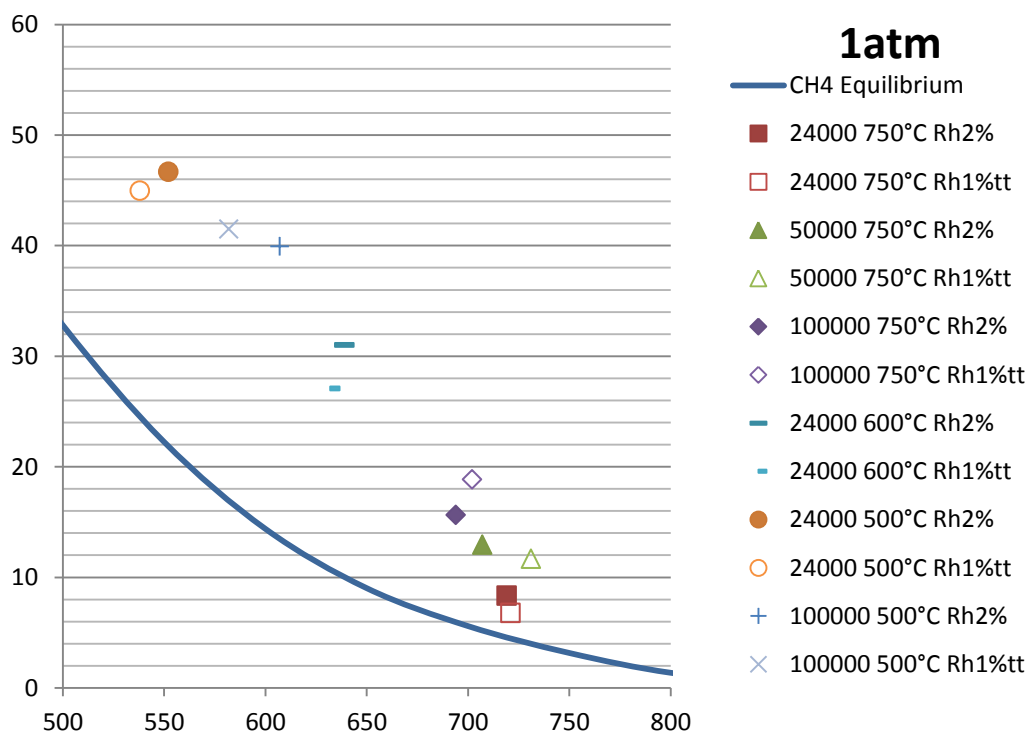


Graph 54. Outlet composition for Rh1% Mg₆₈Al₃₂ (blue bars) compared with Rh1% Mg₆₈Al₃₂tt (red bars) at 1bar, 24'000h⁻¹ and 750°C.

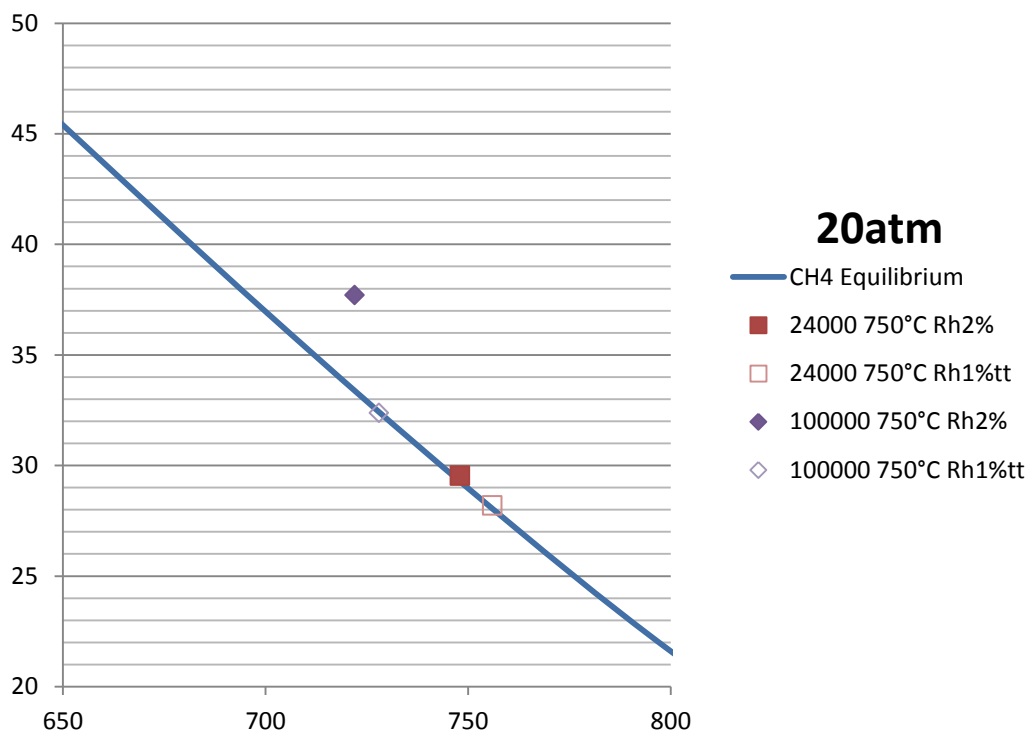


Graph 55. Outlet composition for Rh2% Mg₆₈Al₃₂ (blue bars) compared with Rh1% Mg₆₈Al₃₂tt (red bars) at 1bar, 24000h⁻¹ and 750°C.

The methane composition in the outlet stream obtained with the catalyst thermally treated is significantly lower the composition obtained with the standard Rh1% catalyst (Graph 54) meant a closer value to the equilibrium one. Also if compared with the results obtained with the Rh2% the catalyst is slightly more active. In Graph 55 the control test is showed as comparison because there is a lack of reduction for the Rh 2% as discussed in 3.6.1. Increasing the GHSV the the catalyst thermally treated confirm his improved activity at low pressure tests and also at high pressure as showed in Graph 56 and Graph 57. In particular at 20bar the equilibrium is reache not only at 24'000h⁻¹ but also at 100'000h⁻¹ in which the Rh1% Mg₆₈Al₃₂ and the Rh2% Mg₆₈Al₃₂ were close but they still did not reach the equilibrium.



Graph 56. Equilibrium curve for the CH₄ outlet composition compared with the real composition obtained with exHT's catalysts containing 2% and 1% of Rh after a different thermal treatment. Equilibrium curve is calculated with CEA-NASA.



Graph 57. Equilibrium curve for the CH₄ outlet composition compared with the real composition obtained with exHT's catalysts containing 2% and 1% of Rh after a different thermal treatment. Equilibrium curve is calculated with CEA-NASA.

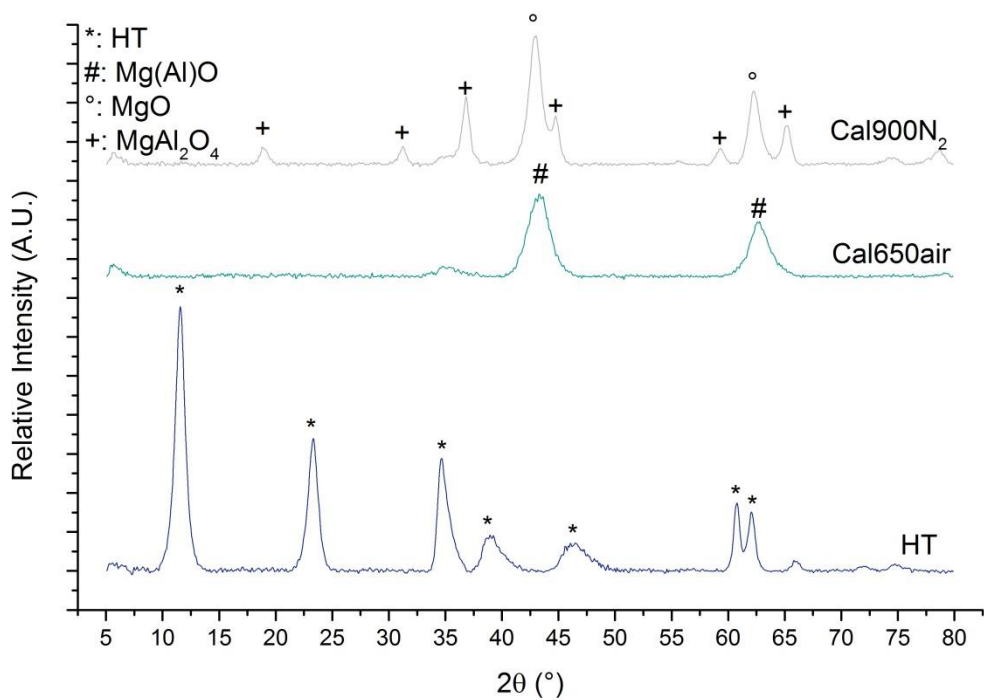
For better interpretation a full table with data is showed.

T (°C):	750	750	750	750	750	750	750	600	500	500	750
GHSV (h ⁻¹):	24'000	24'000	24'000	24'000	50'000	100'000	100'000	24'000	24'000	100'000	24'000
P(bar):	1	10	20	1	1	1	20	1	1	1	1
H ₂	68.8	57.3	52.3	68.2	63.9	58.6	49.0	53.0	39.3	41.5	68.2
CO	22.2	12.5	10.2	20.3	19.5	16.9	9.7	9.6	3.2	6.5	20.6
CH ₄	5.6	22.5	28.2	6.8	11.7	18.9	32.4	27.1	45.0	41.5	6.7
CO ₂	3.5	7.7	9.3	4.7	4.8	5.6	8.9	10.3	12.6	10.6	4.5
Tot	100.0	100.0	100.0	100.0	100.0	100.0	100.0	100.0	100.0	100.0	100.0
X _{CH₄}	82.1	47.3	40.9	78.6	67.5	54.3	36.5	42.3	26.0	29.2	78.9
S _{CO}	86.4	61.9	52.3	81.2	80.2	75.1	52.2	48.2	20.3	38.0	82.1
H ₂ /CO	3.1	4.6	5.1	3.4	3.3	3.5	5.1	5.5	12.3	6.4	3.3
Catalytic bed outlet temperature (°C)	707	752	746	756	714	721	728	632	538	582	710

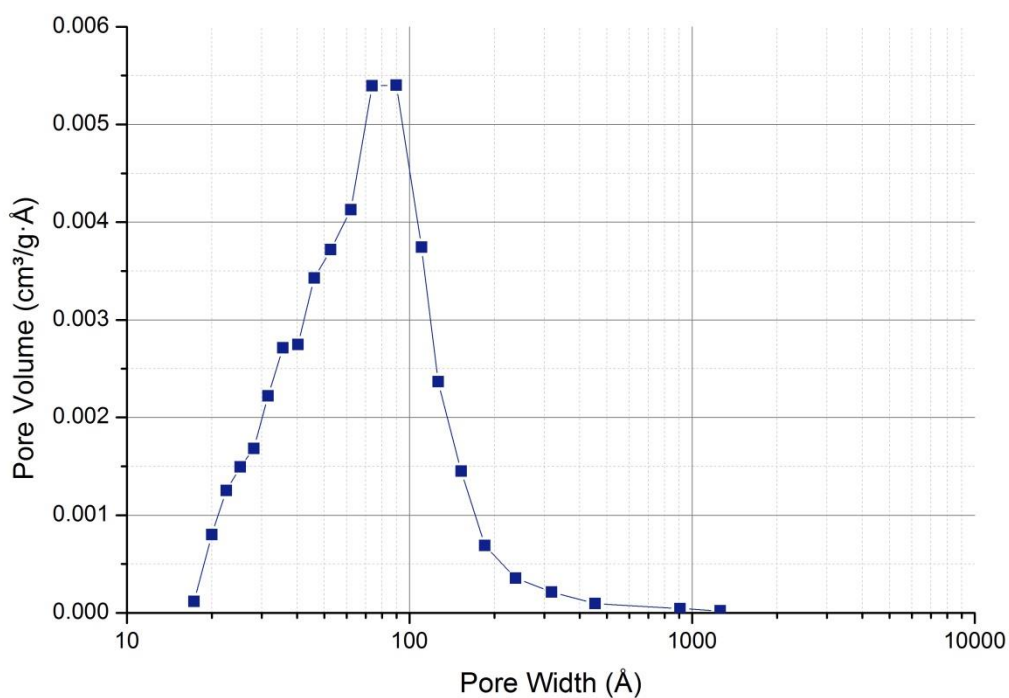
Table 17. Complete results obtained with Rh1%Mg₆₈Al₃₂tt. In blue are showed the control tests.

3.6.5 Rh3% Mg₆₈Al₃₂

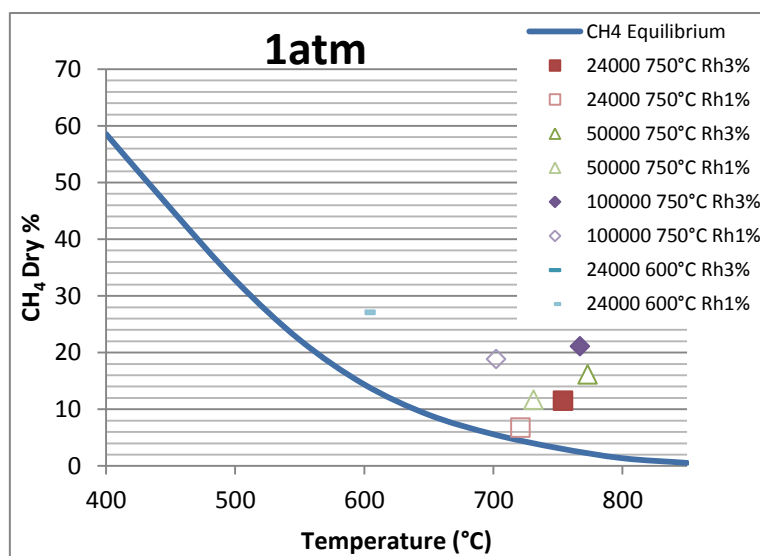
The catalyst has been prepared by co-precipitation route then calcined at 900°C for 12h. The XRD analysis of the sample before calcination shows a typical pattern for an HT precursors in which the active metal is not directly detectable due to its solubility in the matrix. The calcined sample at 650°C shows only the amorphous Mg(Al)O phase while, after, reduction and calcination at 900°C in N₂ stream only two phases are detected: MgO and MgAl₂O₄ in which the third metal is solved. The pore size distribution of Rh3% Mg₆₈Al₃₂exHT sample calcined at 650°C shows one broad pore region in the range of pore distribution curve from 30Å to 110Å with high BET surface area of 215m²g⁻¹



Graph 58. XRD patterns of HT precursor and calcined samples.



Graph 59. BJH pore size distribution of Rh3% Mg₆₈Al₃₂.



Graph 60. Equilibrium curve for the CH₄ outlet composition compared with the real composition obtained with exHT's catalysts containing 3% and 1% of Rh. Equilibrium curve is calculated with CEA-NASA.

The comparison of Rh1% and Rh3% exHT's vs. the equilibrium curve shows the improvement at low residence time of catalyst containing higher amount of active phase.

3.6.6 Structured Catalysts

The Rh3% Mg₆₈Al₃₂ has been used as coating for honeycomb support in order to directly compare the industrial catalyst with the catalyst produced in laboratory. So the company partner of the project impregnated the industrial ceramic support with Rh3% Mg₆₈Al₃₂ and the catalyst has been tested in the laboratory plant. The plant has been modified for this scope in order to load a honeycomb of 25.4mm of diameter. With this rig was impossible to work at high pressure due to the fact that the reactor, for simplicity, was made in quartz.

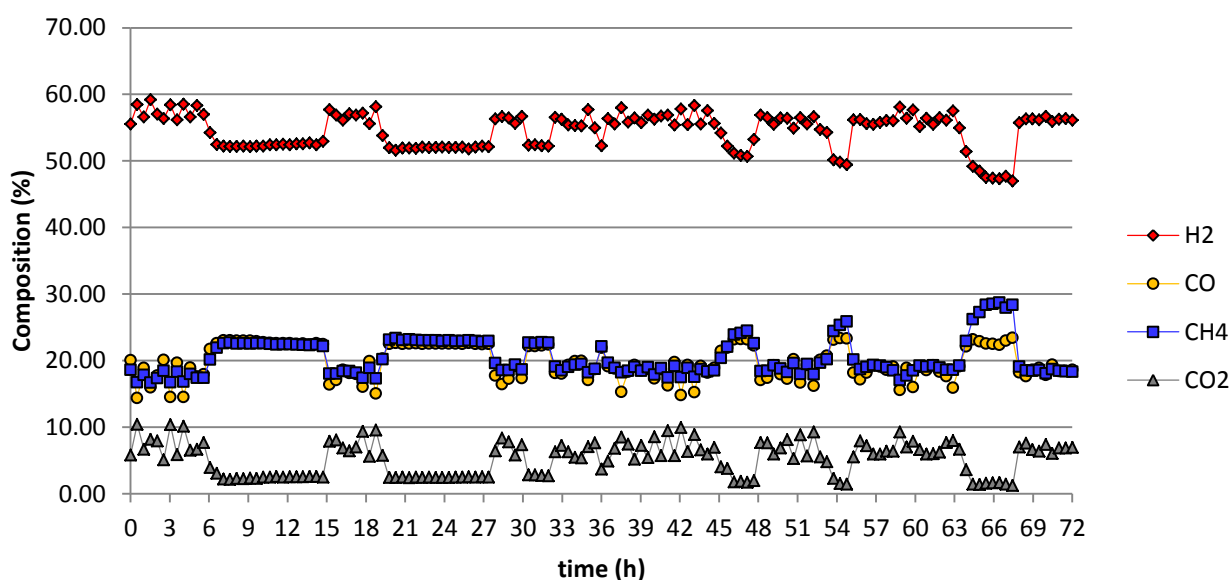
3.6.6.1 Honeycomb catalyst

The IC and the Rh-Mg/Al catalysts have been coated on honeycomb monolith with 64 channels per inch and tested in a modified plant of higher capacity. The catalyst has been tested using two space velocities (12'000 and 24'000 h⁻¹) corresponding to a residence time of 150 and 300ms in a reactor having an i.d. of 25.4mm with a bed length of approximately 25mm. The outlet methane concentration was lower for the Rh1% Mg₆₈Al₃₂ in the two reaction conditions, confirming the enhanced performances of this catalytic material. The performances of the UniBO catalyst show the same exit methane concentration (i.e. same conversion) with respect to the industrial catalyst by doubling the space velocity i.e. reducing the residence time from 300 to 150ms, demonstrating the possibility of increasing productivity. The tests on the Rh

catalyst have been carried out for three days showing constant results and demonstrating the stability of the catalyst. The catalyst will be tested in the Chieti pilot plant by Technimont and a patent is under consideration in the consortium board to exploit the research results.

	12'000h ⁻¹		24'000h ⁻¹	
	Industrial Cat.	Rh3% supported	Industrial Cat.	Rh3% supported
H ₂	61.1 %	60.8 %	56.5 %	56.3 %
CO	17.8 %	18.8 %	14.4 %	17.7 %
CH ₄	15.9 %	12.6 %	21.9 %	17.6 %
CO ₂	5.5 %	7.8 %	7.1 %	8.4 %

Table 18. Comparison of structured industrial catalyst and the supported Rh3%exHT at 12'000h⁻¹ and 24000h⁻¹ in a 25.4mm i.d. quartz reactor.



Graph 61. Long test run (72h) with Rh3% Mg₆₈Al₃₂ supported on industrial honeycomb.

4 CONCLUSIONS

In this work, in order to support a new GTL scheme the oxy-reforming process and a new catalyst for the production of H₂ and CO have been developed. This work was part of an European project, NextGTL, , the aim was to demonstrate that a new route for the production of liquid fuel from methane is possible.

The research proven the possibility to run a process in non-conventional CPO and reforming reaction conditions characterized by a S/C ratio of 0.7 and a O₂/C ratio of 0.21. A smoothed thermal profile as consequence of exothermic oxidation reaction and endothermic reforming reaction in the same reactor region have been observed.

The reaction have been tested form 1-20 bar at 750°C changing the residence time from 150 to 36 ms. Low pressure tests have been shown to be kinetically controlled and in most of the case did not reach the equilibrium condition even at higher residence time, while the high pressure tests have been shown to give results much more close to the thermodynamic equilibrium.

On this bases the catalyst development has been carried investigating different active phase and formulation using the low pressure tests to discriminate among the catalyst activity and the high pressure tests to prove the activity and stability in industrial conditions.

Ru0.1% and Ru1% Mg₆₈Al₃₂ did not showed good catalytic activity due to the segregation of RuO₂ from the matrix, effect particularly visible in the XRD pattern of the Ru1% Mg₆₈Al₃₂. This is not visible for Ru0.1% but the tests did not showed a catalytic activity. Ru0.1%<Ru1%<Rh1%

The Mg/Al ratio influence the distribution of the active metal in the matrix due to the different solubility of the metal in the spinel MgAl₂O₄ phase and in the MgO. Two different ratio with 1% of Rh have been tested Mg/Al:80/20 and Mg/Al:68/32. The TPR analysis showed that the reducibility of the Rh from the matrix change while TEM show that some difference have been observed also in the particle dimension. On the bases of the performances during the catalytic activity tests the Rh Mg/Al:68/32 has been selected as catalyst for further development.

Rh1%/CeZrO₂ have been prepared and tested in order to evaluate the effect of a support with oxygen mobility and O²⁻ sink properties on the activity. The catalyst is less active than the

selected Rh on Mg/Al even if the Rh1% CeZrO₂ catalyst has an higher amount of Rh in the 1 ml catalytic bed due to the higher bulk density.

The insertion of a 2nd active metal have been tested to change the reactivity of the system. In this work two bimetallic catalyst have been tested: Ni₈Rh_{0.15}Mg₆₀Al_{31.85} (NRexHT) and (Pt/Rh:2.5/1)1%/Ce_{0.75}Zr_{0.25}O₂ (PRCZO). These catalyst showed higher catalytic activity but deactivate rapidly due to the formation of coke for the NRexHT and due to the sintering of the Pt on the PRCZO.

A semi industrial catalyst has been tested in order to compare the obtained good results with Rh1% Mg₆₈Al₃₂ with a real reference catalyst. Rh1% Mg₆₈Al₃₂ once again showed best results.

Different thermal treatment of the Rh1% Mg₆₈Al₃₂ showed as is possible to promote the Rh reduction from the structure to the surface. Calcination at lower temperature produce a MgAlO defective structure increasing the Rh mobility and reducibility. Therefore a 650°C calcination, then a reduction to 750°C and a second calcination in N₂ stream have been developed to increase the dispersion of the active phase visible by the TEM images and by chemisorption analysis. Rh1% Mg₆₈Al₃₂tt showed better catalytic activity of Rh2% Mg₆₈Al₃₂ and of Rh1% Mg₆₈Al₃₂.

In order to support the catalyst on an industrial honeycomb a scale up of the catalyst has been thought increasing the amount of the active phase in order to obtain a total amount of 1% of Rh in the final structured catalyst.

The RhMg₆₈Al₃₂ catalyst has been tested after coating on a honeycomb monolith and compared with the industrial catalyst in the same shape. The catalyst developed from UniBO show higher performance by increasing the methane conversion and allow the increase of the productivity of factor two i.e. by reducing the residence time and keeping the same conversion. The catalyst stability has been demonstrated on 3 days tests and the honeycomb catalyst will be tested in the pilot plant in Chieti.

5 REFERENCES

1. BRANDVOLD, T. A.; KOCAL, J. A. A process for the direct production of methanol. WO2007073532, 28 Jun 2007.
2. CHEN, W.; BRANDVOLD, T. A.; BRICKER, M. L.; KOCAL, J. A.; WALENGA, J. T. A process for the production of methanol from methane using a metal trifluoroacetate catalyst. WO2007073533, 28 Jun 2007.
3. CUMMINGS, D. R. Improvements in the utilisation of methane. WO2007260574, 21 Dec 2007.
4. RICHARDS, A. K. Manufacture of dimethyl ether or olefins from methane using DI(METHYL-SULFONYL) PEROXIDE as radical initiator. WO2007136425, 29 Nov 2007.
5. IACCINO, L. L.; LATTINER, J. R. Production of aromatic hydrocarbons and syngas from methane. WO2008002343, 03 Gen 2008.
6. SCHUBERT, M.; MUELLER, U.; TEICH, F.; KIESSLICH, F.; POPLOW, F. Process for preparing unsaturated hydrocarbons. WO2007144324, 21 Dec 2007.
7. IACCINO, L. L.; SANGAR, N.; STAVENS, E. L. Production of aromatic hydrocarbon from methane. WO2007067285, 14 Jun 2007.
8. ENI SPA. *World Oil and Gas Review*. [S.l.]. 2012.
9. ZENNARO, R. Syngas Chem. Symp., Dresden (2006).
10. FLEISCH, H. Syngas Chem. Symp., Dresden (2006).
11. BASINI, L.; BARTOLINI, A.; LUPI, G.; CLERICI, G. C. E. Catalytic partial oxidation process for producing synthesis gas. US7368482, 06 May 2008.
12. RITTER, J. A.; EBNER, A. D. State-of-the-art Adsorption and membrane separation processes for hydrogen production in the chemical and petrochemical industries. *Separation Science and Techn.*, **6** (2007). 42 pp.1123-1193.

-
13. BARBA, D.; GIACOBBE, F.; DE CESARIS, A.; FARACE, A.; IAQUANIELLO, G. Membrane reforming in converting natural gas to hydrogen (part one). *International Journal of Hydrogen Energy*, **14** (2008). 33 pp.3700-3709.
 14. PALO, D. R. Methanol Steam Reforming for Hydrogen Production. *Chem. Reviews*, **107** (2007). p. 3992.
 15. MUNDSCHAU, M. V. Dense inorganic membranes for production of hydrogen from methane and coal with carbon dioxide sequestration. *Catal. Today*, **118** (2006). p. 12.
 16. PAGLIERI, S. Palladium membranes. *Nonporous Inorganic Membranes* (2006). p. 77.
 17. GAO, H. Chemical stability and its improvement of palladium-based metallic membranes. *I&EC Research* **43** (2004) 6920., **43** (2004). p. 6920.
 18. UEMIYA, S. Brief Review of Steam Re-forming Using a Metal Membrane Reactor. *Topics in Catal.*, **29** (2004). p. 79.
 19. BAKER, R. W. Future Directions of Membrane Gas Separation Technology. *I&EC Research*, **41** (2002). p. 1393.
 20. FERREIRA-APARICIO, P.; BENITO, M. J.; SANZ, L. J. *Catalysis Reviews*, **47** (2005). p. 491.
 21. RUSTRUP-NIELSEN, J. R. *Catalysis Today*, **63** (2000). p. 159.
 22. ARMOR, J. N. *Applied Catalysis A*, **176** (1999). p. 159.
 23. ARMOR, J. N. *Catalysis Letters*, **101** (2005). p. 131.
 24. PEÑA, M. A.; GÓMEZ, J. P.; J.L.G., F. *Applied Catalysis A*, **144** (1996). p. 7.
 25. TWIGG, M. V. **Catalyst Handbook**. 2nd. ed. [S.l.]: Wolf Publishing, 1989.
 26. RUSTRUP-NIELSEN, J. R. *Stud. Surf. Sci. Catal., Natural Gas Conversion VII*, **147** (2004). p. 121.
 27. LUTZ, A. E.; BRADSHAW, R. W.; KELLER, J. O.; WITMER, D. E. *Int. J. Hydrogen Energy*, **28** (2003). p. 159.

-
28. JAROSCH, K.; EL SOLH, T.; DE LASA, H. I. *Chem. Eng. Sci.*, **57** (2002). p. 3439.
29. WEI, J.; IGLESIA, E. *Journal of Catalysis*, **224** (2004). p. 370.
30. WEI, J.; IGLESIA, E. *Journal of Catalysis*, **225** (2004). p. 116.
31. CHEN, D.; BJORGUM, E.; LODENG, R.; CHRISTENSEN, K. O.; HOLMEN, A. *Stud. Surf. Sci. Catal., Natural Gas Conversion VII*, **147** (2004). p. 139.
32. MATSUMURA, Y.; NAKAMORI, T. *Appl. Catal. A*, **258** (2004). p. 107.
33. CHOUDARY, T. V.; GOODMAN, D. W. *J. Molec. Catal. A*, **163** (2000). p. 9.
34. ALSTRUP, B.; CLAUSEN, S.; OLSEN, C.; SMITS, R. H. H.; RUSTRUP-NIELSEN, J. R. *Stud. Surf. Sci. Catal., Natural Gas Conversion V*, **119** (2002). p. 5.
35. TAKEIRA, K.; SHISHIDO, T.; KONDO, M. *Journal of Catalysis*, **207** (2002). p. 307.
36. TSYGANOK, A. I.; TSUNODA, T.; HAMAKAWA, S.; SUZUKI, K.; TAKEHIRA, K.; HAYAKAWA, T. *Journal of Catalysis*, **213** (2003). p. 213.
37. TAKEHIRA, K.; SHISHIDO, T.; SHOURO, D.; MURAKAMI, K.; HONDA, M.; KAWABATA, T.; TAKAKI, K. *App. Catal. A* (2005). 279 p. 41.
38. OHI, T.; MIYATA, T.; LI, D.; SHISHIDO, T.; KAWABATA, T.; SANO, T.; TAKEHIRA, K. *Appl. Catal. A*, **308** (2006). p. 194.
39. FONSECA, A.; ASSAF, E. M. *J. Power Sources*, **142** (2005). p. 154.
40. STURZENEGGER, M.; D'SOUZA, L.; STRUIS, R. P. W. J.; STUCKI, S. *Fuel*, **85** (2006). p. 1599.
41. PROVENDIER, H.; PETIT, C.; ESTOURNÈS, C.; LIBS, S.; KIENNEMANN, A. *Appl. Catal. A*, **180** (2000). p. 163.
42. FOLETTI, E. L.; ALVES, R. W.; JAHN, S. L. *J. Power Sources*, **161** (2006). p. 531.
43. KEGHOUCHE, N.; CHETTIBI, S.; LATRÈCHE, F.; BETTAHAR, M. M.; BELLONI, J.; MARIGNIER, J. L. *Radiation Physics and Chemistry*, **74** (2005). p. 185.

-
44. YAMAZAKI, O.; TOMISHIGE, K.; FUJIMOTO, K. *Appl. Catal. A*, **136** (1996). p. 49.
45. TOMISHIGE, K.; CHEN, Y.; YAMAZAKI, O.; HIMENO, Y.; KOGANEZAWA, Y.; FUJIMOTO, K. *Stud. Surf. Sci. Catal., Natural Gas Conversion V*, **119** (1998). p. 1998.
46. SISWANA, N. P.; TRIMM, D. L.; CANT, N. W. *Stud. Surf. Sci. Catal., Natural Gas Conversion V*, **119** (1998). p. 789.
47. DONG, W.; ROH, H.; JUN, K.; PARK, S.; OH, Y. *Appl. Catal. A*, **226** (2002). p. 63.
48. OH, Y.; ROH, H.; JUN, K.; BAEK, Y. *Intern. J. Hydrogen Energy*, **28** (2003). p. 1387.
49. ROH, H.; JUN, K.; PARK, S. *Appl. Catal. A*, **251** (2003). p. 275.
50. ZHANG, Q.; LI, Y.; XU, B. *Catalysis Today*, **98** (2004). p. 601.
51. BOROWIECKI, T.; DENIS, A.; GAC, W.; DZIEMBAJ, R.; PIWOWARSKA, Z.; DROZDEK, M. *Appl. Catal. A*, **274** (2004). p. 259.
52. TAKAHASHI, R.; SATO, S.; SODESAWA, T.; YOSHIDA, M.; TOMIYAMA, S. *Appl. Catal. A*, **273** (2004). p. 211.
53. URASAKI, K.; SEKINE, Y.; KAWABE, S.; KIKUCHI, E.; MATSUKATA, M. *Appl. Catal. A*, **286** (2005). p. 23.
54. WANG, J. S. B.; TAI, Y. L.; DOW, W. P.; HUANG, T. J. *Appl. Catal. A*, **218** (2001). p. 69.
55. WANG, J. B.; KUO, L. E.; HUANG, T. J. *Appl. Catal. A*, **249** (2003). p. 93.
56. WANG, J. B.; HSIAO, S. Z.; HUANG, T. J. *Appl. Catal. A*, **246** (2003). p. 197.
57. SAUVET, A. L.; IRVINE, J. T. S. *Solid State Ionics*, **167** (2004). p. 1.
58. WANG, Y.; CHIN, Y. H.; ROZMIAREK, R. T.; JOHNSON, B. R.; GAO, Y.; WATSON, J.; TONKOVICH, A. Y. L.; VANDER WIEL, D. P. *Catal. Today*, **98** (2004). p. 575.
59. ISHIHARA, A.; QIAN, E. W.; FINAHARI, I. N.; SUTRISNA, I. P.; KABE, T. *Fuel*, **84** (2005). pp.1462-1468.
60. CRACIUN, R.; DANIELL, W.; KNÓZINGER, H. *Appl. Catal. A*, **37** (1997). p. 225.

-
61. ROSTRUP-NIELSEN, J. R. *Catal. Tod.*, **37** (1997). p. 225.
62. BARTHOLOMEW, C. H. *Appl. Catal. A*, **212** (2001). p. 17.
63. BARTHOLOMEW, C. H. *Catal. Rev. – Sci. Eng.*, **24** (1982). p. 67.
64. ARMOR, J. N.; MARTENAK, D. J. *Appl. Catal. A*, **206** (2001). p. 231.
65. TRIMM, D. L. *Catal Tod.*, **37** (1997). p. 233.
66. ROSTRUP-NIELSEN, J. R. *Stud. Surf. Sci. Catal. - "Natural gas conversion II"*, **81** (1994). p. 25.
67. ROSTRUP-NIELSEN, J. R. *J. Catal.*, **85** (1984). p. 31.
68. SEHESTED, J.; GELTEN, J. A. P.; REMEDIAKIS, I. N.; BENGAARD, H.; NORSKOV, J. K. *J. Catal.*, **223** (2004). p. 432.
69. SEHESTED, J.; CARLSON, A.; JANSSENS, T. V. W.; HANSEN, P. L.; DATYE, A. K. *J. Catal.*, **197** (2001). p. 200.
70. CAMPBELL, C. T.; PARKER, S. C.; STARR, D. E. *Science*, **298** (2002). p. 811.
71. SEHESTED, J. *J. Catal.*, **217** (2003). p. 417.
72. HU, Y. H.; RUCKENSTEIN, E. *Adv. Catal.*, **48** (2004). p. 297.
73. CHOUDHARY, V. R.; RAJPUT, A. M.; PRABHAKAR, B. *Catal. Lett.*, **15** (1992). p. 363.
74. CHOUDHARY, V. R.; RAJPUT, A. M.; PRABHAKAR, B. *J. Catal.*, **139** (1993). p. 326.
75. CHOUDHARY, V. R.; RAJPUT, A. M.; RANE, V. H. *Catal. Lett.*, **16** (1992). p. 269.
76. CHOUDHARY, V. R.; RAJPUT, A. M.; RANE, V. H. *J. Phys. Chem*, **96** (1992). p. 8686.
77. CHOUDHARY, V. R.; SANSARE, S. D.; MAMMAN, A. S. *Appl. Catal. A*, **90** (1992). p. L1.
78. HU, Y. H.; RUCKENSTEIN, E. *Ind. Eng. Chem. Res.*, **37** (1998). p. 2333.
79. BASILE, F.; FORNASARI, G. T. F. V. A. *Catal. Tod.*, **64** (2001). p. 54.

-
80. GAVALAS, G. R.; PHICHITCUL, C.; VOECKS, G. E. *J. Catal.*, **88** (1984). p. 54.
81. HICKMAN, D. A.; SCHMIDT, L. D. *J. Catal.*, **138** (1992). p. 267.
82. TAKEHIRA, K. *Catalysis Surveys from Japan*, **6** (2002). p. 19.
83. REYNIERS, M.; DE SMET, C. R. H.; MENON, P. G.; MARIN, G. B. *Cattech.*, **6** (2002). p. 140.
84. BOND, G.; TAHIR, S. F. *Appl. Catal.*, **1** (1991). 71
85. AUGUSTINE, R. L. **Heterogeneous Catalysis for the Synthetic Chemist**. New York: Marcel Dekker, Inc, 1996. 287 p.
86. AVILA, M. S. Catalizadores de Platino Soportado Sobre Óxidos Reducibles Para La Eliminación De Compuestos Orgánicos Volátiles. *PhD. Thesis* (2011). Disponível em: <<http://bibliotecavirtual.unl.edu.ar:8180/tesis/handle/1/322?locale=es>>. Acesso em: 15 Febrary 2013.
87. TAKEHIRA, K. Highly dispersed and stable supported metal catalysts prepared by solid phase crystallization method. *Catalysis Surveys from Japan*, **1/2** (2002). 6
88. MOMMA, K.; IZUMI, F. VESTA 3 for three-dimensional visualization of crystal, volumetric and morphology data. *J. Appl. Crystallogr.*, **44** (2011). pp.1272-1276.
89. DRITS, V. A.; BOOKIN, A. S. **Layered Double Hydroxides: Present and Future**. New York: Vincente Rives, Nova Science Publishers, Inc., 2001. ISBN 1-59033-060-9.
90. REICHLER, W. T.; KANG, S. Y.; EVERHARDT, D. S. *Journal of Catalysis*, **101** (1986). p. 352.
91. LABAJOS, F. M.; RIVES, V.; ULIBARRI, M. A. Effect of hydrothermal and thermal treatment on the physicochemical properties of Mg-Al hydrotalcite-like materials. *Journal of Materials Science*, **27** (1992). pp.1546-1552.
92. VELU, S.; SUZUKI, K.; OKAZAKI, M.; OSAKI, T.; TOMURA, S.; OHASHI, F. Synthesis of new Sn-incorporated layered double hydroxides and their thermal evolution to mixed oxides. *Chem. Mater.*, **11** (1999). pp.2163-2172.

-
93. SHISHIDO, T.; SUKENOBU, M.; MORIOKA, H.; KONDO, M.; TAKAKI, K.; TAKEHIRA, K. Partial Oxidation of methane over Ni/Mg-Al oxide catalysts prepared by solid phase crystallization method from Mg-Al hydrotalcite-like precursors. *Applied Catalysis A: General*, **1-2** (2002). 223 pp.35-42.
94. BASILE, F.; FORNASARI, G.; POLUZZI, E.; VACCARI, A. Catalytic partial oxidation and CO₂-reforming on Rh- and Ni- based catalysts obtained from hydrotalcite-type precursors. *Applied Clay Science*, **5-6** (1998). 13 pp.329-345.
95. BASILE, F.; BENITO, P.; FORNASARI, G.; VACCARI, A. Hydrotalcite-type precursors of active catalysts for hydrogen production. *Applied Clay Science*, **1-2** (2010). 48 pp.250-259.
96. BASILE, F.; BENITO, P.; FORNASARI, G.; GAZZOLI, D.; PETTITI, I.; ROSETTI, V.; VACCARI, A. Ni-catalysts obtained from silicate intercalated HTlcs active in the catalytic partial oxidation of methane: influence of the silicate content. *Catalysis Today*, **1-2** (2009). 142 pp.78-84.
97. TAKEIRA, K.; SHISHIDO, T.; WANG, P.; KOSAKA, T.; TAKAKI, K. Autothermal reforming of CH₄ over supported Ni catalysts prepared from Hydrotalcite-like anionic clay. *Journal of catalysis*, **1** (2004). 221 pp.43-54.
98. BASILE, F.; FORNASARI, G.; ROSETTI, V.; TRIFIRÒ, F.; VACCARI, A. Effect of the Mg/Al ratio of the hydrotalcite-type precursor on the dispersion and activity o. *Catalysis Today*, **91-92** (2004). pp.293-297.
99. BASILE, F.; FORNASARI, G.; GAZZANO, M.; VACCARI, A. Rh, Ru and Ir catalysts obtained by HT precursors: effect of the thermal evolution and composition on the material structure and use. *Journal of Materials Chemistry*, **12** (2002). pp.3296-3303.
100. BASILE, F.; FORNASARI, G.; GAZZANO, M.; KIENNEMANN, A.; VACCARI, A. Preparation and characterization of a stable catalyst for the partial oxidation of methane. *Journal of Catalysis*, **2** (2003). 217 pp.245-252.
101. YATES, J. T. J.; DUNCAN, T. M.; VAUGHAN, R. W. Infrared spectra of chemisorbed CO on Rh. *Journal of Chemical Physics* (1979). 71 p. 3908.
102. ERDÖHELYI, A.; SOLYMOSI, F. Effects of the support on the adsorption and dissociation

-
- of CO and the reactivity of surface carbon on Rh catalysts. *Journal of Catalysis*, **2** (1983). 84 pp.446-460.
103. TRAUTMANN, S.; BAERNS, M. Infrared Spectroscopic Studies of CO Adsorption on Rhodium Supported by SiO₂, Al₂O₃, and TiO₂. *Journal of Catalysis*, **2** (1994). 150 pp.335-344.
104. KUNDAKOVIC, L.; MULLINS, D. R.; OVERBURY, S. H. Adsorption and reaction of H₂O and CO on oxidized and reduced Rh/CeO_x(111) surfaces. *Surface Science*, **1** (2000). 457 pp.51-62.
105. FINOCCHIO, E.; BUSCAI, E.; FORZATTI, P.; GROPPI, G.; A., B. State of supported rhodium nanoparticles for methane catalytic partial oxidation (CPO); FT-IR studies. *Langmuir*, **20** (2007). 23 pp.10419-10428.
106. HADJIIVANOV, K.; IVANOVA, E.; DIMITROV, L.; KNÖZINGER, H. FTIR spectroscopic study of CO adsorption on Rh-ZSM-5: detection of Rh +-CO species. *Journal of Molecular Structure*, **1-3** (2003). 661-662 pp.459-463.
107. VAN'T BLIK, H. F. J.; VAN ZON, J. B. A. D.; HULZINGA, T.; VIS, J. C.; KONINGSBERGER, D. C.; PRINS, R. n extended X-ray absorption fine structure spectroscopy study of a highly dispersed Rh/Al₂O₃ catalyst: the influence of CO chemisorption on the topology of rhodium. *Journal of Physical Chemistry*, **13** (1983). 87 pp.2264-2267.
108. PRIMET, M. Infrared study of CO chemisorption on zeolite and alumina supported rhodium. *Journal of the Chemical Society, Faraday Transactions 1* (1978). 74 pp.2570-2580.
109. BASU, P.; PANAYOTOV, D.; YATES, J. T. Rhodium-carbon monoxide surface chemistry: the involvement of surface hydroxyl groups on Al₂O₃ and SiO₂ supports. *Journal of the American Chemical Society*, **7** (1988). 110 pp.1074-2081.
110. BASILE, F.; BERSANI, I.; DEL GALLO, P.; FIORILLI, S.; FORNASARI, G.; GARY, D.; MORTERA, R.; ONIDA, B.; VACCARI, A. In Situ IR Characterization of CO Interacting with Rh Nanoparticles Obtained by Calcination and Reduction of Hydrotalcite-Type Precursors. *International Journal of Spectroscopy* (2011). p. 8.

-
111. ROSETTI, V. Catalysts for H₂ production (2007).
112. KORUP, O.; GOLDSMITH, C. F.; WEINBERG, G.; GESKE, M.; KANDEMIR, T.; SCHLÖGL, R.; HORN, R. Catalytic partial oxidation of methane on platinum investigated by spatial reactor profiles, spatially resolved spectroscopy, and microkinetic modeling, **297** (2013). pp.1-16.
113. BASILE, F.; FORNASARI, G.; TRIFIRÒ, F.; VACCARI, A. Partial oxidation of methane: Effect of reaction parameters and catalyst composition on the thermal profile and heat distribution, **64** (2001). 1-2 pp.245-252.
114. BASILE, F.; BENITO, P.; FORNASARI, G.; MONTI, M. S. E.; TONELLI, D.; VACCARI, A. Novel Rh-based structured catalysts for the catalytic partial oxidation of methane, **157** (2010). 1-4 pp.183-190.
115. FAURE, R. et al. Foam-supported catalysts tailored for industrial steam reforming processes, **175** (2010). pp.241-244.
116. HAYNES, W. M. **CRC Handbook of Chemistry and Physics Internet Version**. [S.I.]: [s.n.], 2013.
117. SATO, T.; DOSAKA, K.; ISHITSUKA, M.; HAGA, E. M. . O. J., **193** (1993). p. 187.
118. FEGLEY, B.; BARRINGER, A., **32** (1984). p. 187.
119. TANI, E.; YOSHIMURA, M.; SOMIYA, S., **66** (1983). 7 p. 506.
120. LEITENBURG, C.; TROVARELLI, A.; ZAMAR, F.; MASCIO, S.; DOLCETTI, G.; LLORCA, J. (1995). p. 2181.
121. MUROTA, T.; HASEGAWA, T.; AOZASA, S.; MATSUI, H.; MOTOYAMA, M., **193** (1993). p. 298.
122. BASILE, F.; FORNASARI, G.; TRIFIRÒ, F.; VACCARI, A. Rh-Ni synergy in the catalytic partial oxidation of methane: surface phenomena and catalyst stability. *Catalysis Today*, **3** (2002). 77 pp.215-223.
123. BASILE, F.; BASINI, L.; D'AMORE, M.; FORNASARI, G.; GUARINONI, A.; MATTEUZZI, D.; DEL PIERO, G.; TRIFIRÒ, F.; VACCARI, A. Ni/Mg/Al/ anionic clay derived catalysts

for the catalytic partial oxidation of methane. *Journal of Catalysis* (1998). 173 pp.247-256.

First of all I would like to thank Dr. Francesco “Luca” Basile for his help and his support during these three years of work, I’m sure that without him this work would not been possible. I would like also to thanks Prof. Ferruccio Trifirò and Prof. Angelo Vaccari for gave me the opportunity to do this job. Thanks also to Prof. Fabrizio Cavani, Prof. Giuseppe Fornasari and Dr. Stefania Albonetti for tolerate me and my bad character every day for the last three years.

I would like to thanks also INSTM for trusting in me and European Commission who financed the NEXT-GTL project FP7-NMP-2008-LARGE-2: Catalysts and sustainable processes to produce liquid fuels from coal and natural gas.